UNIVERSITÀ
DEGLI STUDI
FIRENZE

DOTTORATO DI RICERCA IN
SCIENZE AGRARIE E AMBIENTALI

CICLO XVIII

Produttività colturale e sostenibilità dei sistemi agro-fotovoltaici in risposta ai cambiamenti climatici

Settore Scientifico Disciplinare

AGR /02

Dottorando

Dott. Moretta Michele

Supervisore

Prof. Bindi Marco

Coordinatore

Prof. Viti Carlo

Supervisor

Prof. Bindi Marco
Department of Agriculture, Food, Environment and Forestry (DAGRI)
University of Florence
Piazzale delle Cascine 18, 50144 Florence, Italy
Phone: +39 055 2755791
Email: marco.bindi@unifi.it

Co-supervisors

Dr. Moriondo Marco
Institute of BioEconomy, Italian National Research Council (IBE-CNR)
Via Caproni 8, 50145 Florence, Italy
Phone: +39 055 3288257
Email: marco.moriondo@cnr.it

Dr. Riccardo Rossi
Department of Agriculture, Food, Environment and Forestry (DAGRI)
University of Florence
Piazzale delle Cascine 18, 50144 Florence, Italy
Phone: +39 0552755886
Email: r.rossi@unifi.it

Dr. Enrico Palchetti
Department of Agriculture, Food, Environment and Forestry (DAGRI)
University of Florence
Piazzale delle Cascine 18, 50144 Florence, Italy
Phone: +39 0552755800
Email: enrico.palchetti@unifi.it

Acknowledgements

This PhD thesis is the result of three years of intense but rewarding work, encapsulated in a few pages that represent an important chapter in my life. Many people have accompanied and supported me on this journey of growth, not only intellectual but also personal. The time has therefore come to thank them all.

I would like to express my deep gratitude to Prof. Marco Bindi for giving me this opportunity and for his constant professional support.

My heartfelt thanks go to Dr. Riccardo Rossi and Dr. Marco Moriondo, whose exceptional scientific guidance has been fundamental to the achievement of this work. I am deeply grateful for their supervision, their brilliant insights, and their constant encouragement throughout these years. Beyond the research itself, they provided invaluable support during the most challenging moments, when everything seemed to go wrong. Their trust, generosity, and human warmth have been a source of strength and motivation. These are not just words - without them, none of this would have been possible. They have been true pillars in the successful completion of these three years of research. I sincerely wish that everyone, in their academic journey and in life, may have the privilege of meeting people as inspiring, generous, and genuine as they are.

A special thanks goes to Dr. Enrico Palchetti, without whose guidance the experiments described in this thesis would not have been possible. I owe to him, in large part, my entry into the academic and research world. Over the past five years, he has constantly supported and encouraged me, welcoming me with trust and guiding me through the most delicate moments. It is thanks to the path I have followed in our office, and to the freedom he has given me to learn from my mistakes, that I have been able to grow both personally and professionally. Beyond my PhD journey, his trust has allowed me to gain valuable experience in project writing, teaching undergraduate students, and understanding both the beauty and the challenges that exist within the university environment.

I am grateful to Prof. Frank De Ruijter and Dr Bernardo Maestrini for welcoming me to the Wageningen University and Research Centre, where I had the privilege of working with brilliant researchers and extraordinary people. Thanks to them, I have also experienced research outside Italy, savoured the beauty of the Dutch countryside and shared ideas and discussions that made me feel at home.

A special thought goes to Gloria Padovan, who has never left me alone throughout these years and has always been by my side in every experiment. She has been like an older sister - always ready to help when I was struggling and always available for a kind conversation. I sincerely wish her the very best for her future, both in life and in her career. May God bless you, Gloria.

I would like to thank all the people who have been part of my journey over these three years, Luisa, Anna, Sergi, Lina, Gianni, Roberto, Camilla, Paolo, Olga, Giacomo, Aldo, Lorenzo, Bob, Luca and all my colleagues at DAGRI. Each of you has left something good and positive within me, something I will carry with me for the rest of my life. I truly hope to continue working with people like you, and I wish that the future brings you nothing but happiness and success.

A special thought goes to Giovanna, who, from above, is surely still getting upset about my messy desk but smiling at every goal I've achieved in these experiments. There will always be a small place for you, and every year on May 21st, one of the candles will always be yours.

Finally, my deepest gratitude goes to Mina, my pillar over the past twelve years. Without her sacrifices during the most difficult times and her constant support in everyday life, I would not have been able to overcome the fears and anxieties that often seemed insurmountable. You have always put me first, setting yourself aside, and this achievement is as much yours as it is mine. I truly hope that life will give us many more moments of joy and success to celebrate together, for all the years to come.

Thank you all.

Table of Contents

Abstract

Agrivoltaic systems (AVS) represent an innovative land-management strategy that enables the simultaneous production of food and renewable energy on the same area of land. By integrating crops and photovoltaic modules, they increase land-use efficiency and contribute to achieving climate neutrality as well as food and energy security targets. In the context of climate change, water scarcity, and growing energy demand, AVS therefore offer a concrete solution capable of mitigating conflicts between agricultural production and electricity generation. However, the presence of photovoltaic structures alters the crop microclimate by reducing solar irradiance, lowering air temperature, and increasing relative humidity, with variable effects on photosynthesis, plant growth, and yield depending on the cultivated species. It is thus essential to test the effectiveness of AVS on crops, understanding how they respond to heterogeneous shading and how system design can be adapted accordingly.

Reliable assessment of these crop responses requires continuous, high-resolution monitoring. Traditional field measurements, while accurate, are labor-intensive and difficult to scale up; hence, there is a need for integrated methodologies that combine optical sensing, process-based modeling, and energy-flow analysis. Against this background, the present thesis aims to provide tools and knowledge for the design of Agro-photovoltaic installations that maximize agricultural production without compromising energy efficiency.

In the framework of the PhD project, the research focused on the development of monitoring and modelling tools for crop production in AVS. Building on these premises, **Chapter 3** presents an image-driven modelling approach for fAPAR-derived biomass estimation in alfalfa cultivated under fixed photovoltaic panels in central Italy. A hybrid method combining proximal sensing (2D time-lapse RGB and 3D LiDAR scans) with the process-based SSM-iCrop2 model was implemented to quantify daily biomass accumulation. Although both 2D and 3D imaging reproduced fAPAR dynamics well, 2D imagery ensured the best

trade-off between temporal resolution and accuracy. By forcing the crop model with 2D-derived fAPAR and radiation data simulated in GroIMP, the system successfully captured growth cycles, mowing events and shading impacts across two seasons, demonstrating the feasibility of low-cost, high-frequency biomass monitoring in AVS.

Building on these findings, **Chapter 4** integrates 3D radiation modelling with crop growth simulations to analyse shading effects on alfalfa across different AVS designs (fixed and dynamic panels). A detailed GroIMP reconstruction of each AVS layout enabled precise calculation of direct and diffuse radiation and its spatial variability. Coupling these data with SSM-iCrop2 allowed the prediction of light interception, water balance and yield under variable shading regimes. The study provided useful design elements to minimize productive losses while simultaneously optimizing renewable energy generation, demonstrating how the integration of data and modelling can support site-specific agronomic management and the optimal configuration of photovoltaic panels.

Chapter 5 moves beyond crop modeling and investigates how microclimatic gradients induced by photovoltaic panels (shading and redistribution of rainwater runoff) influence pasture composition at the field scale. Along transects laid perpendicular to the panel rows, the seasonal composition of the vegetation and the aboveground biomass were monitored. Grasses predominated overall, whereas legumes were favored in the inter-row areas with lower shading. Yield patterns reflected the combined control of light availability and redistributed water, showing maxima at the panel edges and reductions in the most shaded zones, thereby highlighting management opportunities for targeted mowing and grazing.

In line with this approach, **Chapter 6** explores the ecological implications of microclimatic gradients generated by AVS, with a specific focus on their effects on vegetation composition and soil biological quality. Through seasonal surveys conducted in a Mediterranean AVS pasture, the chapter integrates vegetation and

mesofaunal indicators to analyse the functional responses of plant communities and soil microarthropods along the shading gradient induced by photovoltaic panels. The analysis is based on the combined use of the Pasture Value (PV) index and the QBS-ar index, which assess forage quality and soil biological fertility, respectively. The results reveal clear seasonal and spatial variations. In spring, when contrasts in radiation and temperature are most pronounced, inter-row zones exhibit significantly higher PV and QBS-ar values. These areas support a co-dominance of light-demanding legumes and a richer mesofaunal community. Conversely, the under-panel zones, subjected to combined shading and altered water regimes (either drought or waterlogging), are dominated by stress-tolerant forb species and display lower soil biological quality. In autumn, although overall biological activity tends to decrease, a partial recovery of soil fauna is observed, favoured by the accumulation of litter and greater thermo-hygrometric stability.

Riassunto

I sistemi agro-fotovoltaici rappresentano una strategia innovativa di gestione del territorio che consente la produzione simultanea di cibo ed energia rinnovabile sulla stessa superficie agricola. Integrando colture e moduli fotovoltaici, essi aumentano l'efficienza d'uso del suolo e contribuiscono al raggiungimento degli obiettivi di neutralità climatica, sicurezza alimentare ed energetica. Nel contesto dei cambiamenti climatici, della scarsità idrica e della crescente domanda di energia, i sistemi agrivoltaici offrono dunque una soluzione concreta in grado di mitigare i conflitti tra produzione agricola e generazione elettrica. Tuttavia, la presenza delle strutture fotovoltaiche modifica il microclima colturale, riducendo la radiazione solare incidente, abbassando la temperatura dell'aria e aumentando l'umidità relativa, con effetti variabili sulla fotosintesi, sulla crescita delle piante e sulla produttività, a seconda della specie coltivata. È quindi essenziale verificare l'efficacia dei sistemi agrivoltaici sulle colture, comprendendo come esse rispondano a condizioni di ombreggiamento eterogenee e come il design dell'impianto possa essere adattato di conseguenza.

Una valutazione affidabile di tali risposte richiede un monitoraggio continuo e ad alta risoluzione. Le misurazioni tradizionali in campo, sebbene accurate, risultano laboriose e difficili da estendere su ampia scala; emerge quindi la necessità di metodologie integrate che combinino sensori ottici, modellistica di processo e analisi dei flussi energetici. Parallelamente, è fondamentale ampliare la prospettiva oltre la sola produttività colturale, includendo le implicazioni ecologiche e pedologiche dei sistemi agro-fotovoltaici. Le modifiche microclimatiche indotte dai pannelli, come la riduzione della radiazione, la variazione della temperatura e la redistribuzione dell'acqua piovana, possono infatti influenzare non solo la crescita delle colture, ma anche la composizione della vegetazione, i cicli biogeochimici e la fertilità biologica del suolo. La presente tesi mira dunque a fornire strumenti e conoscenze per la progettazione di sistemi agro-fotovoltaici capaci di ottimizzare la produzione agricola ed energetica, salvaguardando al contempo la biodiversità e la qualità biologica del suolo, elementi chiave per la sostenibilità a lungo termine degli agroecosistemi.Nell'ambito del progetto di dottorato, la ricerca si è concentrata sullo sviluppo di strumenti di monitoraggio e modellizzazione della produzione colturale nei sistemi agrivoltaici.

Sulla base di queste premesse, il **Capitolo 3** presenta un approccio modellistico basato su immagini per la stima della biomassa a partire dal fAPAR (frazione di radiazione fotosinteticamente attiva assorbita) in colture di erba medica *(alfalfa)* coltivate sotto pannelli fotovoltaici fissi nell'Italia centrale. È stato sviluppato un metodo ibrido che combina il telerilevamento prossimale (immagini RGB 2D acquisite in time-lapse e scansioni 3D LiDAR) con il modello di simulazione colturale SSM-iCrop2 per quantificare l'accumulo giornaliero di biomassa. Sebbene entrambe le tecniche di imaging abbiano riprodotto correttamente le dinamiche di fAPAR, le immagini 2D hanno garantito il miglior compromesso tra risoluzione temporale e accuratezza. Forzando il modello colturale con i dati di fAPAR derivati dalle immagini 2D e con la radiazione simulata in GroIMP, il sistema ha riprodotto con successo i cicli di crescita, gli sfalci e gli effetti dell'ombreggiamento su due stagioni, dimostrando la fattibilità di un monitoraggio della biomassa a basso costo e ad alta frequenza nei sistemi agrivoltaici.

Sviluppando ulteriormente questi risultati, il **Capitolo 4** integra la modellistica tridimensionale della radiazione con simulazioni di crescita colturale per analizzare gli effetti dell'ombreggiamento sull'erba medica in diversi sistemi agrivoltaici (a pannelli fissi e dinamici). Una ricostruzione dettagliata in GroIMP di ciascun layout pianta-pannello ha consentito di calcolare con precisione la radiazione diretta e diffusa e la sua variabilità spaziale all'interno dei sistemi agrivoltaici. L'integrazione di questi dati nel modello SSM-iCrop2 ha permesso di prevedere LAI, bilancio idrico e la resa sotto regimi di ombreggiamento variabili. Lo studio ha fornito elementi utili alla progettazione per minimizzare le perdite produttive ottimizzando al contempo la produzione di energia rinnovabile, dimostrando come l'integrazione tra dati e modelli possa supportare la gestione agronomica sito-specifica e la configurazione ottimale dei pannelli.

Il **Capitolo 5,** si svincola dalla modellistica colturale e valuta come i gradienti microclimatici indotti dai pannelli (ombreggiamento e deflusso dell'acqua piovana) influenzino la composizione dei pascoli a scala di campo. Lungo transetti perpendicolari alle file di pannelli, sono stati monitorati la composizione stagionale della vegetazione e la biomassa. Le graminacee hanno predominato complessivamente, mentre le leguminose sono risultate favorite nelle interfila con minore ombreggiamento. I pattern di resa hanno riflesso il controllo combinato di luce e acqua redistribuita, con massimi ai bordi dei pannelli e riduzioni nelle zone più ombreggiate, evidenziando leve gestionali utili per lo sfalcio e il pascolamento mirato.

Sulla stessa line, il **Capitolo 6** approfondisce le implicazioni ecologiche dei gradienti microclimatici generati dai sistemi agrivoltaici, con particolare attenzione ai loro effetti sulla composizione della vegetazione e sulla qualità biologica del suolo. Attraverso rilievi stagionali condotti in un pascolo mediterraneo in regime agrivoltaico, il capitolo integra indicatori vegetazionali e mesofaunistici per analizzare le risposte funzionali delle comunità vegetali e dei microartropodi del suolo lungo il gradiente di ombreggiamento indotto dai pannelli fotovoltaici. L'analisi si basa sull'utilizzo congiunto dell'indice di Valore Pascolo (PV) e dell'indice QBS-ar per valutare, rispettivamente, la qualità foraggera e la fertilità biologica del suolo. I risultati evidenziano chiare differenze stagionali e spaziali. In primavera, quando le variazioni di radiazione e temperatura sono più marcate, le zone interfilari presentano valori significativamente più elevati di PV e QBS-ar, grazie alla co-dominanza di leguminose eliofile e a comunità mesofaunistiche più ricche. Al contrario, le zone sotto-pannello, soggette a ombreggiamento e a regimi idrici alterati (siccità o ristagno), ospitano specie erbacee più tolleranti allo stress e mostrano valori inferiori di qualità biologica del suolo. In autunno, sebbene l'attività biologica complessiva risulti ridotta, si osserva un parziale recupero della fauna edafica, favorito dall'accumulo di lettiera e da una maggiore stabilità termo-igrometrica.

Chapter 1.

General background

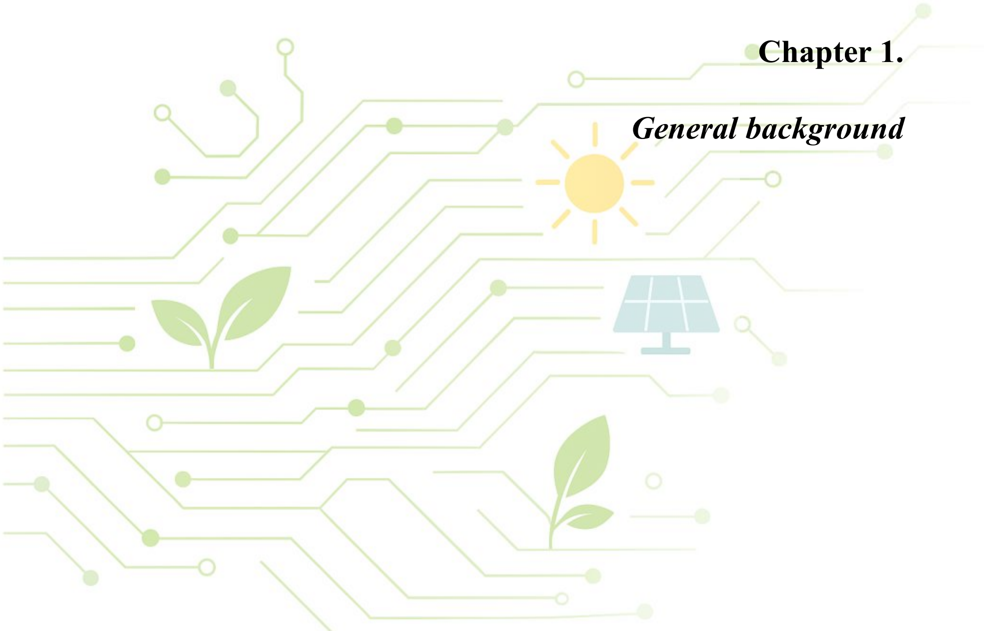

Chapter 1 provides a general background on Agrivoltaic systems, reflecting the global challenges of food security

and renewable energy conversion and highlighting the evolution of innovative technologies and monitoring methodologies for accurately quantifying crop and environmental traits.

PhD candidate's contribution

Michele Moretta wrote all sections of the chapter.

1.1 Agrivoltaic: an overview

Agrivoltaic systems (AVS), also known as agrophotovoltaics, represent an innovative land-use strategy that combines agricultural production with photovoltaic (PV) energy generation on the same land area (Dupraz et al., 2011). The concept was first proposed in Japan in the early 2000s, when Nagashima developed a prototype that allowed crops to grow beneath elevated PV modules while sharing excess solar radiation with energy conversion technologies (Tajima and Iida., 2021). A few years later, one of the first experimental field installations was established in France, near Montpellier, in 2010, paving the way for the scientific evaluation of the co-location of crops and PV modules. Since then, the technology has spread rapidly worldwide, particularly in Europe, Asia, and North America, with large-scale deployments in countries such as China, where some AVS plants now exceed several hundred megawatts of installed capacity (Toledo et al.,2021; Wadley et al.,2022)

The rationale behind AVS lies in their ability to mitigate the competition between food and energy conversion by enhancing land-use efficiency (Trommsdorff et al.,2016). In conventional PV installations, agricultural land is often removed from production, fueling conflicts over soil conservation and food security. In contrast, AVS maintain agricultural activity beneath or between PV panels, thereby offering a dual function: food production and renewable energy generation. This dual use of land is particularly relevant in the context of climate change, rising energy demand, and the urgent need to achieve targets of carbon neutrality, such as those outlined in the European Green Deal (Impallomeni et al.,2025). Moreover, AVS installations may be more socially acceptable than traditional ground-mounted PV farms, as they preserve agricultural functions and can provide diversified income sources for farmers (Thomas et al., 2023).

Beyond the socio-economic rationale, AVS also deliver important environmental and microclimatic benefits. Several studies have demonstrated that PV modules can alter the microenvironment beneath the array, reducing incoming solar radiation, lowering air and soil temperatures by 1-4 °C, and increasing relative humidity (Omer et al.,2025; Thum et al.,2025). These conditions can alleviate heat stress in crops, reduce soil evaporation, and enhance water-use efficiency (WUE). Indeed, systematic reviews report WUE improvements ranging from 20 to 47% under AVS configurations compared with open-field conditions

(Omer et al., 2025; Pascalis et al., 2025). Such effects are particularly valuable in arid and semi-arid regions, where water scarcity is a major constraint to agricultural productivity (Sturchio.,2024). By moderating evapotranspiration, AVS can reduce irrigation demand, thereby contributing to sustainable water management. At the same time, the shading created by PV panels must be carefully managed, as excessive light reduction can compromise photosynthetically active radiation (PAR) availability and reduce yields in light-demanding crops such as maize or kiwifruit (Magarelli et al.,2024).

The design of AVS is highly variable and strongly influences both energy and crop performance. Configurations include stilted or overhead systems, where modules are elevated above 2 m to allow agricultural machinery to pass underneath, and inter-row systems, in which panels are installed at lower heights and crops are cultivated between rows. Greenhouse-integrated PV solutions represent another emerging application, often using semi-transparent modules to modulate light transmission while generating electricity. Recent technological innovations include bifacial PV panels, dynamic tracking systems, and semi-transparent or spectrally selective modules, all aimed at optimizing light distribution for both crops and energy conversion (Lu et al.,2025). Panel orientation, tilt angle, ground coverage ratio (GCR), and spacing are critical design parameters that determine the trade-off between shading intensity, crop suitability, and overall system efficiency (Dupraz.,2024)

Despite their promise, AVS also face several challenges. Economically, the high initial investment and additional structural requirements for elevated PV systems may limit adoption, particularly for smallholder farmers. From a technical perspective, shading heterogeneity, increased complexity of farm operations, and potential risks such as wind load impacts or soil erosion from concentrated runoff require careful design (Zidane et al.,2025; Jung et al.,2021).

Furthermore, while literature demonstrates positive outcomes for shade-tolerant crops (e.g., leafy vegetables, forage species), yield reductions remain a concern for light-sensitive crops under dense PV arrays. These trade-offs underscore the need for site-specific design strategies and robust modelling tools capable of predicting both crop and energy yields before installation (Zainali et al.,2025).

Policy frameworks are increasingly shaping the development of AVS. Countries such as Germany, Japan, and the United States have introduced regulations that limit allowable yield reductions under AVS compared with reference open-field conditions. For example, in Germany, agricultural yields under AVS must not decline by more than one third, while in Japan the reduction threshold is 20%. In Massachusetts (USA), regulations stipulate that crops must receive at least 50% of full sunlight, and in Catalonia (Spain), irradiation reduction is limited to 40% for most crops (Campana et al.,2024).

These rules illustrate the importance of balancing renewable energy supply with agricultural output and highlight the necessity of integrating agronomic research with PV engineering and policy design.

Overall, AVS systems offer a promising pathway for sustainable land management, simultaneously addressing energy, food, and water security challenges. By enhancing land-use efficiency, mitigating climate risks, and contributing to renewable energy targets, AVS systems are positioned as a cornerstone of future sustainable agriculture. Nevertheless, their widespread deployment requires overcoming economic, technical, and regulatory barriers, as well as developing standardized metrics and long-term field studies. For these reasons, AVS systems are increasingly recognized not only as a technological innovation but also as an integrative strategy within the broader Water–Energy–Food nexus (Zainali et al.,2025).

1.2 Advances in Agrivoltaic System

Over the past two decades, AVS systems have evolved from experimental prototypes into increasingly complex and scalable solutions for the dual use of land (Mengi et al.,2023; Wydra et al.,2023; Patel et al.,2023) Early designs were characterized by fixed, ground-mounted photovoltaic arrays with limited integration of crop production, often resulting in significant trade-offs between energy generation and agricultural output. Recent technological progress, however, has led to the development of diversified AVS configurations aimed at optimizing both crop productivity and energy yield (Soto-Gomez et al.,2024).

One of the most relevant advances concerns the structural design of AVS installations. Elevated stilt-mounted systems now allow the passage of agricultural machinery, enabling the cultivation of a wide range of crops beneath solar panels. Dynamic tracking structures, which adjust the tilt angle of panels during the day, have been introduced to modulate shading intensity and distribute light more evenly. In parallel, novel photovoltaic materials such as bifacial, semi-transparent, and spectrally selective modules are being tested to maximize the transmission of photosynthetically active radiation (PAR) while maintaining high conversion efficiency. These innovations directly address one of the main limitations of early AVS systems: excessive and heterogeneous shading. (Lu et al.,2015).

In addition to structural innovations, significant progress has been made in modeling and monitoring tools. Process-based crop models integrated with solar radiation simulations are increasingly employed to predict biomass accumulation, water use efficiency, and yield–energy trade-offs under AVS conditions. Complementary to modeling, proximal sensing technologies (e.g., RGB imagery, multispectral and hyperspectral sensors, LiDAR) have improved the ability to monitor phenotypic traits and detect plant responses to variable shading. Such approaches not only provide higher spatial and temporal resolution than conventional field surveys but also support the calibration and validation of simulation models, thereby enhancing their predictive reliability (Ahemd et al.,2025).

From a systemic perspective, advances also include the integration of AVS into greenhouse structures, vineyards, and orchards, where crop physiology and microclimate management can particularly benefit from controlled light conditions. Pilot studies have demonstrated that leafy vegetables, forage species, and certain horticultural crops show positive or neutral responses to AVS-induced shading, whereas light-demanding crops still require site-specific optimization (Liu et al.,2023).

Despite their promise, AVS still face technical and socio-economic challenges. Economically, the high initial investment and additional structural requirements for elevated PV systems may limit adoption, particularly for smallholder farmers (Zidane et al., 2025) . From a technical perspective, shading heterogeneity, increased complexity of farm operations, and potential risks such as wind load impacts or soil erosion from concentrated runoff require careful design (Weselek et al., 2019; Mazzeo et al., 2025) . Furthermore, standard performance metrics for evaluating the agricultural and energetic outcomes of AVS systems are still lacking, as highlighted in recent simulation and modelling studies (Zainali et al., 2025) . Finally, large-scale adoption requires regulatory frameworks to balance renewable energy generation with the preservation of agricultural productivity, a need emphasised by design-oriented literature discussing trade-offs and policy constraints (Toledo & Scognamiglio, 2021)

Overall, advances in AVS highlight the importance of a multidisciplinary approach that integrates engineering, agronomy, and data science. Future developments will likely depend on the capacity to design flexible and cost-effective systems, while simultaneously providing robust tools for predicting crop responses and guiding sustainable management under variable shading conditions. In this context, continuous and integrated monitoring emerges as a key enabler to address these limitations, providing the data and decision-support tools needed to evaluate system performance, anticipate crop responses, and guide adaptive management.

1.3 Monitoring System in AVS

The performance and sustainability of AVS strongly depend on the ability to monitor both environmental conditions and crop responses under dynamic shading. Monitoring is therefore not only a technical requirement but also a strategic component for optimizing land productivity, energy yield, and resource use efficiency. In Italy, concerns about the potential impact of AVS on food production have prompted the government to issue the Guidelines on Agri-Voltaic Plants (Ministry of Environment and Energy Security, 2022; https://www.mase.gov.it). These guidelines explicitly mandate continuous monitoring of key agronomic and microclimatic parameters-including crop productivity, soil moisture retention and fertility, air temperature, and wind speed-to ensure the long-term sustainability of both agricultural outputs and energy generation.

Achieving such comprehensive monitoring remains challenging because of the complex interactions between crops and AVS structures. Traditional field surveys, while accurate, are labor-intensive and difficult to scale (Gower et al., 1999). To complement on-site measurements, crop growth models coupled with shading-dynamics simulations have been proposed as predictive tools for estimating biomass accumulation, water use efficiency, and crop yield–energy trade-offs in AVS (Amaducci et al., 2018; Mengi et al., 2023). Nevertheless, uncertainties in quantifying shading effects and plant physiological responses can limit the precision of these approaches, highlighting the need for integrated monitoring frameworks that combine modeling with high-resolution sensing.

To meet these needs, AVS installations increasingly rely on advanced, integrated monitoring solutions. Early systems depended mainly on conventional point measurements of temperature, soil moisture, or radiation, but recent developments combine proximal sensing, remote sensing, and computational modeling to capture the full complexity of AVS environments. Fixed sensor networks, often connected through Internet of Things (IoT) platforms, enable real-time collection of microclimatic data such as air temperature, relative humidity, wind speed, soil water content, and photosynthetically active radiation (Grubbs et al., 2024; Agostini et al., 2021; Muñoz-García et al., 2024). These continuous data streams are crucial for understanding the microclimate beneath the panels and for dynamically adjusting irrigation, fertilization, and energy management strategies (Zito et al., 2024).

In parallel, remote sensing technologies have become increasingly relevant. Satellite imagery and drone-based multispectral or hyperspectral surveys provide spatially explicit information on vegetation indices (e.g., NDVI, PRI), canopy structure, and early stress signals, complementing ground-based observations (Muñoz-García et al., 2024). Drones allow high-resolution and rapid mapping of crop performance across heterogeneous shading patterns, integrating seamlessly with proximal measurements (Zito et al., 2024).

Another promising avenue is the use of simulation models and decision-support tools, such as Computational Fluid Dynamics (CFD) for microclimate analysis and PVsyst® for energy prediction. When calibrated with in situ measurements, these models enable the optimization of panel geometry, tilt, and spacing, thereby supporting a more balanced trade-off between light distribution and energy efficiency (Torrente et al., 2024; Xie et al., 2022). Complementary indicators have also been proposed: for instance, the Ground Coverage Ratio (GCR) serves as a simple yet powerful predictor of agricultural productivity under different shading intensities, with yields generally maintained above 80 % when GCR remains below 25 % (Dupraz 2023). Similarly, advanced methods that separate direct and diffuse PAR have improved the accuracy of predicting photosynthetic responses under heterogeneous radiation regimes (Ma Lu et al., 2024; Thomas et al., 2023).

The integration of these monitoring technologies and analytical tools into decision support systems (DSSs) allows for adaptive, evidence-based management. Such platforms provide actionable insights to farmers, energy operators, and policymakers, fostering informed decisions on irrigation scheduling, crop selection, and system design. Although challenges such as high costs, data interoperability, and the need for specialized expertise remain, continuous and integrated monitoring is increasingly recognized-both in Italy and internationally-as a cornerstone for the sustainable design, operation, and upscaling of AVS (De Francesco et al., 2025; cf. references therein such as Grubbs et al., 2024; Zito et al., 2024).

1.4 Remaining knowledge gaps

The current state of the art in AVS still highlights significant gaps in knowledge that hinder effective, large-scale deployment. First, there is a lack of standardization of models and shared benchmarks that would allow for an objective comparison of different methodologies for simulating irradiation, microclimate, crop growth, and photovoltaic production. Added to this is the difficulty of integrating energy and agronomic components into a single platform, as well as adapting models to local specificities (climate, soil, crop species), especially in the presence of complex canopy structures and variable weather conditions. Moreover, most current simulations rely on historical or average climate data, with limited incorporation of future climate scenarios. This represents a major limitation, as climate change is expected to alter the frequency and intensity of extreme events, temperature regimes, and precipitation patterns, all of which could significantly influence crop performance and energy efficiency in AVS. Integrating climate projections into AVS modelling frameworks would provide critical insights into the long-term resilience and adaptive capacity of crops under dynamic shading and microclimatic conditions, supporting the design of climate-smart AV solutions tailored to future agricultural and energy challenges.

In addition to these technical and modelling challenges, much less attention has been devoted to understanding the ecological consequences of photovoltaic installations on agricultural ecosystems. The presence of panels alters not only light and temperature regimes but also rainwater redistribution, vegetation dynamics and soil biological activity. These processes can modify the composition and productivity of grassland and forage systems and influence key indicators of soil biological quality, such as the abundance and diversity of soil microarthropods. Despite their importance for long-term system sustainability, these aspects are rarely quantified and remain poorly integrated into AVS assessment frameworks. Addressing these ecological gaps requires field-based studies that combine vegetation and soil biological monitoring under real shading conditions. Such approaches can reveal how Agrivoltaic layouts reshape habitat heterogeneity and ecosystem functionality, providing essential insights to guide design choices and management practices that ensure not only energy efficiency and crop productivity but also biodiversity conservation and soil health. Moreover, the cascading effects of altered microclimatic and structural conditions may extend to aboveground fauna, potentially reshaping the diversity and spatial distribution of insects, pollinators, and other animal species that contribute to agroecosystem functioning. Despite their importance for long-term system sustainability, these aspects are rarely quantified and remain poorly integrated into AVS assessment frameworks.

There also remain uncertainties about microclimatic processes, such as the combined effects of humidity, rainfall, wind, evapotranspiration, dynamic albedo and soiling, and their impact on both crop yield and photovoltaic module efficiency. Finally, there is still a lack of consolidated methodologies for the joint optimisation of agricultural and energy yields in compliance with regulatory constraints. Bridging these gaps will require interdisciplinary approaches, public databases and full-scale validation campaigns.

Among the many knowledge gaps that still characterize the field of AVS, some of these aspects have been explored in this thesis.

References

Agostini, A., Colauzzi, M., & Amaducci, S. (2021). Innovative agrivoltaic systems to produce sustainable energy: An economic and environmental assessment. Applied Energy, 281, 116102. https://doi.org/10.1016/j.apenergy.2020.116102

Ahmed, R., Izaz, M. H. B., Manik, K. H., Khatun, H., Nath, A., Mim, J. J., & Hossain, N. (2025). Advancements in agrivoltaic systems for enhanced sustainable energy utilization: A review. *Environmental Challenges, 20*, 101299. https://doi.org/10.1016/j.envc.2025.101299

Amaducci, S., Yin, X., & Colauzzi, M. (2018). Agrivoltaic systems to optimise land use for electric energy production. Applied Energy, 220, 545–561. https://doi.org/10.1016/j.apenergy.2018.03.081

Dupraz, C. (2024). Assessment of the ground coverage ratio of agrivoltaic systems as a proxy for potential crop productivity. *Agroforestry Systems, 98*, 2679–2696. https://doi.org/10.1007/s10457-023-00906-3

Dupraz, C., Marrou, H., Talbot, G., Dufour, L., Nogier, A., & Ferard, Y. (2011). Combining solar photovoltaic panels and food crops for optimising land use: Towards new agrivoltaic schemes. Renewable Energy, 36(10), 2725–2732. https://doi.org/10.1016/j.renene.2011.03.005

Gower, S. T., Kucharik, C. J., & Norman, J. M. (1999). Direct and indirect estimation of leaf area index, fAPAR, and net primary production of terrestrial ecosystems. *Remote Sensing of Environment, 70*(1), 29–51. https://doi.org/10.1016/S0034-4257(99)00056-5

Grubbs, E. K., Gruss, S. M., Schull, V. Z., Gosney, M. J., Mickelbart, M. V., Brouder, S., Gitau, M. W., Bermel, P., Tuinstra, M. R., & Agrawal, R. (2024). Optimized agrivoltaic tracking for nearly-full commodity crop and energy production. *Renewable and Sustainable Energy Reviews, 191*, 114018. https://doi.org/10.1016/j.rser.2023.114018

Impallomeni, G., Filianoti, F., & Barreca, F. (2025). The role of agriculture for the European energy requests: Agrivoltaic systems. In L. Sartori, P. Tarolli, L. Guerrini, G. Zuecco, & A. Pezzuolo (Eds.), *Biosystems engineering promoting resilience to climate change* (Lecture Notes in Civil Engineering, Vol. 586, pp. 776–782). Springer. https://doi.org/10.1007/978-3-031-84212-2_96

Liu, W., Omer, A. A. A., & Li, M. (2023). Agrivoltaic: Challenge and progress. Agronomy, 13(7), 1934. https://doi.org/10.3390/agronomy13071934

Lu, M., Camporese, M., Ma, T., Haworth, M., & Campana, P. E. (2025). Selective light transmission in agrivoltaics: Modeling light spectra and photosynthetic rate. Nexus, 2(3), 100074. https://doi.org/10.1016/j.ynexs.2025.100074

Magarelli, A., Mazzeo, A., & Ferrara, G. (2024). Fruit crop species with agrivoltaic systems: A critical review. *Agronomy*, *14*(4), 722. https://doi.org/10.3390/agronomy14040722

Mazzeo, D., Di Zio, A., Pesenti, C., & Leva, S. (2025). Optimizing agrivoltaic systems: A comprehensive analysis of design, crop productivity and energy performance in open-field configurations. Applied Energy, 390, 125750. https://doi.org/10.1016/j.apenergy.2025.125750

Ministry of Ecological Transition, "Guidelines on Agrivoltaic Installations, Italy," 2022.

Mite, C., & Scognamiglio, A. (2021). Agrivoltaic systems design and assessment: A critical review and a descriptive model towards a sustainable landscape vision (three-dimensional agrivoltaic patterns). *Sustainability, 13*, 6871. https://doi.org/10.3390/su13126871

Omer, A. A. A., Li, M., Zhang, F., Hassaan, M. M. E., El Kolaly, W., Zhang, X., Lan, H., Liu, J., & Liu, W. (2025). Impacts of agrivoltaic systems on microclimate, water use efficiency, and crop yield: A systematic review. Renewable and Sustainable Energy Reviews, 221, 115930. https://doi.org/10.1016/j.rser.2025.115930

Paschalis, A., Bonetti, S., & Fatichi, S. (2025). Controls of ecohydrological grassland dynamics in agrivoltaic systems. Earth's Future, 13, e2024EF005183. https://doi.org/10.1029/2024EF005183

Sturchio, M. A., Kannenberg, S. A., & Knapp, A. K. (2024). Agrivoltaic arrays can maintain semi-arid grassland productivity and extend the seasonality of forage quality. Applied Energy, 356, 122418. https://doi.org/10.1016/j.apenergy.2023.122418

Thomas, S. J., Thomas, S., Sahoo, S. S., Ajith Kumar, G., & Awad, M. M. (2023). Solar parks: A review on impacts, mitigation mechanism through agrivoltaics and techno-economic analysis. Energy Nexus, 11, 100220. https://doi.org/10.1016/j.nexus.2023.100220

Thum, C. H., Okada, K., Yamasaki, Y., & Kato, Y. (2025). Impacts of agrivoltaic systems on microclimate, grain yield, and quality of lowland rice under a temperate climate. *Field Crops Research, 326*, 109877. https://doi.org/10.1016/j.fcr.2025.109877

Trommsdorff, M., Dhal, I. S., Özdemir, Ö. E., Ketzer, D., Weinberger, N., & Rösch, C. (2022). Agrivoltaics: Solar power generation and food production. In S. Gorjian & P. E. Campana (Eds.), *Solar energy advancements in agriculture and food production systems* (pp. 159–210). Academic Press. https://doi.org/10.1016/B978-0-323-89866-9.00012-2

Weselek, A., Ehmann, A., Zikeli, S., Lewandowski, I., Schindele, S., & Högy, P. (2019). Agrophotovoltaic systems: Applications, challenges, and opportunities. A review. *Agronomy for Sustainable Development, 39*, 35. https://doi.org/10.1007/s13593-019-0581-3

Zito, F., Giannoccaro, N. I., Serio, R., & Strazzella, S. (2024). Analysis and Development of an IoT System for an Agrivoltaics Plant. Technologies, 12(7), 106. https://doi.org/10.3390/technologies12070106

.

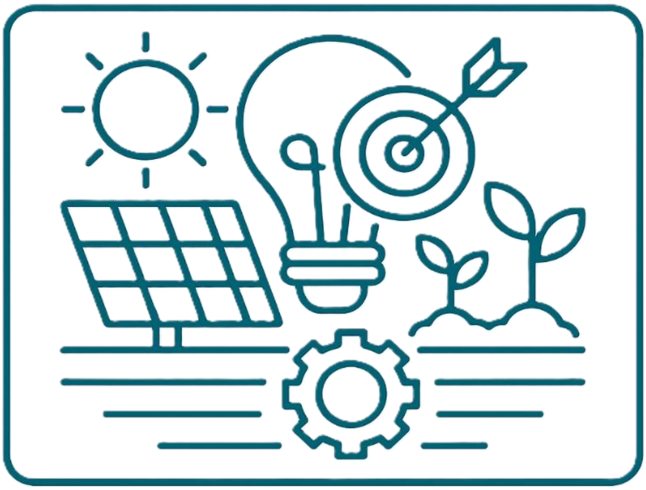

Chapter 2.

Aim and outline

Chapter 2. Shows the objectives and structure of the thesis.

PhD candidate's contribution

Michele Moretta wrote the entire chapter.

2.1 Aim and outline of the research

The PhD research aims to develop integrated and validated methodologies to optimize the management and design of agrivoltaic (AV) systems, fostering synergies between agricultural production and renewable energy generation. The research is structured into three main thematic areas:

A1. Integration of crop monitoring tools

A2. Application of modelling approaches

A3. Field-based ecological assessment

1. *Monitoring Tools (A1)*: The research investigates low-cost monitoring techniques, aligned with the Ministry of Ecological Transition (MITE) guidelines, for their application in AV systems. The study focuses on comparing two methods for estimating the fractional photosynthetically active radiation (fPAR) intercepted by crops, a key factor in assessing crop biomass growth and yield potential. It contrasts the extraction of Green Indices from 2D images captured with timelapse phototraps against the use of 3D images obtained via LiDAR technology. These methodologies were tested during the first two years of the project in a grassland AV systems. Results indicate that 2D imagery provides greater temporal accuracy, making it more suitable for herbaceous cover crops due to the ability to obtain images on both daily and hourly scales. Conversely, the 3D methodology, while less precise in temporal resolution, offers greater accuracy in morphological detail, and it is therefore more appropriate for row crops.
2. *Modeling Approach (A2):* The project examines shading effects on alfalfa in two AVS (fixed and bi-axial panels) during the 2023-2024 growing seasons. Using the GROIMP platform, an alfalfa growth model was parameterized with literature data and a 3D reconstruction of the AV systems. The model simulates light distribution and interception using an inverse path tracking algorithm with Monte-Carlo integration, considering solar panels and other geometries. Applied to open-field and AV systems in Ravenna (fixed) and Mantova (bi-axial), it simulates alfalfa growth based on local

practices. Key parameters like Leaf Area Index, biomass, and yield were validated through destructive sampling. This approach aims to optimise the design of AV systems for sustainable integration between energy and agriculture, advancing research in the field of renewable energy and AVS.

3. *Field ecological assessment (A3):* This work aims to evaluate the ecological effects of agrivoltaic systems on pasture vegetation and soil biological quality by analyzing seasonal dynamics and spatial variability along a shading gradient. Specifically, the objective is to investigate how microclimatic heterogeneity affects plant functional composition and soil mesofaunal communities. By integrating vegetation and Soil Biological Quality (QBS-ar) based soil quality indicators such as PV the study seeks to identify key ecological drivers (e.g., light, temperature, and moisture) and provide science-based recommendations for optimizing AV system design and grazing management to support biodiversity and soil functionality.

Chapter 3.

Towards Crop Monitoring in Agro-Photovoltaic Systems: An Image-driven Modeling Approach for fAPAR-derived Biomass Estimation

Chapter 3. has been based on the study:

Moretta, M., Moriondo, M., Leolini, L., Padovan, G., Staglianó, N., Palchetti, E., Lanini, G. M., Bindi, M., & Rossi, R. (2025). Towards crop monitoring in agro-photovoltaic systems: An image-driven modeling approach for fAPAR-derived biomass estimation. *European Journal of Agronomy, 170*, 127748. https://doi.org/10.1016/j.eja.2025.127748

Towards Crop Monitoring in Agro-Photovoltaic Systems: An Image-driven Modeling Approach for fAPAR-derived Biomass Estimation

Michele Moretta [1], Marco Moriondo[2], Luisa Leolini[1*], Gloria Padovan[1], Nicolina Staglianó[1], Enrico Palchetti[1], Giuseppe Mario Lanini[2], Marco Bindi[1] and Riccardo Rossi[1]

[1]Department of Agriculture, Food, Environment and Forestry (DAGRI), University of Florence, Piazzale delle Cascine 18, 50144, Florence, Italy.

[2] Institute of BioEconomy of the National Research Council (CNR-IBE), via Madonna del Piano 10, 50019, Sesto Fiorentino il, Italy.

Abstract

Agro-Photovoltaic (APV) systems optimize land use by integrating agriculture with renewable energy supply, offering a sustainable solution to contemporary address the growing global food demand and mitigate climate change impacts. However, the heterogeneous shading conditions inherent to APV systems may affect crop growth and productivity, highlighting the need for innovative and accurate monitoring methods to ensure consistent production levels. In this context, the present study proposed and tested a hybrid approach that combines proximal sensing with process-based crop models to estimate biomass accumulation within an APV system. Firstly, the performance of two-dimensional (2D) and three-dimensional (3D) imagery in capturing the phenotypic adaptations of alfalfa (*Medicago sativ*a L.) over two consecutive growing seasons (i.e., 2023 and 2024) was assessed by empirically modeling fluctuations in the fraction of absorbed photosynthetically active radiation (fAPAR). Although the comparative analysis always revealed a strong correlation between observed and image-derived fAPAR values ($R^2 = 0.74$), the 2D-based models demonstrated higher accuracy than the 3D approach (RMSE = 0.07 *vs* 0.09, rRMSE = 10.83% *vs* 17.16%, AIC = -44.91 *vs* -56.27, respectively). Consequently, the daily fAPAR estimates derived from 2D data were used to force the SSM-iCrop2 alfalfa growth model, providing accurate predictions of biomass accumulation both in 2023 ($R^2 = 0.96$, RMSE = 36.26 g m^{-2}, rRMSE = 21.35%, AIC = 151.37) and 2024 ($R^2 = 0.88$, RMSE = 46.98 g m^{-2} , rRMSE = 30.55%, AIC = 129.07) when compared with field survey data. These findings demonstrate how the proposed image-based data assimilation approach can be used as a potential tool for monitoring plant adaptation to varying shading conditions in APV systems. Moreover, its proven ability to predict crop yield with high spatio-temporal accuracy could inform mowing management strategies, optimizing production efficiency while aligning with sustainable agricultural and energy goals.

Keywords: Alfalfa; GroIMP; LiDAR; process-based modeling; timelapse image

Highlights

- A hybrid approach for crop monitoring in Agro-Photovoltaic (APV) systems is proposed
- Image-derived data well reproduced alfalfa's daily fAPAR fluctuations in APV system
- Integrating fAPAR with radiation and crop models produced accurate biomass estimates
- This approach detected plant responses to varying shading, rainfall, and mowing events
- The proposed method could inform data-driven mowing strategies in APV systems

Nomenclature

Acronym	Full Name
APV	Agro-Photovoltaic
VI	Vegetation index
R	Red channel
G	Green channel
B	Blue channel
CF	Color filter
PAR	Photosynthetically Active Radiation
fAPAR	Fraction of Absorbed Photosynthetically Active Radiation
LA	Leaf area [cm^2]
SLA	Specific Leaf Area [$cm^2\ g^{-1}$]
FTSW	Fraction of Transpirable Soil Water

ET	Evapotranspiration
LAI	Leaf Area Index
R^2	Coefficient of determination
RMSE	Root Mean Square Error
rRMSE	Relative RMSE
AIC	Akaike Information Criterion
LiDAR	Light detection and ranging
ROI	Region of interest
DOY	Day of the year

3.1 Introduction

The interconnected challenges of meeting growing global demands for energy and food and mitigating climate change's impacts urgently require innovative solutions. In this context, the Agro-Photovoltaic (APV) system emerges as a promising technology that combines renewable solar energy generation with agricultural production, enabling more efficient land use for dual purposes (Dinesh and Pearce, 2016). This integrated approach is gaining increasing attention from European policymakers, as it supports the goals of the European Green Deal by promoting the sustainable use of natural resources without compromising agricultural productivity (Trommsdorff et al., 2022). The strategic importance of APV systems is particularly evident in EU countries facing challenges such as high solar radiation and water scarcity, where their dual benefits are especially valuable (Zahrawi and Aly, 2024). Among these regions, Italy stands out due to its Mediterranean climate, characterized by abundant irradiance and concomitant droughts, making it one of the most promising locations for APV installations (Fattoruso et al., 2024). In fact, crops cultivated in semi-arid and arid regions may take advantage of the partial or total shading provided by APV structures, which enhances their water use efficiency by increasing soil moisture retention and mitigating temperatures (Amaducci et al., 2018; Touil et al., 2021; Weselek et al., 2019). By contrast, Mohammedi et al. (2023) demonstrated that while the irrigation demand for tomatoes grown in southern Italy under APV was reduced by 15-20%, the significant decrease in photosynthetically active radiation (PAR) resulted in yield losses ranging from 28% to 58%. Similarly, some studies report improved water use efficiency and soil moisture retention for lettuce grown in APV systems (Adeh et al., 2018; Elamri et al., 2018a), while others highlighted significant yield reductions due to limited light availability (Campana et al., 2021). A comparable pattern has been observed in wheat, where the effects of shading on the one hand reduce water stress and on the other lead to lower yields (Weselek et al., 2021). The variability of these results is further supported by Jo et al. (2022), who reported that legume and vegetable crops show inconsistent responses over two years, highlighting the complexity and species-specific nature of APV impacts.

The uncertainty regarding the impact of APV systems on food production has led the Italian government to regulate their adoption through the "Guidelines on Agri-Voltaic Plants", issued by the Ministry of Environment and Energy Security in 2022 (available online at: https://www.mase.gov.it/). These guidelines mandate continuous monitoring of key agronomic parameters, including crop productivity, soil moisture retention and fertility, as well as microclimatic factors like air temperature and wind power, thereby ensuring the long-term sustainability of agricultural and energy outputs. Achieving effective monitoring in APV systems presents significant challenges due to the complex interactions between crops and APV structures. Traditional field surveys, while accurate, are labor-intensive and impractical for large-scale monitoring (Gower et al.,1999). To support this task, crop growth models (CGMs) combined with shadow dynamics simulations have been proposed as tools to estimate theoretical crop growth, water use, and crop yield-energy trade-offs in APV systems (e.g., Amaducci et al., 2018; Mengi et al., 2023). However, uncertainties regarding shading effects on crop development may limit their effectiveness.

The reduced incoming solar radiation influences specific plant phenotypic traits, which must be explicitly incorporated into modeling approaches to enhance accuracy. In this context, studies have shown that limited light availability leads to significant changes in biomass partitioning, particularly between shoots and roots. For instance, Bebre et al., (2022) observed that plants under shading conditions prioritize above-ground growth, optimizing light capture by increasing leaf surface area, while reducing allocation to below-ground structures. Further evidence from Potenza et al., (2022) and Scarano et al., (2024) indicated that SLA tends to increase under shaded environments. This adaptation implies that plants develop thinner leaves with a larger surface area relative to their biomass, optimizing light capture to counter reduced solar radiation availability compared to full sunlight conditions. Thus, neglecting these adaptations in APV-based models risk underestimating leaf area and biomass distribution, ultimately leading to inaccuracies in crop yield predictions and limiting the reliability of studies examining energy-crop trade-offs (Ramos-Fuentes et al., 2023). This complexity introduces further challenges for current models, which often lack the resolution required to accurately simulate plant responses to fluctuating light conditions. Moreover, the absence of field-validated data exacerbates these issues, restricting their accuracy and applicability in real-world APV environments (Marrou et al., 2013; Weselek et al., 2019).

Proximal sensing technologies, leveraging their high spatio-temporal resolution and freedom from visual obstructions inherent to overhead remote observations, emerge as promising solutions for in-field, real-time phenotypic data collection (Wang and Fang, 2020). A range of imaging sensors, including hyperspectral, multispectral and red, green and blue (RGB) cameras, have been effectively employed for quantifying complex phenological traits inferred from specific morpho-colorimetric indexes (Laveglia et al., 2024) Notably, the RGB-based phenotyping offers a cost-effective and accessible approach for effectively analysing plant characteristics associated with growth dynamics and responses to external stimuli (Anderson et al., 2016; Liu et al., 2013; Migliavacca et al., 2011; Parmentier et al., 2021; Sonnentag et al., 2012; Westergaard-Nielsen et al., 2013). The acquisition and processing of two-dimensional (2D) color images using conventional digital cameras have been widely employed for non-destructive monitoring of plant phenology and biomass accumulation in various ecosystems, including forests and arid grasslands. Several studies have demonstrated the potential of repeated digital imaging in tracking vegetation dynamics and extracting key vegetation indices (VIs) that can serve as proxies for plant growth and productivity. For instance, Richardson et al., (2009) highlighted the strong correlation between VIs derived from time-lapse imagery and seasonal variations in canopy greenness, providing valuable insights into plant physiological responses to environmental changes. Similarly, Kurc and Benton, (2010) demonstrated that chromatic coordinates from digital images could effectively assess vegetation cover and biomass fluctuations in arid grasslands. Despite the proven effectiveness of 2D-imagery for phenological monitoring, research exploring the use of RGB-based VIs to estimate biomass accumulation under variable shading conditions remains largely unexplored.

The reconstruction of three-dimensional (3D) digital models allows for a more in-depth and comprehensive analysis of complex plant traits associated with adaptation to specific environmental conditions, such as canopy size, leaves distribution, and light interception efficiency (Rossi et al., 2022a). By capturing the spatial arrangement of plant components, 3D-modeling enables a precise investigation of how plants react to varying levels of shading, which is a critical aspect in APV scenarios. In this context, the integration of structural insights directly provided by Light Detection and Ranging (LiDAR) data with spectral information obtained from spectral-based imagery has proven effective in modeling canopy structure and light interception dynamics (Chen et al., 2017; Crommelinck and Höfle, 2016; Guo et al., 2019). However, these systems can be cumbersome for widespread adoption in APV systems, as they typically require the simultaneous deployment of multiple proximal and/or remote sensors. Recently developed handheld devices offer a more practical solution by consolidating both LiDAR and imaging capabilities into a single unit (Treccani et al., 2024), thus streamlining proximal fAPAR-related data collection in agricultural environments usable to feed CGMs and estimate key agronomic parameters, such as biomass accumulation and yield.

Although some studies have previously used the fAPAR to force CGMs of various crops, including sugarcane (Muller et al., 2020) and grapevine (Leolini et al., 2023), these approaches primarily rely on remote sensing data, resulting unsuitable for the unique context of APV systems. On the other hand, while proximal sensing measurements provide spatially and temporally accurate information about fAPAR-related phenotypic traits, they fall short of delivering a comprehensive understanding of the physiological processes driving their variability within the field. This underscores the necessity of integrating proximal sensing data with CGMs to fully reproduce crop responses to the fluctuating environmental conditions typical of APV systems, thus enabling more accurate predictions of agronomic parameters.

To fill this gap, our work was structured in two phases. The initial step involved the development and testing of empirical models based on proximal sensing to accurately reproduce the fAPAR of alfalfa. Subsequently, the best-performing empirical model was used to simulate the daily fAPAR trend over the 2023 and 2024 growing seasons, which will serve as a forcing factor in the SSM-iCrop2 alfalfa growth model (Soltani et al., 2020). The simulated results were then compared with observed field data to assess the predictive performance of the model under APV conditions.

3.2 Materials and Methods

3.2.1 Study area and experimental design

This study was conducted in 2023 and 2024 at a fixed-panel APV located in Sant'Alberto, Ravenna, Italy (44°30'36.69" N - 12°9'18.72" E; Fig. 1-Site A), within a region (i.e., central Italy) well-suited for the deployment of Agrivoltaic systems due to its high solar irradiation and productive agricultural land.

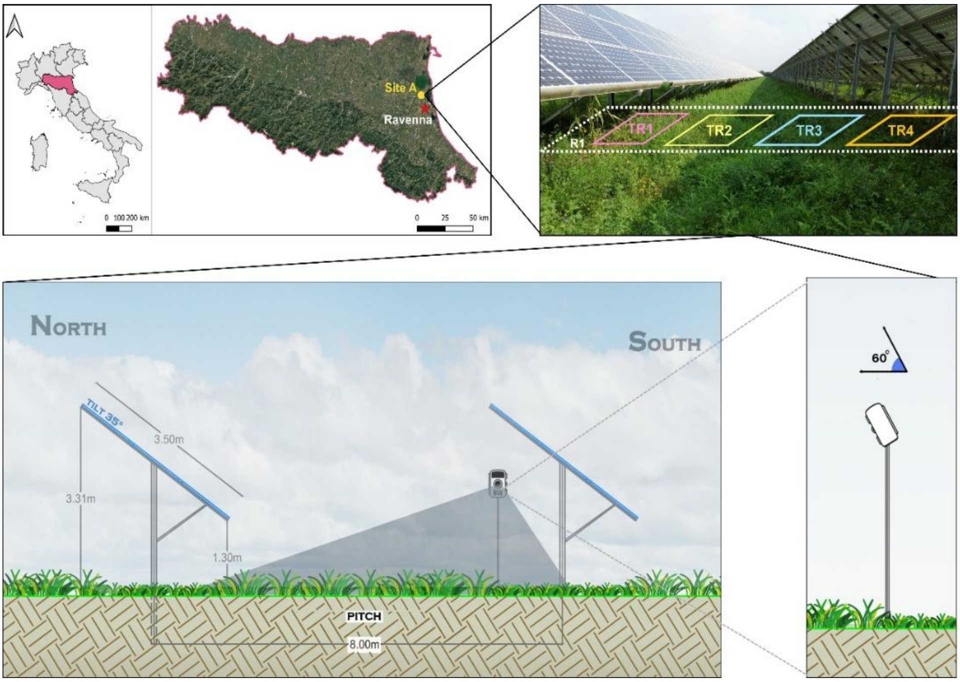

Figure 1. Study site location and technical layout of permanent alfalfa meadow. The figure shows the arrangement of treatments (TR1, TR2, TR3 and TR4) within an alfalfa transect replicate (R1) along with the position and orientation of the time-lapse camera.

The site of study (Fig. 1), operational since 2012, has an annual energy production capacity of 45,000,000 kWh and features a 70-hectare permanent alfalfa (*Medicago sativa* L.) meadow. The area is predominantly flat, with elevations ranging from 4 to 8 m above sea level and a temperate climate characterized by hot summers and cold winters. The annual average temperature is 15°C, with 5°C in January and a peak of 25.6°C in July. Rainfall averages 767 mm per year, with relatively even distribution across the seasons. November is the wettest month, with an average rainfall of 87 mm, while January is the driest, with only 49 mm of precipitation. Meteorological data for the experimental growing period were recorded at the local weather station.

The ground-mounted photovoltaic panels are south-oriented and positioned at an angle of 35° (Fig. 1). The solar panel tables are 3.5 m wide, with 8 m spacing between the center of each row, resulting in a Ground Cover Ratio (GCR) of 38%. The lowest edge of the panels is 1.30 m, while the highest edge reaches 3 m. The alfalfa was sown in 2020 after an initial light plowing to a depth of approximately 30 cm, followed by tilling. The soil was then rolled to ensure proper seed contact and terrain consolidation.

The experimental setup consisted of 9 areas, each characterized by 4 treatments representing different gradients of APV shadow: the front edge of each panel, where all rainwater drains off (TR1), the uncovered interspace adjacent to each panel (TR2), the back edge of each panel (TR3), and the central part under each panel (TR4).

To monitor the effect of different shading treatments on the growth and development of alfalfa throughout its entire cycle, one time-lapse camera (ScoutGuard BG590-K2-45mHD; Scubla®, Remanzacco, Udine, Italy) was strategically positioned on poles-oriented northward at the height of 2 m. The camera was set at a fixed angle of 60 degrees, capturing angular areas of 18 m² and 21 m² from the horizontal in each frame so as to guarantee a comprehensive monitoring of the analyzed transect. Since the camera position was fixed, the scene remained unchanged from day to day.

3.2.2 Data collection and processing

3.2.2.1 2D imaging

One RGB 2D-digital image with a resolution of 7,000x5,252 pixels was automatically acquired every hour from 08:00 AM to 08:00 PM by the camera, resulting in 12 pictures per day. In particular 7,824 images were recorded on the alfalfa from 1 DOY 2023 to 271 DOY 2024, allowing to monitor all growth stages of the meadow grass, including spring and summer mowing events (i.e., the 167 and 240 DOY 2023 and the 108, 134 and 198 DOY 2024, respectively). To avoid altering the framing of the scene during the experimental period, the images were transferred to a workstation only at the end of the experiments and processed in the MATLAB® environment (version R2023a; The MathWorks Inc.®, Natick, MA, USA) to extract morpho-colorimetric parameters of the photographed vegetation.

For the study area, non-overlapped Regions Of Interest (ROIs; Fig. 2.1) corresponding to the shading conditions (i.e., TR1, TR2, TR3) were manually digitized on a reference image and then automatically applied to the entire dataset. In this context, the TR4 area was excluded from the analysis due to obstruction caused by both the photovoltaic panel and nearby vegetation, which hindered visibility and prevented the acquisition of data comparable to the other treatments. A multi-step thresholding approach was implemented using the MATLAB® inbuilt Color Thresholder tool to remove soil pixels from ROIs. Initially, RGB images were converted to the International Commission on Illumination (CIE) L*a*b* (L* = luminosity, a* = red/green coordinate, b* = yellow/blue coordinate) and YCbCr (Y = brightness; Cb = blue-difference chroma component; Cr = red-difference chroma component) color spaces, where pre-established thresholds were iteratively applied (Fig. S1). The segmentation of foreground objects (i.e., vegetation) was, thus, achieved by intersecting the resulting binary masks. Further refinement involved eliminating connected components smaller than 0.005% of the total imaged area. The number of remaining pixels was computed as the Total projected plant area (Duan et al., 2018)

To ensure consistency in feature extraction across different shading conditions and image acquisition times, a procedure was devised to correct non-uniform brightness (Fig. 2.2) and normalize the individual RGB channels (Fig. 2.3). Specifically, a disk-shaped structuring element with a radius of 55 pixels, fully fitting within the canopy of alfalfa plants, was defined and applied to perform a morphological opening operation, consisting of an erosion followed by a dilation. This technique effectively smoothed large-scale brightness variations in the image framework by applying a binary-valued 2D neighborhood, where the center pixel (origin) of the structuring element determines which pixels are included in the morphological computation, as previously described by Soille (2003). Following the principles of the top-hat transformation (Morales and Ginori, 2013; Wang et al., 2014), the resulting opened image was then subtracted pixel-by-pixel from its then pixel-by-pixel the original image, yielding processed ROIs with uniform illumination. The intensity of each pixel's red (R), green (G), and blue channel (B) was normalized relative to its respective maximum value assumed within the same image (R_{max}, G_{max}, and B_{max}; Eq. (1)), following Yang and Cho, (2021). Finally, the normalized red (R_n), green (G_n), and blue (B_n) values were used to calculate the relative contributions of individual color channels (*r*, *g,* and *b*) to the total RGB intensity of each pixel (Eq. (2)), by ensuring the extraction of comparable colorimetric traits between different ROIs and dates (Fig. 2.3).

$$R_n = (\frac{R}{R_{max}}), G_n = (\frac{G}{G_{max}}), B_n = (\frac{B}{B_{max}}) \tag{1}$$

$$r = \frac{R_n}{(R_n+G_n+B_n)}, g = \frac{G_n}{(R_n+G_n+B_n)}, b = \frac{B_n}{(R_n+G_n+B_n)} \tag{2}$$

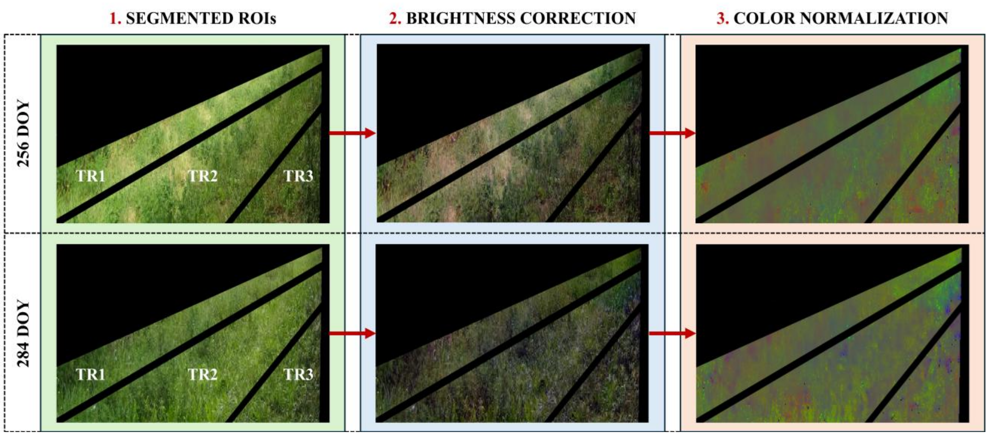

Figure 2. A graphical example of the color normalization applied to the R, G, and B channels of the 2D images to extract comparable colorimetric traits across different ROIs (TR1, TR2, and TR3) and dates (i.e. DOY).

The chromatic coordinates r, g and b were thus used to compute the main vegetation indices (Tab. 1), including Vegetation index (VEG), Color index of vegetation (CIVE), Combination vegetative index (COM), Visible atmospheric resistance index (VARI), Red green blue vegetation index (RGBVI), Modified green ratio vegetation index (MGRVI), Green leaf index (GLI), Normalized green–red difference index (NGRDI), Red ratio (RR), Green ratio (GR), Blue ratio (BR), Woebbecke index (WI). In this context, Excess green (ExG), Excess red (ExR), Excess green minus Excess red ($ExGR$), Alternate excess red ($ExRalt$) and Excess green minus Alternate excess red ($ExGRalt$) color filters were used to segment target vegetation from background objects. Additionally, Otsu's adaptive thresholding algorithm was applied to the tonal image resulting from each ExG, ExR, $ExGR$, $ExRalt$, and $ExGRalt$ calculation to automatically determine the greenness pixels, as similarly reported in Meyer and Neto, (2008). The greenness projected plant area was then computed as the number of greenness pixels and combined in Eq. (3) to derive the Greenness plant area ratio Duan et al., 2018).

$$GPAR_{CF} = \frac{GPPA_{CF}}{TPPA} \tag{3}$$

where *CF* indicates the considered color filters (i.e. ExG, ExR, ExGR, $ExR_{alt,}$ or $ExGR_{alt}$).

Table 1. Vegetation indices extracted in this study from 2D- and 3D-imagery.

Vegetation Index	Acronym	Formula	Reference
Excess green	ExG	$2g - r - b$	(Meyer and Neto, 2008); (Soontranon et al., 2014)
Excess red	ExR	$1.4r - g$	(Meyer and Neto, 2008) (Meyer et al., 2004)
Excess green minus Excess red	ExGR	$ExG - ExR$	(Meyer and Neto, 2008) (Shanmugam and Asokan, 2015) (Soontranon et al., 2014)

Alternate excess red	ExR_{alt}	$1.4r - b$	(Meyer et al., 1999); (Jin et al., 2017)
Excess green minus Alternate excess red	$ExGR_{alt}$	$ExG - ExRalt$	(Riehle et al., 2020)
Vegetation Index	VEG	$\frac{g}{[(r^{0.667})(b^{0.333})]}$	(Hague et al., 2006)
Color Index of Vegetation	CIVE	$0.441r - 0.881g + 0.385b + 18.78745$	(Kataoka et al., 2003)
Combination vegetative index	COM	$0.25ExG + 0.3ExGR + 0.33CIVE + 0.12VEG$	(Guijarro et al., 2011)
Visible atmospheric resistance index	VARI	$\frac{(g - r)}{(g + r - b)}$	(Zhou et al., 2017)
Red green blue vegetation index	RGBVI	$\frac{(g^2 - rb)}{(g^2 + rb)}$	(Bendig et al., 2015)
Modified green ratio vegetation index	MGRVI	$\frac{(g2 - r^2)}{(g2 + r^2)}$	(Bendig et al., 2015)

Green leaf index	GLI	$\frac{(2g - r - b)}{(2g + r + b)}$	(Louhaichi et al., 2001)
Normalized green–red difference index	NGRDI	$\frac{(g - r)}{(g + r)}$	(Tucker, 1979)
Red ratio	RR	$\frac{r}{(r + g + b)}$	(Rivington, 2013; Woebbecke et al., 1995a)
Green ration	GR	$\frac{g}{(r + g + b)}$	(Woebbecke et al., 1995a)
Blue ratio	BR	$\frac{b}{(r + g + b)}$	(Woebbecke et al., 1995a)
Woebbecke index	WI	$\frac{(g - b)}{(r - g)}$	(Woebbecke et al., 1995b)
Greenness plant area ratio	$GPAR_{CF*}$	$\frac{GPPA_{CF}}{TPPA}$	(Duan et al., 2018)

$CF = ExG, ExR, ExGR, ExR_{alt}$ or $ExGR_{alt}$

3.2.2.2 3D scanning

A 3D-scanning was conducted on the 311 DOY in 2022, and on the 89, 143, 186, 212, and 314 DOY in 2023 using a handheld iPad Pro® (Apple Inc., Cupertino, CA, USA) with 11″ Liquid Retina display at 2,388x1,668-pixel resolution, 128 GB of Read Only Memory, 8 GB of Random Access Memory and iPadOS® 17.5.1 operating system (Fig. S2). The LiDAR module integrated into this device works by emitting laser pulses and measuring the time it takes for them to reflect off target objects (i.e., vegetation) using the direct-time-of-flight technology. The mobile-based approach combines depth data (i.e., the distance to various points in the scanned environment) with high-resolution color images captured by a 12MP Wide RGB camera and a 10MP Ultra-Wide RGB camera, allowing for colorized dense point clouds at a 1:1 scale within in-built apps.

The free iOS application *Sacaniverse* (ver. 3.0.0;https://scaniverse.com/) was used to capture the dense point clouds of the study area. The acquisition process, consisting of slowly advancing along the transect direction while continuously rotating the device around the vegetation to ensure full spatial coverage from multiple viewing angles, allowed the monitoring of all treatments (TR1, TR2, TR3, and TR4). The scans were performed in small object mode and then processed in area mode to achieve the highest possible resolution of the reconstructed 3D scene. Each resulting 3D model was exported as a colorized dense point cloud (i.e., LAS format), georeferenced with Universal Transverse Mercator Cartesian coordinates, for subsequent automated analysis within the MATLAB® environment.

Following the workflow of Roussel et al. (2020), the dense point cloud underwent a series of processing steps, including (i) soil classification, (ii) Digital Terrain Model generation, (iii) Digital Surface Model (generation, and (iv) height normalization. The first step involved separating ground and non-ground features using the Cloth Simulation Filter, which classifies points based on how the nodes of a simulated cloth interact with the surface of the inverse point cloud (Zhang et al., 2016). Any remaining noise was automatically removed using the Inverse Voronoi Filtering method. Next, a Triangulated Irregular Network interpolation was employed on the ground-filtered point cloud to generate a digital terrain model with a resolution of 0.05 meters. The digital terrain model was thus subtracted from the original point cloud to produce a digital surface model consisting exclusively of above-ground elements. In the final step of the procedure, a k-nearest neighbor algorithm was applied to normalize the elevation of the digital surface model points relative to the ground model. This removed variations in height caused by terrain irregularities, ensuring that only points with positive z-values (i.e., vegetation) were retained for further analysis.

After normalization, the dense point cloud was clipped according to the predefined spatial coordinates to isolate the ROIs, enabling the subsequent computation of morpho-colorimetric traits. The vegetation indices shown in Table 1 were also extracted from each 3D model, following the procedure previously described. In addition, the average plant height (m) was calculated as the vertical distance from the ground for each *xyz*-point, with duplicates resolved by selecting the maximum *z*-value. The bounding area and volume enveloping all the *xyz*-points were then computed via a 3D-alpha shape approach (α radius equal to 0.33) to extract the average plant area (m^2) and volume (m^3), respectively. Ultimately, the plant area and plant volume were further normalized by dividing their values by the surface area of the bounding box in the *xy*-plane (m^2), which was used as a reference to account for the total spatial distribution of the plants within individual ROIs.

3.2.2.3 Field measurements

PAR measurements (μmol m^{-2} s^{-1}) were taken on 7, 89, 143, 186, 212, and 314 DOY for 2023 and 80, 100, 191 and 268 DOY for 2024 at each alfalfa sample plot (n = 36) using a SunScan canopy analyzer AccuPAR LP-80® ceptometer (Decagon Devices, Inc., WA, USA), following the methodology described by Leolini et al., 2022). This method calculates fAPAR as the ratio between below-canopy PAR (PARb) and above-canopy PAR (PARa), which were acquired under sunny and cloudless conditions between 11:00 AM and 13:00 PM (Eq. 4).

$$fAPAR = 1 - \left(\frac{PAR_b}{PAR_a}\right) \tag{4}$$

On the survey days, the regrowth biomass of alfalfa (g m^{-2}) was harvested by cutting it from a height of 3 cm within a 0.50×0.50 m^2 square positioned at the center of each transect. The samples were then dried in an oven for 48 hours at 60°C to measure the dry weight.

Three alfalfa plants were collected from each sample plot (n = 36) on 89, 143, 186, 212, and 284 DOY in 2023 and on 80, 100, 191 and 268 DOY for 2024. In the laboratory, the leaves removed from each plant were positioned over a background with a standard ruler for scale calibration and photographed from a vertical perspective by a digital RGB camera. The Leaves Area (LA, cm^2) was measured using the open-source software ImageJ® (http://rsbweb.nih.gov/ij/), applying a color-thresholding technique, as similarly described by (Mahmoud et al., 2019). The fresh leaf biomass was then oven-dried at 60 °C until a constant weight was reached, and the Leaf Dry Weight (g) was determined with a precision balance (1,000/0.001 g) to be combined in Eq. (5) for the Specific Leaves Area (SLA, cm^2g^{-1}) computation.

$$SLA = \frac{LA}{LDW} \tag{5}$$

2.2.4 3D simulation of Global Solar Radiation distribution in the APV system

The distribution of global solar radiation in the APV system was simulated in a 3D environment using the GroIMP modeling platform and its associated radiation model (Fig. 3A) (Hemmerling et al., 2008) The GroIMP configuration included an accurate 3D reconstruction of the analyzed APV, and calculations of the radiation intercepted by each object in the scene.

To replicate the layout and site characteristics of the Ravenna APV, the 3D scene in GroIMP was designed with a flat terrain represented by square tiles measuring one meter per side, evenly distributed across a 20x20 m^2 area (Fig. 3). The solar panels were modeled as rectangular surfaces measuring 3.2x3 m, positioned at a height of 2 m and inclined at 35° to their vertical axis. These panels were arranged in seamless rows, spaced 8 m apart, and oriented along the north-south axis.

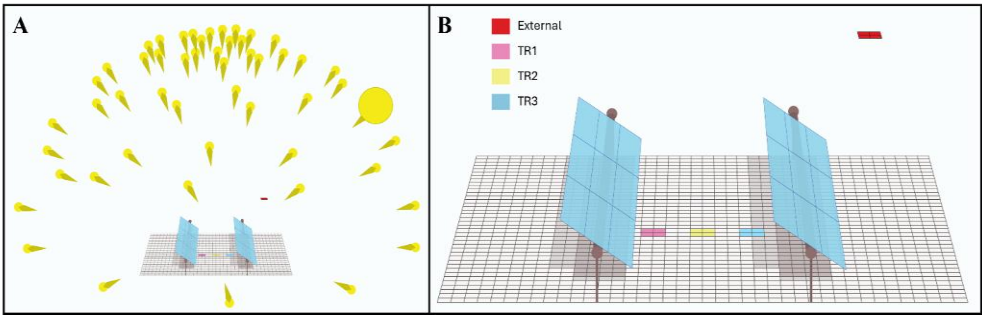

Figure 3. A) Graphical 3D representation of the Ravenna APV System created in GroIMP software. The figure highlights the ground system and the elements representing the sources (orange) of direct and diffuse radiative emission and the position of 72 light nodes in our sky model. **B)** Detailed representation of the position of experimental treatments TR1, TR2, TR3 and external control

The scene is completed by the dynamic simulation of direct and diffuse radiation, which is used to simulate total intercepted radiation by each object over the scene (i.e. solar panels and tiles) during the day. For such a purpose, the scene comprises two different light sources, **i**) a single dynamic light source that simulates the daily course of the sun that represents direct radiation and **ii**) an array of 72 static light sources that cover the hemisphere above the scene regularly positioned in six circles with 12 light sources each, to represent the emission sources of the diffuse radiation. The model, originally proposed in Zhu et al. (2018), was modified to dynamically simulate the partitioning between diffuse and direct radiation in the scene. Specifically, the model includes an initial pre-processing of data for calculating, on an hourly time-step, the elevation of the Sun above the local horizon according to latitude and day of the year (Goudriaan and Van Laar, 1994) to derive the instantaneous global extraterrestrial radiation (Wm^{-2}) (Eq. 6). The ratio between hourly observed ground global radiation (Wm^{-2}), as provided by an external file, and the relevant hourly global extraterrestrial radiation (i.e. Transmissivity, Tr, unitless) is then used as a proxy to calculate the diffuse fraction in global radiation according to (Boland et al., 2008) (Eq. 7). Finally, once calculated, the amount of direct and diffuse radiation hourly radiation (Wm^{-2}) is partitioned by the model, hour by hour to the relevant light sources and light distribution is finally computed by the GroIMP radiation model and integrated over surfaces, according to an inversed Monte Carlo path tracer.

$$GER = e * \sin\beta * (1 + 0.33 * \cos(2\pi * \frac{(t_d - 10)}{365})) \tag{6}$$

where GER is the global extraterrestrial radiation (Wm^{-2}), ε is the solar constant (1,370 Wm^{-2}), t_d is the days from 1st January, and β is the elevation of the sun above the horizon.

$$FDL = \frac{1}{1 + e^{(8.6*Tr-5)}} \tag{7}$$

where *FDL* is the fraction of diffuse radiation (unitless), and *Tr* is the transmissivity (unitless).

According to the distribution of treatments within the plant, hourly global radiation was cumulated over three tiles placed under the slope of the panels (TR1), in the central part between the 2 rows of panels (TR2), and the shaded area under the panels (TR3), respectively (Fig. 3B).

2.3. SSM-iCrop2 model integrated with local fAPAR data and global radiation

SSM-iCrop2 is a process-based model simulating at a daily timestep crop growth and yield of several species including sowing crops and perennial species (Soltani et al., 2020). The structure of the model enables a comprehensive characterization of the study area by incorporating as input data daily minimum $(Tmin)$ and maximum $(Tmax)$ temperatures, cumulative rainfall, and global radiation, and the specification of soil texture, which allows for the determination of the wilting point and field capacity. In its original version, the daily dry matter is simulated as the product between crop intercepted radiation (MJ) and radiation use efficiency (g MJ^{-1}), defined as the unit of biomass produced (g) per unit of intercepted radiation (MJ). Daily dry matter is then partitioned into vegetative and reproductive plant organs based on phenological phases estimated using thermal unit accumulation until a specific growth stage requirement is satisfied. Leaf Area Index (LAI, m^2 m^{-2}) is used to calculate the percentage of radiation intercepted by the canopy (fAPAR) according to Beer's law, where leaf area expansion is calculated as a function of the normalized temperature unit and the maximum expected LAI. A soil water balance module identifies whether the plant is under water stress during the season to derive reducing factors for radiation use efficiency and leaf area growth. The model accounts for positive inputs to the soil water balance, including rainfall and irrigation, as well as losses due to runoff, drainage, and evapotranspiration (ET, mm). For ET calculation, crop transpiration is estimated based on a fixed relationship between biomass production and crop transpiration, defined by the Transpiration Efficiency Coefficient (Pa) (Tanner and Sinclair, 1983). Soil evaporation (, mm) is calculated as the product of potential evapotranspiration (mm) and the fraction of radiation reaching the soil surface, which is adjusted to reflect its actual value based on the number of days since the last rainfall (Rivington, 2013). Accordingly, for a soil characterized by its water content availability (, i.e., the water included between field capacity and wilting point [m^3 m^{-3}]) and total transpirable soil water (mm) (i.e., water content × layer depth [mm]), SSM-iCrop2 tracks day by day the actual water content in the soil depth explored by roots (Actual Transpirable Soil Water, mm) by considering negative and positive water balance terms. The ratio between Actual Transpirable Soil Water and total transpirable soil water (i.e. the fraction of water available for transpiration, FTSW, unitless) is finally used as a reducing factor to rescale crop potential photosynthesis (i.e. radiation use efficiency) and leaf area expansion. For a more accurate description of the model, we recommend reading the original work in Soltani et al. (2020)

In this study, the original SSM-iCrop2 model was modified to integrate daily fAPAR data derived from 2D camera images and global radiation as simulated by GROIMP, enabling the simulation of spatial variability in alfalfa growth conditions within the APV system. Specifically, the fAPAR data were used to force the model by replacing the daily simulation of LAI for each of the three treatments (TR1, TR2, and TR3) in 2023 and 2024, as outlined in the experimental design. This forcing process influenced two key processes within the model: biomass accumulation, which relies on fAPAR to estimate the solar radiation available for photosynthesis, and soil evaporation, which depends on the radiation not intercepted by the canopy and reaching the ground.

Daily global radiation was calculated according to the radiation model of GROIMP considering the areas corresponding to the treatments TR1, TR2, and TR3. Specifically, within the area between two rows of photovoltaic panels simulated in the 3D environment, three tiles measuring 1 square meter each were selected: one placed immediately below the panel slope (TR1), one in the central part of the inter-row area (TR2), and one immediately below the apex of the photovoltaic panels (TR3). For each tile, hourly global radiation calculated by the radiation model was accumulated at a daily time step and used as input data to feed SSM-iCrop2 in 2023 and 2024. Considering that rainfall is intercepted by the photovoltaic panels and the collected water is directed to the area immediately below their slopes, TR1 rainfall data was adjusted to account for this additional water contribution. The adjustment was calculated in Eq. (8), as follows:

$$R_{adjusted} = Prec + (\mathrm{Prec} * A_{panel} * Efficiency) \tag{8}$$

where Prec represent the measured rainfall at the site (mm), A_{panel} is the effective collection area of the panels, calculated in Eq (9):

$$A_{panel} = 3.5m * 1m * \cos(35°) \approx 2.86m^2 \quad (9)$$

The efficiency represents the fraction of rainfall effectively collected and redirected to the ground below the panels, assumed to be 0.9. Tmin and Tmax were assumed to be uniform across the experimental site.

The original model parameters were kept unchanged with respect to the original ones except for radiation use efficiency that was calibrated in 2023 and decreased to 1.5 gMJ^{-1} from the original value 2.0 gMJ^{-1}.

3.2.4 Statistical analysis

The plant height, plant volume and vegetation indices extracted from 2D- and 3D-imagery were used in a multiple linear regression model to estimate fAPAR (Eq. 10). To ensure that the imaged plant characteristics corresponded to those observed during the collection of reference fAPAR measurements under solar zenith conditions, only features extracted from 2D images acquired at 13:00 P.M. were considered. Accordingly, the dataset for each 2D feature consisted of 635 data points for treatment, with one observation per day.

$$fAPAR = \beta_0 + \beta_1 X_1 + \beta_2 X_2 + \ldots + \beta_p X_p + \varepsilon \quad (10)$$

where $X_1, X_2, \ldots, X_p$ are the independent variables (i.e., selected 2D- or 3D-derived traits), β_0 is the intercept, $\beta_1, \beta_2, \ldots, \beta_p$ are the regression coefficients, and ε is the error term.

To define a subset of 2D and 3D image-derived traits that significantly contributed to fAPAR estimates as dependent variables in the relevant models, a multicollinearity analysis was first conducted. Highly collinear variables were thus excluded, keeping only the one most strongly correlated with the observed fAPAR.

Subsequently, a stepwise regression analysis was performed using both forward and backward selection methods, applying stringent criteria for variable inclusion ($p < 0.01$) and exclusion ($p > 0.05$) (StataCorp, 2021). This process identified the most significant predictors of fAPAR, resulting in the development of a final regression model. The model's performance was finally assessed against observed fAPAR using several statistical metrics, including the coefficient of determination (R^2, Eq. (11)), the Root Mean Square Error (RMSE, Eq. (12)), the Relative Root Mean Squared Error (rRMSE, Eq. (13)) and the Akaike Information Criterion (AIC, Eq. (14)).

$$R^2 = \frac{\sum_{i=1}^{n}(O_i - P_i)^2}{\sum_{i=1}^{n}(O_i - \bar{O})^2} \tag{11}$$

$$\text{RMSE} = \left[\sum_{i=1}^{n}\frac{(P_i - O_i)^2}{n}\right]^{0.5} \tag{12}$$

$$\text{rRMSE} = \frac{\left[\sum_{i=1}^{n}\frac{(P_i - O_i)^2}{n}\right]^{0.5}}{\bar{O}} * 100 \tag{13}$$

$$\text{AIC} = 2k - 2\ln(\hat{L}) \tag{14}$$

where O_i is the observed value-i, $\bar{O}$ is the average of the observed values, P_i is the simulated value-i, n is the number of observations, k is the number of estimated parameters in the model and $\hat{L}$ is the maximum value of the likelihood function in the model.

3.3 Results

3.3.1 Comparative performance of 2D and 3D imaging methods

The results of the comparative analysis between 2D- and 3D-derived models for fAPAR estimation in alfalfa are shown in Fig. 4. Limiting to the common treatments (i.e., TR1, TR2, and TR3), both models showed a strong correlation between observed and simulated fAPAR values (R^2 = 0.74 vs 0.73 for the 2D and 3D models, respectively) and similar performance in terms of AIC (AIC = -44.91 vs -47.41 for the 2D and 3D model, respectively), while the 2D model evidenced a lower relative root mean square error (rRMSE = 10.83%) compared to the 3D model (rRMSE = 13.19%). Furthermore, when TR4 is included in the analysis, 3D models' performance did not change significantly, as shown in Fig. 4.

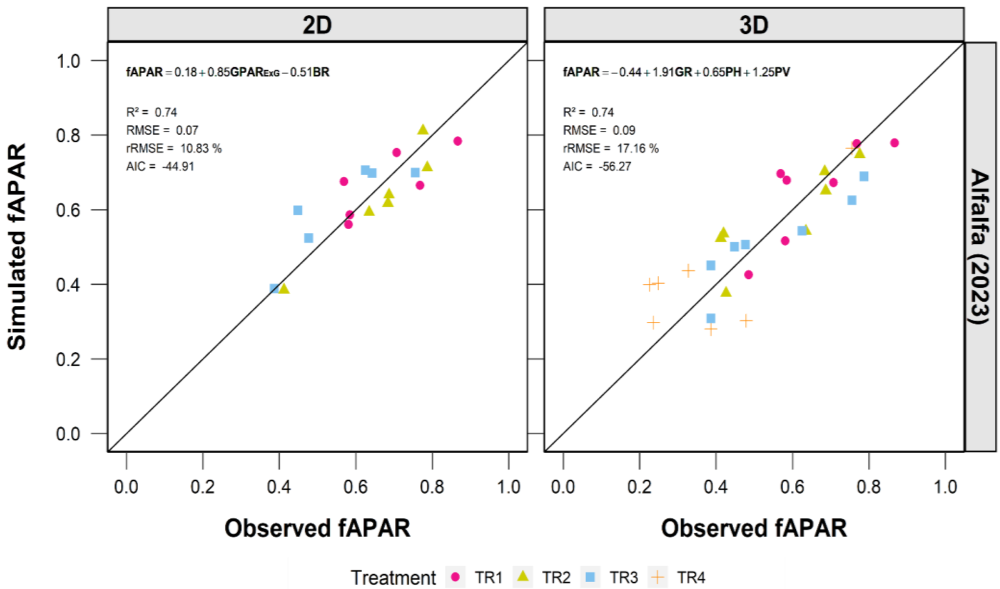

Figure 4. Comparison between observed and simulated alfalfa fraction of absorbed photosynthetically active radiation (fAPAR). The simulated values were modeled using the best predictors derived from 2D- (i.e., Greenness plant area ratio ($GPAR_{ExG}$) and Blue ratio (BR)) and 3D-imaging (i.e., Green ratio (GR), plant height (PH) and plant volume (PV)) for the defined treatments (TR1, TR2, TR3, and TR4) at the infield sampling dates of the 2023 growing season. The black line represents the 1:1 reference line.

3.2 fAPAR daily dynamic reconstruction

Considering that the performance of the 2D and 3D approaches is comparable, but that the 2D approach requires less post-processing and allowed for more continuous data acquisition throughout the season, the 2D-based model was selected for reproducing the daily dynamics of fAPAR in alfalfa meadow (Fig. 5A). The results show that a clear seasonal pattern in fAPAR dynamics exists across different treatments (TR1, TR2, and TR3), with noticeable fluctuations corresponding to management events, such as alfalfa mowing (indicated by red vertical lines).

In detail, during the 2023 season, fAPAR exhibited a marked decline across all treatments after the first mowing event at 160 DOY. Recovery after mowing varied, with TR3 (blue line) showing a faster and more pronounced rebound, reaching pre-mowing fAPAR levels in 39 fewer days compared to TR1. In contrast, TR2 (yellow line) displayed a slower and less complete recovery, lagging behind TR1 and TR3 by 37 DOY throughout the post-mowing period. After the second mowing event at 234 DOY, TR1 showed the fastest recovery, reaching pre-mowing fAPAR levels in approximately 40 days, followed by TR2 with a slightly lower rebound. TR3 shows the slowest and least complete recovery, with consistently lower fAPAR values than the other treatments until 285 DOY.

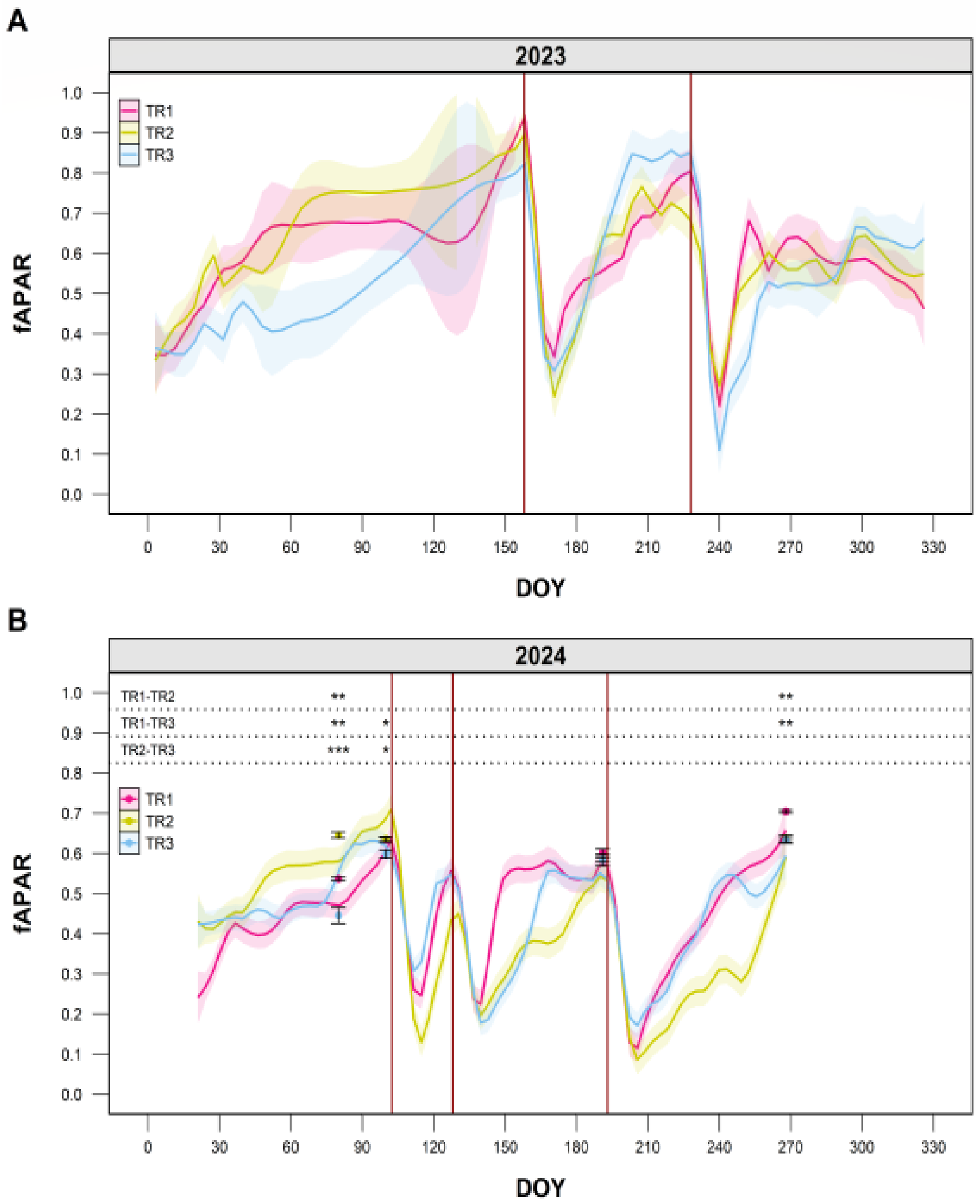

Figure 5. Application of the predictive allometric equations based on 2D-derived data (shown in Fig. 4) in reconstructing the alfalfa daily fAPAR trend throughout (A) 2023 and (B) 2024. The individual

data represents the average value of the 9 replicates and the locally weighted error smooth, while red vertical lines correspond to the alfalfa mowing dates. Each data point indicates the average fAPAR value from three field observations with an error bar (± standard error). Asterisks denote significant differences in observed fAPAR between treatment pairs according to the Tukey post-hoc test (*: $p \leq 0.05$; **: $p \leq 0.01$; ***: $p \leq 0.001$).

These patterns aligned with the observed SLA results (Fig. 6). SLA values were consistently higher in TR3 across all sampling days, particularly on 143 and 212 DOY, although without significant differences compared to TR1 and TR2. Starting from 284 DOY, a sharp decline in SLA was observed for all treatments, indicating a reduction in leaf area relative to dry biomass as the plants approached senescence.

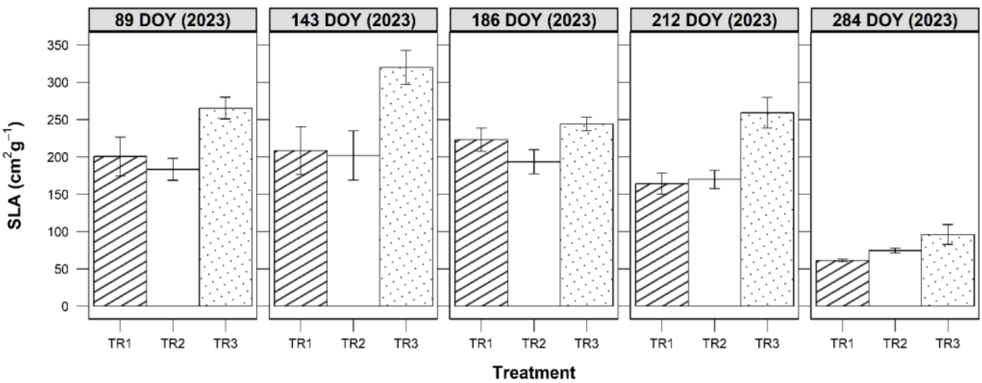

Figure 6. Evolution of Alfalfa Specific Leaf Area across the three ROIs (TR) oversampling dates (DOY) in 2023. Each bar represents the mean value from the replicates, with error bars indicating the standard error.

The set of colorimetric indices used for fAPAR estimation in 2023 (Fig. 4) was also adopted for fAPAR estimation in 2024 to validate the model performances. As shown in Fig. 5B, before the first mowing event at 180 DOY, fAPAR gradually increased across all treatments, with TR1 and TR2 closely aligned, while TR3 remained slightly lower. TR3 exhibited the fastest and most substantial rebound after the first mowing, surpassing the others and suggesting improved microclimatic conditions. TR1 showed a steady recovery, reaching intermediate values, while TR2 displayed the slowest and least complete recovery, consistently lagging behind TR1 and TR3. Following the second mowing, TR1 initially demonstrated the quickest and strongest recovery, regaining pre-mowing levels within 24 days, while TR2 showed a more delayed rebound, requiring 50 days. In contrast, TR3, which had the fastest recovery after the first mowing, experienced a slower response after the second mowing, requiring 32 days to return to pre-mowing levels. After the third mowing, TR1 and TR2 exhibited their longest recovery times, taking 55 and 60 days respectively, whereas TR3 maintained a more moderate recovery time of 36 days.

3.3.3 Yield daily dynamic simulation

The yield analysis for 2023 highlighted the high accuracy of the model forced by daily fAPAR estimation in simulating cumulative dry matter accumulation across different treatments and management practices (Fig. 7A and S3). TR1 consistently exhibited the highest total yield, reaching approximately 1,350 g m^{-2} (13,500 kg $ha^{-}1$) by the end of the season. This productivity is attributed to the greater soil moisture availability observed in TR1 throughout the growing season, as confirmed by the model simulation results (Fig. 8). TR1 maintained consistently higher Fraction of Transpirable Soil Water (FTSW) values, benefiting from localized water redistribution from photovoltaic panels. In contrast, TR2, which accumulated a total yield of approximately 1,150 g m^{-2} (11,500 kg $ha^{-}1$), exhibited a steeper decline in FTSW, indicating a lower capacity to retain soil moisture and a greater susceptibility to water stress. The rapid depletion of soil water in TR2 may have contributed to early growth limitations and lower biomass accumulation compared to TR1. Meanwhile, TR3, the least productive treatment, with a cumulative yield of approximately 700 g m^{-2} (7,000 kg $ha^{-}1$), displayed an intermediate FTSW pattern. The yield trends in 2024 followed a similar ranking among treatments but showed an overall reduction in biomass accumulation

(Fig. 7B and S3). TR1 remained the most productive, although its final yield reached only 950 g m^{-2}, approximately 20% lower than in 2023. The reduction in TR1's yield aligns with a less pronounced contrast in FTSW values among treatments, as the higher frequency of precipitation events in 2024 (160-240 DOY) contributed to a more balanced soil moisture distribution across the experimental plots. Consequently, while TR1 continued to benefit from localized water redistribution, the difference in water availability compared to TR2 and TR3 was less pronounced than in the previous year. TR2 and TR3 also exhibited lower yields in 2024, reaching approximately 700 g m^{-2} and 600 g m^{-2}, respectively.

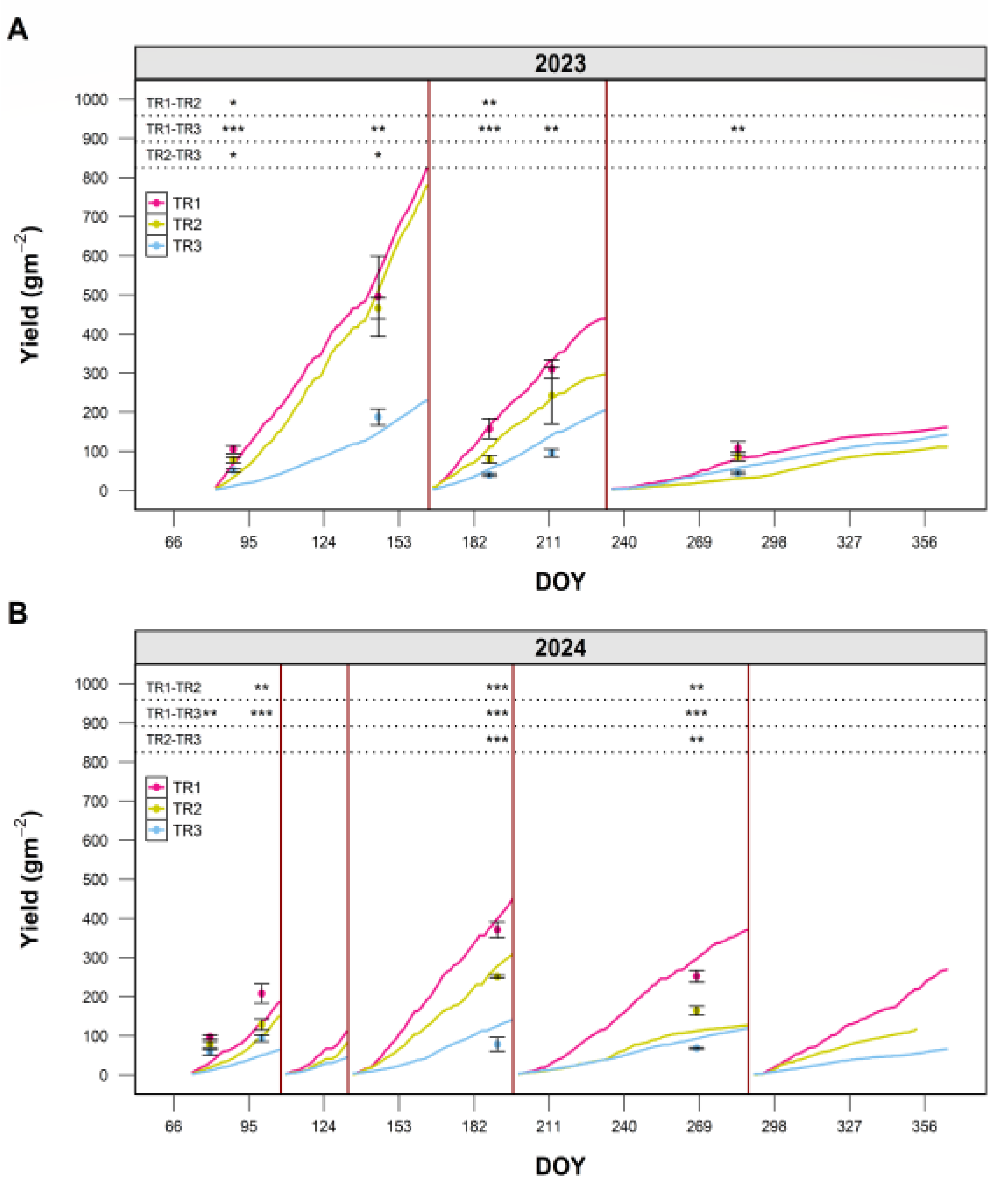

Figure 7. Daily yield progression of alfalfa throughout (A) 2023 and (B) 2024, reconstructed from the 2D image-derived fAPAR data. The red vertical lines correspond to the alfalfa mowing dates. Each data point indicates the average value of yield from three field observations with an error bar (± standard

error). Asterisks denote significant differences in observed yield between treatment pairs according to the Tukey post-hoc test (*: p ≤ 0.05; **: p ≤ 0.01; ***: p ≤ 0.001).

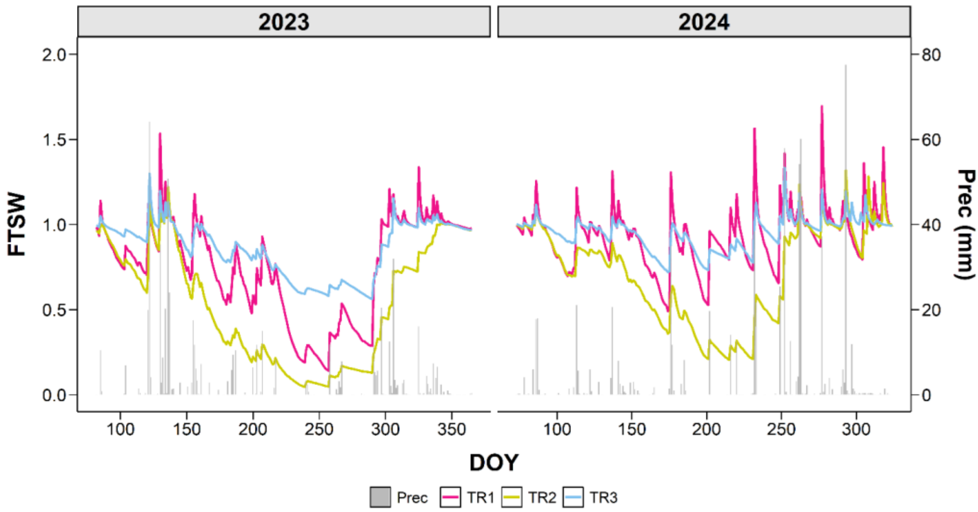

Figure 8. Seasonal trends of the Fraction of Transpirable Soil Water (FTSW) for three treatments (TR1, TR2, TR3) and precipitation (mm) during the years 2023 and 2024.

3.4 Discussion

Non-destructive, accurate and timely monitoring of crop performance within an Agrivoltaic (APV) system is essential for assessing its adaptability to variable shading conditions and ensuring compliance with current Italian regulations. In this study, the effectiveness of a crop model driven by image-derived proximal data was evaluated in capturing the daily growth dynamics of an alfalfa meadow cultivated in an APV environment. The proposed methodology relies on the calculation of specific RGB-based Vegetation Indices (VIs), originally developed to identify temporal and spatial patterns in vegetation phenology (Filippa et al., 2018). Over time, VIs were used as predictors to quantify more complex traits directly associated with plant adaptations to fluctuating external conditions, including fAPAR, leaf area development and biomass accumulation (Richardson et al., 2007, Aasen et al., 2020). This has made image-derived VIs valuable drivers when integrated with simulation models for local estimation of carbon and water fluxes in both natural ecosystems and cropping systems (Zaho et al. 2019; Ganeva et al., 2022; Hufkens et al., 2019).

The present approach addressed the challenge of accounting for complex morphological adaptations, typically induced by variable shading conditions, on a spatially reduced scale that may not be fully represented in traditional crop models. Field surveys confirmed that reduced light availability triggered an adaptive response in the most shaded plants (TR3; Fig. 5), prompting structural adjustments that allowed them to reach levels of intercepted radiation comparable to those observed in the more illuminated plots (TR1 and TR2; Fig. 5). This progressive fAPAR recovery was mediated by an increase in SLA (although not significant, Fig. 6) in TR3 compared to the other treatments, confirming its key role in plant adaptation to shade, as supported by previous studies. For instance, Potenza et al. (2022) reported a 9% increase in SLA for soybeans under a 27% reduction in solar radiation, while Juillion et al. (2023) observed a 22% increase in apple trees grown in APV conditions, where daily shading ranged from 4% to 88%. Similarly, Marrou et al. (2013) demonstrated that lettuce cultivated in an APV system under partial shade increased total leaf area per plant to enhance light capture efficiency. The use of crop simulation models stands out as a solution for consistently predicting the impact of changing exogenous conditions on key agronomic parameters, including yield (Chang et al., 2023; Tahler et al., 2024). However, while the dynamic SLA variations improve the accuracy in estimating state variables (e.g., LAI and biomass accumulation; Li et al. 2023), only a few models incorporate SLA as a sensitive parameter (Asseng et al., 2003; Zhang et al., 2020). This may limit crop model application in contexts such as APV, where the high spatial and temporal variability of environmental factors trigger changes in plants' phenotypic traits (Galleani D'agliano et al., 2024).

Here, the proposed methodology based on image-derived VIs was able to highlight the effect of shading on fAPAR, as a consequence of increased SLA thus reflecting the actual leaf area growth dynamics over two consecutive seasons. VIs derived from RGB images have already demonstrated their effectiveness in reproducing plant fAPAR, although the technical characteristics inherited to the available imaging solutions could influence their applicability in the field. The information provided by planar images, in fact, only offers a simplified representation of the scene, particularly when the increasing architectural complexity of plants, or their development in height, obstructs the capture of detailed data from beneath the observed surface (Rossi et al., 2022b; Nethala et al., 2024). This limitation can be bypassed through information on the three-dimensional structure of plants obtained from LiDAR. As an example, Luo et al. (2014) found that fAPAR of maize is strongly correlated to canopy fractional cover derived from LiDAR. In our experiment, the handheld LiDAR device enabled the measurement of plant morphometric traits , comprehensively representing the actual arrangement of individual organs in the 3D-space, which resulted in reliable predictors of fAPAR (Fig. 4). The integration of spectral data closely linked to chlorophyll content further enhanced the accuracy of the predictive model based solely on plant height and plant volume, highlighting the importance of combining LiDAR-derived morpho-colorimetric information to improve fAPAR prediction (Qin et al., 2018). However, despite being deployable to complex APV environments such as partially obstructed field areas (e.g., TR4), this approach faces limitations in routine, large-scale monitoring due to its high computational demands and scalability challenges (Martinez-Guanter et al., 2019).

The comparable performance of 2D imagery to 3D scanning, along with its cost-effectiveness, low post-processing requirements, and ability to provide high-temporal-resolution data, made this technique eligible as the most suitable for meadow monitoring in an APV environment. Indeed, for low-growing crops like alfalfa, the typical challenge of losing information from the lower canopy layers as the plants grow taller is minimized (Ge et al., 2016). This effectively avoids the need for more complex 3D reconstruction techniques, which instead are necessary to capture the vertical distribution of photosynthetic-related parameters in taller and more intricate plant structures (Gu et al., 2024). In this context, VIs derived from 2D-image sequences proved particularly effective for estimating fAPAR (Fig. 4), aligning with findings obtained for comparable agro-ecosystem such as cereals (Zhou et al., 2013) and grasslands (Wang et al., 2020). Specifically, the integration of BR index, known to be closely associated with chlorophyll content (De Swaef et al., 2021; Nakasagga et al., 2022), with an image-derived feature suited to quantifying the stay-green ability of the plant, such as the greenness plant area ratio , provided the best estimation accuracy by focusing solely on the portion of organs that are actively involved in the photosynthetic process (Guo et al., 2018). The exclusive use of VIS indices, rather than structural metrics, effectively mitigated perspective distortion problems commonly associated with 2D images, which arise due to the camera's position and viewing angle relative to the subject. However, this limitation could become more relevant in applications involving more complex crop architectures, where structural information is required to capture treatment-specific differences that may otherwise be obscured in conventional fixed-position 2D imagery. In such cases, monocular RGB-depth cameras, which simultaneously provide both color and depth data, may represent a suitable solution by enabling a more accurate spatial discrimination of plant morpho-colorimetric features based on their distance from the sensor, without the computational burden of full 3D reconstruction workflows (Yin et al., 2024).

The SSM-iCrop2 crop model, fed with the image-derived fAPAR and incoming radiation data, accurately reproduced the observed decrease in biomass accumulation along the analyzed transects during both 2023 and 2024 growing seasons. The observed recovery in fAPAR in TR3 was not in any case able to fully compensate for reduced cumulative radiation (average reduction of 84% compared to TR1 and TR2; Fig. S4), leading to a significant decrease in total biomass accumulation in TR3 compared to both TR1 (56% and 53% lower in 2023 and 2024, respectively) and TR2 (52% and 50% lower in 2023 and 2024, respectively). These results align with those of Qin et al. (2022) and Tang et al. (2022), who reported alfalfa biomass losses ranging from 30% to 60%, depending on the shading severity.

Despite the limited difference in global radiation and fAPAR (Fig. 5), the model correctly predicted the above-ground biomass trend in TR1 and TR2 treatments. In particular, the model simulates higher above-ground biomass in TR1 compared to TR2, where the localised water harvesting effect induced by the photovoltaic panels, resulted in higher water input to the soil. Indeed, the runoff redirection to TR1 (Fig. 8) supported plant growth during hot-dry periods (150-250 DOY in 2023 and 160-240 DOY in 2024; Fig. S5) by improving yield compared to TR2, that not benefiting from the same water supply, was characterized by a lower FTSW (Fig. 8), which limited biomass assimilation. This runoff effect has already been highlighted in similar works (e.g. Elamri et al., 2018b), where it is reported that photovoltaic panels significantly alter the redistribution of rainwater, with runoff that can reach up to 11 times natural levels, particularly at the edges of the panels, depending on the angle of inclination. Therefore, although no observed soil water content data were available to validate the simulated water dynamics, the good agreement between the observed and simulated biomass data (Fig.7) confirms the ability of a modelling approach, based on the relationship between biomass growth and crop water transpired, to reproduce the dynamics of the system.

Furthermore, in order to capture the interannual yield variability, the model took into account the effect of management (mowing) on biomass accumulation. As an example, in 2024, the higher frequency and amount of rainfall events from June to August (171mm) reduced water stress across the experimental plots with respect to 2023 (133mm); however, this did not translate into increased biomass production during the period, likely due to the more frequent mowing events occurred in 2024 than in 2023 (4 vs 2; Fig. 7). Such a revised strategy ensured a more even distribution of biomass over time, avoiding the growth peaks observed in 2023, but also restricting the maximum yield potential in 2024. In contrast, longer regrowth periods in 2023 led to more pronounced increases in biomass accumulation, although these were followed by more abrupt post-harvest declines, as similarly observed by Siri Prieto et al., (2017) for elephant grass (Pennisetum purpureum L.), giant reed (Arundo donax L.), and switchgrass (Panicum virgatum L.), where more frequent harvests resulted in reduced cumulative biomass.

Therefore, the proposed modeling approach, integrated with real-time data inputs, has proven to be an effective step toward optimizing APV system monitoring and management. By accounting for the complex interplay between shading and water availability, this approach offers a promising future in fine-tuning agricultural productivity.

Despite the fragmented nature of the proposed pipeline, each individual processing step is computationally light and fast to execute. This makes the approach suitable for operational contexts, provided that minimal automation is introduced. However, the validity of the proposed scheme, opens the possibility of implementing this pipeline on a single platform that would manage the remote camera image and weather data acquisition operations, the simulation of radiation and the subsequent biomass simulation in real time, overcoming the constraints imposed using unrelated tools. As an example. in this context, the suggested method could evolve to not only optimize mowing schedules but also provide broader insights into crop performance under varying environmental conditions, while addressing the trade-off between maximizing crop yield and energy. As APV continues to expand, these monitoring tools may become essential for decision-making, helping to adapt to maximizing the overall benefits of dual land-use systems.

3.5 Conclusions

This study represents a promising starting point for continuous, non-destructive biomass monitoring in Agro-Photovoltaic (APV) systems, in line with the Italian APV guidelines. It establishes an innovative proximal monitoring framework, offering a scalable approach to accurately track crop growth dynamics under variable environmental conditions. Initially, the comparison between the 2D and 3D models proposed in this study showed that 2D imaging, due to its satisfactory performance, cost-effectiveness, simplicity, and high temporal resolution, is suitable for routine monitoring of uniform and low-complex crop canopies. This approach was then used to derive daily fAPAR estimates and force SSM-iCrop2 crop growth model to improve the accuracy of alfalfa yield estimation. The model simulations effectively captured interannual variability in biomass accumulation, showing that differences in productivity between 2023 and 2024 were determined not only by total rainfall, but also by its temporal distribution and mowing management. The spatialization of model outputs, through a dynamic assimilation approach of proximal sensing data, aims at optimizing agronomic management in the context of specific microclimatic conditions. This step is preliminary, for example, at the identification of optimal mowing schedules and providing a practical decision-support tool for farmers to maximize productivity while maintaining system efficiency. Despite the promising results obtained in this study, future research should focus on the scalability and applicability of these integrated approaches in different agricultural contexts, leveraging machine learning algorithms to process real-time imaging data and predict crop performance under dynamic shading and water availability conditions. Emerging solutions such as fixed LiDAR cameras and RGB depth systems are being explored, offering the potential for automation and broader deployment in APV monitoring applications. Finally, exploring the physiological mechanisms underlying morphological adaptations, such as variations in SLA, could inform the design of AV systems optimized for specific crops and climates.

Funding

This research did not receive any specific grant from funding agencies in the public, commercial, or not-for-profit sectors.

CRediT authorship contribution statement

Michele Moretta: Conceptualization, Data curation, Methodology, Formal analysis, Investigation, Writing – original draft preparation. **Marco Moriondo:** Conceptualization, Investigation, Methodology, Formal analysis, Software, Writing – review & editing, Supervision**. Luisa Leolini:** Formal analysis, Methodology, Writing – review & editing. **Gloria Padovan:** Investigation, Writing – review & editing. **Nicolina Staglianò:**

Investigation. **Enrico Palchetti:** Project administration, Funding acquisition. **Giuseppe Mario Lanini:** Investigation. **Marco Bindi:** Conceptualization, Methodology, Supervision. **Riccardo Rossi:** Conceptualization, Data curation, Methodology, Formal analysis, Investigation, Software, Writing – review & editing.

Declaration of Competing Interest

The authors declare that they have no known competing financial.

Data Availability

Data will be made available on request.

Acknowledgements

The authors are grateful to Tozzi Green S.p.A. for providing the experimental site and co-funding the research.

References

Aasen, H., Kirchgessner, N., Walter, A., Liebisch, F., 2020. PhenoCams for field phenotyping: using very high temporal resolution digital repeated photography to investigate interactions of growth, phenology, and harvest traits. Frontiers in Plant Science, 11. https://doi.org/10.3389/fpls.2020.00593

Adeh, E.H., Selker, J.S., Higgins, C.W., 2018. Remarkable agrivoltaic influence on soil moisture, micrometeorology and water-use efficiency. PLoS One 13. https://doi.org/10.1371/journal.pone.0203256

Amaducci, S., Yin, X., Colauzzi, M., 2018. Agrivoltaic systems to optimise land use for electric energy production. Appl Energy 220, 545–561. https://doi.org/10.1016/j.apenergy.2018.03.081

Anderson, C.P., Carter, G.A., Funderburk, W.R., 2016. The use of aerial RGB imagery and LIDAR in comparing ecological habitats and geomorphic features on a natural versus man-made barrier island. Remote Sens (Basel) 8. https://doi.org/10.3390/rs8070602

Asseng, S., Turner, N.C., Botwright, T., Condon, A.G., 2003. Evaluating the impact of a trait for increased specific leaf area on wheat yields using a crop simulation model, in: Agronomy Journal. American Society of Agronomy, pp. 10–19. https://doi.org/10.2134/agronj2003.0010

Bebre, I., Marques, I., Annighöfer, P., 2022. Biomass Allocation and Leaf Morphology of Saplings Grown under Various Conditions of Light Availability and Competition Types. Plants 11. https://doi.org/10.3390/plants11030305

Bendig, J., Yu, K., Aasen, H., Bolten, A., Bennertz, S., Broscheit, J., Gnyp, M.L., Bareth, G., 2015. Combining UAV-based plant height from crop surface models, visible, and near infrared vegetation indices for biomass monitoring in barley. International Journal of Applied Earth Observation and Geoinformation 39, 79–87. https://doi.org/10.1016/J.JAG.2015.02.012

Boland, J., Ridley, B., Brown, B., 2008. Models of diffuse solar radiation. Renew Energy 33, 575–584. https://doi.org/10.1016/j.renene.2007.04.012

Campana, P.E., Stridh, B., Amaducci, S., Colauzzi, M., 2021. Optimisation of vertically mounted agrivoltaic systems. J Clean Prod 325. https://doi.org/10.1016/j.jclepro.2021.129091

Chang, Y., Latham, J., Licht, M., Wang, L., 2023. A data-driven crop model for maize yield prediction. Commun Biol 6. https://doi.org/10.1038/s42003-023-04833-y

Chen, Z., Gao, B., Devereux, B., 2017. State-of-the-art: DTM generation using airborne LIDAR data. Sensors (Switzerland). https://doi.org/10.3390/s17010150

Crommelinck, S., Höfle, B., 2016. Simulating an autonomously operating low-cost static terrestrial LiDAR for multitemporal maize crop height measurements. Remote Sens (Basel) 8. https://doi.org/10.3390/rs8030205

De Swaef, T., Maes, W.H., Aper, J., Baert, J., Cougnon, M., Reheul, D., Steppe, K., Roldán-Ruiz, I., Lootens, P., 2021. Applying RGB- and thermal-based vegetation indices from UAVs for high-throughput field phenotyping of drought tolerance in forage grasses. Remote Sensing, 13(1), p.147. https://doi.org/10.3390/rs13010147

Dinesh, H., Pearce, J.M., 2016. The potential of agrivoltaic systems. Renewable and Sustainable Energy Reviews. https://doi.org/10.1016/j.rser.2015.10.024

Duan, L., Han, J., Guo, Z., Tu, H., Yang, P., Zhang, D., Fan, Y., Chen, G., Xiong, L., Dai, M., Williams, K., Corke, F., Doonan, J.H., Yang, W., 2018a. Novel digital features discriminate between drought resistant and drought sensitive rice under controlled and field conditions. Front Plant Sci 9. https://doi.org/10.3389/fpls.2018.00492

Duan, L., Han, J., Guo, Z., Tu, H., Yang, P., Zhang, D., Fan, Y., Chen, G., Xiong, L., Dai, M., Williams, K., Corke, F., Doonan, J.H., Yang, W., 2018b. Novel digital features discriminate between drought resistant and drought sensitive rice under controlled and field conditions. Front Plant Sci 9. https://doi.org/10.3389/fpls.2018.00492

Elamri, Y., Cheviron, B., Lopez, J.M., Dejean, C., Belaud, G., 2018a. Water budget and crop modelling for agrivoltaic systems: Application to irrigated lettuces. Agric Water Manag 208, 440–453. https://doi.org/10.1016/j.agwat.2018.07.001

Elamri, Y., Cheviron, B., Mange, A., Dejean, C., Liron, F., & Belaud, G., 2018b. Rain concentration and sheltering effect of solar panels on cultivated plots. Hydrology and Earth System Sciences, 22(2), pp.1285–1298. https://doi.org/10.5194/hess-22-1285-2018.

Fattoruso, G., Toscano, D., Venturo, A., Scognamiglio, A., Fabricino, M., Di Francia, G., 2024. A Spatial Multicriteria Analysis for a Regional Assessment of Eligible Areas for Sustainable

Agrivoltaic Systems in Italy. Sustainability (Switzerland) 16. https://doi.org/10.3390/su16020911

Filippa, G., Cremonese, E., Migliavacca, M., Galvagno, M., Sonnentag, O., Humphreys, E., Hufkens, K., Ryu, Y., Verfaillie, J., Morra di Cella, U., Richardson, A.D., 2018. NDVI derived from near-infrared-enabled digital cameras: Applicability across different plant functional types. Agric For Meteorol 249, 275–285. https://doi.org/10.1016/j.agrformet.2017.11.003

Galleani D'agliano, A, 2024. Agrivoltaic Modeling: A Sector Overview. Thesis Report.

Ganeva, D., Roumenina, E., Dimitrov, P., Dragov, R., Bozhanova, V., Taneva, K., Gikov, A., Jelev, G., 2022. Phenotypic Traits Estimation and Preliminary Yield Assessment in Different Phenophases of Wheat Breeding Experiment Based on UAV Multispectral Images. Remote Sens (Basel) 14. https://doi.org/10.3390/rs14041019

Ge, Y., Pandey, P., Bai, G., 2016. Estimating fresh biomass of maize plants from their RGB images in greenhouse phenotyping, in: Autonomous Air and Ground Sensing Systems for Agricultural Optimization and Phenotyping. SPIE, p. 986605. https://doi.org/10.1117/12.2228790

Gilardelli, C., Confalonieri, R., Cappelli, G.A., Bellocchi, G., 2018. Sensitivity of WOFOST-based modelling solutions to crop parameters under climate change. Ecol Modell 368, 1–14. https://doi.org/10.1016/j.ecolmodel.2017.11.003

Gonocruz, R.A., Nakamura, R., Yoshino, K., Homma, M., Doi, T., Yoshida, Y., Tani, A., 2021. Analysis of the rice yield under an agrivoltaic system: A case study in Japan. Environments 8, 65. https://doi.org/10.3390/environments8070065

Goudriaan, J., Van Laar, H.H., 1994. Modelling Potential Crop Growth Processes, Current Issues in Production Ecology. Springer Netherlands, Dordrecht. https://doi.org/10.1007/978-94-011-0750-1

Gower, S.T., Kucharik, C.J., Norman, J.M., n.d. Direct and Indirect Estimation of Leaf Area Index, fAPAR , and Net Primary Production of Terrestrial Ecosystems Planet Earth (MTPE), a NASA-initiated program that uses space-, ground-, and aircraft-based measurement.

Graham, E.A., Riordan, E.C., Yuen, E.M., Estrin, D., Rundel, P.W., 2010. Public Internet-connected cameras used as a cross-continental ground-based plant phenology monitoring system. Glob Chang Biol 16, 3014–3023. https://doi.org/10.1111/j.1365-2486.2010.02164.x

Gu, Y., Wang, Y., Wu, Y., Warner, T.A., Guo, T., Ai, H., Zheng, H., Cheng, T., Zhu, Y., Cao, W., Yao, X., 2024. Novel 3D photosynthetic traits derived from the fusion of UAV LiDAR point cloud and multispectral imagery in wheat. Remote Sens Environ 311. https://doi.org/10.1016/j.rse.2024.114244

Guglielmini, A.C., Satorre, E.H., 2002. Shading effects on spatial growth and biomass partitioning of Cynodon dactylon. Weed Res 42, 123–134. https://doi.org/10.1046/j.1365-3180.2002.00268.x

Guijarro, M., Pajares, G., Riomoros, I., Herrera, P., Burgos-Artizzu, X., Ribeiro, A., 2011. Automatic segmentation of relevant textures in agricultural images. Comput Electron Agric 75, 75–83. https://doi.org/10.1016/j.compag.2010.09.013

Guo, T., Fang, Y., Cheng, T., Tian, Y., Zhu, Y., Chen, Q., Qiu, X., Yao, X., 2019. Detection of wheat height using optimized multi-scan mode of LiDAR during the entire growth stages. Comput Electron Agric 165. https://doi.org/10.1016/j.compag.2019.104959

Guo, Z., Yang, W., Chang, Y., Ma, X., Tu, H., Xiong, F., Jiang, N., Feng, H., Huang, C., Yang, P., Zhao, H., Chen, G., Liu, H., Luo, L., Hu, H., Liu, Q., Xiong, L., 2018. Genome-Wide Association Studies of Image Traits Reveal Genetic Architecture of Drought Resistance in Rice. Mol Plant 11, 789–805. https://doi.org/10.1016/j.molp.2018.03.018

Hague, T., Tillett, N.D., Wheeler, H., 2006. Automated crop and weed monitoring in widely spaced cereals. Precis Agric 7, 21–32. https://doi.org/10.1007/s11119-005-6787-1

Hemmerling, R., Kniemeyer, O., Lanwert, D., Kurth, W., Buck-Sorlin, G., 2008. The rule-based language XL and the modelling environment GroIMP illustrated with simulated tree competition. Functional Plant Biology 35, 739–750. https://doi.org/10.1071/FP08052

Hufkens, K., Melaas, E.K., Mann, M.L., Foster, T., Ceballos, F., Robles, M., Kramer, B., 2019. Monitoring crop phenology using a smartphone based near-surface remote sensing approach. Agric For Meteorol 265, 327–337. https://doi.org/10.1016/j.agrformet.2018.11.002

Jin, X., Liu, S., Baret, F., Hemerlé, M., Comar, A., 2017. Estimates of plant density of wheat crops at emergence from very low altitude UAV imagery. Remote Sens Environ 198, 105–114. https://doi.org/10.1016/J.RSE.2017.06.007

Jo, H., Asekova, S., Bayat, M.A., Ali, L., Song, J.T., Ha, Y.S., Hong, D.H., Lee, J.D., 2022. Comparison of Yield and Yield Components of Several Crops Grown under Agro-Photovoltaic System in Korea. Agriculture (Switzerland) 12. https://doi.org/10.3390/agriculture12050619

Juillion, P., Lopez Velasco, G., Fumey, D., Lesniak, V., Genard, M., Vercambre, G. (2022). Shading apple trees with an agrivoltaic system: Impact on water relations, leaf morphophysiological characteristics and yield determinants. Scientia Horticulturae, 306, 111434. https://doi.org/10.1016/j.scienta.2022.111434

Kataoka, T., Kaneko, T., Okamoto, H., Hata, S., 2003. Crop growth estimation system using machine vision. Proceedings of the 2003 IEEE/ASME International Conference on Advanced Intelligent Mechatronics (AIM 2003), Kobe, Japan, 2, pp.B1079–B1083. https://doi.org/10.1109/AIM.2003.1225492

Kurc, S.A., Benton, L.M., 2010. Digital image-derived greenness links deep soil moisture to carbon uptake in a creosotebush-dominated shrubland. J Arid Environ 74, 585–594. https://doi.org/10.1016/j.jaridenv.2009.10.003

Laveglia, S., Altieri, G., Genovese, F., Matera, A., Di Renzo, G.C., 2024. Advances in Sustainable Crop Management: Integrating Precision Agriculture and Proximal Sensing. AgriEngineering 6, 3084–3120. https://doi.org/10.3390/agriengineering6030177

Leolini, L., Bregaglio, S., Ginaldi, F., Costafreda-Aumedes, S., Di Gennaro, S.F., Matese, A., Maselli, F., Caruso, G., Palai, G., Bajocco, S., Bindi, M., Moriondo, M., 2023. Use of remote sensing-derived fPAR data in a grapevine simulation model for estimating vine biomass accumulation and yield variability at sub-field level. Precis Agric 24, 705–726. https://doi.org/10.1007/s11119-022-09970-8

Leolini, L., Moriondo, M., Rossi, R., Bellini, E., Brilli, L., López-bernal, Á., Santos, J.A., Fraga, H., Bindi, M., Dibari, C., Costafreda-aumedes, S., 2022. Use of Sentinel-2 Derived Vegetation Indices for Estimating fPAR in Olive Groves. Agronomy 12. https://doi.org/10.3390/agronomy12071540

Li, Z., Zhan, C., Hu, S., Ning, L., Wu, L., Guo, H., 2023. Implementation of a dynamic specific leaf area (SLA) into a land surface model (LSM) incorporated crop-growth model. Comput Electron Agric 213. https://doi.org/10.1016/j.compag.2023.108238

Liu, L., Peng, D., Hu, Y., Jiao, Q., 2013. A novel in Situ FPAR measurement method for low canopy vegetation based on a digital camera and reference panel. Remote Sens (Basel) 5, 274–281. https://doi.org/10.3390/rs5010274

Louhaichi, M., Borman, M.M., Johnson, D.E., 2001. Spatially located platform and aerial photography for documentation of grazing impacts on wheat. Geocarto Int 16, 65–70. https://doi.org/10.1080/10106040108542184

Luo, S., Wang, C., Xi, X., & Pan, F., 2014. Estimating FPAR of maize canopy using airborne discrete-return LiDAR data. Optics Express, 22, pp.5106–5117. https://doi.org/10.1364/OE.22.005106.

Ma, Q., Su, Y., Guo, Q., 2017. Comparison of Canopy Cover Estimations from Airborne LiDAR, Aerial Imagery, and Satellite Imagery. IEEE J Sel Top Appl Earth Obs Remote Sens 10, 4225–4236. https://doi.org/10.1109/JSTARS.2017.2711482

Mahmoud, M., Mohamed, A., Suliman, A., Puchkov, M., Loktionova, E., 2019. Digitization of Agriculture-Development Strategy.

Marrou, H., Dufour, L., Wery, J., 2013. How does a shelter of solar panels influence water flows in a soil-crop system? European Journal of Agronomy 50, 38–51. https://doi.org/10.1016/j.eja.2013.05.004

Martinez-Guanter, J., Ribeiro, Á., Peteinatos, G.G., Pérez-Ruiz, M., Gerhards, R., Bengochea-Guevara, J.M., Machleb, J., Andújar, D., 2019. Low-cost three-dimensional modeling of crop plants. Sensors (Switzerland) 19. https://doi.org/10.3390/s19132883

Mengi, E., Samara, O.A., Zohdi, T.I., 2023. Crop-driven optimization of agrivoltaics using a digital-replica framework. Smart Agricultural Technology 4. https://doi.org/10.1016/j.atech.2022.100168

Meyer, G., Camargo Neto, J., Jones, D., Hindman, T., 2004. Intensified fuzzy clusters for classifying plant, soil, and residue regions of interest from color images. Comput Electron Agric 42, 161–180. https://doi.org/10.1016/j.compag.2003.08.002

Meyer, G.E., Hindman, T.W., Laksmi, K., 1999. Machine vision detection parameters for plant species identification. Precision Agriculture and Biological Quality, 3543, pp.327–335. https://doi.org/10.1117/12.336896

Meyer, G.E., Neto, J.C., 2008. Verification of color vegetation indices for automated crop imaging applications. Comput Electron Agric 63, 282–293. https://doi.org/10.1016/j.compag.2008.03.009

Migliavacca, M., Galvagno, M., Cremonese, E., Rossini, M., Meroni, M., Sonnentag, O., Cogliati, S., Manca, G., Diotri, F., Busetto, L., Cescatti, A., Colombo, R., Fava, F., Morra di Cella, U., Pari, E., Siniscalco, C., Richardson, A.D., 2011. Using digital repeat photography and eddy covariance data to model grassland phenology and photosynthetic CO2 uptake. Agric For Meteorol 151, 1325–1337. https://doi.org/10.1016/j.agrformet.2011.05.012

Mohammedi, S., Dragonetti, G., Admane, N., Fouial, A., 2023. The Impact of Agrivoltaic Systems on Tomato Crop: A Case Study in Southern Italy. Processes 11. https://doi.org/10.3390/pr11123370

Muller, S.J., Sithole, P., Singels, A., Van Niekerk, A., 2020. Assessing the fidelity of Landsat-based fAPAR models in two diverse sugarcane growing regions. Comput Electron Agric 170. https://doi.org/10.1016/j.compag.2020.105248

Nakasagga, S., Adak, A., Murray, S.C., Rooney, W.L., Hoffmann, L., Wilde, S., Lindsey, R., Nabukalu, P., Cox, S., 2022. Prediction of regrowth and biomass of perennial sorghum using unoccupied aerial systems. Crop Science, 62, pp.2107–2121. https://doi.org/10.1002/csc2.20758

Nethala, P., Um, D., Vemula, N., Montero, O.F., Lee, K., Bhandari, M., 2024. Techniques for Canopy to Organ Level Plant Feature Extraction via Remote and Proximal Sensing: A Survey and Experiments. Remote Sens (Basel). https://doi.org/10.3390/rs16234370

Parmentier, F.J.W., Nilsen, L., Tømmervik, H., Cooper, E.J., 2021. A distributed time-lapse camera network to track vegetation phenology with high temporal detail and at varying scales. Earth Syst Sci Data 13, 3593–3606. https://doi.org/10.5194/essd-13-3593-2021

Potenza, E., Croci, M., Colauzzi, M., Amaducci, S., 2022. Agrivoltaic System and Modelling Simulation: A Case Study of Soybean (Glycine max L.) in Italy. Horticulturae 8. https://doi.org/10.3390/horticulturae8121160

Qin, F., Shen, Y., Li, Z., Qu, H., Feng, J., Kong, L., Teri, G., Luan, H., Cao, Z., 2022. Shade Delayed Flowering Phenology and Decreased Reproductive Growth of Medicago sativa L. Front Plant Sci 13. https://doi.org/10.3389/fpls.2022.835380

Qin, H., Wang, C., Zhao, K., Xi, X., 2018. Estimation of the fraction of absorbed photosynthetically active radiation (fPAR) in maize canopies using LiDAR data and hyperspectral imagery. PLoS One 13. https://doi.org/10.1371/journal.pone.0197510

Ramos-Fuentes, I.A., Elamri, Y., Cheviron, B., Dejean, C., Belaud, G., Fumey, D., 2023. Effects of shade and deficit irrigation on maize growth and development in fixed and dynamic AgriVoltaic systems. Agric Water Manag 280. https://doi.org/10.1016/j.agwat.2023.108187

Richardson, A.D., Braswell, B.H., Hollinger, D.Y., Jenkins, J.P., Ollinger, S. V., 2009. Near-surface remote sensing of spatial and temporal variation in canopy phenology. Ecological Applications 19, 1417–1428. https://doi.org/10.1890/08-2022.1

Richardson, A.D., Jenkins, J.P., Braswell, B.H., Hollinger, D.Y., Ollinger, S. V., Smith, M.L., 2007. Use of digital webcam images to track spring green-up in a deciduous broadleaf forest. Oecologia 152, 323–334. https://doi.org/10.1007/s00442-006-0657-z

Riehle, D., Reiser, D., Griepentrog, H.W., 2020. Robust index-based semantic plant/background segmentation for RGB images. Computers and Electronics in Agriculture, 169, 105201. https://doi.org/10.1016/j.compag.2019.105201.

Rivington, M., 2013. Modelling Physiology of Crop Development, Growth and Yield. By A. Soltani and T. R. Sinclair. Wallingford, UK: CABI (2012), pp. 322, £95.95. ISBN 978-1-84593-970-0. Exp Agric 49, 157–157. https://doi.org/10.1017/s0014479712000774

Rossi, R., Costafreda-Aumedes, S., Leolini, L., Leolini, C., Bindi, M., Moriondo, M., 2022a. Implementation of an algorithm for automated phenotyping through plant 3D-modeling: A practical application on the early detection of water stress. Comput Electron Agric 197. https://doi.org/10.1016/j.compag.2022.106937

Rossi, R., Costafreda-Aumedes, S., Summerer, S., Moriondo, M., Leolini, L., Cellini, F., Bindi, M., Petrozza, A., 2022b. A comparison of high-throughput imaging methods for quantifying plant growth traits and estimating above-ground biomass accumulation. European Journal of Agronomy 141. https://doi.org/10.1016/j.eja.2022.126634

Roussel, J.R., Auty, D., Coops, N.C., Tompalski, P., Goodbody, T.R.H., Meador, A.S., Bourdon, J.F., de Boissieu, F., Achim, A., 2020. lidR: An R package for analysis of Airborne Laser Scanning (ALS) data. Remote Sens Environ. https://doi.org/10.1016/j.rse.2020.112061

Scarano, A., Semeraro, T., Calisi, A., Aretano, R., Rotolo, C., Lenucci, M.S., Santino, A., Piro, G., De Caroli, M., 2024. Effects of the Agrivoltaic System on Crop Production: The Case of Tomato (Solanum lycopersicum L.). Applied Sciences (Switzerland) 14. https://doi.org/10.3390/app14073095

Shanmugam, M., Asokan, R., 2015. A machine-vision-based real-time sensor system to control weeds in agricultural fields. Sens Lett 13, 489–495. https://doi.org/10.1166/sl.2015.3495

Sinclair, T.R., Tanner, C.B., Bennett, J.M., 1984. Water-Use Efficiency in Crop Production.

Siri Prieto, G., Ernst, O., Bustamante, M., 2017. Impact of Harvest Frequency on Biomass Yield and Nutrient Removal of Elephantgrass, Giant Reed, and Switchgrass. Bioenergy Res 10, 853–863. https://doi.org/10.1007/s12155-017-9847-2

Soltani, A., Alimagham, S.M., Nehbandani, A., Torabi, B., Zeinali, E., Dadrasi, A., Zand, E., Ghassemi, S., Pourshirazi, S., Alasti, O., Hosseini, R.S., Zahed, M., Arabameri, R., Mohammadzadeh, Z., Rahban, S., Kamari, H., Fayazi, H., Mohammadi, S., Keramat, S., Vadez, V., van Ittersum, M.K., Sinclair, T.R., 2020. SSM-iCrop2: A simple model for diverse crop species over large areas. Agric Syst 182. https://doi.org/10.1016/j.agsy.2020.102855

Sonnentag, O., Hufkens, K., Teshera-Sterne, C., Young, A.M., Friedl, M., Braswell, B.H., Milliman, T., O'Keefe, J., Richardson, A.D., 2012. Digital repeat photography for phenological research in forest ecosystems. Agric For Meteorol 152, 159–177. https://doi.org/10.1016/j.agrformet.2011.09.009

Soontranon, N., Srestasathiern, P., Rakwatin, P., 2014. Rice growing stage monitoring in small-scale region using ExG vegetation index, in: 2014 11th International Conference on Electrical Engineering/Electronics, Computer, Telecommunications and Information Technology, ECTI-CON 2014. IEEE Computer Society. https://doi.org/10.1109/ECTICon.2014.6839830

Tang, Z., Parajuli, A., Chen, C.J., Hu, Y., Revolinski, S., Medina, C.A., Lin, S., Zhang, Z., Yu, L.X., 2021. Validation of UAV-based alfalfa biomass predictability using photogrammetry with fully automatic plot segmentation. Sci Rep 11. https://doi.org/10.1038/s41598-021-82797-x

Tanner, C.B., Sinclair, T.R., 1983. Efficient water use in crop production: Research or re-search?, in: Limitations to Efficient Water Use in Crop Production. wiley, pp. 1–27. https://doi.org/10.2134/1983.limitationstoefficientwateruse.c1

Thaler, S., Berger, K., Eitzinger, J., Mahnaz, A., Shala-Mayrhofer, V., Zamini, S., Weihs, P., 2024. Radiation Limits the Yield Potential of Main Crops Under Selected Agrivoltaic Designs—A Case Study of a New Shading Simulation Method. Agronomy 14. https://doi.org/10.3390/agronomy14112511

Touil, S., Richa, A., Fizir, M., Bingwa, B., 2021. Shading effect of photovoltaic panels on horticulture crops production: a mini review. Rev Environ Sci Biotechnol. https://doi.org/10.1007/s11157-021-09572-2

Treccani, D., Adami, A., Fregonese, L., 2024. Assessing the effectiveness of LiDAR-based apps on Apple devices to survey indoor and outdoor medium sized areas. The International Archives of the Photogrammetry, Remote Sensing and Spatial Information Sciences XLVIII-2/W8-2024, 431–438. https://doi.org/10.5194/isprs-archives-XLVIII-2-W8-2024-431-2024

Trommsdorff, M., Dhal, I.S., Özdemir, Ö.E., Ketzer, D., Weinberger, N., Rösch, C., 2022. Agrivoltaics: Solar power generation and food production, in: Solar Energy Advancements in Agriculture and Food Production Systems. Elsevier, pp. 159–210. https://doi.org/10.1016/B978-0-323-89866-9.00012-2

Tucker, C.J., 1979. Red and photographic infrared linear combinations for monitoring vegetation. Remote Sens Environ 8, 127–150. https://doi.org/10.1016/0034-4257(79)90013-0

Wang, H., Jia, G., Epstein, H. E., Zhao, H., & Zhang, A. (2020). Integrating a PhenoCam-derived vegetation index into a light use efficiency model to estimate daily gross primary production in a semi-arid grassland. Agricultural and Forest Meteorology, 288, 107983.

Wang, Y., Fang, H., 2020. Estimation of LAI with the LiDAR technology: A review. Remote Sens (Basel). https://doi.org/10.3390/rs12203457

Weselek, A., Bauerle, A., Zikeli, S., Lewandowski, I., Högy, P., 2021. Effects on crop development, yields and chemical composition of celeriac (Apium graveolens L. var. rapaceum) cultivated underneath an agrivoltaic system. Agronomy 11. https://doi.org/10.3390/agronomy11040733

Weselek, A., Ehmann, A., Zikeli, S., Lewandowski, I., Schindele, S., Högy, P., 2019. Agrophotovoltaic systems: applications, challenges, and opportunities. A review. Agron Sustain Dev. https://doi.org/10.1007/s13593-019-0581-3

Westergaard-Nielsen, A., Lund, M., Hansen, B.U., Tamstorf, M.P., 2013. Camera derived vegetation greenness index as proxy for gross primary production in a low Arctic wetland area. ISPRS Journal of Photogrammetry and Remote Sensing 86, 89–99. https://doi.org/10.1016/j.isprsjprs.2013.09.006

Woebbecke, D.M., Meyer, G.E., Von Bargen, K., Mortensen, D.A., 1995a. Color indices for weed identification under various soil, residue, and lighting conditions. Trans. Am. Soc. Agric. Eng. https://doi.org/10.13031/2013.27838.

Woebbecke, D.M., Meyer, G.E., Von Bargen, K., Mortensen, D.A., 1995b. Shape features for identifying young weeds using image analysis. Transactions of the ASABE, 38, 271–281.

Yang, M., Cho, S.I., 2021. High-resolution 3d crop reconstruction and automatic analysis of phenotyping index using machine learning. Agriculture (Switzerland) 11. https://doi.org/10.3390/agriculture11101010

Zahrawi, A.A., Aly, A.M., 2024. A Review of Agrivoltaic Systems: Addressing Challenges and Enhancing Sustainability. Sustainability (Switzerland). https://doi.org/10.3390/su16188271

Zhang, W., Qi, J., Wan, P., Wang, H., Xie, D., Wang, X., Yan, G., 2016. An easy-to-use airborne LiDAR data filtering method based on cloth simulation. Remote Sens (Basel) 8. https://doi.org/10.3390/rs8060501

Zhang, Z., Barlage, M., Chen, F., Li, Y., Helgason, W., Xu, X., Liu, X., Li, Z., 2020. Joint Modeling of Crop and Irrigation in the central United States Using the Noah-MP Land Surface Model. J Adv Model Earth Syst 12. https://doi.org/10.1029/2020MS002159

Zhou, L., He, H. L., Sun, X. M., Zhang, L., Yu, G. R., Ren, X. L., ... & Zhao, F. H. (2013). Modeling winter wheat phenology and carbon dioxide fluxes at the ecosystem scale based on digital photography and eddy covariance data. Ecological informatics, 18, 69-78.

Zhou, X., Zheng, H.B., Xu, X.Q., He, J.Y., Ge, X.K., Yao, X., Cheng, T., Zhu, Y., Cao, W.X., Tian, Y.C., 2017. Predicting grain yield in rice using multi-temporal vegetation indices from UAV-based multispectral and digital imagery. ISPRS Journal of Photogrammetry and Remote Sensing 130, 246–255. https://doi.org/10.1016/J.ISPRSJPRS.2017.05.003

Zhu, J., Dai, Z., Vivin, P., Gambetta, G.A., Henke, M., Peccoux, A., Ollat, N., Delrot, S., 2018. A 3-D functional-structural grapevine model that couples the dynamics of water transport with leaf gas exchange. Ann Bot 121, 833–848. https://doi.org/10.1093/aob/mcx141

.

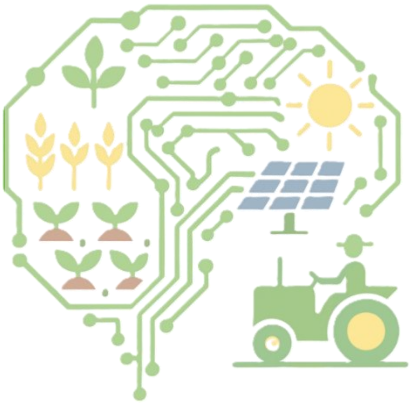

Chapter 4.

Integrated Modelling of Shading Effects on Alfalfa Growth Across Different Agrivoltaic Systems.

Chapter 4. has been based on the study:

Moretta, M., Moriondo, M., Rossi, R., Carvalho, G. M. de C. P., Padovan, G., Dal Prà, A., Palchetti, E., Argenti, G., Staglianò, N., Balingit, A. R., & Leolini, L. (2025). *Integrated modelling of shading effects on alfalfa growth across different agrivoltaic systems*. *Frontiers in Agronomy, 7,1699126.*
https://doi.org/10.3389/fagro.2025.1699126

Integrated Modelling of Shading Effects on Alfalfa Growth Across Different Agrivoltaic Systems

Michele Moretta [1], Marco Moriondo [1,2], Riccardo Rossi [1*], Gabriel Marçal da Cunha Pereira Carvalho [2], Gloria Padovan [1], Aldo Dal Prà [2], Enrico Palchetti [1], Giovanni Argenti [1], Nicolina Staglianò [1], Anna Rita Balingit [1] and Luisa Leolini [1]

[1] Department of Agriculture, Food, Environment and Forestry (DAGRI), University of Florence, Piazzale delle Cascine 18, 50144, Florence, Italy

[2] Institute of BioEconomy of the National Research Council (CNR-IBE), via Madonna del Piano 10, 50019, Sesto Fiorentino, Italy

Keywords: Agrivoltaic System; Alfalfa; GroIMP; Light Interception Modeling; Process-based Crop Model

Abstract

Agrivoltaic systems (AVS) combine agricultural production with solar energy generation on the same land. However, the spatiotemporal variability in light availability caused by panel shading presents a critical challenge for accurately predicting impacts on crop growth and yield. This study introduces a novel modeling framework that integrates a three-dimensional radiative transfer model with a process-based crop growth model, implemented in the GroIMP platform, to simulate the performance of alfalfa (*Medicago sativa* L.) under contrasting AVS conditions. The model accounts for dynamic light interception, canopy temperature variation, and soil water availability. Field experiments were conducted in

northern and central Italy under three conditions: open field (Site A), fixed-panel AVS (Site B), and bi-axial tracking AVS (Site C). At each site, the model was calibrated and validated using field data on leaf area index (LAI) ($R^2 \geq 0.79$, RMSE ≤ 48.61), dry matter yield ($R^2 \geq 0.82$, RMSE ≤ 48.6 g m^{-2}) and canopy temperature ($R^2 = 0.83$, RMSE = 1.24 °C), demonstrating strong agreement with observations. The validated model enabled a detailed assessment of how different panel configurations influence microclimatic conditions, which in turn significantly affected alfalfa growth and biomass production. From this perspective, simulations revealed pronounced spatial gradients driven by shading intensity, system layout, and seasonal dynamics, emphasizing the critical role of AVS design in determining crop performance. In particular, yield differences among treatments reflected microclimatic modifications induced by the panels, with shading and rainfall redistribution likely affecting canopy temperature, soil moisture dynamics, and associated plant water relations. The proposed integrated modeling framework thus provides a robust and scalable tool for AVS design and management, supporting both agronomic planning and the optimization of structural configurations tailored to site-specific climatic conditions. By doing so, it may effectively contribute to the development of more adaptive, efficient, and sustainable agri-energy systems capable of balancing agricultural productivity with renewable energy generation.

Graphical Abstract

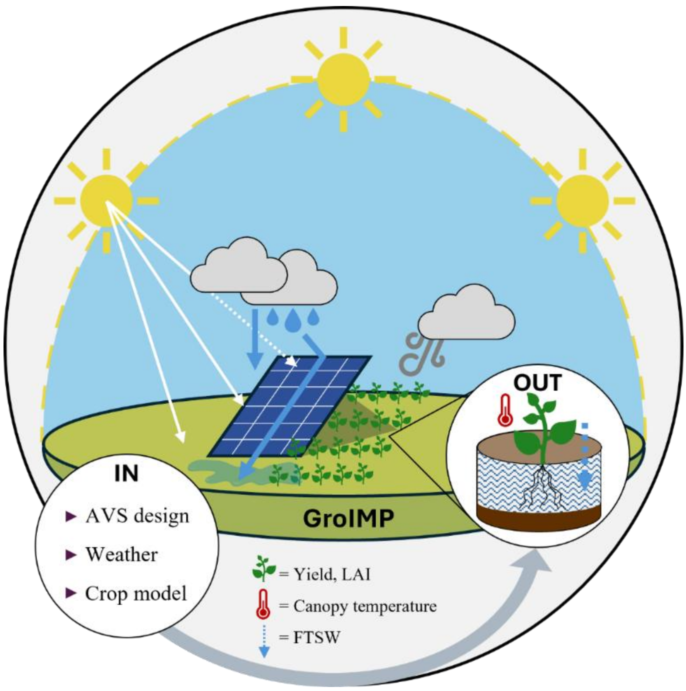

Nomenclature

Acronym	Full Name	Unit of Measurement
ASEV	Actual Soil Evaporation	mm [1]
ATR	Actual Transpiration	mm
AVS	Agrivoltaic Systems	–
B_{crop}	Biomass Crop	g m^{-2} or t ha^{-1}
C_{bio}	Carbon Fraction in Biomass	g C g^{-1} DM
C_c	Chloroplast CO_2 Concentration	µmol mol^{-1}

CF	Cover Factor	Unitless
c_p	Specific Heat of Air	J $K^{-1}m^{-3}$
EPIC	Environmental Policy Integrated Climate model	–
ET	Evapotranspiration	mm
FDL	Fraction of Diffuse Light	Unitless
fPAR	Fraction of Photosynthetically Active Radiation	Unitless
FTSW	Fraction of Transpirable Soil Water	Unitless
G	Soil Heat Flux	W m^{-2}
GER	Global Extraterrestrial Radiation	W m^{-2}
GR	Global Radiation	W m^{-2}
Jmax	Maximum Electron Transport Rate	µmol m^{-2} s^{-1}
K_c	Crop Coefficient	Unitless
MBE	Mean Bias Error	same as variable compared (e.g., g m^{-2} or m^2 m^{-2})
PAR	Photosynthetically Active Radiation	µmol m^{-2} s^{-1}
PC	Partitioning Coefficient	Unitless
PET	Potential Evapotranspiration	mm d^{-1}
PP	Photoperiod	h
PV	Photovoltaic	–
RH	Relative Humidity	%
RMSE	Root Mean Square Error	same as variable compared
Rn	Net Radiation	W m^{-2}

r_s / r_a	Surface / Aerodynamic Resistance	s m^{-1}
RSR	Reduced Solar Radiation	%
RUE	Radiation Use Efficiency	g MJ^{-1}
SENrate	Senescence Rate	m^2 m^{-2}
SF	Stage Factor	Unitless
ShF	Shadow Factor	Unitless
SLA	Specific Leaf Area	m^2 g^{-1}
STICS	Simulateur mulTIdisciplinaire pour les Cultures Standard	–
Ta	Air Temperature	°C
TF	Temperature Factor	Unitless
Tr	Transmissivity	Unitless
VPD	Vapor Pressure Deficit	kPa
WEF	Water–Energy–Food nexus	–
WS	Wind Speed	m s^{-1}
WSF	Water Stress Factor	Unitless
γ	Psychrometric Constant	kPa $°C^{-1}$
Γ^*	CO_2 Compensation Point	µmol mol^{-1}
ΔT	Canopy Temperature minus Air Temperature	°C
ρ_a	Air Density	kg m^{-3}
Φ_2LL	Electron Transport Efficiency of Photosystem II under Limiting Light	mol mol^{-1}

4.1 Introduction

Agrivoltaic systems (AVS) are increasingly recognized as a promising solution to address the interlinked challenges of the Water–Energy–Food (WEF) nexus by integrating agricultural production with renewable energy generation on the same land area (Barron-Gafford et al., 2019). However, this dual-use approach inherently entails trade-offs between crop performance and solar energy capture, making it essential to optimize system design for both efficiency and long-term sustainability. At the same time, the electricity generated by AVS systems can directly power on-farm operations such as irrigation, cooling, or processing, or be exported to the grid, thereby reducing greenhouse gas emissions and creating an additional source of income that reinforces the overall sustainability of the system (Agostini et al., 2021). A key aspect of this optimization lies in understanding how the partial or complete shading induced by photovoltaic (PV) panels alters microenvironmental conditions, particularly light availability, temperature regimes, and soil moisture dynamics, which in turn can significantly affect crop growth and development (Marrou et al., 2013; Ma et al., 2022).

Assessing the complex interactions between AVS components and the physiological drivers of plant response under variable shading is therefore critical to evaluating overall system performance (Choi et al., 2023). Reduced solar radiation has been identified as the primary constraint to crop productivity in AVS (Marrou et al., 2013), leading countries to establish regulatory limits on Ground Coverage Ratios (e.g., Italy, with a 40% GCR limit; Dupraz, 2024). Consequently, ongoing research is increasingly focused on quantifying the heterogeneous impacts of AVS, which depend on the interaction between species-specific sensitivity to shading and the growing season. As outlined by the meta-analysis in Laub et al. (2022), the response of different cultivated species to increasing shading is non-linear. While most crops analyzed (berries, fruits, fruiting vegetables, and forages) tolerate moderate shading, maize and grain legumes exhibit a strong yield reduction even under low shading conditions. In any case, for shading greater than 50%, all the crops proved to be susceptible. However, seasonal variability and management practices also strongly interact with a crop's response to shading. As an example, a two-year field trial on alfalfa recorded a season-by-season effect of moderate shading (25-30%) from PV panels on biomass production where shading proved particularly beneficial during drought periods resulting in increased biomass accumulation (+10%) with respect to full sunlight (Edouard et al., 2023). Wheat, considered a species sensitive to decreased radiation, exhibits different responses not only between varieties but also in response to the prevailing climatic conditions. Laub et al. (2022) observed that in subtropical environments, wheat-maintained yields comparable to open field conditions under low shading, 30% reduced solar radiation (RSR) level, while higher levels of shading resulted in an average yield reduction of 36.2%. Conversely, in temperate regions experiencing low shading levels, a decline in yield of 17.4% and 45.2% was observed under shading conditions exceeding 30% RSR level. These findings emphasize the climate-dependent plasticity of crop responses to shading.

Although existing studies highlight both the opportunities and challenges of AVS deployment, they also expose a major knowledge gap: current evidence remains largely crop- and context-specific, which limits the transferability of results across environmental and agronomic conditions (Laub et al., 2022; Marrou et al., 2013; Amaducci et al., 2018). The strong species-specific responses to shading, combined with the spatio-temporal variability of microclimates induced by photovoltaic structures, underscore the need for systematic data collection across diverse climates and AVS configurations. Yet, the labor and time-intensive nature of field campaigns constrain large-scale evaluations, positioning modelling frameworks as a powerful alternative for assessing AVS impacts on crop performance and resource-use efficiency (Zainali et al., 2025).

Two- (2D) and three-dimensional (3D) simulation platforms coupled with crop growth models, such as EPIC (Campana et al., 2024), GECROS (Amaducci et al., 2018, Bellone et al. 2024), and STICS (Dupraz et al., 2011; Dinesh and Pearce, 2016; Crépeau et al., 2025), have become increasingly common for simulating radiation dynamics, light interception, and biomass production under heterogeneous conditions, including AV systems (Grubbs et al., 2024). These tools have significantly accelerated the evaluation of crop-specific shading responses and the identification of optimal AVS designs balancing energy and agricultural outputs (Bellone et al., 2024). Despite advances in modeling crop-radiation interactions, key methodological gaps remain. Daily-step models (e.g., STICS, EPIC) cannot resolve intra-day radiation dynamics, and even hourly models like GECROS lack full 3D integration to represent canopy light distribution. Moreover, most approaches treat photovoltaic and crop growth modules separately, limiting the understanding of soil-water redistribution and its impact on productivity and system efficiency. Nonetheless, a major limitation persists due to the lack of robust, multi-seasonal experimental datasets for model calibration and validation (Zainali et al., 2025). Where data are available, they are often restricted to a single growing season, limiting the ability to capture interannual variability. This constraint is highlighted by recent studies emphasizing the scarcity of long-term data in European contexts, which undermines the reliability and transferability of the existing models (Zidane et al., 2025; Berrian et al., 2025). For such an example, Mazzeo et al. (2025) proposed a sophisticated simulation approach, yet acknowledged that many yield estimates are still derived from artificially shaded experiments rather than real AVS conditions. Another critical source of uncertainty concerns the type of crop growth model used to estimate biomass responses under AVS conditions. Broadly, these models can be classified into two categories. The first refers to semi-mechanistic models, which simulate crop development on a daily time step using simplified assumptions, most notably, Radiation Use Efficiency to convert intercepted light into biomass (Monteith et al., 1977; Brisson et al., 2002). The second includes process-based models, which rely on a detailed, physiological representation of photosynthesis, operating typically on an hourly scale and incorporating key limiting factors such as water and nitrogen availability (Kirschbaum et al., 1997; Morales et al., 2018; Bellasio, 2019). Semi-mechanistic models are generally easier to parameterize and calibrate due to their lower data requirements, making them suitable for broad-scale applications. However, they may lack the resolution needed to capture intra-daily shading fluctuations typical of AV systems, thus limiting their accuracy in highly dynamic light environments (He et al., 2024, Zainali et al., 2025). In contrast, process-based models are better equipped to simulate the fine-scale effects of fluctuating radiation, but they require extensive input data, including crop-specific biochemical and structural parameters, which are often unavailable or difficult to measure (Prusinkiewicz & Runions, 2012).

Building upon these premises, this study presents the development and validation of a novel modelling framework that integrates a simplified process-based crop growth model with a high-resolution, three-dimensional radiative transfer environment. The framework is specifically designed to resolve the spatial and temporal heterogeneity of intra-daily shading patterns generated by diverse AVS configurations, while capturing feedback processes that are fundamental for a realistic representation of crop productivity under fluctuating light regimes. Its performance was rigorously evaluated using an extensive multi-year dataset collected across contrasting environmental contexts, including open-field conditions, fixed-panel installations, and dual-axis tracking AVS, with alfalfa (*Medicago sativa* L.) employed as a representative model species.

4.2 Materials and Methods

4.2.1 Study area and experimental design

Field trials were conducted across three locations in northern and central Italy (Figure 1), each representing a distinct agronomic and environmental context: (i) an open-field reference site in Montese (Modena; Figure 1-Site A), (ii) a fixed-panel AVS in Sant'alberto (Ravenna; Figure 1-Site B), and (iii) a bi-axial tracking AVS in Borgo Virgilio (Mantova; Figure 1-Site C). These sites were selected to capture a range of radiation regimes and to assess crop performance under different spatial and temporal shading conditions.

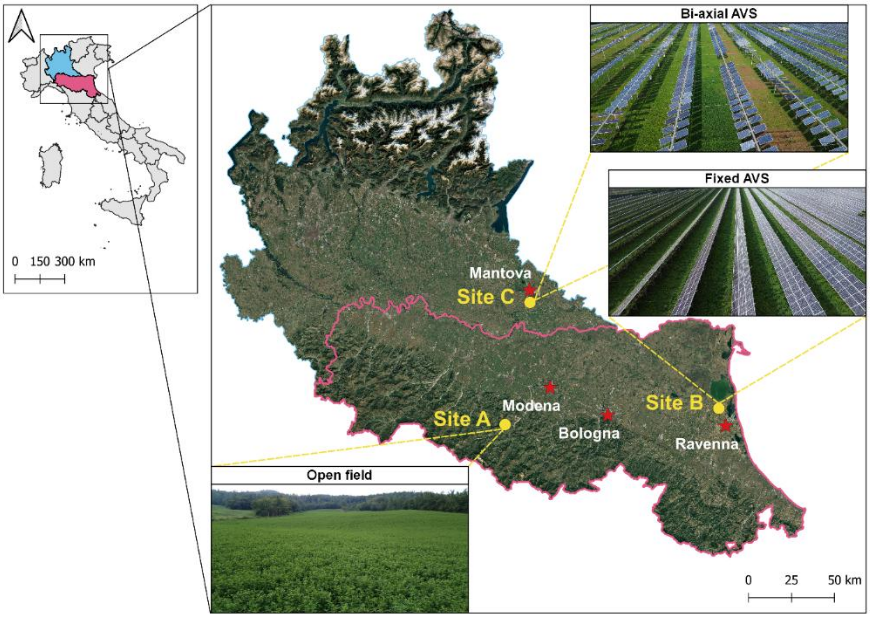

Figure. 1. Location of the open field (Site A), fixed (Site B) and bi-axial (Site C) agrivoltaic system experimental sites.

4.2.1.1 Open-field setup

The open-field study area is located within the 'Terre di Montagna' Consortium, which includes approximately 100 farms dedicated to Parmigiano Reggiano production in the mountainous Apennine regions of Bologna and Modena (Emilia-Romagna, central Italy), at altitudes exceeding 600 meters above sea level. The local soils are mainly composed of sandstone, limestone, and marl, exhibiting variable pH conditions. Climatic data were obtained from the Montese meteorological station (44.4579° N, 10.5899° E), positioned at the center of the study area (Figure S1). The climate is characterized by an average annual temperature of 10.1 °C and mean annual precipitation of 930 mm, with limited drought occurrence during the summer months (Argenti et al., 2021).

4.2.1.2 Fixed Agrivoltaic System

The fixed AVS study site is located in Sant'Alberto (Ravenna, Italy; 44.51019° N, 12.1552° E), a northeastern area of Italy well-suited for AVS implementation due to its high solar radiation and fertile agricultural soils. The site has been operational since 2012 and hosts a 70-hectare alfalfa (*Medicago sativa* L.) meadow, contributing to approximately 45 GWh of electricity per year. The terrain is predominantly flat, with elevations ranging from 4 to 8 m above sea level. The climate is temperate, with hot summers and cold winters, and an average annual temperature of 15 °C (ranging from 5 °C in January to 25.6 °C in July). Annual precipitation averages 767 mm, with November being the wettest month (87 mm) and January the driest (49 mm). Meteorological data were recorded at the local weather station throughout the experimental period (Figure S1). Soils at the site are classified as silty sand in the 0-60 cm layer, composed of 50% sand, 40% silt, and 10% clay. Photovoltaic panels at the site are mounted on south-facing ground structures tilted at a 35° angle. The tables are 3.5 m wide with 8 m spacing between rows, resulting in a Ground Cover Ratio (GCR) of 38%. Panel height varies from 1.3 m at the lower edge to 3.3 m at the upper edge (Figure 2a). Prior to sowing in 2020, the soil was plowed to a depth of 30 cm, then tilled and rolled to ensure good seed-to-soil contact, facilitating successful crop establishment under the AVS configuration.

4.2.1.3 Bi-Axial Agrivoltaic System

The bi-axial AVS experimental site is located in Borgo Virgilio, northern Italy (Mantova; 45.0944° N, 10.7916° E), and has been operational since April 2011. The site spans 11.42 hectares, with approximately 13% of the surface occupied by photovoltaic panels (GCR), each measuring 1 m × 2 m. The total installed capacity is 2,150.4 kWp, distributed across 768 biaxial solar trackers that support 7,680 polycrystalline PV modules (Poly 280 Wp, Bisol Group, Slovenia). The panels are mounted 4.5 m above ground and are capable of dual-axis tracking, with tilt ranges of ±50° along the primary axis and ±40° along the secondary. Soils at the site are classified as silty sand in the 0-60 cm layer, composed of 50% sand, 40% silt, and 10% clay. The pH is slightly alkaline (8.5), with an organic carbon content of 1.1% and total nitrogen of 0.18%. Available phosphorus and exchangeable potassium levels are 76.4 mg kg^{-1} and 810 mg kg^{-1}, respectively.

4.2.2 Data collection

Field data were collected at the three experimental sites - Site A, B and C - throughout the entire seasonal growth cycle of alfalfa. Measurements focused on above-ground dry biomass (AGB, g) and Leaf Area Index (LAI, m^2 m^{-2}), both used for model calibration and validation.

At the open-field site (Figure 1-Site A), surveys were conducted during the 2019 season on four-year-old pure stands of alfalfa. Sampling occurred on three dates (day of year (DOY) 150, 197, and 241), corresponding to spring, summer, and late summer, respectively. For each date, three replicate plots per field were randomly selected. On each sampling date, canopy LAI was first measured using a LI-COR ceptometer (LI-190; LI-COR, USA), with one reading per plot. Subsequently, AGB was harvested within 0.5 × 0.5 m quadrats using battery-powered clippers, following the protocol of Mikhailova et al. (2000). Samples were sealed in plastic bags, transported to the laboratory, and oven-dried at 80 °C for 48 hours until constant weight (Wang et al., 2019).

At the fixed AVS site (Figure 1-Site B), sampling was performed throughout the 2023 and 2024 growing seasons on the following dates: DOY 7, 68, 144, 188, 212, and 314 (2023) and DOY 80, 100, 191, and 268 (2024). A total of 36 sample plots (0.5 × 0.5 m each) were established according to a randomized complete block design, consisting of four treatments (TR1: 6% shading, TR2: 7% shading, TR3: 67% shading, TR4: 82% shading) replicated three times within each of the three blocks distributed across the field (Figure 2a). This layout allowed for the capture of both spatial heterogeneity and treatment effects across the AVS system. Plots were systematically positioned along the shading gradient imposed by the PV panels. On each sampling date, canopy LAI was first measured using an AccuPAR LP-80® ceptometer (Decagon Devices, Pullman, WA, USA). Subsequently, regrowth biomass was harvested to a height of 3 cm within the 0.5 × 0.5 m frame at the plot center. Samples were dried at 60 °C for 48 hours to determine dry matter yield (g m^{-2}). For a detailed description of the site and the relevant sampling protocol, please refer to Moretta et al. (2025).

At bi-axial AVS site (Figure 1-Site C), alfalfa was sown on 20 October 2022 at a density of 300 seeds m^{-2}. Biomass sampling was conducted along 12 m transects arranged within a

12 × 36 m study area. The experimental layout consisted of four treatments (TR1: 27% shading, TR2: 12% shading, TR3: 21% shading, TR4: 34% shading), spaced 3 m apart, each containing three replicate plots within the transect. This arrangement was repeated three times across the study area, resulting in a total of 36 treatment plots. A 1.5 m buffer was maintained at both ends of each transect to minimize edge effects and avoid interference from PV panel supports. Data were collected on DOY 183, 207, 241, and 296 during the 2024 season. On each date, biomass was cut to 3 cm within 0.5 × 0.5 m quadrats at plot centers, then oven-dried at 60 °C for 48 hours for dry matter quantification. Additionally, canopy temperature was measured using a FLIR Ex-Series thermal camera (FLIR Systems, Inc., Wilsonville, OR, USA), positioned approximately 1 cm from the leaf surface, to monitor thermal responses to shading conditions. Meteorological data were recorded at the local weather station throughout the experimental period (Figure S3). Temperature measurements were taken on the same days as biomass sampling, consistently between 10:30 a.m. and 11:30 a.m., always selecting leaves exposed to direct sunlight and avoiding shaded ones.

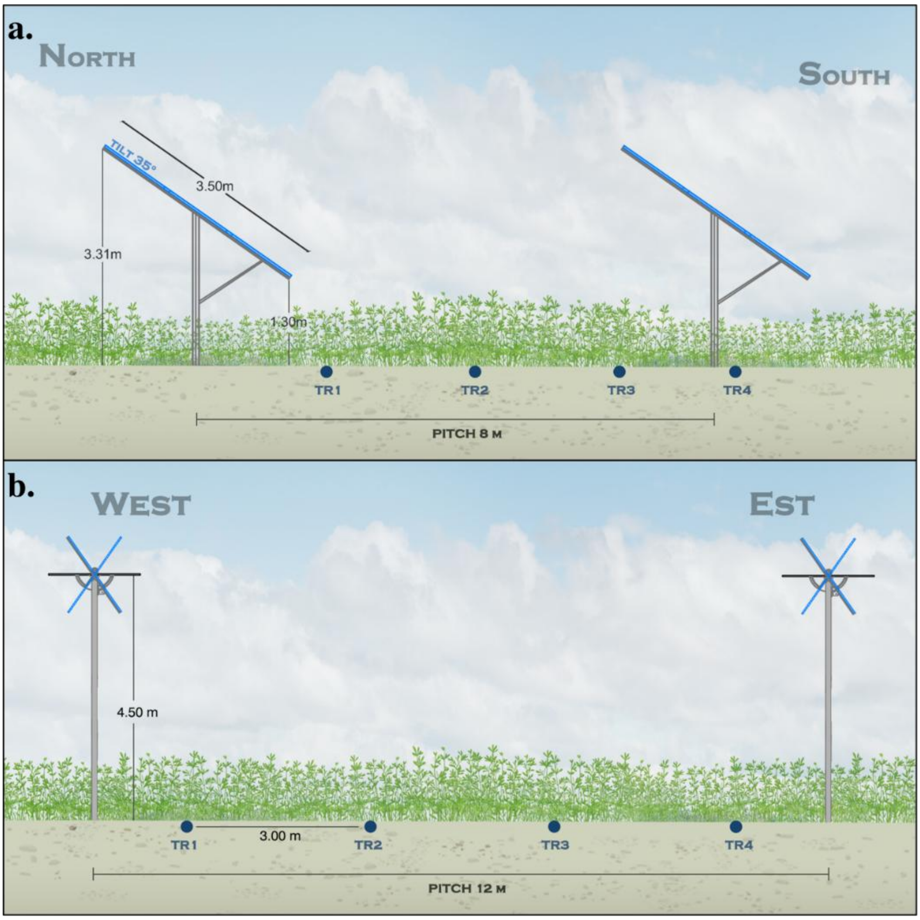

Figure 2. Representation of the fixed (a.; Site B) and bi-axial AVS (b.; Site C), highlighting the spacing between rows, height of the panel in relation to the ground and arrangement of treatments (TR1-TR4).

4.2.3 Integrated Modeling of AVS

4.2.3.1 Framework setup and scene design

To spatially assess the impact of AVS on crop growth, a process-based crop simulation model was embedded within the Growth Grammar-related Interactive Modelling Platform (GroIMP), leveraging its capabilities for three-dimensional modeling, light simulation, and interactive visualization (Kniemeyer et al., 2007). GroIMP is an open-source 3D environment originally developed for functional–structural plant modelling; it supports rule-based scene construction and physically based light simulation through an inverse Monte Carlo ray-tracing algorithm (Kniemeyer et al., 2007; Hemmerling et al., 2008). GroIMP was used to construct virtual 3D scenes representing different AVS layouts, with photovoltaic (PV) panel geometry and spatial distribution explicitly defined. The associated ray-tracing radiation model (Hemmerling et al., 2008; Boland et al., 2018) enabled the simulation of global solar radiation distribution and shadow patterns across the cropping surface. These outputs were used to dynamically drive the crop model and evaluate the spatial effects of shading.

At Site A (Montese, open-field reference), the terrain configuration was simulated in GroIMP using a tile-based approach, with the soil surface partitioned into 1 × 1 m grid elements spanning a 20 × 20 m area.

The same scheme was used to spatially represent the terrain in the AVS layout at the Ravenna (Site B) and Mantova (Site C) experimental sites. In Site B (fixed AVS), PV panels were represented as 3.2 × 3 m rectangular surfaces, mounted at a height of 2 m and tilted at 35° relative to the vertical. Panels were arranged in continuous rows, spaced 8 m apart, and oriented along a north–south axis (Figure 2a).

In the Site C system (bi-axial AVS), panels were modeled as 1 × 2 m surfaces positioned at 4.5 m above ground (Figure 2b). Each panel was assigned two degrees of freedom for solar tracking, with tilt ranges of ±50° and ±40° along the primary and secondary axes, respectively.

4.2.3.2 Radiative environment

Each scene is coupled with a physically based simulation of direct and diffuse solar radiation, aimed at quantifying the total radiation intercepted by each object in the scene (e.g., photovoltaic panels and underlying surfaces) throughout the diurnal cycle. The radiative model is based on the approach originally described by Zhu et al. (2018) and subsequently modified in Moretta et al. (2025).

To this end, the scene incorporates two distinct types of radiative sources: i) a dynamic point light source that emulates the solar trajectory across the sky, representing direct beam radiation; and ii) an array of 72 static point light sources, spatially distributed across six concentric circles (12 sources per circle) to uniformly sample the upper hemisphere and reproduce the angular distribution of diffuse radiation, following the discretization scheme of Zhu et al. (2018).

The model includes a preprocessing step to compute the solar elevation angle on an hourly basis as a function of site latitude and DOY, following the astronomical formulation of Goudriaan and Van Laar (1994). This enables the derivation of instantaneous global extraterrestrial radiation (GER, W m^{-2}) (Eq. 1).

$$GER = \varepsilon \cdot sin\beta \left(1 + 0.33 \cdot \cos\left(\frac{2\pi(t_d - 10)}{365}\right)\right) \tag{1}$$

where GER is the global extraterrestrial radiation (Wm^{-2}), ε is the solar constant (1370 Wm^{-2}), t_d is the days from 1st January, and β is the elevation of the sun above the horizon.

The ratio between the hourly ground-measured global radiation (GR, W m^{-2}), provided by external meteorological data, and the corresponding GER yields the transmissivity coefficient (Tr, dimensionless), which is then used as an input to estimate the diffuse radiation fraction according to the empirical model by Boland et al. (2018) (Eq. 2).

$$FDL = \left(1 + e^{(8.6 \cdot Tr - 5)}\right)^{-1} \tag{2}$$

where *FDL* is the fraction of diffuse radiation (unitless) and *Tr* is the transmissivity (unitless).

Once the partitioning between direct and diffuse components is obtained, the corresponding radiative fluxes (W m^{-2}) are assigned to their respective light sources for each hourly timestep. The distribution of radiative energy within the scene is then computed using the GroIMP radiation model, which employs an inverse Monte Carlo path-tracing algorithm to simulate light transport and integrate intercepted radiation across object surfaces.

4.2.3.3 Crop modelling approach and calibration strategy

The global radiation intercepted at the ground on an hourly time step for each tile simulated in GroIMP, was used as a direct input to drive an Alfalfa growth model embedded in the same platform, which also requires, at the same time resolution, air temperature (Ta,

°C), accumulated rainfall (Rain, mm), relative humidity (RH, %), and wind speed (WS, ms^{-1}) to estimate plant morpho-physiological processes (Figure 3).

The basic structure of the model uses a process-based approach for hourly estimation of biomass accumulation (B_{crop}, g m^{-2}), which is dynamically partitioned to leaves, stems, and roots during the season. Accordingly, in non-limiting conditions:

$$B_{crop} = fPAR \cdot I \cdot RUE \tag{3}$$

where *I* is the incident hourly global solar radiation (MJ m^{-2}) derived from the GroIMP radiation model, *fPAR* is the fraction of incident radiation intercepted by the canopy (unitless), and *RUE* is radiation use efficiency (g MJ^{-1}). $fPAR$ is calculated on an hourly time step according to Sinclair et al. (1992):

$$fPAR = 1 - e^{\left[-LAI \cdot \frac{k}{\sin(alpha)}\right]} \tag{4}$$

where k is the extinction coefficient of light in the canopy, and *alpha* (°) is the angle of sun elevation provided to the growth model by the GroIMP simulation of the daily course of solar track (section 2.3.2). RUE is calculated according to Yin et al. (2021), who modelled the canopy light use efficiency of C3 crops ($\Phi_{CO2canopy}$, mol CO_2 mol^{-1} photon) as:

$$\Phi_{CO2canopy} = \frac{(C_C - \Gamma_*) \cdot \phi_{2LL}}{4 \cdot (C_C + 2\Gamma_*) \cdot (1 + \phi_{2LL} + \frac{\phi_{2LL} \cdot k \cdot I_{inc}}{Jmax})} \tag{5}$$

where C_C is the chloroplast CO_2 level (μmol mol^{-1}), Γ_* is the CO_2 compensation point (μmol mol^{-1}), Φ_{2LL} is the electron transport efficiency of Photosystem II under limiting light (mol mol^{-1}), I_{inc} is incident light photosynthetically active radiation (PAR, μmol m^{-2} s^{-1}), and J_{max} is canopy-top leaf maximum electron transport rate under light-saturating conditions (μmol e^- m^{-2} s^{-1}). Further description of the functional formulations related to temperature sensitivity of Γ_* and J_{max}, as well as the nitrogen-dependent scaling of J_{max} for photosynthetic response, is provided in SI. The parameterisation of the alfalfa growth model is provided in Table S1. Canopy light use efficiency ($CO_{2,canopy}$), calculated in not limiting water conditions, is then converted into *RUE* according to van Oijen et al. (2004) and Yin et al. (2021):

$$RUE = \Phi_{CO2,canopy} \cdot MM \cdot \left(1 - \frac{R}{P}\right) \cdot 4.56 \cdot \frac{0.5}{C_{biom}} \tag{6}$$

where R/P (crop respiration-to-photosynthesis ratio) was set to 0.4 (Yin et al., 2021); MM (the molar mass of carbon) was fixed at 12 g mol^{-1} and a conversion factor of 4.56 was used to translate photosynthetically active radiation (PAR) from MJ to moles of photons, assuming that PAR represents 50% of incoming global solar radiation. The carbon fraction in crop biomass (C_{biom}) was set to 0.48.

Assimilated biomass at the hourly scale is accumulated daily and partitioned to the different organs according to dynamic partitioning coefficients (*PCs, ratio*), which are dependent on photoperiod (*PP*, hours) as provided by the radiative model of GroIMP. Specifically, for *PP* before the spring equinox, *PC* to above ground biomass (AGB, g m^{-2}) (*i.e.*, leaves and shoots) is set to 0.9 while it decreases to 0.67 between the equinox and summer solstice (Brown et al., 2006). After that, as *PP* starts decreasing, *PC* to AGB drops to 0.35, considering that at the end of the season, the plant improves the accumulation of reserve substances in the roots to ensure vegetative recovery after the winter (Teixeira et al., 2007). According to Brown et al. (2006), this stage was assumed to start when *PP* decreases to 1h less than the daylength at solstice.

Biomass partitioned to AGB is further partitioned to leaves (PC_{leaf}) and shoots (PC_{shoots}) according to an allometric equation that assumes an exponential decrease in PC_{leaves} as increased dry matter to AGB (Brown et al., 2006; Teixeira et al., 2009). Accordingly:

$$PC_{leaf} = c \cdot exp\left(\frac{d}{AGB\ 10^{-2} + e}\right) \tag{7}$$

$$PC_{shoots} = 1 - PC_{leaves} \tag{8}$$

Where *c*, *d* and *e* are empirical coefficients shaping the response of *PC* to leaves to AGB (Table S1).

The biomass partitioned to leaves (g m^{-2}) is converted into new leaf area (LAI_{rate}, m^2 m^{-2}) considering biomass investment per unit leaf area (Specific Leaf Area, *SLA*, m^2 g^{-1}).

$$LAIrate_{(t)} = AGB \cdot PC_{leaves} \cdot SLA \tag{9}$$

On the evidence that plants show an increase in *SLA* as an adaptation to shading conditions, as observed in the literature (Scarano et al., 2024; Potenza et al., 2022; Evans &

Poorter, 2001) and the experiment in Site B (Moretta et al., 2025), SLA was dynamically modified over each tile by quantifying the relevant degree of shading. Accordingly, a shadow factor (*ShF*, unitless) is calculated as the ratio between incoming global radiation (*GR*) and that intercepted by each tile (*I*), which ranges between 1, when the radiation intercepted by the tile corresponds to the external global radiation (no shadow), up to 0, corresponding to a complete shadowing:

$$ShF = \frac{I}{GR} \tag{10}$$

The shadow effect on *SLA* is assumed for *ShF* lower than 0.9, where the increase in *SLA* was calculated as:

$$incSLA = SLAmax \cdot (1 - ShF) \tag{11}$$

where $SLAmax$ represents the maximum increment of SLA in response to a complete shadowing according to the results obtained in Site B (0.25; Moretta et al., 2025). inc_{SLA}, calculated on an hourly basis for each tile, is daily averaged and finally used to update the original SLA and the relevant *LAIrate*.

The simulation of LAI is completed by the simulation of leaf area senescent rate (*SENrate*, m^2 m^{-2}) that is modelled by assuming a fixed senescence rate (Fix*SENrate,* m^2 m^{-2}) multiplied by a Stage Factor (*SF*, unitless), a Cover Factor (*CF*, unitless), a Temperature Factor (*TF*, unitless), and a Water Stress Factor (*WSF*, unitless) (Yang et al., 2022).

SF starts linearly increasing from active vegetative growth (*SF*=0) to floral buds' visible stage (BV) (*SF*=0.3). This stage is dependent on daily mean temperature (Tmean, °C) and *PP*, where the attainment of the phase, in the original configuration of Teixeira et al., (2011), is determined by an accumulation of 700 degree days (DDA, °C) (base temperature Tb=0°C) at *PP*=10h, linearly decreasing up to 270 DDA at *PP*>14h condition. After BV, temperature becomes the primary driver of anthesis, defined as the stage when 50% of stems have open flowers. This is initially set to occur at 274 DDA after BV, corresponding to SF=0.6, which increases to 1 in the following stage (grain filling).

CF increases linearly from 0 to 0.5 as LAI increases from 2 to 4, and then continues to increase, reaching a maximum value of 1.5 at LAI 7.

TF is set to 0.1 for mean daily temperatures between 0 and 5 °C, then increases progressively, reaching 1 at 20 °C, and peaking at a maximum of 1.5 at 40 °C.

WSF is assigned a value of 1 when the Fraction of Transpirable Soil Water (FTSW) is greater than 0.5. Below this threshold, WSF increases linearly up to 2 as FTSW decreases down to the wilting point (FTSW = 0.1).

Accordingly:

$$SENrate_{(t)} = FixSENrate \cdot SF \cdot CF \cdot TF \cdot WSF \tag{12}$$

LAI at time *t* is then updated:

$$LAI_{(t)} = LAI_{(t-1)} + LAIrate_{(t)} - SENrate_{(t)} \tag{13}$$

A soil water balance module is integrated to simulate water limitation experienced by the canopy during the growing season and the relevant impact on plant transpiration and photosynthesis. The soil water balance is calculated for a single layer where the total transpirable soil water (TTSW, cm) is estimated considering the water content availability (WCA, cm cm^{-1}) between field capacity and wilting point and the root depth (cm). Assuming no surface runoff, available soil water for the layer ($ATSW_d$, cm) depends on the ATSW of the previous day ($ATSW_{d-1}$, cm), and the positive (rainfall and/or irrigation, mm) and negative contribution (actual evapotranspiration, ET, mm) to the water budget.

$$ATSW_d = ATSW_{(d-1)} + \left(Rainfall_{(d)} + Irrigation_{(d)}\right) - ET_{(d)} \tag{14}$$

where rainfall, irrigation and ET are converted from mm to cm.

The calculation of actual evapotranspiration ET is preceded by the estimation of potential evapotranspiration (PET, mm), that representing the atmospheric evaporative demand under non-limiting water conditions, serves as a reference for deriving ET by incorporating constraints related to soil water availability and crop-specific stress factors. PET is calculated according to Penman-Monteith approach at hourly timestep:

$$PET = \frac{\left(\Delta(R_n - G) + \rho_a c_p \frac{(e_s - e_a)}{r_a}\right)}{\left(\Delta + \gamma\left(1 + \frac{r_s}{r_a}\right)\right)} \lambda^{-1} \tag{15}$$

where λ is the latent heat of vaporization (J Kg^{-1}), Rn is the net radiation (Wm^{-2}), G is the soil heat flux (Wm^{-2}), (e_s-e_a) represents the vapour pressure deficit of the air (VPD, KPa), ρ_a is the mean air density at constant pressure (Kg m^{-3}), c_p is the specific heat of the air (J $K^{-1}m^{-3}$), Δ is the slope of the saturation vapour pressure temperature relationship (KPa $°C^{-1}$), γ is the psychrometric constant (KPa $°C^{-1}$), and r_s and r_a are the surface and aerodynamic resistances (s m^{-1}).

Considering that Rn, G, and VPD data were not available at the experiment sites, they were calculated according to Allen et al. (1998). Hourly net radiation Rn was calculated as the difference between net shortwave radiation (Rns) and net longwave radiation (Rnl). Rns were obtained by correcting incoming solar radiation for surface albedo (assumed 0.23), while Rnl was estimated using the Stefan-Boltzmann law based on hourly air temperature, vapor pressure, and the ratio of measured to clear-sky solar radiation. G was calculated as 10% Rn during the day, to 50% at night. Hourly vapor pressure deficit (VPD) was calculated as the difference between saturated vapor pressure, derived from air temperature, and actual vapor pressure, estimated from observed relative humidity. For more comprehensive information, we recommend consulting the original publication.

Surface resistance (*rs*) was assumed to be 70 s m^{-1} during the day (Allen et al., 1998) and 700 s m^{-1} during the night (e.g. Meyers and Hollinger, 2004) to account for stomatal closure when radiation is missing.

Aerodynamic resistances *ra* is calculated according to Thom and Olivier (1977) as:

$$r_a = \frac{[4.72 \cdot [ln((z-d+z_O)/z_O]^2]}{(\ 1+0.54 \cdot u)} \tag{16}$$

where u is wind speed (ms^{-1}) at reference height z (2 m), d is the zero-displacement height equal to 1.04 $h^{0.88}$ and z_0 the roughness length for momentum and heat transfer equal to 0.062 $h^{1.08}$, where h is the crop height, assumed as a function of accumulated AGB according to a logistic function .

PET is partitioned between plant transpiration and soil evaporation that are then rescaled to the relevant actual values considering the limitations imposed by current water conditions. $fPAR$ is used as a scalar to partition ET between soil and crop, where the proportion of PET allocated to potential transpiration is $fPAR$ and that to potential soil evaporation is 1-$fPAR$ (Marsal et al., 2014). Potential transpiration is rescaled to actual transpiration considering that plant's gas exchange is regulated by the extractable soil water content, expressed by the ratio between ATSW and TTSW (i.e., fraction of transpirable soil water, FTSW, unitless; Sinclair et al., 1999).

$$RelTr = (1 + a \cdot exp(b \cdot FTSW))^{-1}$$
(17)

where $RelTr$ is the fraction of actual to potential transpiration (ranging from 1, when FTSW is not yet limiting potential transpiration, to 0, where FTSW completely inhibits transpiration), and *a* and *b* are empirical parameters shaping the response of RelTr to FTSW. The RelTr is also used to rescale the potential RUE (Eq. 6) to its actual value by considering that the reduction in RUE is directly proportional to the reduction in transpiration (Sinclair et al.,1999; Fig. S3).

Similarly, a rescaling factor for soil evaporation (*RedEvap*) is calculated when soil moisture diverges from a condition equivalent to that of a wet surface, assumed when FTSW>0.5 (Soltani and Sinclair, 2012). *RedEvap* is thus calculated as a function of the square root of time (DYSE, days) since FTSW is lower than 0.5:

$$RedEvap = [(DYSE + 1)^{0.5} - (DYSE)^{0.5}] \tag{18}$$

Finally, actual transpiration (ATR, mm) and soil evaporation (ASEV; mm) are calculated as:

$$ATR = fPAR \cdot PET \cdot Kc \cdot RelTr \tag{19}$$

$$ASEV = (1 - fPAR) \cdot PET \cdot Kc \cdot RelEvap \tag{20}$$

where Kc is the crop coefficient, assumed constant (1.05) during the growing season (Allen et al., 1996).

Considering that the hourly energy balance is calculated as:

$$R_n = G + H + \lambda ET \tag{21}$$

where Rn and G are known terms and actual λET may be calculated as the sum of ATR and ASEV and then converted via λ, the sensible heat H (Wm^{-2}) may be derived as difference and used to calculate the hourly temperature of the canopy (Tc, °C), accounting for the effect of a reduced transpiration on plant temperature (Webber et al., 2018). The Tc is then introduced as a factor affecting photosynthetic efficiency (Γ_* and J_{max}, SI)

$$T_c = T_a + \left(\frac{H \cdot ra}{\rho_a \cdot c_p}\right) \quad (22)$$

By embedding the crop growth model within the same platform as the radiative model in GroIMP, the framework dynamically accounts not only for the effect of absorbed global radiation and PP on plant growth and development but also for the impact of photovoltaic panels water harvesting its subsequent redistribution to the ground area immediately below their slopes. Accordingly, rainfall intercepted by the photovoltaic panels is redistributed onto the ground within the first meter linearly extending from the lower edge of the panels (Moretta et al., 2025):

$$R_a = R_m + R_i \quad (23)$$

where $R_a$is the total daily cumulated total rainfall (mm), including daily measured rainfall (R_m) and that intercepted by the panel (R_i) that is calculated according to:

$$R_i = R_m \cdot A_{panel} \cdot Rc \quad (24)$$

where A_{panel} is the effective collecting area calculated per linear meter of panel and Rc is the precipitation runoff conversion coefficient. In this study, *Rc* was set to 0.9 (90%). A_{panel} is calculated as:

$$A_{panel} = Length \cdot Width \cdot \cos(\alpha) \quad (25)$$

where $Length$ is the length of the panel (m), $Width$ is the width of the panel (m) and α is the tilt angle of the panel relative to the ground norm.

Conversely, the water input below the area under the panels' projection was considered negligible in all cases. In this context, a 1.5 m strip on both sides of each supporting pole, representing the area most influenced by potential rainfall shielding and runoff from the panels, was excluded from the computation domain.

Considering the simplified structure of the model, model calibration was limited to the tuning of a limited subset of parameters, while core physiological and structural parameters remained fixed, as they were derived from experimentally validated sources. Specifically, the calibration considered coefficients and timing of *PC* to above/below ground biomass as these parameters determine the accumulation and subsequent distribution of biomass in the leaves and stem. In addition, the flowering period was considered, as it plays a key role in driving leaf surface senescence.

As such, the model was initially applied over the calibration sites for testing LAI and biomass accumulation (Site A) and phenology (Site B) considering the initial parameterization for phenology and biomass partitioning in accordance with the literature data (Table S1). As a second step, based on the model's performance, the relevant parameters were modified to adjust the model's performance to the observed results.

To further explore the interaction between crop growth, water regime and energy conversion, the calibrated model was used to perform additional simulations (Site C; 2024) varying the pitch distance (spacing between PV panel rows) from 4 m to 16 m every 2m. For each configuration we calculated the relative alfalfa yield of three harvests and the relative PV energy production were calculated, both under non-limiting and water-limiting conditions (50 % reduction in seasonal rainfall).

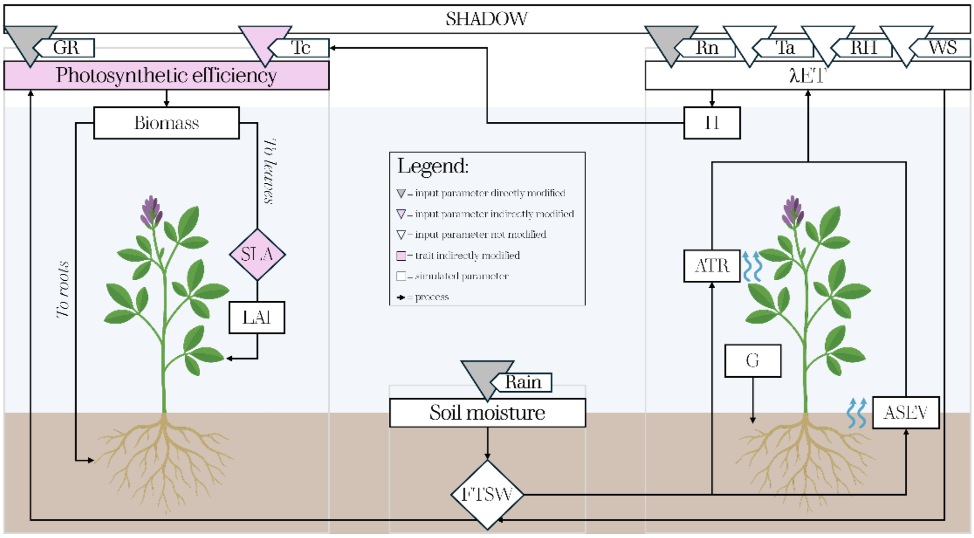

Figure 3. Simplified diagram of the crop modelling framework developed for assessing Alfalfa growth under different AVS. Grey, pink and white triangles indicate model input parameters directly, indirectly and not modified by shading effects, respectively. The remaining pink elements refer to morpho-physiological traits indirectly modified, while the white ones represent the parameters simulated by the model.

4.2.4 Statistical Analysis

To assess the performance of the integrated modeling framework in simulating alfalfa above ground biomass, LAI, and canopy temperature under different AVS configurations, a set of standard statistical indicators was employed. These included the Root Mean Square Error (RMSE), the Mean Bias Error (MBE), and the coefficient of determination (R^2). In addition to these performance metrics, the Akaike Information Criterion (AIC) was calculated to evaluate the trade-off between model accuracy and complexity.

Statistical comparisons between shading treatments were performed using analysis of variance (ANOVA), followed by Tukey's Honest Significant Difference (HSD) post-hoc test to identify differences in biomass accumulation and LAI across spatial positions. For variables measured repeatedly on the same plots across multiple sampling dates, a repeated-measures ANOVA was applied to account for temporal autocorrelation. Normality and homogeneity of variances were tested using the Shapiro–Wilk and Levene's tests, respectively. All statistical analyses were conducted using R software (version 4.4.3; R Core Team, 2025), and significance was accepted at $p < 0.05$ unless otherwise stated.

4.3 Results

4.3.1 Model calibration

Under the initial configuration (Table S1), the model slightly underestimated the DOY of full anthesis recorded in Site B in both 2023 and 2024. In 2023 the first flowering date was recorded on DOY 135 and the second, after the first mowing, on DOY 197, which were simulated respectively on DOY 130 and 190. In 2024, the flowering date was recorded on DOY 186, as the earlier cuts prevented reaching this stage previously and simulated on DOY 180. Accordingly, the thermal time from the bud visible stage to full anthesis was increased from its original value (270 degree-days) to 310 degree-days, resulting in a simulated flowering date within ±1 day of the observed DOY.

Under this configuration, the model was tested in Site A (2019), under open field conditions. In this experimental site, alfalfa showed an observed cumulative production of approximately 1,250 g m^{-2} (12.5 t ha^{-1}) at the end of the 2019 season. The three growing cycles, separated by mowing at DOY 153, 211 and 240, produced about 500, 420 and 330 g m^{-2}, respectively. The LAI peaked at about 5.1 m^2 m^{-2} before the first mowing, followed by decreasing values and subsequent recoveries with peaks of 3.2 and 2.8 m^2 m^{-2} in subsequent cycles. The model well reproduced the growth dynamics of both biomass and LAI for the first two mowings (Figure 4), highlighting the overall consistency of the proposed approach in simulating the process of biomass accumulation and partitioning and the senescence. Conversely, the model failed to adequately capture the regrowth dynamics following the second harvest during the terminal phase of the growing season (Figure 4) highlighting a potential inconsistency in the parameterization that defines the period during which biomass is preferentially allocated to the roots (*i.e.* at the end of growing season), as well as in the associated partitioning coefficient. In terms of predictive performance, the model yielded R^2

= 0.82, RMSE = 48.6 g m⁻², MBE = 12.1 g m⁻², and AIC = 125.4 for biomass, and R^2 = 0.74, RMSE = 0.62, MBE = 0.18, and AIC = 92.7 for LAI in this pre-calibration phase.

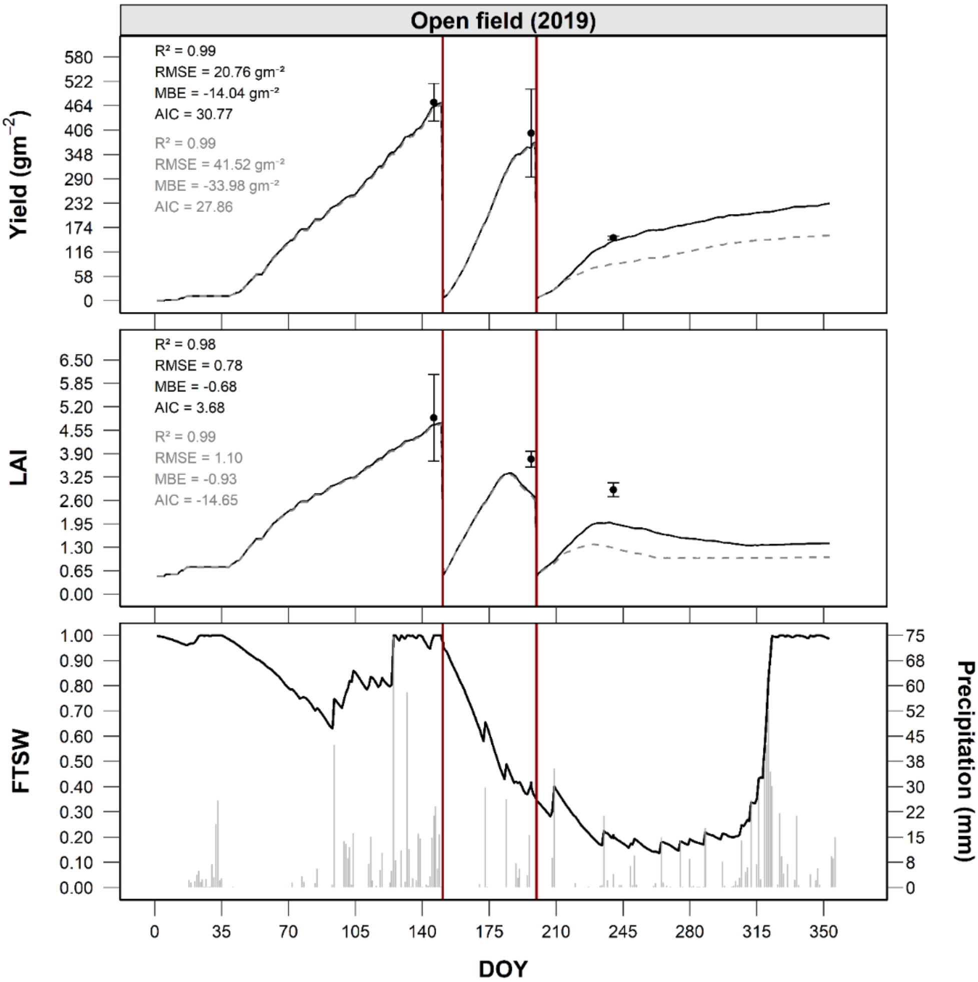

Figure 4. Seasonal dynamics of yield (g m^{-2}), LAI (m^2 m^{-2}), and FTSW under open-field (Site A) conditions in 2019, as a function of DOY. Post-calibration simulations are shown as black solid lines, while pre-calibration simulations are represented by grey dashed lines. Observed data are indicated by points with error bars. The bottom panel illustrates the seasonal course of FTSW (black solid line) together with daily precipitation (grey columns). Vertical red lines indicate dates of full-field harvest.

Accordingly, the *PP* triggering this shift under shortening day length conditions, was tuned in a range -1h (original value) to -2h with respect to the solstice (step 0.5h), considering all possible combinations with *PC* to AGB in the range between 0.35 (original value) and 0.5 (step 0.05). Finally, the best combination *PP-PC* providing the best performance in simulating biomass and LAI was selected.

Quantitative assessment of model performances after this second step improved model performances for both total biomass and LAI predictions. After calibration, the model achieved an R^2 of 0.99, RMSE of 20.76 g m^{-2}, MBE of -14.04 g m^{-2}, and AIC of 30.77 for total biomass. For LAI, the model reached an R^2 of 0.98, RMSE of 0.78, MBE of -0.68, and AIC of 3.68, indicating a substantial enhancement in accuracy and precision compared to the pre-calibration phase.

4.3.2 Fixed Agrivoltaic System

The performance of the calibrated model was evaluated at the fixed AVS (Site B) by comparing simulated and observed dry matter yield of alfalfa under four treatments (TR1-TR4, Fig 5) during the 2023 and 2024 growing seasons.

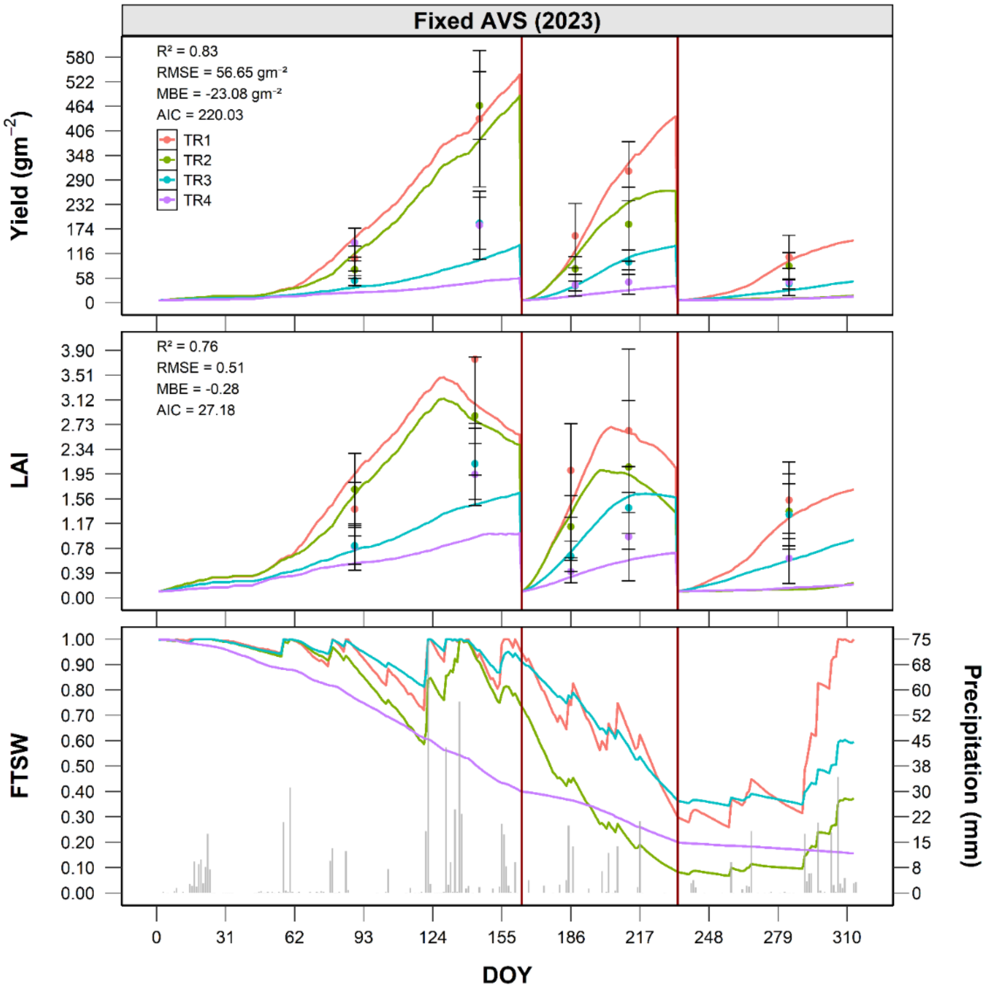

Figure 5. Seasonal dynamics of alfalfa dry matter yield (g m^{-2}), LAI (m^2 m^{-2}), and FTSW under fixed AVS conditions (Site B) in 2023, as a function of DOY. Simulated values are shown as solid lines for four treatments (TR1–TR4), while observed data are represented by points with error bars (mean ± standard error). The bottom panel illustrates the seasonal course of FTSW (solid lines) together with daily precipitation (grey columns). Vertical red lines indicate the dates of full-field harvest.

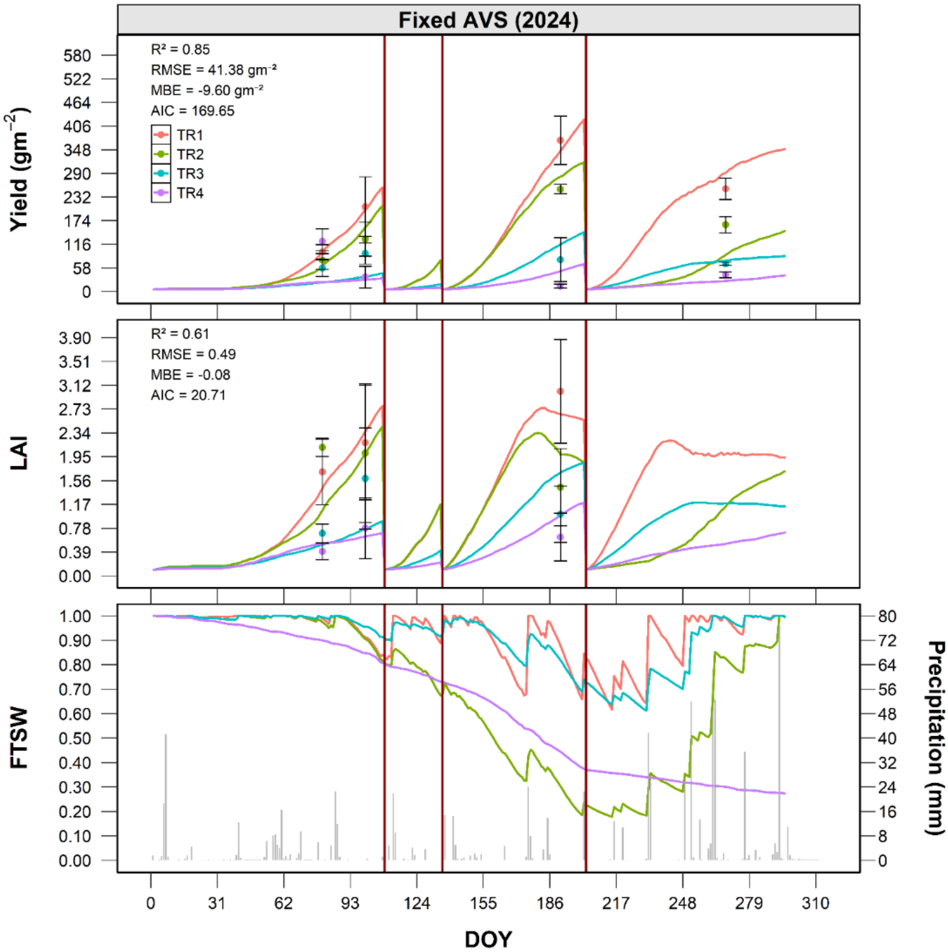

Figure 6. Seasonal dynamics of alfalfa dry matter yield (g m^{-2}), LAI (m^2 m^{-2}), and FTSW under fixed AVS conditions (Site B) in 2024, as a function of DOY. Simulated values are shown as solid lines for four treatments (TR1–TR4), while observed data are represented by points with error bars (mean ± standard error). The bottom panel illustrates the seasonal course of FTSW (solid lines) together with daily precipitation (grey columns). Vertical red lines indicate the dates of full-field harvest.

In 2023 (Figure 5), observed biomass accumulation revealed a clear gradient among treatments: TR1 achieved the highest yields, likely due to increased soil moisture availability from panel-induced runoff, followed by TR2, while TR3 and TR4, located in more heavily shaded areas, showed substantially lower productivity. Before the first cut (DOY 153), TR1 reached approximately 580 g m^{-2}, TR2 510 g m^{-2}, TR3 260 g m^{-2}, and TR4 only 120 g m^{-2}. After the second growth phase (DOY 240), cumulative yields increased to approximately 1,050 g m^{-2} for TR1, 900 g m^{-2} for TR2, 560 g m^{-2} for TR3, and 290 g m^{-2} for TR4. By the end of the season, total annual yields were approximately 1,350 g m^{-2} for TR1, 1,150 g m^{-2} for TR2, 700 g m^{-2} for TR3, and 400 g m^{-2} for TR4. Using TR2 as a reference, this corresponds to a +17.4% increase in TR1, and reductions of -39.1% and -65.2% for TR3 and TR4, respectively. The agreement between observed and simulated values was good (R^2 = 0.83, RMSE = 56.6 g m^{-2}, MBE = -23.1 g m^{-2}).

In 2024 (Figure 6), similar spatial patterns were observed, though overall yields were lower due to different climatic and management conditions, including a higher number of harvests. Before the first cut (DOY 122), TR1 reached approximately 230 g m^{-2}, TR2 200 g m^{-2}, TR3 120 g m^{-2}, and TR4 80 g m^{-2}. After the second growth cycle (DOY 211), yields were around 460 g m^{-2} for TR1, 360 g m^{-2} for TR2, 260 g m^{-2} for TR3, and 160 g m^{-2} for TR4. At the end of the season (DOY 268), cumulative yields were approximately 650 g m^{-2} for TR1, 520 g m^{-2} for TR2, 390 g m^{-2} for TR3, and 280 g m^{-2} for TR4. Compared to TR2, this corresponds to a +25.0% increase in TR1, and reductions of -25.0% and -46.2% for TR3 and TR4, respectively. The model accurately reproduced treatment-based differences in productivity, with overall satisfactory performance also in 2024 (R^2 = 0.85, RMSE = 41.4 g m^{-2}, MBE = 9.6 g m^{-2}), confirming the robustness of the approach for simulating spatially heterogeneous AVS.

The simulation of FTSW in 2023 revealed pronounced differences among treatments, reflecting their spatial arrangement within the fixed AVS system (Figure 5). TR1 consistently maintained the highest FTSW values, remaining above 0.6 for most of the season, supported by localized water redistribution from the northern panel edge. TR2 exhibited a steeper decline after the first harvest, with values approaching 0.5 by mid-season, indicating a faster depletion of soil water. TR3 and TR4, located beneath the panels and with limited direct access to rainfall (particularly TR4), showed the lowest soil moisture availability. In both treatments, FTSW dropped below 0.4 during the central part of the growing season (DOY 150–240), confirming greater exposure to water stress.

In 2024, FTSW dynamics followed a similar spatial gradient, but with overall higher values across all treatments, mainly due to more frequent rainfall events recorded during the summer period (DOY 160–240). Consequently, differences among treatments were less pronounced than in 2023. TR1 again maintained the highest FTSW, although the gap with TR2 and TR3 was reduced. TR4 remained the lowest, but without the sharp decline observed in the previous year.

4.3.3 Bi-Axial Agrivoltaic System

The performance of the calibrated model was evaluated under bi-axial AVS (Site C) conditions during the 2024 growing season. Figure 7 compares simulated and observed dry matter yield for four treatments (TR1 to TR4), corresponding to different shading levels and spatial positions relative to the solar panel configuration. The model demonstrated strong predictive accuracy, with a R^2 of 0.94, RMSE of 39.3 g m^{-2}, and an MBE of -3.4 g m^{-2}, indicating a slight overestimation of yield.

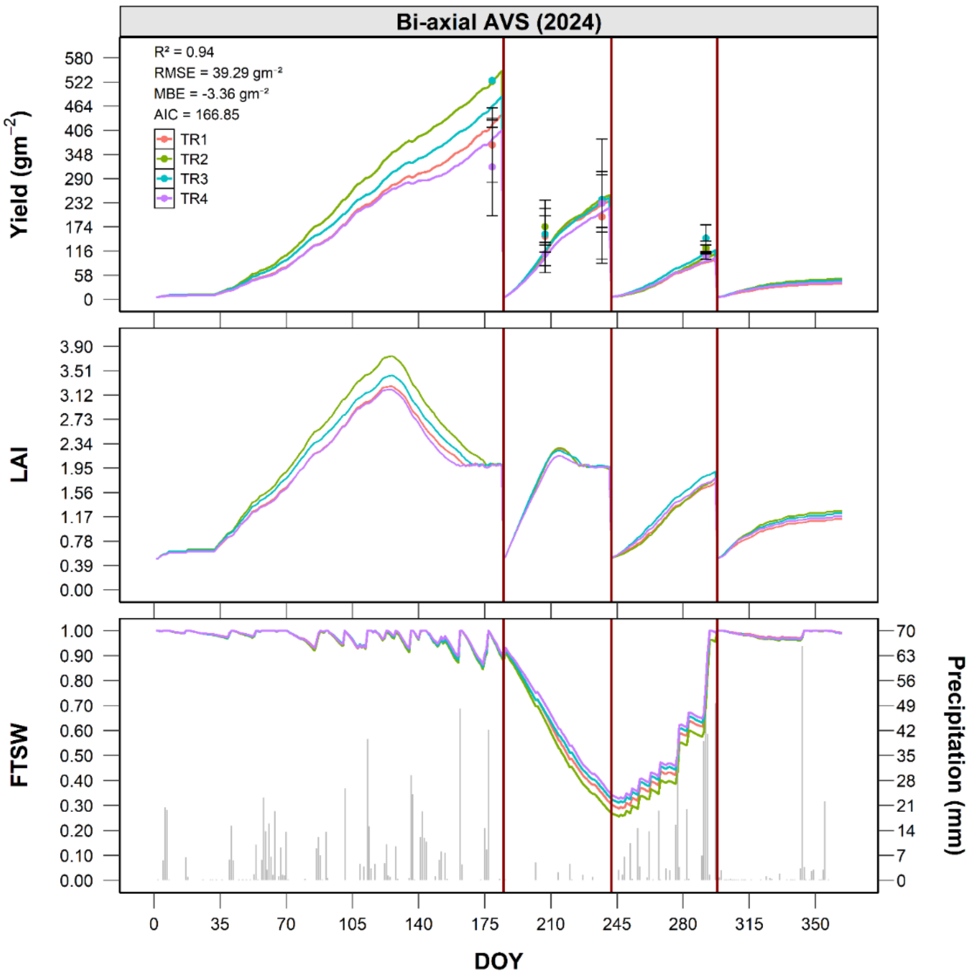

Figure 7. Seasonal dynamics of alfalfa dry matter yield (g m^{-2}), LAI (m^2 m^{-2}), and FTSW under bi-AVS conditions (Site C) in 2024, as a function of DOY. Simulated values are shown as solid lines for four treatments (TR1–TR4), while observed data are represented by points with error bars (mean ± standard error). The bottom panel illustrates the seasonal course of FTSW (solid lines) together with daily precipitation (grey columns). Vertical red lines indicate the dates of full-field harvest.

During the first growth phase (DOY 66-182), TR2 exhibited the highest productivity, reaching approximately 550 g m^{-2}, followed by TR3 and TR1, with yields around 500–520 g m^{-2}. TR4 consistently recorded the lowest yield (~470 g m^{-2}), reflecting a reduction of about

15% compared to TR2. These results highlight the significant influence of spatial positioning and light availability under biaxial tracking systems on biomass accumulation.

In the second regrowth phase (DOY 182-240), TR2 again showed the most vigorous recovery, followed by TR3, TR1, and TR4. Yield differences among treatments remained consistent, with TR4 accumulating approximately 10–15% less biomass than the most productive treatment.

During the final growth phase (DOY 240-298), yield levels among TR1, T2, TR3, and TR4 converged, suggesting a reduced marginal impact of partial shading under late-season conditions. Nonetheless, TR4 maintained a slightly lower cumulative yield, ending the season with approximately 10% less biomass than TR2, reinforcing the adverse effects of sustained shading on alfalfa productivity. Considering the annual cumulative biomass production averaged over harvests, alfalfa grown in Site A (open field, 2019) recorded the highest mean yields. The bi-axial tracking AVS (Site C, 2024) achieved a comparable annual output, remaining generally within about 10 % of the open-field reference. In the fixed-panel AVS (Site B, 2023–2024), when the calculation is restricted to the pre-existing, less shaded corridors (i.e., the productive inter-row areas comparable to TR1 and TR2), the system reached roughly 70 % of open-field alfalfa productivity on an annual basis. In contrast, the persistently shaded corridors contributed negligibly to yearly biomass and would scarcely justify cultivation.

The FTSW simulations show a very similar trend among the four treatments, with no marked differences related to the position with respect to the photovoltaic modules. During the first growth phase, the values remain close to 1, indicating optimal water availability. In the middle of the season (DOY 182-280), a progressive reduction in FTSW is observed, with minimums around 0.3-0.4, consistent with moderate but uniform water stress conditions across the plots. Starting from DOY 280, the recovery of rainfall causes a rapid rise in FTSW towards values close to saturation, restoring conditions that do not limit growth.

4.3.4 Canopy temperature simulation

The simulation of canopy temperature was evaluated at Site C (bi-axial AVS) across four spatial positions (TR1 to TR4) during the 2024 growing season (Figure 8). Observed canopy temperature dynamics varied across treatments and dates, reflecting both spatial heterogeneity and seasonal changes. Canopy temperatures exhibited a clear seasonal trajectory, increasing progressively from early measurements (DOY 183) to a peak during mid-season (DOY 241), followed by a marked decline by late season (DOY 296). Across all sampling dates, the highest temperatures were consistently recorded in the central treatments (TR2 and TR3), which correspond to the areas with the lowest shading levels. The model successfully captured observed trends, including the progressive temperature gradient from heavily shaded (TR1 and TR4) to less shaded areas (TR2 and TR3). On all sampling dates, TR1 and TR4 consistently exhibited lower average canopy temperatures than TR2 and TR3, with the differences being most pronounced at mid-season (DOY 207 and 241). Simulated temperatures closely matched observed data, with slight overestimation in late-season measurements (DOY 296) particularly under TR1. Overall model performance was strong, with a coefficient of determination (R^2) of 0.96 and a low RMSE of 0.87 °C, confirming the accuracy of the simulation in reproducing observed canopy temperature across treatments.

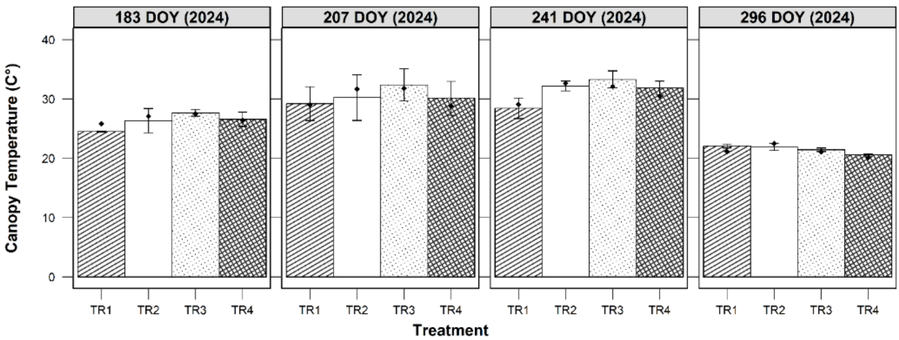

Figure 8. Observed and simulated canopy temperature (°C) for four treatments (TR1-TR4) across four dates (DOY 183, 207, 241, 296) at Site C. Columns show observed means with error bars (mean ± SE), while points represent simulated values.

To assess treatment effects on crop microclimate, canopy temperature was measured and expressed as the difference between canopy and air temperature (ΔT = canopy temperature minus air temperature) across four shading treatments (TR1 to TR4) and four sampling dates (DOY 183, 207, 241, and 296) at the Site C. Observed ΔT values showed clear differences among treatments and dates, reflecting variations in both shading intensity and environmental conditions. On days 207 and 241, corresponding to mid-summer conditions with air temperatures above 30 °C, the largest temperature differences were recorded. The most shaded treatments (TR1 and TR4) consistently exhibited lower canopy temperatures than the least shaded ones (TR2 and TR3), with ΔT differences exceeding 3 °C. On cooler days (183 and 296), when air temperatures were below 25 °C, treatment differences were smaller but still evident. The model accurately reproduced these spatial and temporal patterns, showing good agreement with observed data (R^2 = 0.83, RMSE = 0.88 °C, and MBE = - 0.11 °C; Figure 9), confirming its effectiveness in simulating canopy thermal dynamics under variable shading conditions. Overall model performance in simulating biomass yield and LAI across AVS configurations

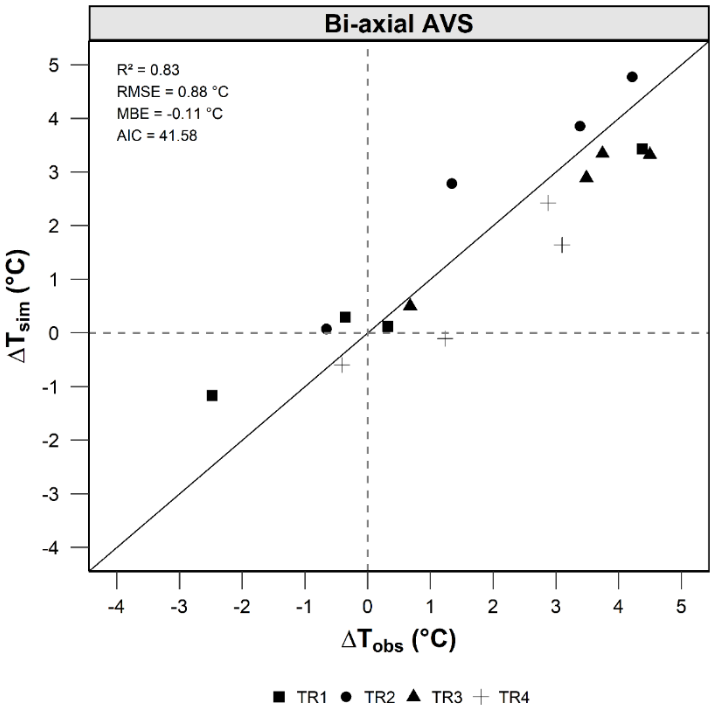

Figure 9. Comparison between simulated (ΔT_{sim}) and observed (ΔT_{obs}) canopy-to-air temperature difference ($\Delta T = T_{canopy} - T_{air}$) across four shading treatments (TR1–TR4) under the bi-axial tracking agrivoltaic system (Site C) during the 2024 growing season.

The accuracy of the integrated modeling framework was assessed by comparing simulated and observed values of yield ($Yield_{sim}$ vs $Yield_{obs}$) and LAI (LAI_{sim} vs LAI_{obs}) across all experimental sites and treatments, including open field, fixed-panel AVS (Site B), and bi-axial tracking AVS (Site C).

As shown in Figure 10A, the model captured yield dynamics with high accuracy (R^2 = 0.94), with a RMSE of 110,34 g m^{-2} and a MBE of –54.7 g m^{-2}, indicating a slight overall underestimation. The wide distribution of treatment-specific data points (TR1 to TR4) confirms the model's robustness in representing productivity across a range of shading intensities and microclimatic conditions. The slight underestimation tendency is more evident under high-yielding conditions (>400 g m^{-2}), where the model showed conservative predictions, likely due to limitations in simulating peak growth phases or resource-unlimited scenarios.

In Figure 10B, the model also accurately reproduced the seasonal dynamics of LAI, with a coefficient of determination of R^2 = 0.96, RMSE =-0.24. Most of the underestimation occurred at moderate to high LAI values (>3), suggesting that the model may slightly underestimate canopy expansion during the most favorable growth periods. Nevertheless, the model successfully represented the full range of LAI development across treatments, confirming its ability to capture both regrowth phases post-harvest and senescence-driven declines.

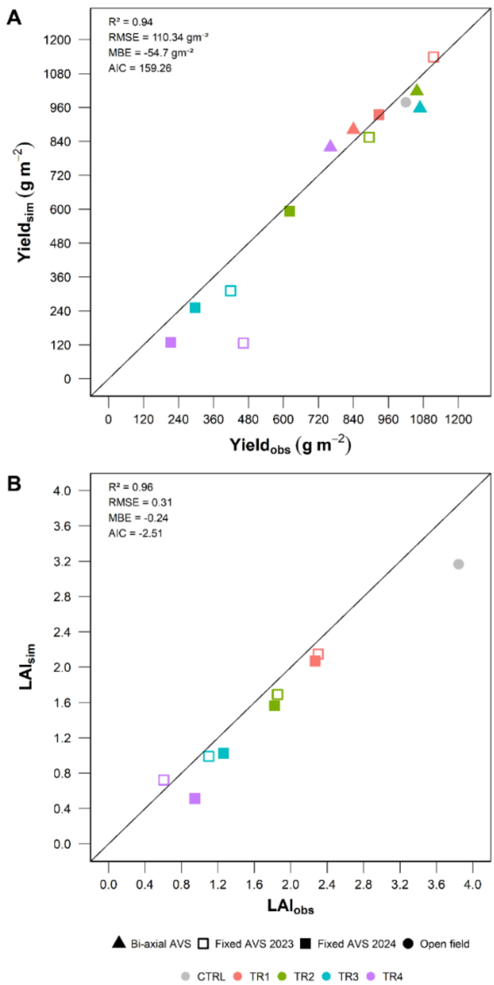

Figure 10. Comparison between simulated and observed values of (A) annual yield (sum per site and treatment) and (B) mean LAI at harvest. Data include open field (Site A), fixed AVS (Site B), and bi-axial AVS (Site C).

4.3.5 Scenario simulations on pitch distance and water availability

Yield and energy production were differently affected by pitch distance depending on water availability (Figure 11). Under non-limiting water, alfalfa yield increased steadily with wider pitch, reflecting improved light interception. Yield penalties at 4 m pitch reached about –50 % for the first harvest, while the second and third harvests showed progressively smaller reductions. In contrast, energy production decreased almost linearly with pitch distance, as larger spacing lowers the installed PV capacity per hectare.

Under water-limiting conditions, the response pattern changed. Moderate shading (pitch 6–8 m) mitigated drought stress by reducing canopy temperature and evapotranspiration, resulting in higher second-harvest yields than both narrower and wider layouts. The first harvest, when soil moisture was still adequate, and the third harvest, constrained by late-season stress, showed smaller differences among pitches. Energy production again declined with increasing pitch, but the agronomic advantage of intermediate spacing partly offset this loss.

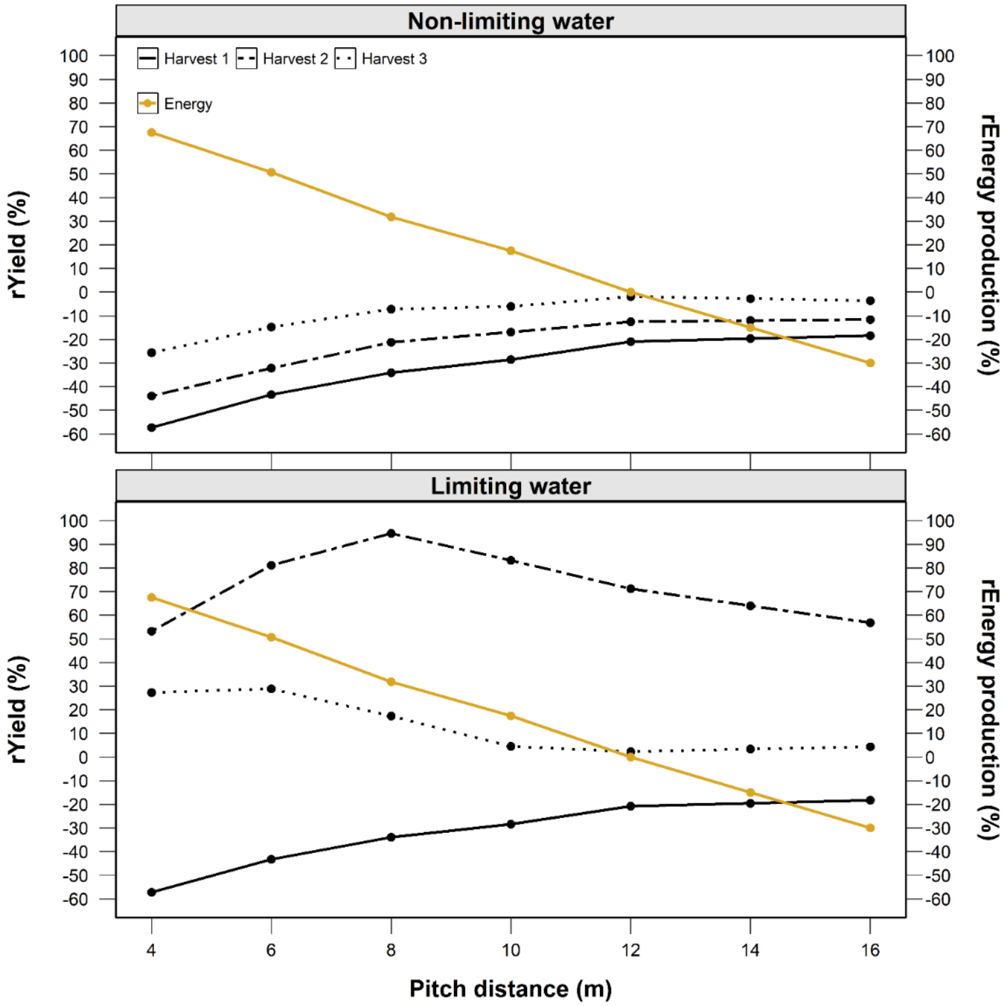

Figure 11. Modelled relative alfalfa yield of three harvests and PV energy production across pitch distances (4–16 m) under non-limiting (top) and water-limiting (bottom; 50 % rainfall) conditions.

4.4 Discussion

This study introduced a novel modeling framework based on the GroIMP platform that integrates a simplified, process-based crop growth model with a three-dimensional radiation transfer environment. The proposed approach enabled an explicit, physics-based simulation of light transport, which successfully quantified radiation interception by the modeled elements (i.e., crop and panels). As highlighted in the literature (Zainali et al., 2025; Amaducci et al., 2018), most existing modeling platforms are not well-suited for AVS because they overlook the critical interaction between panel-induced shading and the morpho-physiological responses of cultivated plants. Such omissions can lead to significant biases in model predictions. To address this gap, our framework was designed to balance parsimony with the ability to capture essential plant-environment feedback. Specifically, it has been developed to simulate the effects of hourly dynamic shading on alfalfa, thereby providing a more accurate assessment of crop performance under AVS conditions. In a recent study, Moretta et al. (2025) explored the impact of shading-induced microclimatic changes on alfalfa grown under the fixed AVS in Ravenna (Site B) by forcing the SSM crop model (Soltani & Sinclair, 2012) with image-derived fAPAR data, thereby circumventing the need to explicitly represent the morpho-physiological acclimation processes usually induced by reduced light availability. Conversely, the new prognostic approach presented here directly accounts for the physiological effects of lower radiation, providing a realistic simulation of alfalfa growth under shade that remains comparable to the forced SSM model.

In fact, the proposed framework incorporates key elements required to distinguish crop growth responses in shaded versus full-light conditions beneath PV panels. This integrated approach enables a more realistic simulation of the combined impacts of shading, drought and heat stress on plant morpho-physiological performance, which are especially critical in a Mediterranean climate where high temperature and low rainfall often limit plant growth during the season (Holmgren et al., 2012; Xu et al., 2020; Acevedo, 2024). The use of the GroIMP platform enabled the simulation of radiation dynamics at an hourly time step within a complex three-dimensional environment. This temporal resolution was crucial to capture the intra-daily variability of shading patterns induced by AVS structures. By explicitly representing these fluctuations, the model improved the realism of light–crop interactions. In contrast, many crop models commonly used to evaluate the effect of AVS on crop productivity such as STICS (Dupraz et al., 2011), EPIC (Campana et al., 2021) and APSIM (Ahmed et al., 2022), operate at a daily time step. While daily resolution is often sufficient to capture long-term growth patterns and seasonal dynamics, it tends to mask strong intra-day variability characteristic of plant–environment interactions under AVS (Artru et al., 2018), including the mitigation of midday photosynthesis depression and the effect of diurnal evapotranspiration patterns (Marrou et al., 2013; Elamri et al., 2018). This reinforces the importance of an hourly timestep for mechanistic modelling approaches (Amaducci et al., 2018; Potenza et al. 2022; Bellone et al., 2024).

Increasing SLA is a key trait underlying plant acclimation to low-light environments, as it enhances light interception per unit biomass (Valladares and Niinemets, 2008). While this plastic adjustment does not always confer a net fitness advantage (Liu et al., 2016), it is consistently observed as part of shade acclimation strategies (Poorter et al., 2009). Importantly, this behavior has also been specifically reported in crops cultivated beneath photovoltaic panels, such as alfalfa (Moretta et al., 2025; Zhang et al., 2017) and corroborated by similar findings in soybean (Potenza et al., 2022), tomato (Scarano et al., 2024), apple (Juilion et al.,2023) and lettuce (Marrou et al.,2013). The need to represent SLA dynamically in response to environmental stresses has recently been emphasized by Zhang et al. (2025) for the WOFOST model, whereas the original version only uses fixed tabular values linked to development stages. Similar limitations exist in the APSIM-Nwheat model (Asseng et al., 2003), while CropSyst (Stöckle et al., 2003) uses even a fixed SLA. APSIM Next Generation, developed for alfalfa, omits SLA altogether and simulates LAI with a double-sigmoid function of thermal time modulated by photoperiod, which further limits its ability to account for stress-induced adjustments in leaf morphology. In contrast, the GroIMP platform introduces a dynamic correction factor for SLA under shade, consistent with observations of Moretta et al. (2025). This adjustment accounts for the degree of shading across canopy zones and the associated variation in SLA, thus capturing the spatio-temporal heterogeneity of the canopy light environment and enabling a more accurate simulation of cumulative radiation interception throughout the growing season.

Increases in SLA are frequently associated with a reduction in the maximum electron transport capacity (J_{max}), reflecting coordinated trait syndromes under shade and leading, in the latter case, to a downregulation of photosynthetic capacity per unit leaf area in shaded environments (Valladares and Niinemets, 2008). Functionally, this adjustment represents an optimization strategy: shaded leaves typically exhibit lower nitrogen per unit area and reallocate it from photosynthetic enzymes toward light-harvesting structures and pigments, including increased SLA, to maximize light capture (Evans, 2001). Such downregulation aligns photosynthetic capacity with available light, while retaining the ability to respond to intermittent high-light pulses (Eichelmann, 2004). Conversely, crop models based on RUE (e.g., APSIM, EPIC, CROPSYST, STICS) typically account for water or nutrient stress on photosynthetic efficiency but ignore shading as a reducing factor. This oversight may bias biomass estimates and systematically underestimate both crop plasticity and the agronomic impacts of shading in AVS. To address this limitation, the GroIMP platform incorporates a response function, following Waring et al. (2023), to account for the effect of shading on the maximum electron transport capacity normalized at 25 °C (J_{max25}). This approach captures well-established acclimation processes of the photosynthetic apparatus to low irradiance (Waring et al., 2023; Dai et al., 2004) and ultimately enhances the realism of photosynthetic simulations under AVS conditions.

The modelling framework explicitly accounts for the interactions between transpiration, leaf temperature, and photosynthetic efficiency through an energy balance approach. In this formulation, reduced transpiration lowers latent heat flux, thereby increasing the proportion of net radiation dissipated as sensible heat. This shift leads to higher leaf temperatures, which are directly resolved by the model's energy balance module and subsequently used to drive photosynthetic efficiency (Eq. 22), thereby capturing the contrasting responses of plants grown under full light versus shaded conditions.

The roof effect induced by PV panels, introduced by Wu et al. (2022) to substantially modify rainfall distribution beneath PV installations, is systematically overlooked in current crop modelling studies on AVS, resulting in an incomplete representation of water dynamics. In contrast, our framework embeds the crop growth model within the 3D representation of the AVS, dynamically accounting for panel-mediated water interception and redistribution to the soil, and explicitly capturing the effects of canopy coverage on field water balance over time.

The simplified structure of the crop model requires calibration of only a few key parameters, primarily those controlling biomass partitioning and phenology, while most values are derived from the literature. This parsimony avoids overfitting to site-specific conditions, a common limitation of models with large parameter sets (Sinclair and Seligman, 2000). As a result, the model achieves greater robustness and transferability across different environments (i.e., open field, fixed AVS and bi-axial AVS).

In the control experiment at Site A, the late-season increase in root allocation occurred later and to a lesser extent than initially described by Brown et al. (2006), suggesting a delayed and reduced investment in belowground growth under experimental Mediterranean conditions. Specifically, the daylength threshold (*PP*) for increasing root partitioning shifted from -1 hour (i.e., when daylength decreases by 1 hour from the solstice) to -2 hours in our study, with the end-of-season partitioning coefficient decreasing from 0.65 to 0.5. This pattern likely reflects a local adaptation to Mediterranean climates, where mild autumn–winter temperatures extend the growing season and thus modify seasonal allocation strategies of Alfalfa. The retrieved partitioning coefficient (0.5) remains in any case within the range reported in the literature (Teixeira et al., 2009).

The calibrated model showed overall good performance results at simulating plant processes, including biomass accumulation, leaf area development and crop temperature, emphasizing differences between fixed and dynamic AVS.

In fixed-panel systems (Site B, 2023–2024), treatments showed marked differences in biomass accumulation. TR1 consistently outperformed the other treatments, with final yield advantages reaching up to 400 g m^{-2} compared to TR4. These yield gaps can be explained by persistent shaded zones in some treatments, especially TR3, where the fixed panel geometry restricted light availability for long periods during the day and across the growing season. When comparing TR1 and TR2, both received almost the same amount of radiation (+4% in TR1 relative to TR2), yet TR1 achieved substantially higher biomass production (+17.4% in 2023 and +25.0% in 2024). The simulations accurately reproduced this trend, capturing the pronounced shading gradients generated by the fixed AVS. This further supports the idea that static shading imposes an asymmetrical distribution of light and accentuates productivity gradients along transects (Tahir & Butt, 2022). In alfalfa, these gradients were not compensated by increased leaf area resulting from higher SLA under shading conditions, highlighting its sensitivity to persistent shading. This classifies alfalfa among light-demanding crops (Argenti et al., 2021), such as corn (Ramos-Fuentes et al., 2023) and kiwifruit (Jiang et al., 2022), which experience significant yield losses under fixed-panel systems. In contrast, shade-tolerant species, including lettuce and other leafy vegetables (Marrou et al., 2013; Elamri et al., 2018), rice (Gonocruz et al., 2021), and winter wheat (Weselek et al., 2019), can maintain stable or even improved yields under similar conditions, benefitting from moderated canopy temperatures, reduced evapotranspiration, and enhanced water-use efficiency. Importantly, the higher biomass production observed in TR1 with respect to TR2 was also accurately captured by the model, indicating that this difference is primarily attributable to water harvesting. Indeed, the additional water input from rainfall intercepted by the panels effectively mitigated summer water stress, underscoring the need to account for panel-driven water redistribution when estimating the effects of photovoltaic structures in open-field conditions (Adeh et al., 2018; Wu et al., 2022; Moretta et al., 2025).

By contrast, in the dual axis tracking system (Site C, 2024), differences among treatments were limited, with final biomass gaps generally below 100 g m^{-2} (≈1 t ha^{-1}). This outcome suggests that panel movement effectively reduced the heterogeneity of light distribution across the field, leading to more uniform yield patterns. A similar conclusion was reached by Edouard et al. (2023), who tested alfalfa under a bi-axial AVS with shading levels ranging from 29% to 44%. In that study, yield differences between shaded and full-sunlight conditions remained within ±10% of annual biomass), confirming that bi-axial tracking systems mitigate spatial variability compared to fixed-panel configurations. Collectively, these results demonstrate that advanced AVS layouts not only reduce average yield penalties but also enhance yield uniformity across space. As shown in similar studies (e.g., Zainali et al., 2025; Asa'a et al., 2025), the temporal dynamics of light availability, rather than total shading percentage alone, play a decisive role in determining crop performance under AVS. Nonetheless, the trade-off between plant growth, biomass production and energy output from the photovoltaic system must be considered, since greater panel mobility or spacing, while beneficial for yield uniformity, may reduce the overall efficiency of electricity generation. The model proved also effective in estimating canopy surface temperature, capturing both its spatial variability within the field and its seasonal dynamics. This outcome indicates a realistic representation of the canopy radiative balance, with an appropriate partitioning of net radiation into latent and sensible heat fluxes. The seasonal patterns of canopy–air temperature differences ($\Delta T = T_{canopy} - T_{air}$) revealed clear treatment effects, with shaded plots (TR1 and TR4) consistently exhibiting lower canopy temperatures compared to the more light-exposed central treatments (TR2-TR3). The model reproduced these dynamics with good accuracy ($R^2 = 0.83$; MBE = –0.11 °C, Figure 9), confirming its ability to capture the complex interactions among water availability, transpiration, and canopy thermal regulation. These mechanisms became particularly evident under water-limiting conditions, as observed on DOY 241 (FTSW < 0.4 in all treatments; Figure 7). On this date, canopy–air temperature differences reached their maximum seasonal range, from values close to zero in the shaded corridor (TR1; $\Delta T \approx 0$ °C) to markedly positive in sun-exposed treatments (up to +4.5 °C in TR2 and +3.1 °C in TR3). The model successfully reproduced this gradient (+3.3 °C in TR3, +1.6 °C in TR4, and +0.3 °C in TR1), highlighting its capacity to simulate the coupling between transpiration and leaf energy balance. These results align with previous studies show that shading mitigates canopy heating and improves leaf thermal regulation (Alves et al., 2022; Chopard et al., 2024). Conversely, in sun-exposed plots, water stress exacerbated canopy warming, limiting transpiration-driven cooling and leading to positive ΔT values (Disciglio et al., 2025). Overall, the ability of the model to reproduce these contrasting responses emphasizes its suitability for exploring the role of microclimatic heterogeneity in modulating crop resilience to water stress and for assessing the potential benefits of shading strategies under future climate scenarios.

The scenario analysis (section 3.5) also highlights the strategic importance of the second harvest, which proved most responsive to moderate shading under drought. By slightly increasing pitch distance or temporarily adjusting panel tilt during this critical regrowth phase, it may be possible to maximize forage yield while limiting the impact on annual energy output. Such seasonal, model-guided adjustments could enhance the resilience and overall efficiency of AVS, aligning biomass production with periods of highest crop sensitivity without substantially reducing electricity generation. Beyond yield responses, our findings indicate that the panel-induced microclimate may foster conditions that promote long-term soil health and fertility. Moderate shading reduces canopy and soil temperatures, which in turn can lower evapotranspiration and slow the decomposition of soil organic matter (Luo et al., 2024). Additionally, rainfall redistribution along panel edges enhances soil moisture availability, supporting nutrient cycling and improving water-use efficiency. Therefore, future research should investigate these dynamics further to develop a comprehensive understanding of the soil–vegetation interplay under AVS, clarifying how improvements in soil conditions affect plant growth and how vegetation feedback, in turn, contribute to the enhancement of soil quality.

These results indicate that by resolving the contrasting impacts of different AVS configurations, the model can provide valuable insights for system design and management. Adaptable tracking architectures appear to enhance crop performance by promoting a more balanced distribution of light, while in fixed-panel systems, targeted management, such as prioritizing cultivation in less shaded inter-row corridors, may help mitigate yield penalties. These findings highlight the potential of integrated modelling approaches to translate morpho-physiological understanding into agronomic recommendations, thereby strengthening the role of modelling in supporting sustainable AVS deployment. In addition, the framework provides key inputs for future cost-benefit assessments and investment planning by quantifying, in advance, the interactions between shading, water dynamics and yield formation that underpin economic performance. This information can help farmers stabilize income, lower water and energy costs, and enhance the long-term profitability of AVS.

At the same time, some limitations should be acknowledged. Although the proposed framework proved robust in reproducing key physiological and yield responses, it does not yet account for certain crop processes (e.g nutrient uptake and limitation or biotic interactions) and for the microclimatic disturbances induced by photovoltaic panels, which may affect canopy-atmosphere interactions. Addressing these aspects would further improve the realism and applicability of the model under diverse agrivoltaic configurations. Another limitation lies in the relatively limited data set available for calibration. The restricted size and diversity of the calibration dataset may reduce the model's capacity to fully capture the variability observed across contrasting environmental conditions, management practices, and crop responses. As a result, further efforts should focus on expanding both calibration and validation datasets to enhance model generalization and reliability.

Photosynthesis was represented using a simplified formulation, with water stress was introduced by scaling assimilation with FTSW (Sinclair et al., 1986). This approach is parsimonious and widely applied (e.g. Moriondo et al., 2019; Leolini et al., 2023; Cui et al., 2024), but it does not explicitly capture stomatal regulation or the differential effects of water stress on biochemical parameters, potentially underestimating transient or heterogeneous stress responses. Further, in this empirical formulation both photosynthesis and transpiration decline when FTSW falls below 0.4 (Figure S2). Although this threshold was not experimentally determined for alfalfa, it is broadly consistent with values reported for other herbaceous legumes, including soybean, chickpea, and field pea (Soltani et al., 1999; Lecoeur & Sinclair, 1996).

Phenological development is driven by air rather than crop temperature, so neither potential shading effects nor the impact of water stress on canopy temperature that may alter thermal time accumulation are captured. Field evidence has previously shown that shading beneath photovoltaic panels can delay the phenological cycle of maize (Ramos-Fuentes et al., 2023) and durum wheat (Dal Prà et al. 2014) by lowering canopy temperature and reducing the incoming radiation. While no treatment-related differences were observed in this study with respect to the timing of phenological stages (e.g., anthesis), a parameterization based on crop temperature would likely offer a more effective representation of shading and water-stress effects, as implemented, for example, in the CropSyst model (Stöckle et al., 2003).

In our model, both photosynthesis and transpiration are scaled according to the fraction of transpirable soil water (FTSW) to account for water stress. This approach provides a simple and practical way to include the first-order effects of soil moisture limitation at the leaf or canopy level (Sinclair and Muchow, 2001). However, it assumes that reductions in photosynthesis and transpiration occur proportionally, which may not reflect plant physiology under drought. Stomatal closure often reduces transpiration more strongly than photosynthesis, leading to an increase in water use efficiency (Chaves et al., 2009). Similarly, photosynthetic capacity can be affected by biochemical limitations, especially under severe stress, whereas transpiration is primarily governed by stomatal behavior and atmospheric demand (Flexas et al., 2004). As a result, the responses of carbon assimilation and water loss to soil drying are generally not strictly proportional, and direct scaling with FTSW may oversimplify these dynamics. Incorporating the reciprocal modulation of stomatal conductance and photosynthetic capacity according to an iterative approach (e.g. Leuning et al., 1995) may preserve physiological realism, allowing carbon assimilation to be consistent to water stress and transpiration.

The model currently neglects the aerodynamic influence of photovoltaic panels, their effect on outgoing longwave radiation, and their potential cooling impact on air temperature, which is assumed constant. Incorporating these processes would improve the realism of simulated microclimatic conditions and canopy–atmosphere interactions under different AVS configurations.

The simulation of water harvesting and rainfall redistribution proved to be an important process influencing crop water balance. However, in bi-axial AVS (Site C), the dynamic movement of the panels makes this process particularly challenging to represent water fluxes as a function of panel orientation, and thus a no-water harvesting assumption was adopted for this configuration. Although the pitch-to-panel width ratio at Site C (12 m x 1.98 m) may have minimized the effect of water redistribution in plant growth, it likely contributed to the similarity in simulated FTSW values between treatments. Therefore, future investigations should account for the perturbations induced by dynamic panel movements on major environmental drivers and their cascading effects on the soil–plant system, as modulated by the pitch-to-panel width ratio.

In the fixed AVS, rainfall flux was assumed to fall perpendicularly to the ground surface, although in reality it reaches the soil at an angle, influenced by wind speed and panel geometry (Wu et al., 2022). This simplification may introduce bias in simulating water harvesting, especially in areas close to the photovoltaic panel. Once these processes are integrated, the framework could evolve into a comprehensive tool for reliably assessing crop performance under diverse AVS configurations and climatic conditions.

4.5 Conclusions

This study presents an integrated, process-based modelling framework designed to simulate the impacts of spatio-temporal shading on alfalfa growth under different AVS configurations. The results show that the system effectively captures the feedback between photovoltaic shading and crop performance. A key strength of the framework lies in its ability to dynamically couple simulated irradiance with crop morpho-physiological processes, reflecting plant adaptation to microclimatic variability. The model reliably reproduced dry matter yield, leaf area, canopy temperature and soil water dynamics across diverse shading scenarios, demonstrating its capacity to represent both light distribution and its interactions with plant physiology. The integration of morpho-physiological realism and computational scalability makes the framework a robust decision-support tool for optimizing AVS design and crop management in a site-specific context, with broad applications in agronomic research and precision agriculture. Incorporating a radiative and crop growth model within the same platform provides a clear advantage over alternative approaches, capturing the bidirectional feedback between shading and crop responses. The framework allows not only estimation of yield impacts under different shading scenarios but also active modulation of shading during key phenological stages. This capability enables targeted increases in light availability when crops are most sensitive, improving the assessment of trade-offs between energy and agricultural output. Overall, the tool supports dynamic, data-driven management of AVS, maximizing the combined benefits of food and electricity production.

Future developments should extend this approach to additional crop species with varying shade tolerance and incorporate other limiting factors, such as nutrient and pest dynamics, to further enhance predictive capacity under real-world agroecosystem conditions.

Conflict of Interest

The authors declare that the research was conducted in the absence of any commercial or financial relationships that could be construed as a potential conflict of interest.

Credit authorship contribution statement

Michele Moretta: Writing – original draft, Methodology, Formal analysis, Data curation, Conceptualization. **Marco Moriondo:** Writing – review & editing, Software, Methodology, Investigation, Formal analysis, Conceptualization. **Riccardo Rossi:** Writing – review & editing, Software, Methodology, Investigation, Formal analysis, Data curation, Conceptualization. **Gabriel Marçal da Cunha Pereira Carvalho:** Writing – review & editing. **Luisa Leolini:** Writing – review & editing, Methodology, Formal analysis. **Gloria Padovan:** Writing – review & editing. **Aldo Dal Prà:** Writing – review & editing, Investigation. **Enrico Palchetti:** Writing – review & editing, Project administration, Funding acquisition. **Giovanni Argenti:** Writing – review & editing, Investigation. **Nicolina Staglianò:** Writing – review & editing, Methodology, Investigation. **Anna Rita Balingit:** Writing – review & editing, Investigation.

Funding

This research received no external funding

Acknowledgements

The authors gratefully acknowledge Tozzi Green S.p.A. and REM TEC s.r.l. for providing access to the experimental sites.

Data Availability Statement

The raw data supporting the conclusions of this article will be made available by the authors, without undue reservation.

References

Acevedo, M., Álvarez-Maldini, C., Dumroese, R. K., González, M., Cartes, E., Bannister, J. R., Sandoval, S., Álvarez, A., & Stange, C. (2024). Decoupling seedling establishment in a shade-intolerant species of a Mediterranean climate: Soil moisture determines survival but growth is promoted by irradiance. Forest Ecology and Management, 569, 122190. https://doi.org/10.1016/j.foreco.2024.122190

Adeh, E. H., Selker, J. S., & Higgins, C. W. (2018). Remarkable agrivoltaic influence on soil moisture, micrometeorology and water-use efficiency. PLoS ONE, 13(11), e0203256. https://doi.org/10.1371/journal.pone.0203256

Ahmed, M. S., Khan, M. R., Haque, A., & Khan, M. R. (2022). Agrivoltaics analysis in a techno-economic framework: Understanding why agrivoltaics on rice will always be profitable. Applied Energy, 323, 119560.

Allen, R. G. (1996). Assessing integrity of weather data for reference evapotranspiration estimation. Journal of Irrigation and Drainage Engineering, 122(2), 97–106. https://doi.org/10.1061/(ASCE)0733-9437(1996)122:2(97)

Allen, R. G., Pereira, L. S., Raes, D., & Smith, M. (1998). Crop evapotranspiration: Guidelines for computing crop water requirements (FAO Irrigation and Drainage Paper No. 56). Food and Agriculture Organization of the United Nations.

Alves, C. M. L., Chang, H.-Y., Tong, C. B. S., Rohwer, C. L., Avalos, L., & Vickers, Z. M. (2022). Artificial shading can adversely affect heat-tolerant lettuce growth and taste, with concomitant changes in gene expression. Journal of the American Society for Horticultural Science, 147(1), 45–52. https://doi.org/10.21273/JASHS05124-21

Amaducci, S., Yin, X., & Colauzzi, M. (2018). Agrivoltaic systems to optimise land use for electric energy production. Applied Energy, 220, 545–561. https://doi.org/10.1016/j.apenergy.2018.03.081

Argenti, G., Parrini, S., Staglianò, N., & Bozzi, R. (2021). Evolution of production and forage quality in sown meadows of a mountain area inside Parmesan cheese consortium. Agronomy Research, 19(2), 344–356, 2021. doi:10.15159/AR.21.061

Artru, S., Dumont, B., Ruget, F., Launay, M., Ripoche, D., Lassois, L., & Garré, S. (2018). How does STICS crop model simulate crop growth and productivity under shade conditions? Field Crops Research, 215, 83–93. https://doi.org/10.1016/j.fcr.2017.10.005

Asa'a, S.-N., Lu, S. M., Kaaya, I., Dupon, O., de Jong, R., van der Heide, A., Bouguerra, S., Radhakrishnan, H. S., Poortmans, J., Campana, P. E., & Daenen, M. (2025). Evaluating the influence of different agrivoltaic topologies on PV energy, crop yields and land productivity in a temperate climate. Renewable Energy, 252, 123528. https://doi.org/10.1016/j.renene.2025.123528

Asseng, S., Turner, N. C., Botwright, T., & Condon, A. G. (2003). Evaluating the impact of a trait for increased specific leaf area on wheat yields using a crop simulation model. Agronomy Journal, 95(1), 10–19. https://doi.org/10.2134/agronj2003.1000b

Barron-Gafford, G. A., Pavao-Zuckerman, M. A., Minor, R. L., Sutter, L. F., Barnett-Moreno, I., Blackett, D. T., Thompson, M., Dimond, K., Gerlak, A. K., Nabhan, G. P., & Macknick, J. E. (2019). Agrivoltaics provide mutual benefits across the food–energy–water nexus in drylands. Nature Sustainability, 2(9), 848–855. https://doi.org/10.1038/s41893-019-0364-5

Bellasio, C. A generalised dynamic model of leaf-level C3 photosynthesis combining light and dark reactions with stomatal behaviour. Photosynthesis Research, 141, 99–118 (2019). https://doi.org/10.1007/s11120-018-0601-1

Bellone, Y., Croci, M., Impollonia, G., Nik Zad, A., Colauzzi, M., Campana, P. E., & Amaducci, S. (2024). Simulation-Based Decision Support for Agrivoltaic Systems. Applied Energy, 369. https://doi.org/10.1016/j.apenergy.2024.123490

Berrian, D., Chhapia, G., & Linder, J. (2025). Performance of land productivity with single-axis trackers and shade-intolerant crops in agrivoltaic systems. Applied Energy, 384, 125471. https://doi.org/10.1016/j.apenergy.2025.125471

Boland, J., Ridley, B., & Brown, B. (2008). Models of diffuse solar radiation. Renewable Energy, 33(4), 575–584. https://doi.org/10.1016/j.renene.2007.04.012

Brisson, N., Ruget, F., Gate, P., Lorgeou, J., Nicoullaud, B., Tayot, X., Plenet, D., Jeuffroy, M.-H., Bouthier, A., Ripoche, D., Mary, B., & Justes, E. (2002). STICS: A generic model for simulating crops and their water and nitrogen balances. II. Model validation for wheat and maize. Agronomie, 22, 69–92. https://doi.org/10.1051/agro:2001005

Brown, H. E., Moot, D. J., & Teixeira, E. I. (2006). Radiation use efficiency and biomass partitioning of lucerne (Medicago sativa) in a temperate climate. European Journal of Agronomy, 25(4), 319–327. https://doi.org/10.1016/j.eja.2006.06.008

Campana, P. E., Stridh, B., Amaducci, S., & Colauzzi, M. (2021). Optimisation of vertically mounted agrivoltaic systems. Journal of Cleaner Production, 325, 129091. https://doi.org/10.1016/j.jclepro.2021.129091

Campana, P. E., Stridh, B., Hörndahl, T., Svensson, S. E., Zainali, S., Lu, S. M., Zidane, T. E. K., de Luca, P., Amaducci, S., & Colauzzi, M. (2024). Experimental results, integrated model validation, and economic aspects of agrivoltaic systems at northern latitudes. Journal of Cleaner Production, 437. https://doi.org/10.1016/j.jclepro.2023.140235

Choi, C. S., Macknick, J., Li, Y., Bloom, D., McCall, J., & Ravi, S. (2023). Environmental Co-Benefits of Maintaining Native Vegetation With Solar Photovoltaic Infrastructure. Earth's Future, 11(6). https://doi.org/10.1029/2023EF003542

Chopard, J., Lopez, G., Persello, S., & Fumey, D. (2024). Modelling Canopy Temperature of Crops With Heterogeneous Canopies Grown Under Solar Panels. AgriVoltaics Conference Proceedings, 1. https://doi.org/10.52825/agripv.v1i.561

Crépeau, M., Jégo, G., Bélanger, G., Strullu, L., Duchemin, M., & Tremblay, G. (2025). Coupling the STICS model and CATIMO equations to simulate the growth and nutritive value of alfalfa. Agronomy Journal, 117, e70045. https://doi.org/10.1002/agj2.70045

Cui, B., Liu, J., Zhang, M. et al. CO2 elevation modulates the growth and physiological responses of soybean (Glycine max L. Merr.) to progressive soil drying. Plant Growth Regul 103, 139–150 (2024). https://doi.org/10.1007/s10725-023-01092-z

Dai, Y., Dickinson, R. E., & , Y. P. (2004). A two-big-leaf model for canopy temperature, photosynthesis, and stomatal conductance. Journal of climate, 17(12), 2281-2299.

Dinesh, H., & Pearce, J. M. (2016). The potential of agrivoltaic systems. In Renewable and Sustainable Energy Reviews (Vol. 54, pp. 299–308). Elsevier Ltd. https://doi.org/10.1016/j.rser.2015.10.024

Disciglio, G., Stasi, A., Tarantino, A., & Frabboni, L. (2025). Microclimate Modification, Evapotranspiration, Growth and Essential Oil Yield of Six Medicinal Plants Cultivated Beneath a Dynamic Agrivoltaic System in Southern Italy. Plants, 14(15), 2428. https://doi.org/10.3390/plants14152428

Dupraz, C. (2024). Assessment of the ground coverage ratio of agrivoltaic systems as a proxy for potential crop productivity. Agroforest Syst 98, 2679–2696. https://doi.org/10.1007/s10457-023-00906-3

Dupraz, C., Marrou, H., Talbot, G., Dufour, L., Nogier, A., & Ferard, Y. (2011). Combining solar photovoltaic panels and food crops for optimising land use: Towards new agrivoltaic schemes. Renewable Energy, 36(10), 2725–2732. https://doi.org/10.1016/j.renene.2011.03.005

Edouard, S., Combes, D., Van Iseghem, M., Ng Wing Tin, M., & Escobar-Gutiérrez, A. J. (2023). Increasing land productivity with agriphotovoltaics: Application to an alfalfa field. Applied Energy, 329, 120207. https://doi.org/10.1016/j.apenergy.2022.120207

Eichelmann, H., Oja, V., Rasulov, B., Padu, E., Bichele, I., Pettai, H., Mänd, P., Kull, O., & Laisk, A. (2005). Adjustment of leaf photosynthesis to shade in a natural canopy: Reallocation of nitrogen. Plant, Cell & Environment, 28(3), 389–401. https://doi.org/10.1111/j.1365-3040.2004.01275

Elamri, Y., Cheviron, B., Lopez, J.-M., Dejean, C., & Belaud, G. (2018). Water budget and crop modelling for agrivoltaic systems: Application to irrigated lettuces. Agricultural Water Management, 208, 440–453. https://doi.org/10.1016/j.agwat.2018.07.001

Evans, J. R. (2001). Photosynthetic acclimation of plants to growth irradiance: the relative importance of specific leaf area and nitrogen partitioning in maximizing carbon gain. Plant, Cell & Environment, 24(8), 755–767. https://doi.org/10.1046/j.1365-3040.2001.00724

Gonocruz, R. A., Nakamura, R., Yoshino, K., Homma, M., Doi, T., Yoshida, Y., & Tani, A. (2021). Analysis of the Rice Yield under an Agrivoltaic System: A Case Study in Japan. Environments, 8(7), 65. https://doi.org/10.3390/environments8070065

Goudriaan, J., Van Laar, H.H., 1994. Current Issues in Production Ecology. In: Modelling Potential Crop Growth Processes. Springer Netherlands, Dordrecht. https://doi.org/ 10.1007/978-94-011-0750-1

Grubbs, E. K., Gruss, S. M., Schull, V. Z., Gosney, M. J., Mickelbart, M. v., Brouder, S., Gitau, M. W., Bermel, P., Tuinstra, M. R., & Agrawal, R. (2024). Optimized agrivoltaic tracking for nearly-full commodity crop and energy production. Renewable and Sustainable Energy Reviews, 191. https://doi.org/10.1016/j.rser.2023.114018

He, Y., Wang, Y., Friedel, D., Lang, M., & Matthews, M. L. (2024). Connecting detailed photosynthetic kinetics to crop growth and yield: A coupled modelling framework. in silico Plants, 6(2), diae009. https://doi.org/10.1093/insilicoplants/diae009

Hemmerling, R., Kniemeyer, O., Lanwert, D., Kurth, W., Buck-Sorlin, G., 2008. The rule-based language XL and the modelling environment GroIMP illustrated with simulated tree competition. Functional Plant Biology 35, 739–750. https://doi.org/10.1071/FP08052

Holmgren, M., Gómez-Aparicio, L., Quero, J.L. et al. Non-linear effects of drought under shade: reconciling physiological and ecological models in plant communities. Oecologia 169, 293–305 (2012). https://doi.org/10.1007/s00442-011-2196-5

Jiang, S., Tang, D., Zhao, L., Liang, C., Cui, N., Gong, D., Wang, Y., Feng, Y., Hu, X., & Peng, Y. (2022). Effects of different photovoltaic shading levels on kiwifruit growth, yield and water productivity under 'agrivoltaic' system in Southwest China. Agricultural Water Management, 269, 107675. https://doi.org/10.1016/j.agwat.2022.107675

Juillion, P., Lopez, G., Fumey, D., Lesniak, V., Génard, M., & Vercambre, G. (2024). Combining field experiments under an agrivoltaic system and a kinetic fruit model to understand the impact of shading on apple carbohydrate metabolism and quality. Agroforestry Systems. Advance online publication. https://doi.org/10.1007/s10457-024-00965-0

Kirschbaum, M., Küppers, M., Schneider, H. et al. Modelling photosynthesis in fluctuating light with inclusion of stomatal conductance, biochemical activation and pools of key photosynthetic intermediates. Planta 204, 16–26 (1997). https://doi.org/10.1007/s0042500502

Laub, M., Pataczek, L., Feuerbacher, A., Zikeli, S., & Högy, P. (2022a). Contrasting yield responses at varying levels of shade suggest different suitability of crops for dual land-use systems: A meta-analysis. Agronomy for Sustainable Development, 42, 83. https://doi.org/10.1007/s13593-022-00783-7

Lecoeur, J., Wery, J., & Sinclair, T. R. (1996). Model of leaf area expansion in field pea subjected to soil water deficits. Agronomy Journal, 88(3), 467–472. https://doi.org/10.2134/agronj1996.00021962008800030018

Leolini, L., Bregaglio, S., Ginaldi, F., Costafreda-Aumedes, S., Di Gennaro, S. F., Matese, A., Maselli, F., Caruso, G., Palai, G., Bajocco, S., Bindi, M., & Moriondo, M. (2023). Use of remote sensing-derived fPAR data in a grapevine simulation model for estimating vine biomass accumulation and yield variability at sub-field level. Precision Agriculture, 24, 705–726. https://doi.org/10.1007/s11119-022-09970-8

Liu, X., Chen, F., Barlage, M., Zhou, G., & Niyogi, D. (2016). Noah-MP-Crop: Introducing dynamic crop growth in the Noah-MP land surface model. Journal of Geophysical Research: Atmospheres, 121(23), 13,953–13,972. https://doi.org/10.1002/2016JD025597

Ma, L. S., Zainali, S., Stridh, B., Avelin, A., Amaducci, S., Colauzzi, M., & Campana, P. E. (2022). Photosynthetically active radiation decomposition models for agrivoltaic systems applications. Solar Energy, 244, 536–549. https://doi.org/10.1016/j.solener.2022.05.046

Marrou, H., Dufour, L., & Wery, J. (2013). Microclimate under agrivoltaic systems: Is crop growth rate affected in the partial shade of solar panels? Agricultural and Forest Meteorology, 177, 117–132. https://doi.org/10.1016/j.agrformet.2013.04.012

Marsal, J., Johnson, S., Casadesus, J., Lopez, G., Girona, J., & Stöckle, C. (2014). Fraction of canopy intercepted radiation relates differently with crop coefficient depending on the season and the fruit tree species. Agricultural and Forest Meteorology, 184, 1–11. https://doi.org/10.1016/j.agrformet.2013.08.008

Mazzeo, D., Di Zio, A., Pesenti, C., & Leva, S. (2025). Optimizing agrivoltaic systems: A comprehensive analysis of design, crop productivity and energy performance in open-field configurations. Applied Energy, 390, 125750. https://doi.org/10.1016/j.apenergy.2025.125750

Meyers, T. P., & Hollinger, S. E. (2004). An assessment of storage terms in the surface energy balance of maize and soybean. Agricultural and Forest Meteorology, 125(1–2), 105–115. https://doi.org/10.1016/j.agrformet.2004.03.001

Mikhailova, E.A., Bryant, R.B., Cherney, D.J.R., Post, C.J., & Vassenev, I.I. (2000). Botanical composition, soil and forage quality under different management regimes in Russian grasslands. Agriculture, Ecosystems & Environment 80(3), https://doi.org/10.1016/S0167-8809(00)00148-1

Monteith, J. L. (1977). Climate and efficiency of crop production in Britain. Philosophical Transactions of the Royal Society of London. B, Biological Sciences, 281(980), 277–294. https://doi.org/10.1098/rstb.1977.0140

Morales, A., Kaiser, E., Yin, X., et al. Dynamic modelling of limitations on improving leaf CO2 assimilation under fluctuating irradiance. Plant Cell Environ. 2018; 41: 589–604. https://doi.org/10.1111/pce.13119

Moretta, M., Moriondo, M., Leolini, L., Padovan, G., Staglianó, N., Palchetti, E., Lanini, G. M., Bindi, M., & Rossi, R. (2025). Towards crop monitoring in agro-photovoltaic systems: An image-driven modeling approach for fAPAR-derived biomass estimation. European Journal of Agronomy, 170, 127748. https://doi.org/10.1016/j.eja.2025.127748

Moriondo, M., Leolini, L., Brilli, L., Dibari, C., Tognetti, R., Giovannelli, A., Rapisarda, B., Battista, P., Caruso, G., Gucci, R., Argenti, G., Raschi, A., Centritto, M., Cantini, C., & Bindi, M. (2019). A simple model simulating development and growth of an olive grove. European Journal of Agronomy, 105, 129–145. https://doi.org/10.1016/j.eja.2019.02.002

Poorter, H., Niinemets, Ü., Poorter, L., Wright, I.J. and Villar, R. (2009), Causes and consequences of variation in leaf mass per area (LMA): a meta-analysis. New Phytologist, 182: 565-588. https://doi.org/10.1111/j.1469-8137.2009.02830

Potenza, E., Croci, M., Colauzzi, M., & Amaducci, S. (2022). Agrivoltaic System and Modelling Simulation: A Case Study of Soybean (Glycine max L.) in Italy. Horticulturae, 8(12), 1160. https://doi.org/10.3390/horticulturae8121160

Prusinkiewicz, P., & Runions, A. (2012). Computational models of plant development and form. New Phytologist, 193(3), 549–569. https://doi.org/10.1111/j.1469-8137.2011.04009.x

Ramos-Fuentes, I. A., Elamri, Y., & Cheviron, B. (2023). Effects of shade and deficit irrigation on maize growth and development in fixed and dynamic AgriVoltaic systems. Agricultural Water Management, 280, 108183. https://doi.org/10.1016/j.agwat.2023.108183

Scarano, A., Semeraro, T., Calisi, A., Aretano, R., Rotolo, C., Lenucci, M. S., Santino, A., Piro, G., & De Caroli, M. (2024). Effects of the Agrivoltaic System on Crop Production: The Case of Tomato (Solanum lycopersicum L.). Applied Sciences, 14(7), 3095. https://doi.org/10.3390/app14073095

Sinclair, T. R., & Muchow, R. C. (1999). Radiation use efficiency. In D. L. Sparks (Ed.), Advances in Agronomy (Vol. 65, pp. 215–265). Academic Press. https://doi.org/10.1016/S0065-2113(08)60914-1

Sinclair, T. R., & Seligman, N. (2000). Criteria for publishing papers on crop modeling. Field Crops Research, 68(3), 165–172. https://doi.org/10.1016/S0378-4290(00)00105-2.

Sinclair, T. R., Shiraiwa, T., & Hammer, G. L. (1992). Variation in crop radiation-use efficiency with increased diffuse radiation. Crop Science, 32(5), 1281–1284. https://doi.org/10.2135/cropsci1992.0011183X003200050043

Sinclair, T.R., 1986. Water and nitrogen limitations in soybean grain production. I. Model development. Field Crops Research, 15(2), 125–141.Sinclair, T. R., & Ludlow, M. M. (1986). Influence of soil water supply on the plant water balance of four tropical grain legumes. Functional Plant Biology, 13(3), 329–341. https://doi.org/10.1071/PP9860329

Soltani, A., & Sinclair, T. R. (2012). Modelling physiology of crop development, growth and yield. Wallingford, UK: CABI. ISBN 978-1-84593-970-0

Soltani, A., Khooie, F. R., Ghassemi-Golezani, K., & Moghaddam, M. (2000). Thresholds for chickpea leaf expansion and transpiration response to soil water deficit. Field Crops Research, 68(3), 205–210. https://doi.org/10.1016/S0378-4290(00)00122-2

Steduto, P., Hsiao, T. C., & Fereres, E. (2007). On the conservative behavior of biomass water productivity. Irrigation Science, 25(3), 189–207. https://doi.org/10.1007/s00271-007-0064-1

Stöckle, C. O., Donatelli, M., & Nelson, R. (2003). CropSyst, a cropping systems simulation model. European Journal of Agronomy, 18(3–4), 289–307. https://doi.org/10.1016/S1161-0301(02)00109-0

Tahir, Z., & Butt, N. Z. (2022). Implications of spatial-temporal shading in agrivoltaics under fixed tilt & tracking bifacial photovoltaic panels. Renewable Energy, 190, 167–176. https://doi.org/10.1016/j.renene.2022.03.078

Teixeira, E. I., Brown, H. E., Meenken, E. D., & Moot, D. J. (2011). Growth and phenological development patterns differ between seedling and regrowth lucerne crops (Medicago sativa L.). European Journal of Agronomy, 35(1), 47–55. https://doi.org/10.1016/j.eja.2011.03.006

Teixeira, E. I., Moot, D. J., & Brown, H. E. (2009). Modelling seasonality of dry matter partitioning and root maintenance respiration in lucerne (Medicago sativa L.) crops. Crop and Pasture Science, 60(8), 778–784. https://doi.org/10.1071/CP08409

Teixeira, E. I., Moot, D. J., Brown, H. E., & Fletcher, A. L. (2007). The dynamics of lucerne (Medicago sativa L.) yield components in response to defoliation frequency. European Journal of Agronomy, 26(4), 394–400. https://doi.org/10.1016/j.eja.2006.12.005

Thom, A.S. and Oliver, H.R. (1977), On Penman's equation for estimating regional evaporation. Q.J.R. Meteorol. Soc., 103: 345-357. https://doi.org/10.1002/qj.49710343610

Valladares, F., & Niinemets, Ü. (2008). Shade tolerance, a key plant feature of complex nature and consequences. Annual Review of Ecology, Evolution, and Systematics, 39, 237–257. https://doi.org/10.1146/annurev.ecolsys.39.110707.173506

Van Oijen, M., Dreccer, M. F., Firsching, K.-H., & Schnieders, B. J. (2004). Simple equations for dynamic models of the effects of CO_2 and O_3 on light-use efficiency and growth of crops. Ecological Modelling, 179(1), 39–60. https://doi.org/10.1016/j.ecolmodel.2004.05.002

Wang, G., Liu, S., Liu, T., Fu, Z., Yu, J., & Xue, B. (2019). Modelling above-ground biomass based on vegetation indexes: a modified approach for biomass estimation in semi-arid grasslands. International Journal of Remote Sensing 40(10), 3835−3854. doi: 10.1080/01431161.2018.1553319

Waring, E. F., Perkowski, E. A., & Smith, N. G. (2023). Soil nitrogen fertilization reduces relative leaf nitrogen allocation to photosynthesis. Journal of Experimental Botany, 74(17), 5166–5180. https://doi.org/10.1093/jxb/erad195

Webber, H., White, J. W., Kimball, B. A., Ewert, F., Asseng, S., Eyshi Rezaei, E., Pinter, P. J. Jr., Hatfield, J. L., Reynolds, M. P., Ababaei, B., Bindi, M., Doltra, J., Ferrise, R., Kage, H., Kassie, B. T., Kersebaum, K.-C., Luig, A., Olesen, J. E., Semenov, M. A., … Martre, P. (2018). Physical robustness of canopy temperature models for crop heat stress simulation across environments and production conditions. Field Crops Research, 216, 75–88. https://doi.org/10.1016/j.fcr.2017.11.005

Weselek, A.; Ehmann, A.; Zikeli, S.; Lewandowski, I.; Schindele, S.; Högy, P., 2019. Agrophotovoltaic systems: applications, challenges, and opportunities. A review. Agron. Sustain. Dev. 39:35. https://doi.org/10.1007/s13593-019- 0581-3

Wu, C., Liu, H., Yu, Y., Zhao, W., Liu, J., Yu, H., & Yetemen, O. (2022). Ecohydrological effects of photovoltaic solar farms on soil microclimates and moisture regimes in arid Northwest China: A modeling study. Science of the Total Environment, 802, 149946. https://doi.org/10.1016/j.scitotenv.2021.149946

Xu, Z., Jiang, Y., Jia, B., Zhou, G., & Li, Y. (2020). Combined effects of heat and drought stress on the photosynthesis, chlorophyll fluorescence, and antioxidant defense of alfalfa (Medicago sativa L.). Photosynthetica, 58(5), 1217–1226. https://doi.org/10.32615/ps.2020.083

Yang, X., Brown, H. E., Teixeira, E. I., & Moot, D. J. (2022). Development of a lucerne model in APSIM next generation: 2. Canopy expansion and light interception of genotypes with different fall dormancy ratings. European Journal of Agronomy, 139, 126570. https://doi.org/10.1016/j.eja.2022.126570

Yang, Y., Bechelen, T., Dufour, L., & Lauri, P. É. (2022). Light distribution and productivity in apple trees trained to different architectures under photovoltaic panels. Agricultural and Forest Meteorology, 323, 109029. https://doi.org/10.1016/j.agrformet.2022.109029

Yin, X., Busch, F. A., Struik, P. C., & Sharkey, T. D. (2021). Evolution of a biochemical model of steady-state photosynthesis. Plant, Cell & Environment, 44(9), 2811–2837. https://doi.org/10.1111/pce.14070

Zainali, S., Lu, S. M., Fernández-Solas, Á., Cruz-Escabias, A., Fernández, E. F., Zidane, T. E. K., Honningdalsnes, E. H., Nygård, M. M., Leloux, J., Berwind, M., Trommsdorff, M., Amaducci, S., Gorjian, S., & Campana, P. E. (2025). Modelling, simulation, and optimisation of agrivoltaic systems: a comprehensive review. Applied Energy, 386, 125558. https://doi.org/10.1016/j.apenergy.2025.125558

Zhang, C., Campana, P., Yang, J., Zhang, J., & Yan, J. (2017). Can solar energy be an alternative choice of milk production in dairy farms? A case study of integrated PVWP system with alfalfa and milk production in dairy farms in China. Energy Procedia, 105, 3953–3959. https://doi.org/10.1016/j.egypro.2017.03.822

Zhang, Y., Homma, K., Shi, L., Wang, Y., Qiao, H., & Zha, Y. (2025). Improving crop modeling by simultaneously incorporating dynamic specific leaf area and leaf area index: A two-year experiment. Agricultural Systems, 227, 104357. https://doi.org/10.1016/j.agsy.2025.104357

Zhu, J., Dai, Z., Vivin, P., Gambetta, G.A., Henke, M., Peccoux, A., Ollat, N., Delrot, S., (2018). A 3-D functional-structural grapevine model that couples the dynamics of water transport with leaf gas exchange. Ann. Bot. 121, 833–848. https://doi.org/ 10.1093/aob/mcx141.

Zidane, T. E. K., Zainali, S., Bellone, Y., Guezgouz, M., Khosravi, A., Ma, L. S., Tekie, S., Amaducci, S., & Campana, P. E. (2025). Economic evaluation of one-axis, vertical, and elevated agrivoltaic systems across Europe: A Monte Carlo Analysis. Applied Energy, 391, 125826. https://doi.org/10.1016/j.apenergy.2025.125826

Chapter 5.

The Impact of Photovoltaic on Permanent Grassland Composition and Productivity in Central Italy

Chapter 5 has been based on the study:

Moretta,M.,Rossi,R.,Padovan, G., Staglianò,N.,Palchetti, E.,Campana,P.E., Bindi, M., Moriondo, M.

(2025). The Impact of Photovoltaic on Permanent Grassland Composition and Productivity in Central Italy.

AgriVoltaics Conference Proceedings, *3*.

https://doi.org/10.52825/agripv.v3i.1372

The Impact of Photovoltaic on Permanent Grassland Composition and Productivity in Central Italy

Michele Moretta[1], Riccardo Rossi[1] ,Gloria Padovan[1],Nicolina Staglianò[1],Enrico Palchetti[1], Marco Bindi[1], Pietro Elia Campana[2], and Marco Moriondo[3]

[1]Department of Agriculture, Food, Environment and Forestry, DAGRI, University of Florence,50144 Firenze, IT

[2] Mälardalen University, Future Energy Center, Västerås, Sweden

[3] Institute of BioEconomy, Italian Research Council (IBE-CNR),50145, Sesto Fiorentino, IT

*Correspondence: Michele Moretta, michele.moretta@unifi.it

Abstract. Climate change and population growth put a strain on energy and food resources, prompting a shift to renewable energy. The EU is aiming for 40 per cent renewable energy by 2030 and photovoltaic solar systems are expected as the primary source of electricity by 2035. However, the expansion of photovoltaics generates conflicts over land use, especially in agriculture. Agrivoltaic (AV) systems, which integrate photovoltaic panels with agricultural practices, offer a promising solution by providing crops with partial shade, thus potentially mitigating excessive sunlight and reducing water stress. This study evaluates the effects of an AV system on a 70 ha pasture in Ravenna, Italy, examining changes in pasture composition and productivity. In order to identify variations along the shadow gradient, four sampling areas were chosen along the transect perpendicular to the panel row, where plant species were identified and crop biomass sampled throughout the growing season in 2023. The results revealed a dominant presence of Grasses, with percentages of Leguminous ranging from 20 to 40% in less shaded areas, and other species present mainly in shaded areas, particularly in the back edge of the panel. Biomass yield showed considerable variation along the transect, with higher yields near the panels and lower below the central panels. The biomass peaks highlight the role of shading, sunlight and water drainage in production. These results emphasize the critical influence of shading in AV systems, providing insights for optimizing pasture management and crop selection to increase productivity under different light conditions.

Keywords: Agrivoltaic System, Grassland, Renewable energy

5.1 Introduction

Climate change and population growth are creating significant pressures on energy and food supply while the EU has stipulated that 40 percent of energy consumption must come from renewable resources by 2030 to mitigate greenhouse gas emissions. Advances in photo-voltaic (PV) technology and lower production costs are key to this transition. The International Energy Agency (IEA) predicts that solar PV will become the main source of electricity generation by 2035, with a capacity of 16% of global electricity production (International Energy Agency .,2023). This rapid expansion leads to land-use conflicts, emphasizing the need to consider the impact of photo-voltaic installations on arable land.

To address these challenges, an innovative concept has been proposed: Agrivoltaic (AV), a system that combines food and photovoltaic energy conversion on the same land. This system involves installing photovoltaic panels over crops, providing partial shading that can protect crops from excessive sunlight and reduce evapotranspiration during periods of water and heat stress (Dupraz et al.,2011; Marrou et al., 2013).

In this context, Italy is moving towards sustainable growth to meet EU targets with AV systems playing a crucial role. Over the next decade, the number of AV systems in Italy is expected to increase, supported also by PNRR funding (Ministry of Ecological Transition.,2022).

Studies on AV systems have examined several crops, including lettuce, potatoes, maize, winter wheat, rice, raspberries, cherry tomatoes and chillies. The results indicate a nonlinear relationship between crop yields and reductions in solar radiation for all crop types. Most crops can tolerate up to a 15% reduction in solar radiation, exhibiting a yield decline that is less than proportional (Reher et al.,2024; Touil et al.,2021; Laub et al.,2022). Herbaceous species, such as fescue and alfalfa, seem promising for growing under AV systems as they suffer water stress during summer and shading could improve their growth during these periods (Dupraz., 2024; Andrew et al.,2024; Edouard et al.,2023). However, further research is needed to understand how micro-environments under solar panels interact with management strategies and influence botanical composition and forage production (Madej et al.,2024).

This study presents a one-year investigation of the impact of an agrivoltaic system on a pasture ecosystem in Italy, with the objective of quantifying the adaptive responses of pasture composition and productivity in different areas of an agrivoltaic field.

5.2 Materials and Methods

The study was conducted in 2023 at a large agrivoltaic (AV) system in Ravenna, Italy, at Sant'Alberto (44°30'36.69" N, 12°9'18.72" E), where fixed photovoltaic panels are installed on a 70 ha permanent grassland. The grassland was sown in 2018, both between and beneath the panels, maintaining a 50 cm distance on both the right and left sides of the poles supporting the panels, and consists of a mixture of *Festuca arundinacea*, *Dactylis glomerata*, *Trifolium repens*, and *Medicago sativa*.The panels are 3 m long, have an inclination of 35 degrees with respect to the horizontal plane and are oriented along east-west direction. The side closest to the ground is mounted at a height of 1.30m, while the far side at 3 meters. The space between the poles supporting the structure is 8 meters, resulting in a Ground Coverage Ratio (GCR) of 38%. The experimental setup consisted of 3 randomized blocks with 3 replicas each, characterized by 4 selected areas along the transect perpendicular to the panel rows: G1, G2, G3, and G4 (Fig.1).

The sampling started in November 2022 and the last date was April 9, 2024 (sampling dates are specified in Fig. 1 and 2).

To investigate the impact of the AV system on grassland growth, species identification was conducted in each area, determining the percentage of Grasses, Leguminous, and Other species (GLA categories). Furthermore, to assess the influence on grassland productivity, systematic mowing was performed within designated 0.5 m x 0.5 m square plots for each area. The samples were dried at 65°C for 48 hours to calculate the percentage of dry matter and subsequently weighed.

This setup allowed for a detailed analysis of the effects of AV shading on both species composition and biomass yield of the grassland, providing insights into the interactions between AV systems and underlying vegetation.

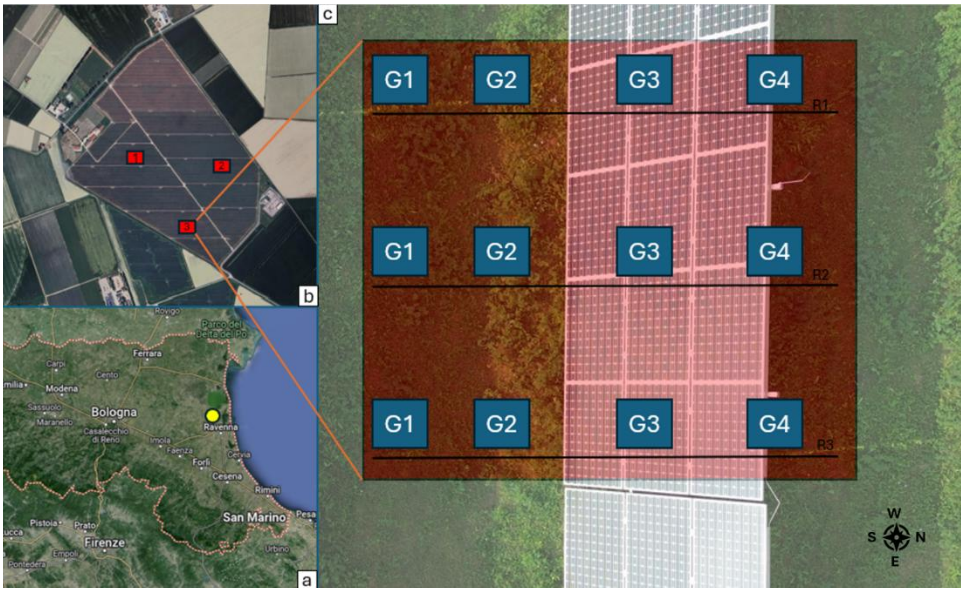

Figure 1. a) Location of the site in Emilia-Romagna, Italy. b) Experimental Field, Experimental Blocks in red. C) Spatial representation of sampling Areas. G1: the uncovered interspace adjacent to each panel; G2: front edge of each panel; G3: beneath the center of each panel; G4: back edge of each panel.

5.3 Results

In Fig. 2, a distinct pattern is evident where Grasses (G) have a predominant presence in most of the samples analyzed. Leguminosae (L), on the other hand, exhibit variable percentages ranging from 20% to 40%. The other species (O) shows a significant presence in some samples, particularly in the back edge of each panel, G4 group.

In the sample collected on 23 May 2023, the G3 group shows a very high predominance of Grasses, amounting to 90%. In the sample of 11 October 2023, group G1 shows a high proportion of other species, at 40%.

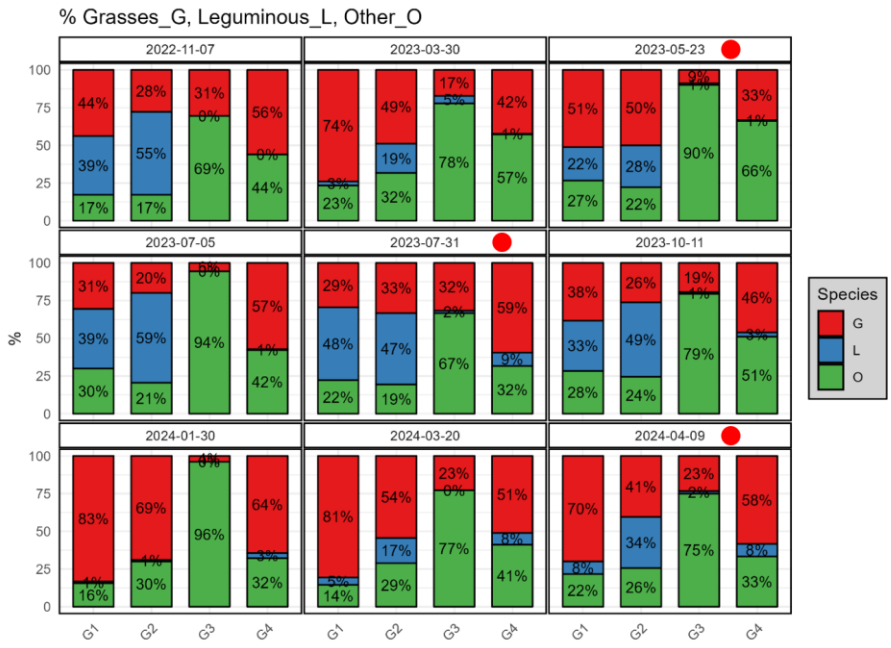

Figure 2. Evolution of the average GLO % detected in the sampling plots during the experiment.

In summary, in the sunniest areas, specifically G1 and G2, legumes tend to dominate over grasses and other species, particularly during the warmest periods. Conversely, in shadier areas, legumes are less prevalent. In G3, grasses and legumes consistently constitute a minority compared to other species. However, in G4, grasses exhibit an ability to adapt to conditions of very low direct radiation.

Fig.3 clearly illustrates how the biomass yield varies significantly over time and between the different distance groups. The most obvious peaks are observed on 23 May 2023, with group G1 and G2 showing significantly higher yields, and on 5 July 2023 with a peak for G2. Other increases are observed in the mowing periods, such as 31 July 2023 and 9 April 2024. However, in general, yields tend to be low, with only a few significant increases on certain dates and groups. The influence of the shading gradients of the AV panels is evident: the areas adjacent to the panels (G1 and G2) show a stronger seasonal trend and higher yields overall, influenced only by partial shading in the morning (G1). In 2023, the total biomass yield on five sampling dates was about 8.5 T DM/ha in the open locations (G1 and G2) and 4.8 T DM/ha under the panels (G3 and G4). This translates into a relative biomass yield of

78%, taking the yield of G2 as the reference point. The areas under the panels (G3 and G4) maintain more stable but generally lower yields, further suggesting the critical role of sunlight exposure and rainwater drainage in biomass production in these environments.

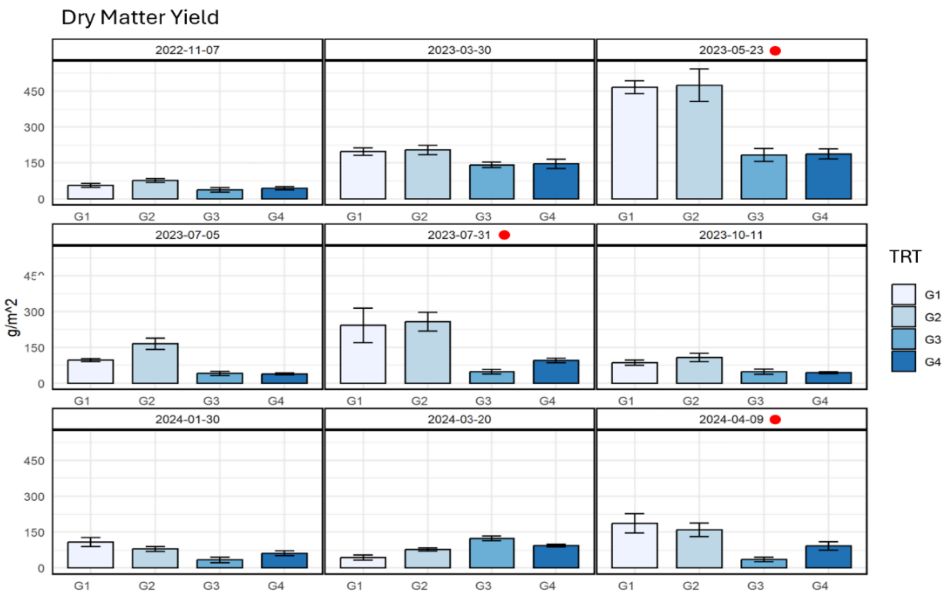

Figure 3. Barplots depicting the production of dry weight biomass (g/m2) in sampling plots during the experiment. The red icon indicates the harvest date.

5.4 Conclusion

This study demonstrates how the botanical composition and productivity of permanent grassland within Agrivoltaic (AV) systems with fixed photovoltaic panels are significantly influenced by shading conditions. Grasses were found to be the dominant species across most samples, while Leguminous and other species varied in presence depending on the shading gradient and temporal factors. Biomass yields showed notable variation, with higher yields observed in areas adjacent to the panels (G1 and G2) and lower, more consistent yields under the center (G3) and rear edge (G4) of the panels. The data suggest that optimizing shading management, such as increasing panel spacing or using adjustable tracking systems, could mitigate the negative effects of shading and potentially improve grassland productivity.

These findings offer preliminary insights that can help farmers explore species-specific strategies and adaptive grassland management practices to mitigate the challenges of shading and optimize the benefits of AV systems. The results of this study can be used as input into crop simulation models for future AV plant designs. Future agrivoltaic systems should explore strategies aimed at improving radiation management and water storage, supported by further research measuring key environmental factors such as light availability, soil moisture, and water dynamics.

Data availability statement

Data available upon reasonable request.

Author contributions

Conceptualization: Michele Moretta, Riccardo Rossi, Marco Moriondo **Data curation:** Michele Moretta, Riccardo Rossi, Marco Moriondo, Gloria Padovan. **Formal analysis**: Michele Moretta, Riccardo Rossi. Funding acquisition: Marco Bindi, Enrico Palchetti **Investigation:** Michele Moretta, Riccardo Rossi, Gloria Padovan, Marco Moriondo, Nicolina Staglianò. **Methodology:** Michele Moretta, Riccardo Rossi, Gloria Padovan, Marco Moriondo,Nicolina Staglianò, Pietro Elia Campana **Resources:** Enrico Palchetti, Marco Moriondo, Marco Bindi. **Writing – original draft:** Michele Moretta, Riccardo Rossi, Gloria Padovan, Marco Moriondo

Competing interests

The authors declare no competing interests

Funding

This material is based upon work supported byTozzi Green S.p.A., Ravenna, Italy.

Acknowledgement

The authors like to thank Tozzi Green S.p.A. for funding part of the activities.

References

Andrew, A. C., Higgins, C. W., Smallman, M. A., Prado-Tarango, D. E., Rosati, A., Ghajar, S., Graham, M., & Ates, S. (2024). Herbage and sheep production from simple, diverse, and legume pastures established in an agrivoltaic production system. Grass and Forage Science, 79(2), 294–307. doi: https.doi.org/10.1111/gfs.12653

C. Dupraz, "Assessment of the ground coverage ratio of agrivoltaic systems as a proxy for potential crop productivity," Agrofor. Syst., vol. 98, pp. 2679–2696, 2024, doi: https.doi.org/10.1007/s10457-023-00906-3

C. Dupraz, H. Marrou, G. Talbot, L. Dufour, A. Nogier, and Y. Ferard, "Combining solar photovoltaic panels and food crops for optimising land use: Towards new agrivoltaic schemes," Renew. Energy, vol. 36, no. 10, pp. 2725–2732, Oct. 2011, doi: https://doi.org/10.1016/j.renene.2011.03.005

H. Marrou, L. Guilioni, L. Dufour, C. Dupraz, and J. Wéry, "Microclimate under agrivoltaic systems: Is crop growth rate affected in the partial shade of solar panels?," Agric. Forest Meteorol., vol. 177, pp. 117–132, Apr. 2013, doi: https://doi.org/10.1016/j.agrformet.2013.04.012

International Energy Agency (2023), World Energy Outlook 2023, IEA,

J. Madej, L. Loan, C. Picon-Cochard, C. l'Ecluse, C. Cogny, L. Michaud, M. Roncoroni, and D. Colosse, "One Year of Grassland Vegetation Dynamics in Two Sheep-Grazed Agrivoltaic Systems," AgriVoltaics Conf. Proc., vol. 1, no. 1, Jan. 2024, doi: https.doi.org/10.52825/agripv.v1i.692

Laub, M., Pataczek, L., Feuerbacher, A. et al. Contrasting yield responses at varying levels of shade suggest different suitability of crops for dual land-use systems: a meta-analysis. Agron. Sustain. Dev. 42, 51 (2022). https://doi.org/10.1007/s13593-022-00783-7

Ministry of Ecological Transition, "Guidelines on Agrivoltaic Installations, Italy," 2022.

S. Edouard, D. Combes, M. Van Iseghem, M. Ng Wing Tin, and A. J. Escobar-Gutiérrez, "Increasing land productivity with agriphotovoltaics: Application to an alfalfa field," Appl. Energy, vol. 329, no. 120207, Jan. 2023, doi: https.doi.org/10.1016/j.apenergy.2022.120207

S. Touil, A. Richa, M. Fizir, and B. Bingwa, "Shading effect of photovoltaic panels on horticulture crops production: A mini review," Rev. Environ. Sci. Bio/Technol., vol. 20, no. 2, pp. 281–296, 2021.

T. Reher et al., "Potential of sugar beet (Beta vulgaris) and wheat (Triticum aestivum) production in vertical bifacial, tracked, or elevated agrivoltaic systems in Belgium," Appl. Energy, vol. 359, p. 122679, 2024, doi: https://doi.org/10.1016/J.APENERGY.2024.122679

Chapter 6.

Assessing the Impact of Agrivoltaic System on Pasture Plant and Soil Microarthropod Communities

Chapter 6 has been based on the study:

Michele Moretta, Filippo Gallese, Enrico Palchetti, Riccardo Rossi, France Joshua Rabit, Marco Moriondo, Giacomo Santini, Anita Maienza and Alberto Masoni

Submitted in: Journal of Sustainable Agriculture and Environment, Wiley

Assessing the Impact of Agrivoltaic Shading on Plant and Microarthropod Community Composition

Michele Moretta[1], Riccardo Rossi[1*], Enrico Palchetti[1], Marco Moriondo[2], France Joshua Rabit[3], Giacomo Santini[3], Filippo Gallese[2], Anita Maienza[2], Marco Bindi[1] and Alberto Masoni[3]

[1] Department of Agriculture, Food, Environment and Forestry (DAGRI), University of Florence (UNIFI), Piazzale delle Cascine 18, 50144, Florence, Italy

[2] Institute of BioEconomy of the National Research Council (CNR-IBE), via Madonna del Piano 10, 50019, Sesto Fiorentino (FI), Italy

[3] Department of Biology (BIO), University of Florence (UNIFI), Via Madonna del Piano 6, 50019, Sesto Fiorentino (FI), Italy

ABSTRACT

Agrivoltaic systems (AVS) integrate renewable energy production with agricultural use, creating novel microclimatic gradients that can affect ecosystem structure and function. However, the ecological consequences of these gradients on vegetation composition and soil biological quality remain poorly understood, particularly in pasture-based AVS configurations. In this study, we investigated seasonal and spatial changes in plant functional groups and soil microarthropod communities across shading gradients in a Mediterranean AVS pasture. Functional plant composition and biomass were assessed alongside the Pasture Value (PV) and the Soil Biological Quality-arthropods (QBS-ar) index as proxies for forage and soil biological quality. Results revealed marked seasonal differences driven by panel-induced microclimatic variability. In spring, when temperature and radiation contrasts were most pronounced, significant heterogeneity emerged across treatments, with higher PV and QBS-ar values in the inter-row zones, characterized by higher irradiance and adequate soil moisture. These areas supported the co-dominance of legumes and a richer assemblage of microarthropods, indicating a positive relationship between productive, nitrogen-fixing vegetation and soil faunal diversity. Conversely, shaded zones beneath panels, exposed to either combined shading and dryness or shading and waterlogging, hosted more stress-tolerant forb species and exhibited lower QBS-ar values, reflecting reduced biological quality under microclimatic extremes. This study highlights how integrative indicators such as PV and QBS-ar can effectively guide pasture management strategies aimed at optimizing forage productivity while preserving soil biological quality. Their combined use may also serve as a practical tool for long-term monitoring of soil fertility and ecosystem functioning in agrivoltaic grasslands.

Keywords: Functional biodiversity; Pasture integrity; PV index; QBS-ar index; Shading gradient

6.1. Introduction

The degradation of soil biological quality is one of the major problems that modern agriculture has to face (Karlen et al., 2015). Over recent decades, this issue has often been - linked with intensively industrialized, unsustainable agricultural practices that accelerate resource depletion, reduce ecosystem functioning, and increase vulnerability to extreme climatic events. Conventional agriculture, characterized by intensive tillage, the massive use of fertilizers, pesticides, and herbicides, may maximize short-term productivity but negatively affects sustainability and biodiversity (Le Campion et al., 2020). Furthermore, while the European Green Deal (European Commission, 2019) aims to achieve climate neutrality by 2050 through the promotion of the energy transition and the expansion of renewable energy sources, it may simultaneously lead to the unintended loss of arable and fertile lands.

Agrivoltaic systems (AVS), which integrate photovoltaic energy production with agricultural activities such as crop cultivation or livestock grazing, have emerged as a promising solution to mitigating this land-use conflict (Goetzberger & Zastrow, 1982; Al Mamun et al., 2022). Ongoing technological advances and the decreasing cost of photovoltaic modules have further stimulated interest in large-scale, ground-mounted AVS installations (Meneguzzo et al., 2015; Rosslowe & Petrovich, 2025). In particular, systems combining livestock grazing (e.g., sheep) with photovoltaic infrastructures have gained attention for their potential to modulate vegetation growth, reducing excessive biomass accumulation and management requirements, while maintaining sufficient forage availability and delivering additional ecological and economic co-benefits (Kochendoerfer et al., 2019; Byrnes et al., 2018; Freehill-Maye, 2020; Udroiu, 2023). For instance, pasture-based AVS have shown to maintain comparable lamb growth rates to open fields (≈120 g head^{-1} day^{-1}), while allowing for higher stocking densities and reduced water consumption under shaded conditions. Moreover, partial shading from photovoltaic panels helps preserve forage productivity during the summer, enhances animal welfare by mitigating heat stress, and increases overall land-use efficiency up to 200% through the joint production of renewable energy and livestock products (Andrew et al., 2021). However, potential trade-offs affecting crop yields and livestock feed must be considered in integrated AVS to maintain an optimal balance between agricultural production and energy generation.

As a matter of fact, the installation of AVS directly affects plant growth and development by modifying local microclimatic conditions through dynamic shading, which alters solar radiation, air and soil temperatures, and water availability (Weseleck et al.,2019; Amaducci et al.,2018; Moretta et al., 2024; Moretta et al 2025). Beneath photovoltaic panels, temperatures are often lower and more stable, particularly during hot seasons (Armstrong et al., 2016; Yue et al., 2021), and soil moisture may increase due to reduced evaporation, although the magnitude of this effect depends on module layout, spacing, and seasonal precipitation patterns (Hassanpour Adeh et al., 2018; Papadopoulos & Pantera, 2023). These changes have been observed to improve organic carbon stocks (Luo et al., 2024), while they may also entail potential risks such as salinization, reduced infiltration capacity, and increased pH (Chen et al., 2025). In turn, such modifications can influence plant productivity, community composition, and overall ecosystem functioning in context-dependent ways (Armstrong et al., 2014; Zhang et al., 2024). In temperate and cool climates, shading typically reduces biomass and species richness beneath the panels, whereas in Mediterranean environments, lower solar radiation can alleviate heat stress and enhance forage quality and availability, especially for shade-tolerant grasses (Vaverková et al., 2022; Adeh et al., 2019; Gill, 2024; Moretta et al., 2024).

Nonetheless, plant responses to exogenous factors remain difficult to generalize even within a single environment, as they vary depending not only on local conditions but also on species-specific functional traits and adaptation strategies. In this context, grasses are generally more tolerant to shade and respond positively to increased moisture, while legumes may be constrained by limited nodulation and lower carbon assimilation under reduced irradiance (Pang et al., 2019; Van Sambeek et al., 2007). Moreover, shallow-rooted annuals may struggle under dry conditions caused by limited rainfall when growing beneath partially or fully panel-covered zones, whereas deep-rooted species can access water redistributed by photovoltaic modules to surrounding areas (Pierret et al., 2016; Nippert & Holdo, 2015). Consequently, plant community composition adapts to the shading gradients induced by AVS, resulting in spatial variations of soil organic matter content and nutrient availability (Bertoldo et al., 2024).

These different patterns form the basis of bottom-up processes typical of grassland ecosystems, where the quality and abundance of plant-derived resources, such as root exudates and litter, drive the distribution of soil biota, including microarthropods (van

Eekeren et al., 2022). Such interactions are further reinforced by feedback effects, as the decomposition of organic matter and nutrient recycling by microarthropods enhance soil fertility and can thus promote the growth and development of key plant species for agricultural or grazing purposes (Menta et al., 2023; Orgiazzi et al., 2016). Recent studies have provided more detailed evidence of these dynamics. For instance, Fusco et al. (2023) demonstrated that, across contrasting Alpine habitats, soils harboring richer and more functionally diverse microarthropod communities, such as those in undisturbed forest, showed significantly higher biological quality and nutrient turnover, thereby fostering vegetation stability and productivity even under different management regimes. Similarly, Culliney (2013) emphasized the pivotal ecological roles of soil fauna, particularly detritivorous arthropods, in accelerating decomposition rates and nutrient cycling, ultimately enhancing soil structure and fertility.

At the same time, pedofauna is highly sensitive to varying edaphic conditions, which can strongly influence their activity, spatial distribution, and ecosystem functions (Delcourt et al., 2023; Erktan et al., 2020). In disturbed or compacted soils, epiedaphic and hemiedaphic microarthropods often dominate, whereas euedaphic forms are more prevalent in well-structured, biologically active soils (Lavelle et al., 2006; Wallwork, 1970; Maienza et al.,2023). Moderate shading and increased soil moisture under AVS can favor soil fauna, while excessive humidity or reduced organic inputs may depress its diversity and abundance (Moscatelli et al., 2022; Meloni et al., 2020). Furthermore, the optical properties of photovoltaic panels, including reflection and polarization, may also affect microarthropods orientation and behavior, contributing to the multifaceted faunal responses under AVS installations (Fox et al., 2007; Egri et al., 2016).

Given this complex functional diversity of vegetation and microarthropod communities in response to panel-induced microenvironmental variability, it is crucial to adopt approaches that allow for the characterization and assessment of their composition and interrelationships, in order to optimize the management of productive AVS. Among indices based on plant species composition previously proposed as proxies for forage quality and pasture integrity, the Pasture Value (PV) index stands out for its simplicity, stability over time and broad applicability (Argenti et al., 2006, 2017). This synthetic indicator quantifies the overall pastoral quality of a plant community by weighing species according to their forage value and has been widely used in Mediterranean and alpine grasslands to assess the ecological and productive status of pastures, providing valuable guidance for conservative grazing management (Argenti and Lombardi, 2012; Pornaro et al., 2019; Pittarello et al., 2018). On the other hand, the Soil Biological Quality-arthropods (QBS-ar) index offers a practical and affordable means to characterize soil arthropod communities without requiring species-level identification, relying on eco-morphological traits to infer their adaptation to edaphic conditions (Parisi et al., 2001, 2005; Menta et al., 2018; Gallese et al., 2025; Mantoni et al., 2021; D'Avino et al., 2023; Naglič et al., 2024). Although these indices perform well individually, they have not yet been applied in an integrated and comprehensive manner to capture the combined effects of shading gradients on both plant and soil arthropod communities and their interactions within an AVS.

Based on these premises, the present study aims to provide a comprehensive understanding of how microclimatic gradients induced by photovoltaic modules influence both plant and soil microarthropod community composition in a managed Mediterranean pasture. To this end, by jointly assessing PV and QBS-ar indices across two seasons and multiple shading treatments (CT, TRI–TR4), our approach captured the effects of shading intensity and precipitation patterns on above- and below-ground biodiversity and ecosystem functioning, providing critical insights to support the optimized management of agrivoltaic pastures.

6.2 Materials and Methods

6.2.1 Study area and experimental design

The study was conducted at the fixed APV located in Sant'Alberto (Ravenna, Italy; 44.51019° N, 12.1552° E), within the Po River Valley. This site, working since 2012, covers approximately 70 ha and consists of a permanent alfalfa (*Medicago sativa* L.) meadow integrated with ground-mounted photovoltaic panels.

The land-soil-ground is flat, ranging from 4 to 8 m a.s.l., and is characterized by a temperate climate with hot summers and cold winters. Mean annual temperature is 15 °C (minimum 5 °C in January; maximum 25.6 °C in July), and annual precipitation averages 767 mm, with November as the wettest month (87 mm) and January the driest (49 mm).

According to the official pedological cartography of the Emilia-Romagna Region (1:250.000; Figure 1), approximately two-thirds of the study area fall within class 2Aa, corresponding to soils in morphologically depressed areas of the alluvial plain. These soils are flat, with slopes typically ranging from 0.05% to 0.1%; very deep; fine-textured; calcareous; moderately alkaline; and characterized by moderate oxygen availability. The remaining portion belongs to class 3Ad, representing soils in morphologically elevated areas of the alluvial plain. These are also flat, with slopes generally between 0.08% and 0.3%; very deep; medium-textured; calcareous; moderately alkaline; and with oxygen availability varying from good to moderate. Overall, the soils can be classified as silty sand in the 0–60 cm layer, with an average composition of approximately 50% sand, 40% silt, and 10% clay (Regione Emilia-Romagna, 2024).

Photovoltaic modules are mounted on south-facing ground structures tilted at 35°, with tables 3.5 m wide and rows spaced 8 m apart, resulting in a ground cover ratio (GCR) of 38%. Panel height varies between 1.3 m at the lower edge and 3.3 m at the upper edge, creating a clear shading gradient across the field. The installation contributes about 45 GWh of electricity annually.

Before sowing in 2020, the soil was plowed to a 30 cm depth, tilled, and rolled to ensure optimal seed–soil contact and crop establishment under the AVS configuration. The site is managed under a rotational grazing system using Sardinian sheep breeds, with photovoltaic panel rows spacing and layout designed to minimize interference with grazing activity and pasture management.

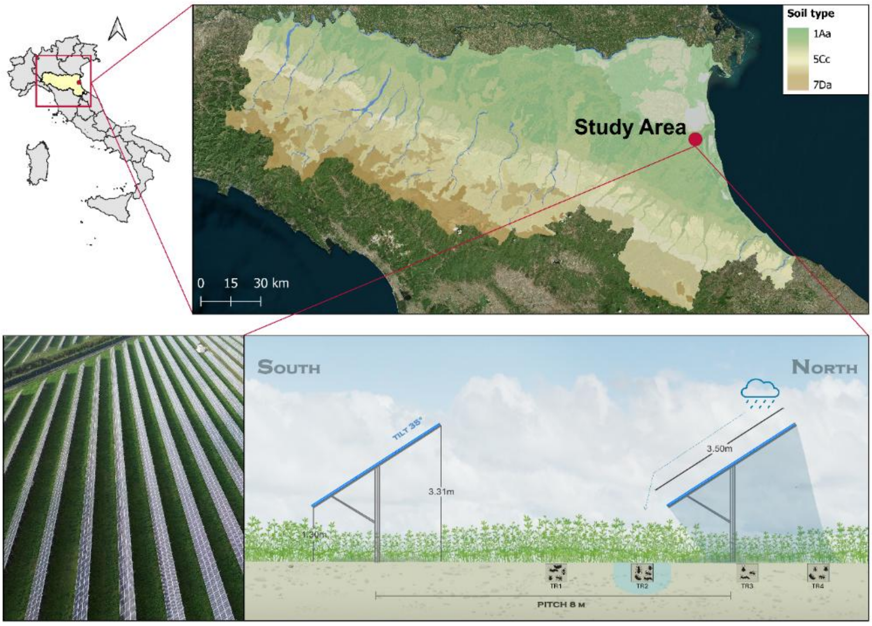

Figure 1. Location and technical layout of the study area, along with the disposition of the sampling treatments (TR1, TR2, TR3 and TR4). The soil map (1:250.000) is based on the official pedological cartography of the Emilia-Romagna Region, encompassing soil units ranging from delta plain soils (1Aa) to those of the lower (5Cc) and upper Apennines (7Da; source: https://geoportale.regione.emilia-romagna.it/).

The field experiment was carried out at the fixed APV site following a randomized complete block design with three blocks (B1, B2, B3) randomly distributed across the study area. Within each block, three transects were laid out perpendicular to the photovoltaic panel rows to capture spatial heterogeneity in light exposure and shading. Along the photovoltaic-induced shading gradient (Figure 1), four treatments were defined: TR1 (inter-row fully exposed, without run-off, ~7% of shading), TR2 (inter-row partially shaded with water run-off from panels, ~6% of shading), TR3 (front under-panel, ~67% of shading), and TR4 (rear under-panel, ~82% of shading). In addition, three external control areas were established along the eastern (CT1), south-eastern (CT2), and south (CT3) edges of the APV system. These control plots were not affected by panel shading or runoff but were cultivated and managed in the same way as the panel-covered meadow area.

6.2.2 Data Collection and processing

During two representative seasons (i.e., autumn 2023 and spring 2024), microenvironmental parameters, plant and microarthropod communities were surveyed within each block × treatment × replicate combination to assess the effects of the AVS on soil and biological components. All sampling plots were situated in areas where sheep grazing had been suspended since late summer 2022, in order to minimize short-term effects on soil and vegetation conditions.

6.2.2.1 Microenvironmental Data

Air temperature (T, °C) and relative humidity (RH, %) were recorded every 15 minutes using data loggers with built-in T/RH sensors (HOBO® Pro v2, Onset Computer Corporation, Pocassette, MA, USA) positioned outside (CT1), between (TR1) and under the photovoltaic panels (TR3). In addition, soil volumetric water content and soil temperature were determined in triplicate using a portable time-domain reflectometry probe (FieldScout TDR 350, Spectrum Technologies Inc., Aurora, IL, USA) on day of year (DOY) 326 (Autumn 2023), and on DOY 100 (Spring 2024).

Furthermore, an integrated modeling framework was adopted, based on the image-driven approach recently developed by Moretta et al. (2025). This framework combines proximal sensing data with a process-based crop model (SSM-iCrop2) to dynamically simulate crop growth responses under variable light and soil moisture conditions typical of AVS. Within this setup, daily estimates of the Fraction of Transpirable Soil Water (FTSW) and Intercepted Soil Radiation (ISR, MJ m^{-2} day^{-1}) were computed for the considered treatments using the validated SSM-iCrop2 model, forced with site-specific boundary conditions. In particular, FTSW was calculated using the water balance sub-model and represents the fraction of soil water between the wilting point and field capacity, while ISR was computed as the difference between incoming solar radiation and the fraction intercepted by the canopy. To capture the short- to mid-term effects of these microenvironmental variables on plant and soil communities, rather than their immediate daily fluctuations, the data were averaged over the 15 days preceding the sampling date. The model accounted for rainfall, runoff, drainage, and evapotranspiration when estimating the soil water balance, while ISR was derived through the three-dimensional GroIMP radiation module, which simulates the spatial partitioning of direct and diffuse radiation within the photovoltaic layout. For a detailed description of the modeling workflow and its validation, readers referred to Moretta et al. (2025).

6.2.2.2 Plant Data

On the same sampling days (DOY 326, 2023 and DOY 100, 2024), the botanical composition of the pasture was assessed in each experimental unit using a 1 × 1 m quadrat, randomly placed within each treatment area. Plant species were visually identified by a single experienced observer to minimize human bias between sampling dates. The relative cover of plant species (%) was then quantified and classified into three functional groups: palatable grasses (G), legumes (L), and species belonging to other botanical families (O). Within a pasture system, G typically represents the primary forage component providing bulk biomass, L contributes to nitrogen fixation and improve forage quality, and O includes forbs and non-leguminous plants, which may influence biodiversity and ecosystem functions (Menta et al., 2011; Birkhofer et al.,2011). Based on the collected data, a Pasture Value (PV) index was calculated for each experimental unit following the methodology of Argenti et al. (2017; Eq. 1).

$$PV = \frac{\Sigma SC_i \cdot SI_i}{5} \quad (1)$$

where SC_i is the relative cover (%) of each *i*-botanical species within the sampled quadrat, and SI_i is the specific index of forage value for that species, ranging from 0 to 5. For the functional groups considered in this study, the *SI* values were assigned as follows based on Argenti et al. (2006): G = 1.95, L = 2.99, O = 0.29.

Subsequently, for each treatment, three plants from the most representative species of the functional groups were collected, placed in separate bags, and refrigerated until processing. In the laboratory, leaves from each sample were individually detached, arranged on a white background, and photographed perpendicularly from above using a tripod-mounted digital camera. A metric ruler with millimeter markings was included in each image as a scale reference to calibrate measurements in the ImageJ® imaging software (https://imagej.nih.gov/ij/). The total leaf area of each plant was quantified (cm^2) using a color-thresholding approach and then averaged across the three replicates to obtain the mean total leaves area per species and treatment.

6.2.3 Microarthropod Data

The assessment of soil microarthropod communities was carried out through soil sampling performed on DOY 326 (2023) and DOY 100 (2024), following the standardized QBS-ar protocol proposed by D'avino et al. (2024). Both sampling dates were selected when soil temperature ranged from approximately 14 °C (DOY 326) to 24 °C (DOY 100) and soil moisture was close to field capacity, ensuring optimal conditions for the detection of active soil fauna (Table S1). To prevent escape of soil fauna during collection, the vegetation above each sampling point was clipped prior to soil removal. For each treatment (TR1–TR4) along the transects and in the controls (CT1-CT3), three undisturbed soil subsamples were collected at 0–10 cm depth (10 × 10 × 10 cm soil cube), avoiding the transition between the plough layer and the subsoil (Figure 2.A-C). In total, 78 soil samples were collected, including 72 from treatment plots (2 time points × 3 blocks x 4 treatments × 3 replicates) and 6 from control plots (2 time points × 3 blocks × 1 treatment × 1 replicate).

Samples were immediately placed in sealed black plastic containers and transported to the laboratory (within 4 h), where they were processed for microarthropod extraction using Berlese–Tullgren funnels. Specifically, each soil sample was placed under a 60 W incandescent lamp positioned approximately 30 cm above the funnel for seven days, creating a gradual light–heat gradient that induced the migration of arthropods from the soil matrix into the collecting vials (Figure 2.D). Collected specimens were examined under a stereomicroscope (Carl Zeiss Vision Italia Spa, Varese, Italy) at 80× magnification and identified into morpho-functional groups according to the eco-morphological index (EMI) used for QBS-ar evaluation (Parisi et al., 2005). Microarthropods were further categorized as epiedaphic ($1 < EMI \leq 4$), hemiedaphic ($4 < EMI \leq 8$), or euedaphic ($8 < EMI < 20$) as reported in Menta et al. (2015). For each morpho-functional group, the highest EMI score was recorded and subsequently summarized to calculate the QBS-ar for the associated soil sample, according to D'Avino et al. (2024).

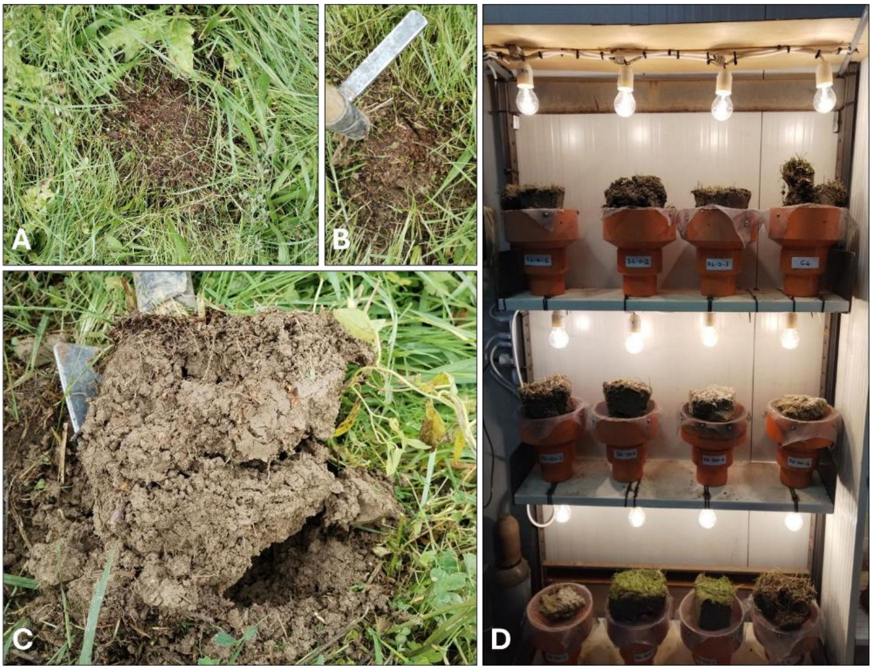

Figure 2. Procedure adopted for soil sampling and extraction of microarthropods in the AVS. **(A)** Removal of the vegetation layer at the sampling point. **(B)** Collection of a standardized soil cube (10 × 10 × 10 cm) using a steel corer. **(C)** Example of an extracted soil sample prior to laboratory processing. **(D)** Berlese-Tullgren funnels used for microarthropod extraction, with soil samples placed under a light–heat gradient to induce organism migration into the collecting vials.

6.2.3 Statistical Analysis

All statistical analyses were performed using R software (v. 4.3.3; R Core Team, 2024). The considered variables, including relative cover (%) of plant functional groups (G, L, O), relative abundance (%) of soil microarthropod functional groups (Epiedaphic, Hemiedaphic, Euedaphic), Plant Vegetation index (PV), Soil Biological Quality index (QBS-ar), Intercepted Soil Radiation (ISR), and Fraction of Total Soil Water (FTSW), were preliminarily tested for normality using the *Shapiro–Wilk* test and for homogeneity of variances using the *Levene* test. The percentage data were arcsine square-root transformed, while the remaining variables were log-transformed to achieve normality and satisfy the assumption of homogeneity of variances.

Differences in the mean values among treatments (CT, TR1–TR4) within each season (autumn and spring) and between seasons for the same treatment were assessed using one-way analysis of variance (ANOVA). *Treatment* and *season* were included as fixed effects, while *block* was treated as a random factor to account for spatial dependence within the experimental design, which was found to be not significant ($p > 0.05$). When significant differences were detected ($p < 0.05$), pairwise comparisons of means were performed using Tukey's HSD test. Finally, the relationships between the variables across treatments were evaluated using the Pearson correlation coefficient (r).

6.3 Results

6.3.1 Plant Community Composition

Across seasons, clear shifts were observed in the relative abundance of functional groups (Figure S1.A). Grasses (G) significantly decreased from autumn to spring ($p < 0.05$), while legumes (L) and other species (O) showed no significant seasonal variation.

During both sampling campaigns, consistent differences also emerged in the relative cover of functional groups along the shading gradient imposed by the photovoltaic panels (Figure 3). G represented the dominant component in both seasons, particularly in the control (CT) and front under-panel (TR3) treatments, where their cover was significantly higher than in the other plots. In autumn, grass cover peaked in CT and TR3, whereas inter-row (TR1) and rear under-panel (TR4) areas displayed lower values. L prevailed in TR1 and TR2 across both seasons, showing markedly higher percentages than in the shaded treatments, with the highest values recorded in spring. In contrast, TR3 and TR4 exhibited negligible legume presence, indicating that these under-panel conditions were unsuitable for nitrogen-fixing species. Conversely, O became increasingly dominant toward the shaded zones, particularly in TR4, where they reached the highest cover in both seasons. In spring, TR4 values were significantly greater than those of all other treatments, while in autumn the same trend was evident though less pronounced, with O species nearly absent in CT, TR1, and TR2 but sharply increasing under TR3 and TR4.

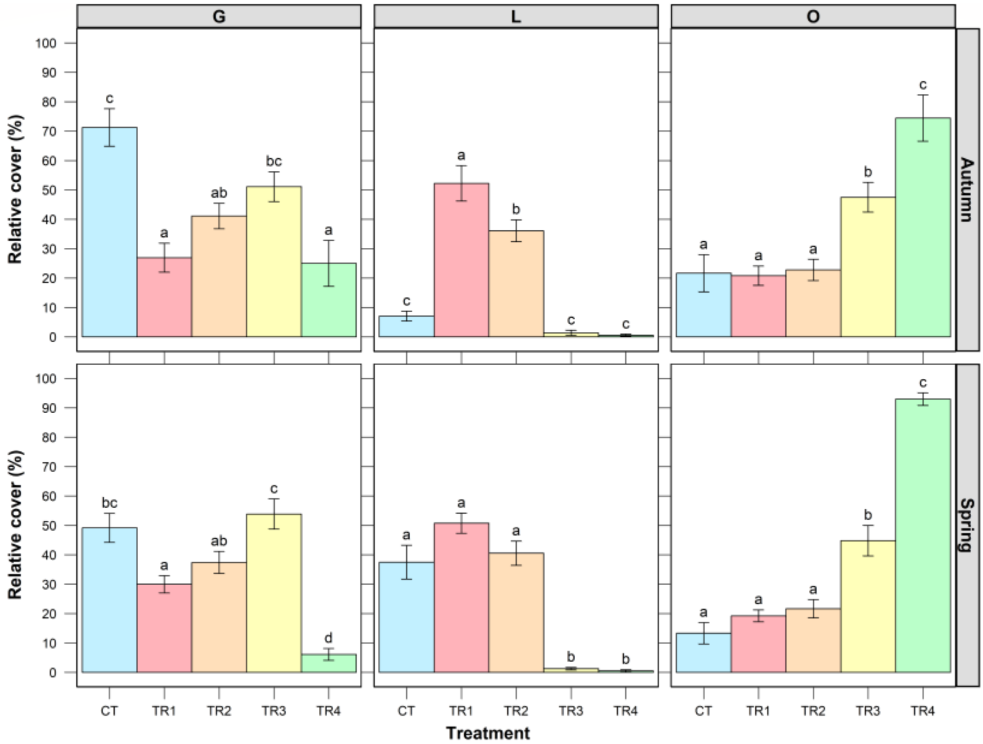

Figure 3. Average (± standard error) relative cover (%) of plant functional groups (G, L, O) across treatments (CT, TR1–TR4) and seasons (autumn and spring). Different letters above bars indicate significant differences among treatments within the same functional group and season according to Tukey's HSD test ($p < 0.05$).

6.3.2 Microarthropod Community Composition

The taxonomic composition of the soil arthropod community reflected these functional patterns, with Acarina and Collembola representing the dominant groups across all treatments and seasons (Table S2). In autumn, Acarina abundance was particularly high in TR2 and TR4, while Collembola peaked in TR2 and declined under the shaded positions (TR3–TR4). Minor taxa such as Hymenoptera, Coleoptera larvae, and Isopoda contributed to seasonal and spatial variability, showing higher occurrence in spring and in the rear under-panel area (TR4).

Seasonal differences in the relative abundance of microarthropod functional groups were observed (Figure S4.B). Epiedaphic taxa represented the largest proportion of the community in both autumn and spring, with no significant variation between seasons ($p > 0.05$).

Hemiedaphic microarthropods were significantly more abundant in autumn compared to spring ($p < 0.05$), accounting for over 60% of individuals in autumn and less than 40% in spring. Similarly, Euedaphic organisms showed a higher relative abundance in autumn than in spring ($p < 0.05$), although the magnitude of the seasonal difference was smaller compared to the hemiedaphic group.

These seasonal trends in functional group composition were further influenced by the distance from the crop row, as reflected in the treatment effects (Figure 4). In autumn, epiedaphic organisms were significantly more abundant in CT, TR1, and TR2, with no differences among them, whereas TR3 and TR4 exhibited a strong reduction in density ($p < 0.05$). A similar trend was observed for hemiedaphic microarthropods, which peaked in CT and were significantly lower in TR3 and TR4. Euedaphic organisms followed the same spatial pattern, with the highest densities in TR1 and TR2 and significantly lower values in TR3 and TR4.

In spring, overall densities were lower than in autumn, with no significant differences among treatments for epiedaphic and hemiedaphic groups. Nevertheless, Euedaphic microarthropods displayed a moderate decrease from CT to TR4, with significantly higher densities in CT compared to TR3 and TR4 ($p < 0.05$), while TR1 and TR2 showed intermediate values.

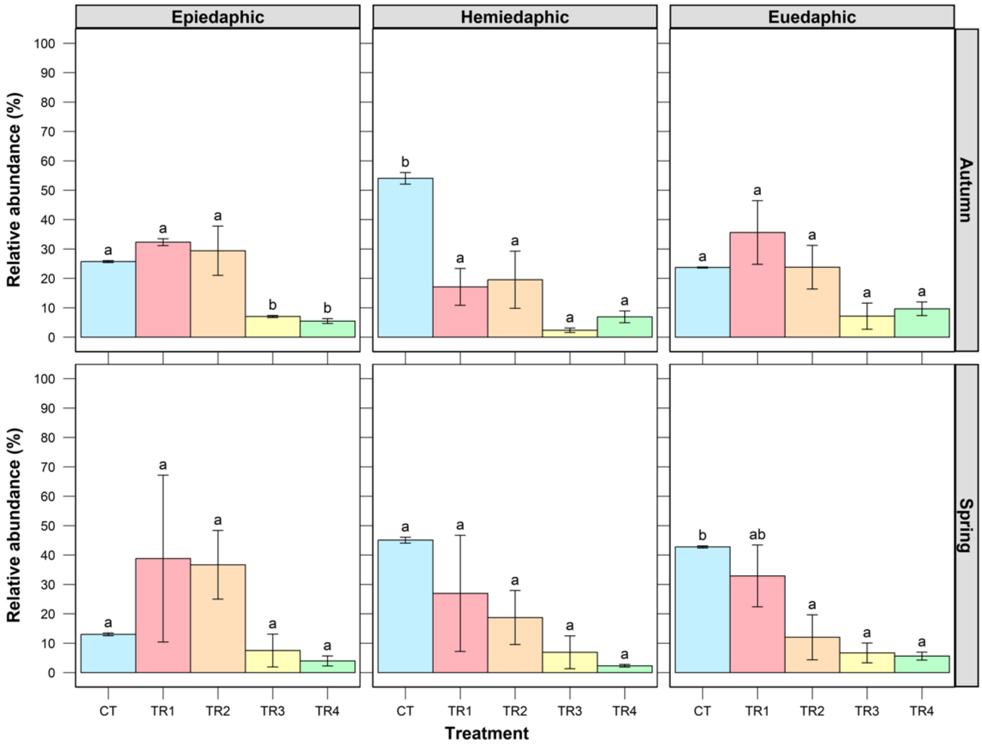

Figure 4. Average (± standard error) relative abundance (%) of soil microarthropod functional groups (Epiedaphic, Hemiedaphic, Euedaphic) across treatments (CT, TR1–TR4) and seasons (autumn and spring). Different letters above bars indicate significant differences among treatments within the same microarthropod functional group and season according to Tukey's HSD test ($p < 0.05$).

6.3.3 Impact of AVS on PV and QBS-ar

Both the PV and QBS-ar indexes showed clear and significant differences among treatments and between sampling seasons (Figure 5).

In terms of the PV index, the control treatment showed significantly lower values in autumn compared to spring ($p < 0.05$). Treatments TR1 and TR2 maintained consistently high PV values across both seasons, with no significant differences between them. In TR3, PV values were intermediate and not significantly different between autumn and spring, while TR4 showed the lowest PV percentages in both seasons. Notably, TR4 exhibited a significant seasonal decrease ($p < 0.05$), indicating reduced plant cover in spring.

The QBS-ar index revealed more marked seasonal variations. In TR2, TR3, and TR4, index values were significantly higher in autumn than in spring ($p < 0.05$), suggesting that soil biological quality declined under increased distance from the tree row during the spring season. In contrast, CT and TR1 did not show significant seasonal differences. Overall, the highest QBS-ar values were observed in TR2 and TR4 during autumn, indicating more favorable soil biological conditions at these distances during that period.

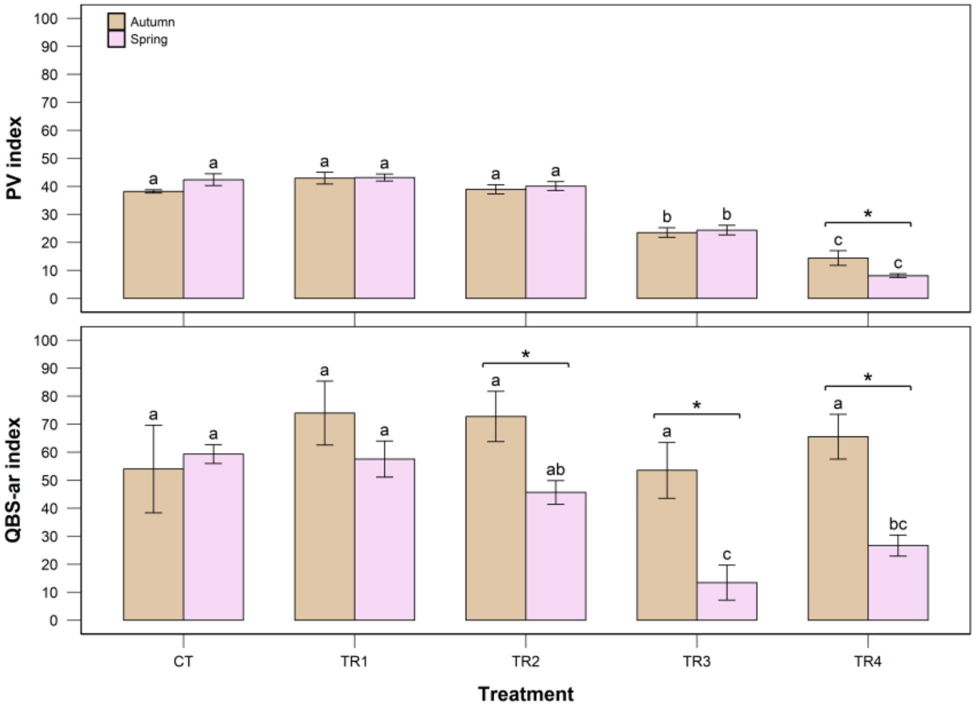

Figure 5. Average (± standard error) PV and QBS index across treatments (CT, TR1–TR4) and seasons (autumn and spring). Different letters above bars indicate significant differences among treatments within the same season according to Tukey's HSD test ($p < 0.05$), while asterisks denote significant differences between seasons for the same treatment ($p < 0.05$).

6.3.4 Relationships Between Plant and Microarthropod Community Composition

Given that significant differences in both PV and QBS-ar index were observed only in spring (Figure 5), all subsequent analyses were therefore focused on this sampling period. The PCA conducted on the combined dataset of microenvironmental, vegetation, and soil microarthropod indicators revealed a clear spatial segregation among treatments (Figure 6).

The first two principal components accounted for 82.6% of the total variance (PC1 = 52.7%; PC2 = 31.2%). Along PC1, the strong positive correlation between ISR and both PV and QBS-ar indices indicated that radiation was the primary driver of pasture productivity and soil quality across the shading gradient. Accordingly, inter-row areas characterized by higher irradiance (i.e., TR1 and TR2) were positioned on the positive side of PC1. Nevertheless, water redistribution also appeared to influence these patterns. Specifically, PV was higher in TR1, where full irradiance occurred but soil moisture was more limited, whereas the QBS-ar vector pointed toward TR2, where rainwater runoff from the panels increased soil moisture availability. In contrast, TR3 and TR4 (under-panel areas) clustered on the negative side, corresponding to shaded zones with lower light availability and reduced plant development. Along PC2, both the FTSW and the QBS-ar index showed positive loadings, clearly separating TR4 from the other treatments. This pattern indicates that the rear under-panel areas (TR4), despite their reduced vegetation cover, maintained higher soil moisture levels and supported distinct soil faunal communities. The persistent shading at this position likely limited evapotranspiration, resulting in localized water accumulation and almost constant soil moisture conditions.

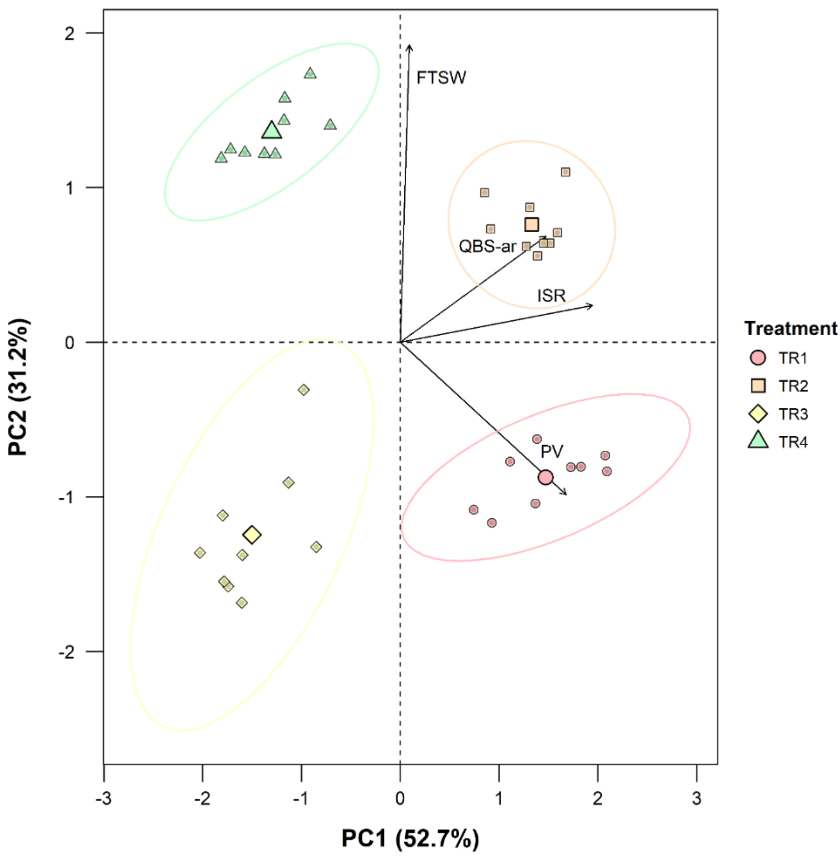

Figure 6. Principal Component Analysis (PCA) biplot showing the distribution of observations by treatment (TR1–TR4) during spring (DOY 100). Individual points represent replicates, while larger points indicate group centroids. Ellipses depict 95% confidence intervals for each treatment. Variable vectors (arrows) illustrate the contribution and direction of each measured variable to the first two principal components (PC1 and PC2), with the percentage of variance explained indicated on the axes. Variables included are Plant Vegetation index (PV), Soil Biological Quality index (QBS-ar), Fraction of Total Soil Water (FTSW), and Intercepted Soil Radiation (ISR).

Correlation analyses further supported the observed relationships among vegetation traits and microarthropod assemblages (Figure 7). In spring, the relative abundance of Euedaphic microarthropods was strongly and positively correlated with legume cover (r = 0.86) and negatively with "Other" species (r = -0.65), showing little relationship with grasses (r = 0.06). Hemiedaphic forms showed positive correlations with both grasses (r = 0.45) and legumes (r = 0.76), but a strong negative correlation with "Other" species (r = -0.80), indicating a preference for vegetation with greater legume and grass cover. Epiedaphic taxa also exhibited positive associations with legumes (r = 0.73) and to a lesser extent with grasses (r = 0.32), while being negatively related to "Other" species (r = -0.70).

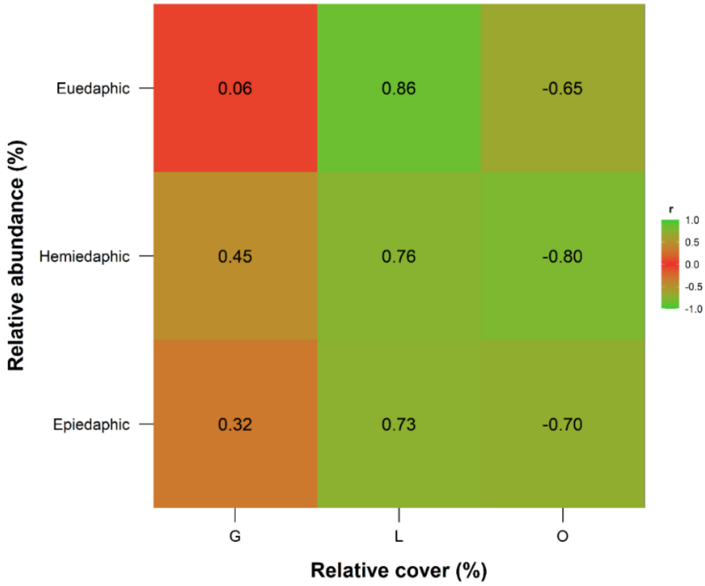

Figure 7. Heatmap showing Pearson's correlation coefficients (r) between relative abundance (%) and relative cover (%) of plant (G, L, O) and soil microarthropod (Euedaphic, Hemiedaphic, Epiedaphic) functional groups, respectively, during spring (DOY 100).

6.4 Discussion

This study provides novel insights into the functioning of pasture ecosystems within AVS, showing how microclimatic gradients created by photovoltaic panels shape both plant functional composition and soil biological quality. In particular, seasonal patterns emerged as key drivers of ecological variability, affecting both plant community assemblage and soil faunal across shading intensities.

During autumn, the overall integrity of the AVS-managed pasture, as indicated by the PV and QBS-ar indices, remained largely unaffected by panel-induced microclimatic variations (Figure 5). This stability can be attributed to the reduced biological activity of both plants and soil microarthropods under the generally unfavorable conditions characteristic of the Mediterranean cold season. Indeed, perennial grass growth is inherently constrained during the autumn-winter period by a combination of low temperatures and limited light availability, reflecting an adaptive strategy that promotes cold acclimation and ensures plant survival (Wingler and Hennessy, 2016). In our study, this seasonal pattern is confirmed by the pronounced decline in total canopy leaf area of key pasture species, including *Dactylis glomerata* L. (-30.06 %), *Trifolium repens* L. (-46.98 %), and *Medicago sativa* L. (-25.74 %), during autumn compared to spring (Figure S2). The reduction occurred consistently across all panel shading treatments, reflecting the generally low solar radiation at the experimental site (Figure S3), which minimized gradient-related differences. On the other hand, soil microarthropods, although generally resilient to cold, are known to respond to freezing risk by migrating to deeper soil layers (Holmstrup et al., 2018). This behavior likely explains the observed reduction in the relative abundance of epiedaphic organisms beneath photovoltaic panels (i.e., TR3 and TR4), where the lowest recorded autumnal temperatures (Figure S4) may have prompted them to seek refuge in subsurface strata (Siepel, 1994). Nevertheless, the QBS-ar index, which integrates the entire soil microarthropod community, buffered localized reductions in surface-dwelling organisms and reflected the overall stability of soil biological quality, in line with previous observations by Kardol et al. (2011).

Conversely, distinct differences in both plant functional composition and soil microarthropod communities became apparent during the spring season. This pattern was driven by active vegetative regrowth and increases in temperature and solar radiation, which amplified contrasts in resource availability, particularly light and water, across treatments. Notably, areas lacking rainfall redistribution from the photovoltaic panels but fully exposed to solar radiation (i.e., CT and TR1) favored the presence of therophyte plant species (i.e., *Geranium dissectum* L. and *Veronica persica* Poir.), reflecting their ecological adaptation to drier habitats with higher evapotranspiration rates (Midolo et al., 2024). Under high-shading conditions, plant distribution patterns indicate that light availability, rather than soil moisture, was the primary driver, as shown by the presence of shade-tolerant species beneath the photovoltaic panels (i.e., *Bromus mollis* L., *Daucus carota* L. and *Rumex alpinus* L.), where both dry (TR3) and moist (TR4) soils supported comparable plant assemblages (Jungová et al., 2025; Loarca et al., 2024). In this context, legumes, being typically heliophilous, predominantly colonized areas with high irradiance (i.e., TR1-TR2), whereas shaded zones (i.e., TR3-TR4) were mainly occupied by grasses and more stress-tolerant, ruderal taxa (Walgenbach and Marten, 1981; Lin et al., 1999; Qin et al., 2010). This functional differentiation has direct implications for forage yield, as demonstrated by Pang et al. (2019), who reported that under moderate or dense shading conditions, leguminous species exhibit reduced adaptability and lower productivity compared to grasses. Consequently, the high irradiance in TR1 provided favorable conditions for the establishment and growth of key forage legumes, thereby driving the association with the highest PV index (Figure 6).

Legumes play a crucial role in maintaining soil fertility and biological quality in pastures through biological nitrogen fixation (Ledgard and Steele, 1992). As demonstrated by Kanté et al. (2021), their rhizodeposition significantly increases soil enzymatic activity and microbial efficiency by providing readily available carbon and nitrogen compounds, thus promoting greater trophic complexity within the soil food web. Similarly, Ma et al. (2022) demonstrated that root exudate hotspots create favorable microhabitats for soil fauna, which foster greater functional diversity among microarthropods. Overall, these mechanisms likely explain the spatial pattern observed in our study, where microarthropod relative distribution mirrored that of legumes along the shading gradient, with higher values recorded in the inter-row areas. This is further supported by the strong positive correlation between legume relative cover and microarthropod abundance across soil layers, coupled with a negative association with low-forage-value species (O; Figure 7). The latter, lacking nitrogen-fixing capacity, prevailed under less favorable microclimatic conditions, either warmer and drier soils (TR3) or excessively moist environments prone to waterlogging (TR4), and were consequently ineffective in sustaining soil biological quality.

The integrated modeling framework adopted in this study (Moretta et al., 2025) was instrumental in characterizing these microclimatic gradients. By coupling process-based simulations of FTSW and ISR with field data, the model allowed us to quantify the combined effects of shading and soil water availability on plant-soil interactions, thereby providing a mechanistic explanation for the patterns observed across treatments. Consistent with these patterns, the QBS-ar index showed a clear tendency toward the microclimatic conditions under TR2 (Figure 6), where optimal combinations of soil moisture and irradiance were recorded (Table S3). This finding supports the notion that soil biological quality reaches its maximum under moist and thermally favorable conditions (Meloni et al., 2020; Moscatelli et al., 2022), which simultaneously promote the growth and functional performance of key pasture plant species.

The integration of PV and QBS-ar indices, as applied in the present study, highlighted the value of a comprehensive, site-specific assessment of AVS pastures to guide targeted management strategies that optimize both forage production and soil health. Such a consideration aligns with the broader principles outlined by Bacon et al. (2025), who advocate for a multi-disciplinary approach in AVS grazing systems, balancing energy production, animal welfare, and ecological integrity through adaptive, site-specific strategies. Practically, novel pasture management actions, such as rotational grazing or virtual fencing, should consider the heterogeneous distribution and functional composition of plant species across shading gradients and inter-row areas, aligning rest and grazing periods with ecological variability. Maintaining soil quality remains critical to these strategies, as it directly influences plant community composition, forage value, and overall pasture productivity. Therefore, future research should be extended to exploring the reciprocal interactions between grazing animals and AVS pastures, including: (i) the effects of selective feeding on the distribution of plant species and soil microarthropods, and (ii) the role of animal excreta in modulating soil biological quality. Adopting such integrated, site-tailored approaches will be essential for sustaining both ecological function and productive capacity in pasture-based AVS systems.

6.5. Conclusions

This study highlights how agrivoltaic systems (AVS) influence both plant and soil communities in pasture ecosystems through microclimatic gradients induced by photovoltaic panels. Across shading treatments, light availability and soil moisture jointly drove plant-soil interactions, with legumes supporting soil fertility and enhancing microarthropod communities. The combined use of PV and QBS-ar proved effective to capture fine-scale ecological variation, offering potential guidance for informed site-specific management strategies. In this context, future studies should further explore the interactions between grazing animals and AVS pastures, providing valuable insights for designing more resilient and biodiversity-friendly agroenergy systems. Overall, these studies underscore the value of microarthropods as indicators for assessing and monitoring soil quality, particularly in view of their potential integration within the framework of the Soil Monitoring Law, emanated by the Council of the European Union in 2024.

Funding

This research did not receive any specific grant from funding agencies in the public, commercial, or not-for-profit sectors.

CRediT authorship contribution statement

Michele Moretta: Conceptualization, Data curation, Methodology, Formal analysis, Investigation, Writing – original draft preparation. **Riccardo Rossi**: Conceptualization, Data curation, Investigation, Writing – original draft preparation. **Enrico Palchetti**: Project administration, Funding acquisition; Writing – review & editing. **France Joshua Rabit**: Investigation, Data curation, Writing – review & editing, Supervision. **Marco Moriondo**: Formal analysis, Methodology, Writing – review & editing. **Giacomo Santini**: Project administration; Writing – review & editing. **Filippo Gallese**: Formal analysis, Methodology, Writing – review & editing. **Anita Maienza**: Formal analysis, Methodology, Writing – review & editing. **Marco Bindi**: Funding acquisition, Writing – review & editing. **Alberto Masoni**: Investigation, Conceptualization, Methodology, Supervision, Writing – review & editing.

Declaration of Competing Interest

The authors declare that they have no known competing financial.

Data Availability

Data will be made available on request.

Acknowledgements

The authors are grateful to Tozzi Green S.p.A. for providing the experimental site and co-funding the research.

References

Adeh EH, Good SP, Calaf M, et al. Solar PV power potential is greatest over croplands. Sci Rep. 2019;9:11442. https://doi.org/10.1038/s41598-019-47803-3

Al Mamun MA, Dargusch P, Wadley D, Zulkarnain NA, Abdul Aziz A. A review of research on agrivoltaic systems. Renew Sustain Energy Rev. 2022;161:112351. https://doi.org/10.1016/j.rser.2022.112351

Andrew AC, Higgins CW, Bionaz M, Smallman MA, Ates S. Pasture production and lamb growth in agrivoltaic system. AIP Conf Proc. 2021;2361(1):060001. https://doi.org/10.1063/5.0055889

Amaducci S, Yin X, Colauzzi M. Agrivoltaic systems to optimise land use for electric energy production. Appl Energy. 2018;220:545–561. https://doi.org/10.1016/j.apenergy.2018.03.081

Argenti G, Bianchetto E, Ferretti F, Staglianò N. Proposal of a simplified method for pastures assessment in forest planning. Forest@ J Silvic For Ecol. 2006;3(2):275–280. https://doi.org/10.3832/efor0367-0030275

Argenti G, Lombardi G. The pasture-type approach for mountain pasture description and management. Ital J Agron. 2012;7(4):e39. https://doi.org/10.4081/ija.2012.e39

Argenti G, Bianchetto E, Ferretti F. Proposta di un metodo semplificato per la valutazione del valore pastorale nella pianificazione forestale. Ann Silvic Res. 2017;41(2):67–73. https://doi.org/10.12899/asr-1377

Armstrong A, Ostle NJ, Whitaker J. Solar park microclimate and vegetation management effects on grassland carbon cycling. Environ Res Lett. 2016;11(7):074016. https://doi.org/10.1088/1748-9326/11/7/074016

Armstrong A, Waldron S, Whitaker J, Ostle NJ. Wind farm and solar park effects on plant–soil carbon cycling: uncertain impacts of changes in ground-level microclimate. Glob Change Biol. 2014;20(6):1699–1706. https://doi.org/10.1111/gcb.12437

Bacon B, Calvert D, Hodge DL, Waller DM. Agrivoltaic grazing systems for a sustainable future: a multi-disciplinary review. Earth’s Future. 2025;13(2):e2023EF003675. https://doi.org/10.1029/2023EF003675

Bertoldo G, Chiodi C, Gavinelli F, Li S, Cagnin M, Del Todesco Frisone D, et al. Agrivoltaic panel shading influences soil nutrient dynamics and microbial community structure in a wheat-cultivated field [Preprint]. SSRN. 2024. https://ssrn.com/abstract=5379179

Birkhofer K, Diekötter T, Boch S, Fischer M, Müller J, Socher S, Wolters V. Soil fauna feeding activity in temperate grassland soils increases with legume and grass species richness. Soil Biol Biochem. 2011;43(11):2200–2207. https://doi.org/10.1016/j.soilbio.2011.07.008

Byrnes RC, Eastburn DJ, Tate KW, Roche LM. A global meta-analysis of grazing impacts on soil health indicators. J Environ Qual. 2018;47(4):758–765. https://doi.org/10.2134/jeq2017.08.0313

Chen H, Wu W, Li C, Lu G, Ye D, Ma C, Li G. Ecological and environmental effects of global photovoltaic power plants: a meta-analysis. J Environ Manage. 2025;373:123785. https://doi.org/10.1016/j.jenvman.2025.123785

Culliney TW. Role of arthropods in maintaining soil fertility. Agriculture. 2013;3(4):629–659. https://doi.org/10.3390/agriculture3040629

D'Avino L, Bigiotti G, Vitali F, Tondini E, L'Abate G, Jacomini C, et al. QBS-ar and QBS-ar_BF index toolbox for biodiversity assessment of microarthropod community in soil (version 3.0) [Dataset]. Zenodo. 2024. https://doi.org/10.5281/zenodo.14070537

Delcourt N, Dupuy N, Rébufa C, Aupic-Samain A, Foli L, Farnet-Da Silva A-M. Rapid assessment of land use legacy effect on forest soils: a case study on microarthropods used as indicators in Mediterranean post-agricultural forests. Forests. 2023;14(11):2223. https://doi.org/10.3390/f14112223

Egri Á, Farkas A, Kriska G, Horváth G. Polarization sensitivity in Collembola: an experimental study of polarotaxis in the water-surface-inhabiting springtail Podura aquatica. J Exp Biol. 2016;219(16):2567–2576. https://doi.org/10.1242/jeb.139295

Erktan A, Or D, Scheu S. The physical structure of soil: determinant and consequence of trophic interactions. Soil Biol Biochem. 2020;148:107876. https://doi.org/10.1016/j.soilbio.2020.107876

European Commission. Communication from the Commission to the European Parliament, the European Council, the Council, the European Economic and Social Committee and the Committee of the Regions: European Green Deal, COM(2019) 640 final, 11 December 2019. Brussels: European Commission; 2019.

Fox GL, Coyle-Thompson CA, Bellinger PF, Cohen RW. Phototactic responses to ultraviolet and white light in various species of Collembola, including the eyeless species Folsomia candida. J Insect Sci. 2007;7(1):22. https://doi.org/10.1673/031.007.2201

Freehill-Maye L. A new vision for farming: chickens, sheep, and… solar panels. The Christian Science Monitor. 2020 Apr 23.

Fusco T, Fortini L, Casale F, Jacomini C, Di Giulio A. Assessing soil quality of Italian Western Alps protected areas by QBS-ar: impact of management and habitat type on soil microarthropods. Environ Monit Assess. 2023;195(11):1287. https://doi.org/10.1007/s10661-023-11880-9

Gallese F, Gismero-Rodriguez L, Govednik A, Giagnoni L, Lumini E, Suhadolc M, et al. Soil microarthropods as tools for monitoring soil quality: the QBS-ar index in three European agroecosystems. Agriculture. 2025;15(1):89. https://doi.org/10.3390/agriculture15010089

Gill B. Agrivoltaics – sheep grazing in solar farms; good for both. Agriculture Victoria – Energy Smart Farming. 2024 Apr 30.

Goetzberger A, Zastrow A. On the coexistence of solar-energy conversion and plant cultivation. Int J Solar Energy. 1982;1(1):55–69. https://doi.org/10.1080/01425918208909875

Hassanpour Adeh E, Selker JS, Higgins CW. Remarkable agrivoltaic influence on soil moisture, micrometeorology and water-use efficiency. PLoS One. 2018;13(11):e0203256. https://doi.org/10.1371/journal.pone.0203256

Holmstrup M, Ehlers BK, Slotsbo S, Ilieva-Makulec K, Sigurdsson BD, Leblans NIW, et al. Functional diversity of Collembola is reduced in soils subjected to short-term, but not long-term, geothermal warming. Funct Ecol. 2018;32(5):1304–1316. https://doi.org/10.1111/1365-2435.13058

Jungová M, Kadlecová M, Pavlů V, Lejšová-Svobodová L, Svoboda P, Martinková Z. Ecological implications of germination temperature on native and invasive Rumex spp. Plant Environ Interact. 2025;6(2):e70045. https://doi.org/10.1002/pei3.70045

Kanté M, Riah-Anglet W, Cliquet J-B, Trinsoutrot-Gattin I. Soil enzyme activity and stoichiometry: linking soil microorganism resource requirement and legume carbon rhizodeposition. Agronomy. 2021;11(11):2131. https://doi.org/10.3390/agronomy11112131

Kardol P, Reynolds WN, Norby RJ, Classen AT. Climate change effects on soil microarthropod abundance and community structure. Appl Soil Ecol. 2011;47(1):37–44. https://doi.org/10.1016/j.apsoil.2010.11.001

Karlen DL, Rice CW. Soil degradation: will humankind ever learn? Sustainability. 2015;7(9):12490–12501. https://doi.org/10.3390/su70912490

Kochendoerfer N, Hain L, Thonney ML. The agricultural, economic and environmental potential of co-locating utility-scale solar with grazing sheep. Cornell Univ Atkinson Cent Sustain Future. 2019.

Lavelle P, Decaëns T, Aubert M, Barot S, Blouin M, Bureau F, Rossi J-P. Soil invertebrates and ecosystem services. Eur J Soil Biol. 2006;42:S3–S15. https://doi.org/10.1016/j.ejsobi.2006.10.002

Ledgard SF, Steele KW. Biological nitrogen fixation in mixed legume/grass pastures. Plant Soil. 1992;141:137–153. https://doi.org/10.1007/BF00011314

Le Campion A, Oury FX, Heumez E, Rolland B. Conventional versus organic farming systems: dissecting comparisons to improve cereal organic breeding strategies. Org Agric. 2020;10:63–74. https://doi.org/10.1007/s13165-019-00249-3

Lin CH, McGraw RL, George MF, Garrett HE. Shade effects on forage crops with potential in temperate agroforestry practices. Agrofor Syst. 1999;44:109–119. https://doi.org/10.1023/A:1006205116354

Loarca J, Liou M, Dawson JC, Simon PW. Evaluation of shoot-growth variation in diverse carrot (Daucus carota L.) germplasm for genetic improvement of stand establishment. Front Plant Sci. 2024;15:1342512. https://doi.org/10.3389/fpls.2024.1342512

Luo J, Luo Z, Li W, Shi W, Sui X. The early effects of an agrivoltaic system within a different crop cultivation on soil quality in dry–hot valley eco-fragile areas. Agronomy. 2024;14(3):584. https://doi.org/10.3390/agronomy14030584

Ma W, Tang S, Dengzeng Z, Zhang D, Zhang T, Ma X. Root exudates contribute to belowground ecosystem hotspots: a review. Front Microbiol. 2022;13:937940. https://doi.org/10.3389/fmicb.2022.937940

Maienza A, Remelli S, Verdinelli M, Baronti S, Crisci A, Vaccari FP, Menta C. A magnifying glass on biochar strategy: long-term effects on the soil biota of a Tuscan vineyard. J Soils Sediments. 2023;23(4):1733–1744. https://doi.org/10.1007/s11368-023-03447-5

Mantoni C, Pellegrini M, Dapporto L, Del Gallo MM, Pace L, Silveri D, Fattorini S. Comparison of soil biology quality in organically and conventionally managed agro-ecosystems using microarthropods. Agriculture. 2021;11(10):1022. https://doi.org/10.3390/agriculture11101022

Meloni F, Civieta BF, Zaragoza JA, Moraza ML, Bautista S. Vegetation pattern modulates ground arthropod diversity in semi-arid Mediterranean steppes. Insects. 2020;11(1):59. https://doi.org/10.3390/insects11010059

Meneguzzo F, Ciriminna R, Albanese L, Pagliaro M. The great solar boom: a global perspective into the far-reaching impact of an unexpected energy revolution. Energy Sci Eng. 2015;3(6):499–509. https://doi.org/10.1002/ese3.98

Menta C, Leoni A, Gardi C, et al. Are grasslands important habitats for soil microarthropod conservation? Biodivers Conserv. 2011;20:1073–1087. https://doi.org/10.1007/s10531-011-0017-0

Menta C, Conti FD, Pinto S, Bodini A. Soil biological quality index (QBS-ar): 15 years of application at global scale. Ecol Indic. 2018;85:773–780. https://doi.org/10.1016/j.ecolind.2017.11.030

Menta C, Remelli S, Andreoni M, Gatti F, Sergi V. Can grasslands in photovoltaic parks play a role in conserving soil arthropod biodiversity? Life. 2023;13(7):1536. https://doi.org/10.3390/life13071536

Menta C, Tagliapietra A, Caoduro G, Zanetti A, Pinto S. IBS-BF and QBS-ar comparison: two quantitative indices based on soil fauna community. EC Agric. 2015;2(5):427–439.

Midolo G, Axmanová I, Divíšek J, Dřevojan P, Lososová Z, Večeřa M, et al. Diversity and distribution of Raunkiær's life forms in European vegetation. J Veg Sci. 2024;35:e13229. https://doi.org/10.1111/jvs.13229

Moretta M, Moriondo M, Leolini L, Padovan G, Staglianó N, Palchetti E, et al. Towards crop monitoring in agro-photovoltaic systems: an image-driven modeling approach for fAPAR-derived biomass estimation. Eur J Agron. 2025;170:127748. https://doi.org/10.1016/j.eja.2025.127748

Moretta M, Rossi R, Padovan G, Staglianó N, Palchetti E, Bindi M, Moriondo M. The impact of photovoltaic on permanent grassland composition and productivity in Central Italy. AgriVoltaics Conf Proc. 2024;3. https://doi.org/10.52825/agripv.v3i.1372

Moscatelli MC, Marabottini R, Massaccesi L, Marinari S. Soil properties changes after seven years of ground mounted photovoltaic panels in Central Italy coastal area. Geoderma Reg. 2022;29:e00500. https://doi.org/10.1016/j.geodrs.2022.e00500

Naglič V, Šibanc N, Grebenc T, Bertoncelj I. Soil mesofauna diversity in agricultural systems of Slovenia using the QBS index and its modifications. Acta Biol Slov. 2024;68(1).

Nippert JB, Holdo RM. Challenging the maximum rooting depth paradigm in grasslands and savannas. Funct Ecol. 2015;29:739–745. https://doi.org/10.1111/1365-2435.12390

Orgiazzi A, Panagos P, Yigini Y, Dunbar MB, Gardi C, Montanarella L, Ballabio C. A knowledge-based approach to estimating the magnitude and spatial patterns of potential threats to soil biodiversity. Sci Total Environ. 2016;545–546:11–20. https://doi.org/10.1016/j.scitotenv.2015.12.091

Pang K, Van Sambeek JW, Navarrete-Tindall NE, Lin CH, Jose S, Garrett HE. Responses of legumes and grasses to non-, moderate, and dense shade in Missouri, USA. I. Forage yield and its species-level plasticity. Agrofor Syst. 2019;93(1):11–24. https://doi.org/10.1007/s10457-017-0112-3

Papadopoulos A, Pantera A. Solar parks effect on soil properties: initial results. CEST2023 Proc. 2023. https://doi.org/10.30955/gnc2023.00316

Parisi V. La qualità biologica del suolo: un metodo basato sui microartropodi. Acta Nat Ateneo Parmense. 2001;37:105–114.

Parisi V, Menta C, Gardi C, Jacomini C, Mozzanica E. Microarthropod communities as a tool to assess soil quality and biodiversity: a new approach in Italy. Agric Ecosyst Environ. 2005;105(1–2):323–333. https://doi.org/10.1016/j.agee.2004.02.002

Pierret A, Maeght J-L, Clément C, Montoroi J-P, Hartmann C, Gonkhamdee S. Understanding deep roots and their functions in ecosystems: an advocacy for more unconventional research. Ann Bot. 2016;118(4):621–635. https://doi.org/10.1093/aob/mcw130

Pittarello M, Lonati M, Gorlier A, Perotti E, Probo M, Lombardi G. Plant diversity and pastoral value in alpine pastures are maximized at different nutrient indicator values. Ecol Indic. 2018;85:518–524. https://doi.org/10.1016/j.ecolind.2017.10.064

Pornaro C, Basso E, Macolino S. Pasture botanical composition and forage quality at farm scale: a case study. Ital J Agron. 2019;14(4):1480. https://doi.org/10.4081/ija.2019.1480

Qin FF, Shen YX, Zhou JG, Wang QS, Sun ZC, Wang B. Seedling morphology and growth responses of nine Medicago sativa varieties to shade conditions. Acta Pratacult Sin. 2010;25:1263–1267. https://doi.org/10.3724/SP.J.1077.2010.01263

Regione Emilia-Romagna, Servizio Geologico, Sismico e dei Suoli. Catalogo dei suoli. Bologna: Regione Emilia-Romagna; 2024 [Consulted 2025 Sept 05]. Available from: https://agri.regione-emilia-romagna.it/Suoli/

Rosslowe C, Petrovich B. European Electricity Review 2025. London: Ember; 2025.

Siepel H. Life-history tactics of soil microarthropods. Biol Fertil Soils. 1994;18:263–278. https://doi.org/10.1007/BF00570628

Udroiu N-A. The use of agrivoltaic systems, an alternative for Romanian farmers. Sci Pap Ser D Anim Sci. 2023;66(2):410–420.

Vaverková MD, Winkler J, Uldrijan D, Ogrodnik P, Vespalcová T, Aleksiejuk-Gawron J, Koda E. Fire hazard associated with different types of photovoltaic power plants: effect of vegetation management. Renew Sustain Energy Rev. 2022;162:112491. https://doi.org/10.1016/j.rser.2022.112491

Walgenbach RP, Marten GC. Release of soluble protein and nitrogen in alfalfa: III. influence of shading. Crop Sci. 1981;21:859–862. https://doi.org/10.2135/cropsci1981.001118

Wallwork JA. Ecology of soil animals. London: McGraw-Hill; 1970.

Wingler A, Hennessy D. Limitation of grassland productivity by low temperature and seasonality of growth. Front Plant Sci. 2016;7:1130. https://doi.org/10.3389/fpls.2016.01130

Weselek A, Ehmann A, Zikeli S, Lewandowski I, Schindele S, Hogy P. Agrophotovoltaic systems: applications, challenges, and opportunities—a review. Agron Sustain Dev. 2019;39:35. https://doi.org/10.1007/s13593-019-0581-3

Yue S, Guo M, Zou P, Wu W, Zhou X. Effects of photovoltaic panels on soil temperature and moisture in desert areas. Environ Sci Pollut Res. 2021;28:17506–17518. https://doi.org/10.1007/s11356-020-11742-8

Zhang J, Li Z, Tao J, Ge Y, Zhong Y, Wang Y, Yan B. Observed impacts of ground-mounted photovoltaic systems on the microclimate and soil in an arid area of Gansu, China. Atmosphere. 2024;15(8):936. https://doi.org/10.3390/atmos15080936

Van Sambeek JW, Navarrete-Tindall NE, Garrett HE, Lin CH, McGraw RL, Wallace DC. Ranking the shade tolerance of forty-five candidate groundcovers for agroforestry plantings. Temp Agroforester. 2007;15(4):10 p.

van Eekeren N, Jongejans E, van Agtmaal M, Guo Y, van der Velden M, Versteeg C, Siepel H. Microarthropod communities and their ecosystem services restore when permanent grassland with mowing or low-intensity grazing is installed. Agric Ecosyst Environ. 2022;323:107682. https://doi.org/10.1016/j.agee.2021.107682

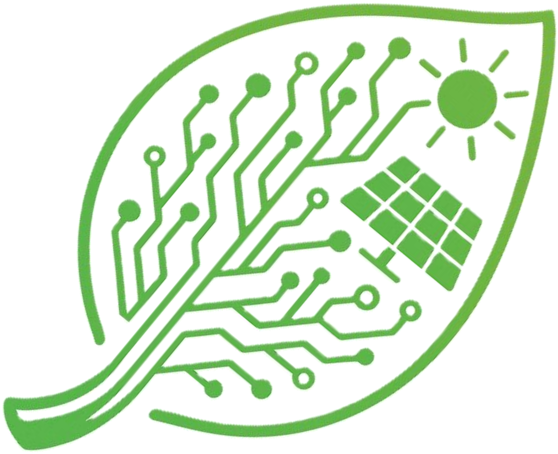

Chapter 7.

General conclusions

Chapter 7. shows the conclusions of the thesis.

PhD candidate's contribution

Michele Moretta wrote the entire chapter.

7.1 General conclusions

The research presented in this PhD thesis explored the integration of agricultural production and renewable energy generation within Agrivoltaic systems, providing new methodological and conceptual tools to assess and optimize their performance. By combining multi-scale monitoring, radiation modelling, and process-based crop simulation, this work contributed to a deeper understanding of how heterogeneous shading affects crop growth, productivity, and resource-use efficiency under AVS configurations.

Across the experimental and modelling frameworks developed, three main advances were achieved.

First, as discussed in *Chapter 3*, the thesis demonstrated that low-cost proximal sensing can effectively capture crop dynamics in complex shaded environments, representing a promising step toward continuous, non-destructive monitoring of biomass in AVS. This study established an innovative image-driven monitoring framework, aligned with the Italian AVS guidelines, and offered a scalable and replicable approach to accurately track crop growth dynamics under variable environmental and microclimatic conditions.

Initially, the comparative analysis between 2D and 3D imaging models revealed that 2D imagery, owing to its satisfactory performance, simplicity, cost-effectiveness, and superior temporal resolution, is particularly suitable for routine monitoring of uniform and low-complexity canopies such as alfalfa. The 2D-derived data were therefore used to estimate daily fAPAR values and to force the process-based SSM-iCrop2 crop growth model, enhancing its ability to reproduce biomass accumulation under heterogeneous shading. This integration enabled the model to capture interannual variability in alfalfa productivity, demonstrating that yield differences between 2023 and 2024 were influenced not only by total rainfall but also by its temporal distribution and mowing management practices.

Beyond its methodological contribution, the dynamic assimilation of proximal sensing data provided a practical foundation for site-specific agronomic management. The spatialization of model outputs offered valuable insight into crop heterogeneity, enabling the identification of optimal mowing schedules and supporting decision-making tools for farmers aimed at maximizing productivity while maintaining the overall energy-agricultural efficiency of AVS. Despite these promising results, further work is required to expand the scalability and transferability of the framework across different crops and climates. The integration of machine learning algorithms for real-time data processing and the use of fixed LiDAR or RGB-depth cameras could further automate monitoring and improve model prediction under dynamic shading and water availability. Moreover, deeper investigation of physiological adaptations, such as variations in Specific Leaf Area (SLA), may guide the design of AVS configurations tailored to specific species and environments.

Overall, the framework developed in Chapter 3 establishes a foundation for data-driven and adaptive monitoring in agrivoltaics, bridging the gap between high-resolution field observation and process-based modelling, and paving the way toward an integrated, intelligent management of AVS that harmonizes agricultural productivity with renewable energy generation.

Second, as discussed in *Chapter 4*, the integration of 3D radiation modelling with process-based crop simulations provided a mechanistic understanding of how AVS design parameters- such as panel height, spacing, and tilt- modulate light distribution, microclimate, and crop performance. The coupling between GroIMP and SSM-iCrop2 highlighted the central role of spatial variability in intercepted radiation and water balance, enabling the identification of design configurations that minimize yield penalties while sustaining high energy output.

This integrated, process-based modelling framework dynamically linked simulated irradiance with crop morpho-physiological processes, successfully reproducing dry matter yield, leaf area development, canopy temperature, and soil water dynamics (FTSW) across a range of shading scenarios. The capacity to simulate canopy-level microclimate, including cooling effects of shading, proved essential for evaluating crop water-use efficiency and resilience to thermal stress - two critical aspects under Mediterranean and semi-arid conditions. By combining morpho-physiological with computational scalability, the approach established a robust decision-support tool for optimizing both AVS design and site-specific management, with broad applicability in agronomic research and precision agriculture.

Beyond its immediate findings, this work demonstrates the strategic value of integrated modelling frameworks for advancing AV research. By unifying biophysical processes and system geometry within a single simulation environment, it becomes possible to explore tailored design strategies that balance agricultural productivity and photovoltaic efficiency. Future developments should extend this approach to different crops with variable shade tolerance and incorporate additional limiting factors such as nutrient availability, pest pressure, and soil heterogeneity. These improvements would further strengthen model predictive capacity and contribute to a new generation of adaptive, data-driven tools for the sustainable deployment of AV technologies.

Third, as presented in *Chapter 5*, the evaluation of AVS impacts on permanent grassland ecosystems provided new insights into the long-term interactions between photovoltaic installations and natural forage systems in Mediterranean environments. This research explored how partial shading and altered microclimatic regimes beneath photovoltaic panels influence grassland composition and productivity across multiple growing seasons.

Importantly, these vegetation responses were paralleled by significant improvements in soil biological activity, as evidenced by the QBS-ar (Soil Biological Quality) index presented within the same research framework presented in *Chapter 6*. The study highlights how AVS influence both plant and soil communities in pasture ecosystems through microclimatic gradients induced by photovoltaic panels. Across shading treatments, light availability and soil moisture jointly drove plant-soil interactions, with legumes supporting soil fertility and enhancing microarthropod communities. The combined use of PV and QBS-ar indices proved effective in capturing fine-scale ecological variation, offering valuable guidance for site-specific and informed management strategies. In this context, future research should further explore the interactions between grazing animals and AVS pastures, providing insights for the design of more resilient and biodiversity-friendly agroenergy systems. Overall, these studies underscore the value of microarthropods as indicators for assessing and monitoring soil quality, particularly in view of their potential integration within the framework of the Soil Monitoring Law adopted by the Council of the European Union in 2024.

Taken together, these outcomes advance the scientific foundation for data-driven AV design and management, where continuous monitoring and model integration serve as key enablers for adaptive decision-making. The methodological framework developed in this work can be extended to a wide range of crops and climatic zones, paving the way for predictive, multi-objective optimization of future AVS installations.

Beyond their technical implications, the findings reinforce the role of AVs as a strategic instrument for climate adaptation, land-use efficiency, and resource conservation. By fostering a synergistic coexistence between energy and agriculture, AVS systems can contribute significantly to rural development and to the transition toward a carbon-neutral economy. However, their widespread adoption will depend on coherent policy frameworks, economic incentives, and long-term experimental validation to ensure their environmental and socio-economic sustainability.

Supplementary Material

Supplementary Material contains all the annexes separated in Chapters. The Supplementary Material includes also the List of Tables and Figures and the List of Scientific Contributions.

1. Supplementary Material Chapter III

Towards Crop Monitoring in Agro-Photovoltaic Systems: An Image-driven Modeling Approach for fAPAR-derived Biomass Estimation

Table S1 Correlations and statistics between observed and VIs-derived fAPAR data obtained in alfalfa over each treatment.

Technology	Treatment	Statistic index			
		R^2	RMSE	rRMSE	AIC
2D Imaging	TR1	0.59	0.07	10.65	-12.53
	TR2	0.92	0.05	7.77	-16.87
	TR3	0.75	0.08	14.17	-11.18
3D Imaging	TR1	0.64	0.077	11.89	-10.76
	TR2	0.72	0.075	13	-13.14
	TR3	0.80	0.08	14.88	-16.09
	TR4	0.54	0.13	33.29	-5.62

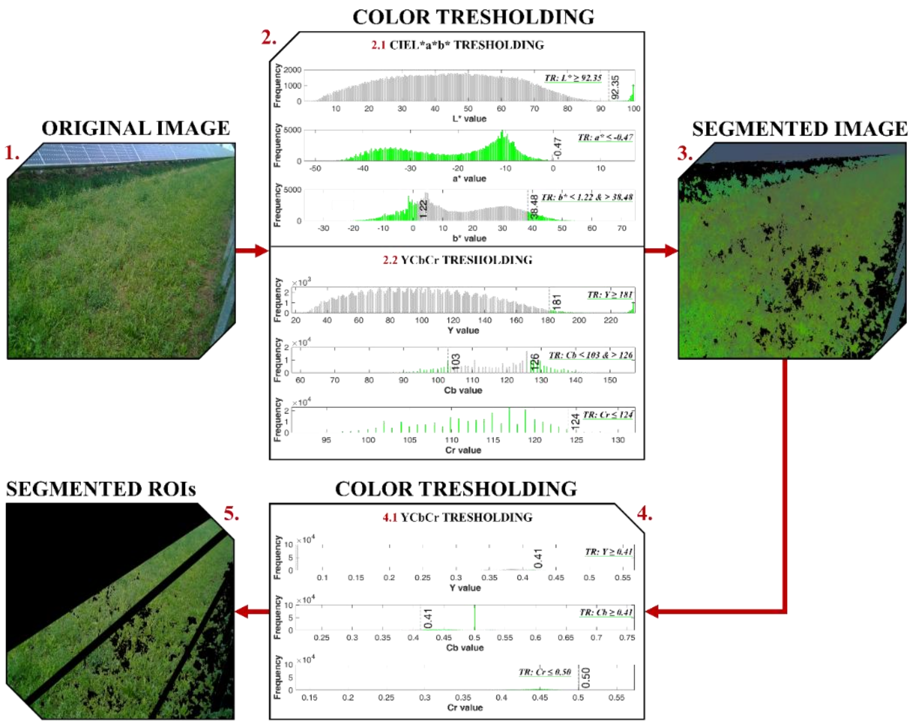

Figure S1. Visual overview of the color thresholding approach used for the automatic segmentation of vegetation in the analyzed ROIs. The green bars highlight the regions in each channel of the CIEL*a*b*and YCbCr color spaces that fall within the applied thresholds (TR).

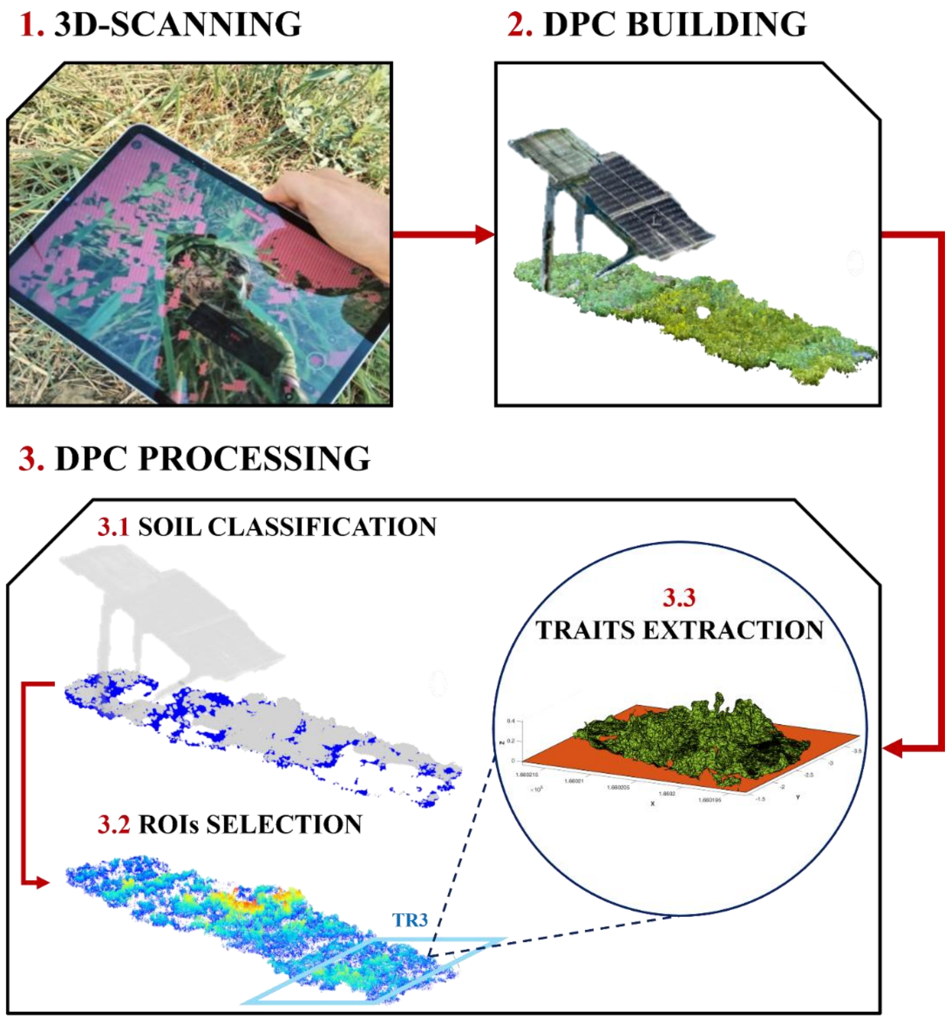

Figure S2. Graphical workflow of the applied methodology for 3D-modeling, including (1) 3D scanning using a handheld LiDAR device, (2) reconstruction of a dense point cloud (DPC) via the built-in *Scaniverse* app, and (3) semi-automated processes for (3.1) soil removal, (3.2) selection of regions of interest (ROIs), and (3.3) extraction of morpho-colorimetric traits. In step 3.3, the orange area represents the bounding box in the *xy*-plane, used to normalize the average plant area (PA, m^2) and volume (PV, m^3).

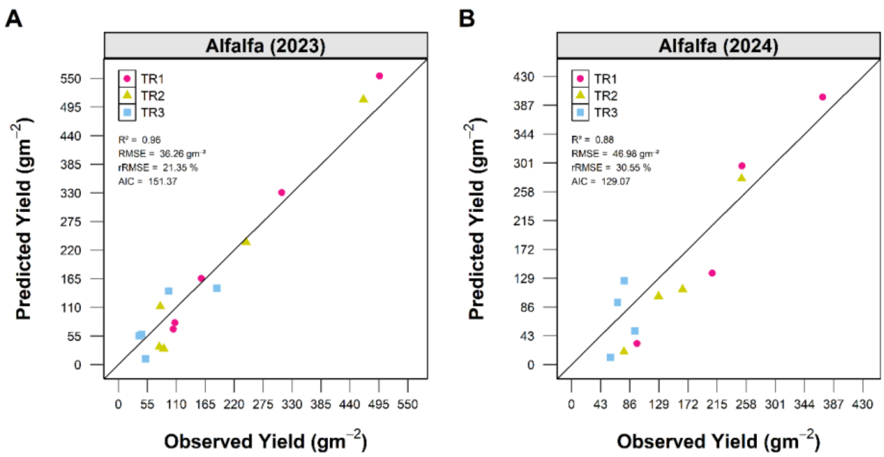

Figure S3. Comparison of the observed alfalfa yield with the predicted values modeled using the 2D image-derived fAPAR data for the defined treatments (TR1, TR2 and TR3) at the (**A**) 2023 and (**B**) 2024 infield sampling dates. The black line represents the 1:1 reference line.

Radiation distribution in AVS

Global radiation was simulated here under standard conditions throughout the year, considering a constant transmissivity factor for each day (0.75) to better highlight the different irradiance along the analyzed transect. The external condition follows a typical seasonal pattern, with radiation gradually increasing from the beginning of the year, reaching a peak around DOY 180-210 at approximately 32 MJ m^{-2} d^{-1}, and subsequently declining towards the end of the year. In contrast, the three treatments under the AVS exhibited distinct radiation patterns influenced by varying degrees of shading. TR1 and TR2 displayed similar trends to the external condition but with moderate reductions in GR, particularly noticeable at the beginning and end of the growing season. The maximum radiation observed in these treatments was slightly lower than the external values, indicating a partial shading effect that allows for relatively favorable light conditions for plant growth. On the other hand, TR3 experienced a significant reduction in GR throughout the entire year, with the lowest radiation levels recorded among the treatments. The GR values in TR3 peaked at lower levels and displayed a bimodal pattern, with smaller peaks occurring around DOY 50 and 300, suggesting pronounced shading effects that may be influenced by the positioning of solar panels or seasonal variations in light availability.

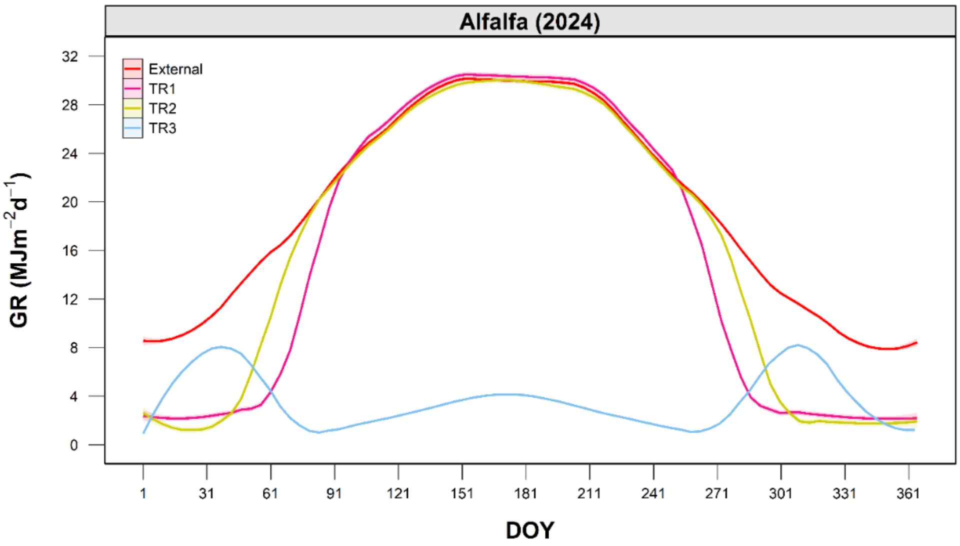

Figure S4. Daily global radiation (GR, MJ m^{-2} d^{-1}) trends over the year 2024 for external conditions and three treatments (TR1, TR2, and TR3).

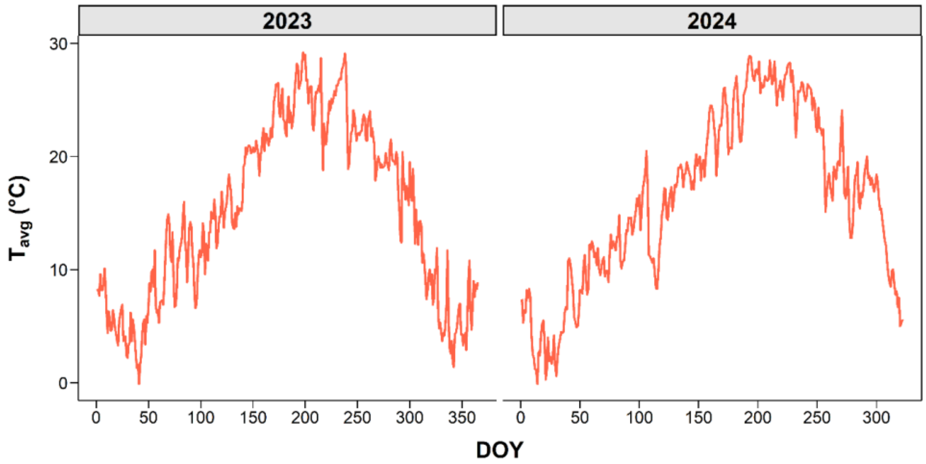

Figure S5. Daily trend of average temperatures (T_{avg}, °C) registered for the 2023 and 2024 growing seasons.

2. Supplementary Material Chapter IV

Integrated Modelling of Shading Effects on Alfalfa Growth Across Different Agrivoltaic Systems

A full explanation of the approach is presented in Yin et al. (2021), of which this document provides only a brief overview; for more comprehensive information, we recommend consulting the original publication.

The model $\Phi_{CO2,canopy}$ [Eq. 1] considers the effect of CO_2 concentration on photosynthetic efficiency, but also responds to temperature, which affects both the CO_2-compensation point Γ_*, [Eq. 2] and the maximum electron transport rate J_{max}, [Eq. 3].

$$\Phi_{CO2,canopy} = \frac{(C_C - \Gamma_*)\cdot \phi_{2LL}}{4\cdot(C_C + 2\Gamma_*)\cdot\left(1 + \phi_{2LL} + \frac{\phi_{2LL}\cdot k\cdot I_{inc}}{J_{max,0}}\right)} \qquad [1]$$

$$\Gamma_* = \Gamma_{*25}\cdot A_{rr(T)} = \Gamma_{*25}\cdot exp\left[\frac{E}{R}\left(\frac{1}{298} - \frac{1}{T}\right)\right] \qquad [2]$$

$$J_{max} = J_{max25}\cdot A_{rr*(T)} = J_{max25}\cdot exp\left[\frac{E}{R}\left(\frac{1}{298} - \frac{1}{T}\right)\right]\cdot \frac{1 + exp\left[\frac{H}{R}\left(\frac{S}{H} - \frac{1}{298}\right)\right]}{1 + exp\left[\frac{H}{R}\left(\frac{S}{H} - \frac{1}{T}\right)\right]} \qquad [3]$$

$$J_{max25} = \chi\,(n - n_b) \qquad [4]$$

In Equation [1], chloroplast CO_2 concentration C_C was set to 0.5 of ambient CO_2 (Yin et al., 2014) and the electron transport efficiency of photosystem II under limiting light Φ_{2LL} was set to 0.8 mol mol^{-1} (Baker,2008).

In Equation [2], $A_{rr(T)}$ is the standard Arrhenius equation, where R is the universal gas constant (8.314 J K^{-1} mol^{-1}), and E is the activation energy (J mol^{-1}). The value of E for Γ_* is set to 32,000 J mol^{-1} (Yin et al., 2014).

In Equation [3], $A_{rr*(T)}$ is a modified Arrhenius equation, where H is the deactivation energy (J mol^{-1}) and S is the entropy term (J K^{-1} mol^{-1}). The value of H is set to 200,000 J mol^{-1}, that of S to 650 J K^{-1} mol^{-1} (Harley et al., 1992). Considering that E for J_{max} ranges from 30,000 J mol^{-1} for temperate to 97,000 J mol^{-1} for warm-climate grown crops (Yin and van Laar, 2005) since alfalfa is a crop adapted to a Mediterranean climate (Argenti et al., 2021), for our simulation, we considered E to be close to that of warm-climate grown crops and assumed 85,000 J mol^{-1}.

Equation [4] (Harley et al.,1992; Yin and Struik, 2016) defines the response of J_{max} (µmol m^{-2} s^{-1}) to leaf nitrogen content (N, g m^{-2}), where n_b is the base leaf nitrogen content for photosynthesis (gNm^{-2}). The slope factor χ has a value of about 100 µmol $(gN)^{-1}$ s^{-1}, and the value of (n - n_b) for a top leaf in the canopy was set to 1.5 gN m^{-2}.

Considering that a shaded environment reduces J_{max25} with respect to full-light conditions (Waring et al., 2023), we accounted for this effect by dynamically decreasing J_{max25} from its control conditions (assumed 150 μmol m^{-2} s$^{-1,}$ considering the maximum value obtained for Glycine max in Waring et al., 2023, in unstressed conditions), depending on the degree of shadowing on hourly time scale

$$J_{max25}(f_{shade}) = J_{max25,full} \cdot e^{-kl \cdot f_{shade}} \quad [5]$$

where f_{shade} is the degree of shadowing (*i.e.,* the ratio between locally intercepted and external global radiation, unitless), $J_{max25,\,full}$ is J_{max25} in sunlight conditions. *Kl* defines the rate at which J_{max25} decreases as a function of shading, here calibrated according to the results in Waring et al. (2023) (*kl* = 1.3).

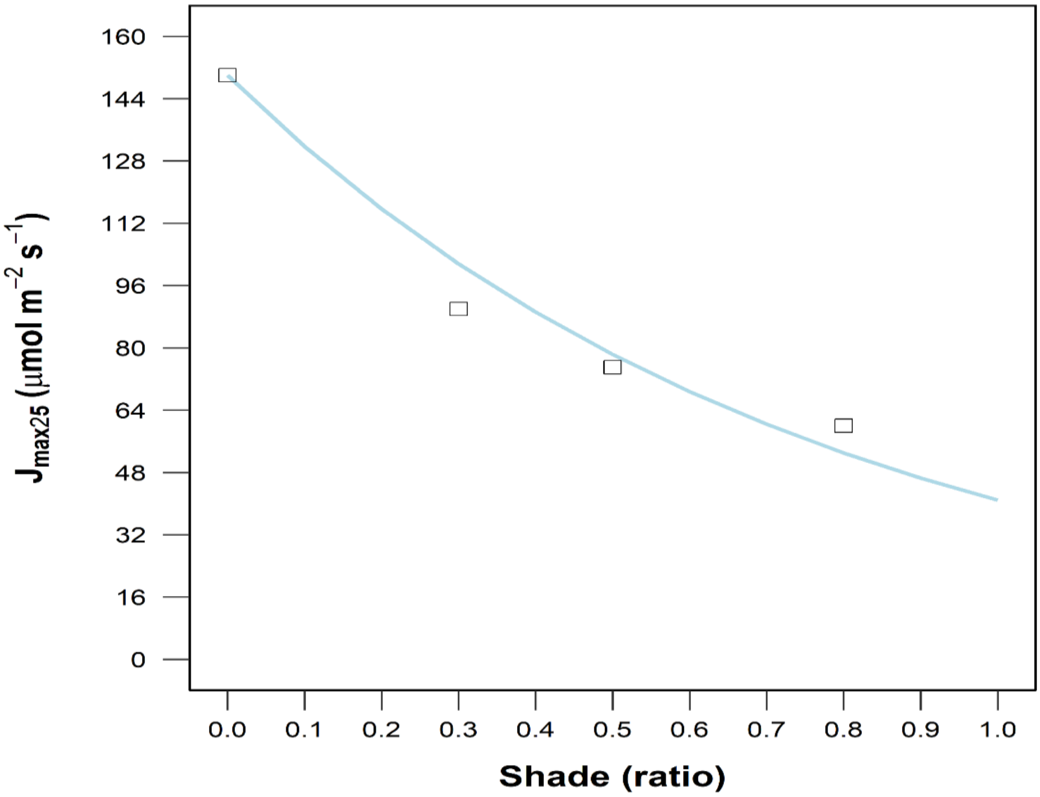

Figure S1. The effect of shading on J_{max25} is parametrized in Equation [5] according to the results of Waring et al. (2025) on Glycine max (open squares). Full light conditions (Shade=0) correspond to 1662 μmol m^{-2} s^{-1}.

The effect of soil moisture on potential transpiration and leaf area expansion was calculated according to:

$$RelTr = \ (1 + a \cdot exp\ exp\ (b \cdot FTSW)\ )^{-1} \quad [6]$$

where *RelTr* represents the ratio between the actual value of transpiration/RUE and its corresponding reference value under non-limiting water conditions. *FTSW* denotes the Fraction of Transpirable Soil Water, which is used as an indicator of soil water availability. The parameters *a* and *b* correspond to the shape coefficients that define the sensitivity of the process to soil water deficit, as reported in Table S1 and in Figure S2

Figure S2. The effect of FTSW on plant transpiration and RUE according to Equation [6], parametrized for *a* and *b* as in Table S1.

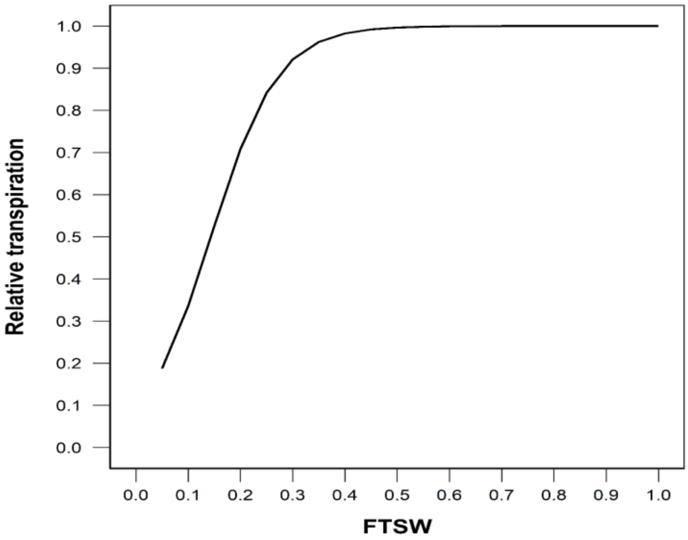

Table S1. List of parameters of the alfalfa growth model. The calibrated parameters are shown in bold.

Parameter	Description	Value	Unit	References
Phenology				
Tb	Base temperature for development	0	°C	Brown et al. (2006)
DDA to BV	Degree days to the bud visible stage (PP=10h)	700	°C	Teixeira et al. (2011)
	Degree days to the bud visible stage (PP>14h)	270	°C	Teixeira et al. (2011)
DDA from BV to anthesis	Degree days accumulated to the anthesis stage	274 (310)	°C	Teixeira et al. (2011)
Leaf area development				
FixSENrate	Senescence rate	0.20	$m^2 m^{-2}$	Yang et al. (2022)
SLAmax	Maximum increment of specific leaf area under complete shading	0.25	Unitless	Moretta et al. (2025)
Light interception and photosynthesis				
a	Shape parameter for RelTr	9.5	Unitless	Bellini et al. (2023)
b	Shape parameter for RelTr	-15.7	Unitless	Bellini et al. (2023)
C_C	Chloroplast CO_2 concentration	0.5 amb_{CO2}	$\mu mol\ mol^{-1}$	Yin et al. (2014)
Γ^*_{25}	CO_2-compensation point at reference temperature (25°C)	35	$\mu mol\ mol^{-1}$	Yin et al. (2014)
H	Deactivation energy	200,000	$J\ mol^{-1}$	Harley et al., 1992
S	Entropy	650	$J\ K^{-1}\ mol^{-1}$	Harley et al., 1992
E	Activation energy (Γ^*)	32,000	$J\ mol^{-1}$	Yin et al., 2014
	Activation energy (Jmax)	85,000	$J\ mol^{-1}$	Assumed
χ	Slope factor	100	$\mu mol\ (g\ N)^{-1}\ s^{-1}$	Yin and Struik, (201
n-nb	Leaf nitrogen (difference between base leaf nitrogen and top layer content)	1.5	gNm^{-2} leaf	Assumed
Kc	Crop coefficient	1.05	Unitless	Allen et al. (1998)
Φ_{2LL}	Electron transport efficiency of Photosystem II under limiting light	0.8	$mol\ mol^{-1}$	Baker (2008)
R/P	Respiration/photosynthesis ratio	0.4	Unitless	Yin et al. (2021)

Table S1 (continued)

Biomass accumulation and partitioning					
c	Coefficient for AGB partitioning to leaf		0.26	Unitless	Teixeira et al. (2009)
d	Coefficient for AGB partitioning to leaf		0.68	Unitless	Teixeira et al. (2009)
e	Coefficient for AGB partitioning to leaf		0.43	Unitless	Teixeira et al. (2009)
PC_{AGB}	Partitioning coefficient to AGB	PP<spring equinox	0.9	Unitless	Brown et al. (2006)
	Partitioning coefficient to AGB	summer solstice> PP>spring equinox	0.67	Unitless	
	Partitioning coefficient to AGB	summer solstice-1h (-2h)> PP	0.35 (0.5)	Unitless	

References

Allen, R. G., Pereira, L. S., Raes, D., & Smith, M. (1998). Crop evapotranspiration: Guidelines for computing crop water requirements (FAO Irrigation and Drainage Paper No. 56). Food and Agriculture Organization of the United Nations.

Argenti, G., Parrini, S., Staglianò, N., & Bozzi, R. (2021). Evolution of production and forage quality in sown meadows of a mountain area inside Parmesan cheese consortium. Agronomy Research, 19(2), 344–356, 2021. doi:10.15159/AR.21.061

Baker N. R. (2008). Chlorophyll fluorescence: a probe of photosynthesis in vivo. Annual review of plant biology, 59, 89–113. https://doi.org/10.1146/annurev.arplant.59.032607.092759

Bellini, E., Moriondo, M., Dibari, C., Bindi, M., Staglianò, N., Cremonese, E., Filippa, G., Galvagno, M., & Argenti, G. (2023). VISTOCK: A simplified model for simulating grassland systems. European Journal of Agronomy, 142, 126647. https://doi.org/10.1016/j.eja.2022.126647

Brown, H. E., Moot, D. J., & Teixeira, E. I. (2006). Radiation use efficiency and biomass partitioning of lucerne (Medicago sativa) in a temperate climate. European Journal of Agronomy, 25(4), 319–327. https://doi.org/10.1016/j.eja.2006.06.008

Harley, P. C., Loreto, F., Di Marco, G., & Sharkey, T. D. (1992). Theoretical considerations when estimating the mesophyll conductance to CO2 flux by analysis of the response of photosynthesis to CO2. Plant physiology, 98(4), 1429-1436. https://doi.org/10.1104/pp.98.4.1429

Moretta, M., Moriondo, M., Leolini, L., Padovan, G., Staglianó, N., Palchetti, E., Lanini, G. M., Bindi, M., & Rossi, R. (2025). Towards crop monitoring in agro-photovoltaic systems: An image-driven modeling approach for fAPAR-derived biomass estimation. European Journal of Agronomy, 170, 127748. https://doi.org/10.1016/j.eja.2025.127748

Soltani, A., F. R. Khooie, K. Ghassemi-Golezani, and M. Moghaddam. "Thresholds for chickpea leaf expansion and transpiration response to soil water deficit." (2000): 205-210.

Teixeira, E. I., Brown, H. E., Meenken, E. D., & Moot, D. J. (2011). Growth and phenological development patterns differ between seedling and regrowth lucerne crops (Medicago sativa L.). European Journal of Agronomy, 35(1), 47–55. https://doi.org/10.1016/j.eja.2011.03.006

Teixeira, E. I., Moot, D. J., & Brown, H. E. (2009). Modelling seasonality of dry matter partitioning and root maintenance respiration in lucerne (Medicago sativa L.) crops. Crop and Pasture Science, 60(8), 778–784. https://doi.org/10.1071/CP08409

Waring, E. F., Perkowski, E. A., & Smith, N. G. (2023). Soil nitrogen fertilization reduces relative leaf nitrogen allocation to photosynthesis. Journal of Experimental Botany, 74(17), 5166–5180. https://doi.org/10.1093/jxb/erad195

Yang, X., Brown, H. E., Teixeira, E. I., & Moot, D. J. (2022). Development of a lucerne model in APSIM next generation: 2. Canopy expansion and light interception of genotypes with different fall dormancy ratings. European Journal of Agronomy, 139, 126570. https://doi.org/10.1016/j.eja.2022.126570

Yin, X., & van Laar, H. H. (2005). Crop systems dynamics: An ecophysiological simulation model of genotype-by-environment interactions. Wageningen Academic Publishers. https://doi.org/10.3920/978-90-8686-539-0

Yin, X., Belay, D. W., van der Putten, P. E. L., Struik, P. C., & Harbinson, J. (2014). Accounting for the decrease of photosystem photochemical efficiency with increasing irradiance to estimate quantum yield of leaf photosynthesis. Photosynthesis Research, 122(3), 323–335. https://doi.org/10.1007/s11120-014-0030-8

Yin, X., Busch, F. A., Struik, P. C., & Sharkey, T. D. (2021). Evolution of a biochemical model of steady-state photosynthesis. Plant, Cell & Environment, 44(9), 2811–2837. https://doi.org/10.1111/pce.14070

Yin, X., Struik, P.C. (2016). Crop Systems Biology: Where Are We and Where to Go?. In: Yin, X., Struik, P. (eds) Crop Systems Biology. Springer, Cham. https://doi.org/10.1007/978-3-319-20562-5_10

3. Supplementary Material Chapter IV

Assessing the Impact of Agrivoltaic System on Pasture Plant and Soil Microarthropod Communities

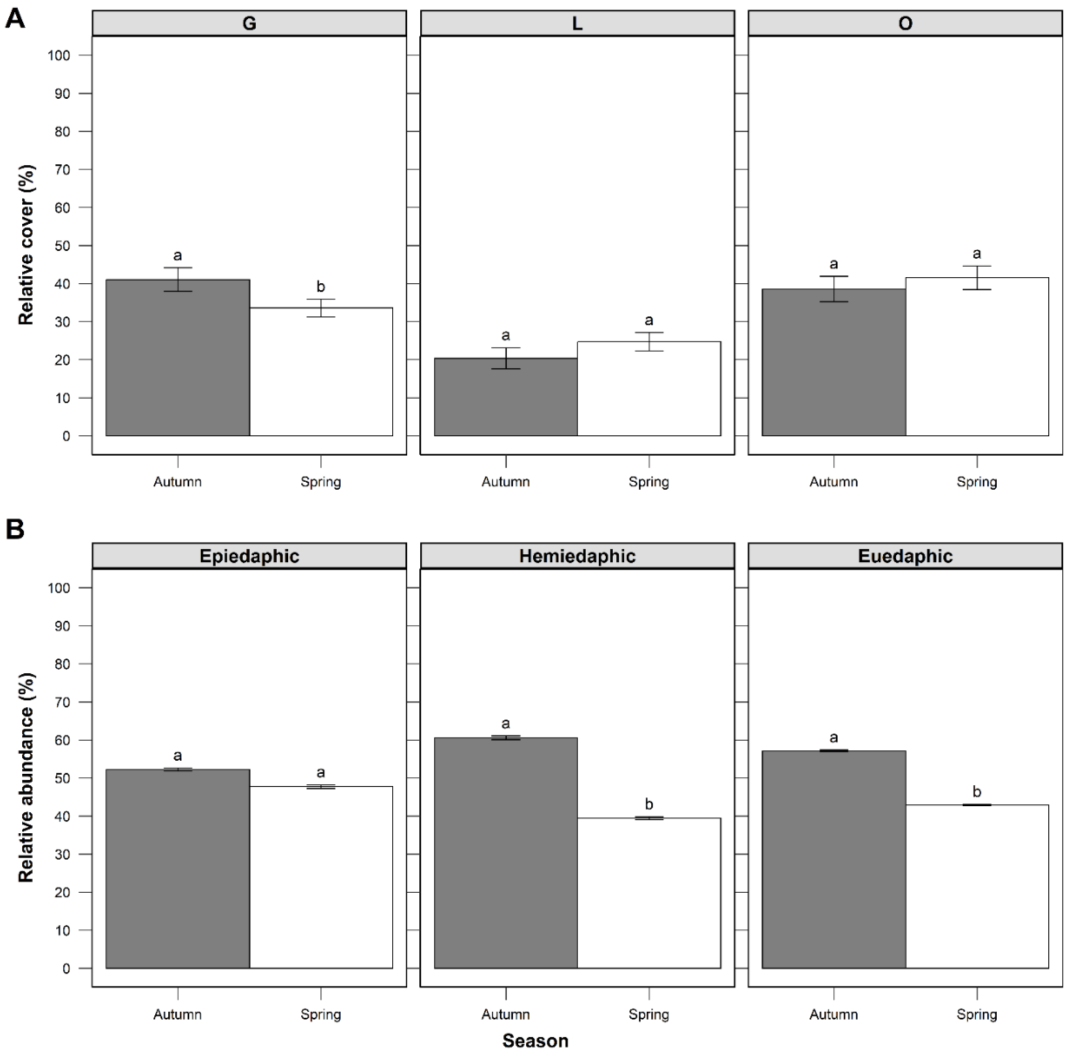

Figure S1. Average (± standard error) **(A)** relative cover (%) of plant functional groups (G, L, O) and **(B)** relative abundance (%) of soil microarthropod functional groups (Epiedaphic, Hemiedaphic, Euedaphic), across seasons (autumn and spring). Different letters above bars indicate significant differences among seasons within the same plant or microarthropod functional group according to Tukey's HSD test ($p < 0.05$).

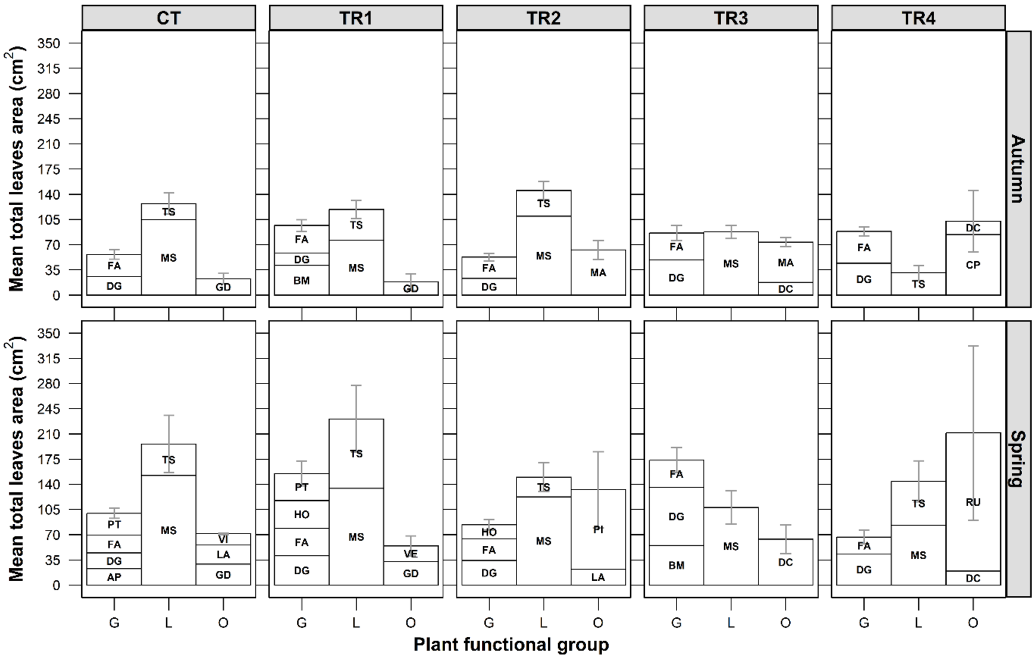

Figure S2. Mean (± standard error) total leaves area (cm^2) of the most representative species within each functional group (G, L, O) sampled across treatments (CT, TR1–TR4) and seasons (autumn and spring). Species included are *Festuca arundinacea* Scchreb. (FA), *Dactylis glomerata* L. (DG), *Trifolium repens* L. (TS), *Medicago sativa* L. (MS), *Bromus mollis* L. (BM), *Geranium dissectum* L. (GD), *Malva sylvestris* L. (MA), *Daucus carota* L. (DC), *Crepis pontana* L. (CP), *Poa trivialis* L. (PT), *Alopecurus pratensis* L. (AP), *Vicia faba* L. (VI), *Lamium maculatum* L. (LA), *Holcus lanatus* L. (HO), *Veronica persica* Poir. (VE), *Picris hieracioides* L. (PI), and *Rumex alpinus* L. (RU).

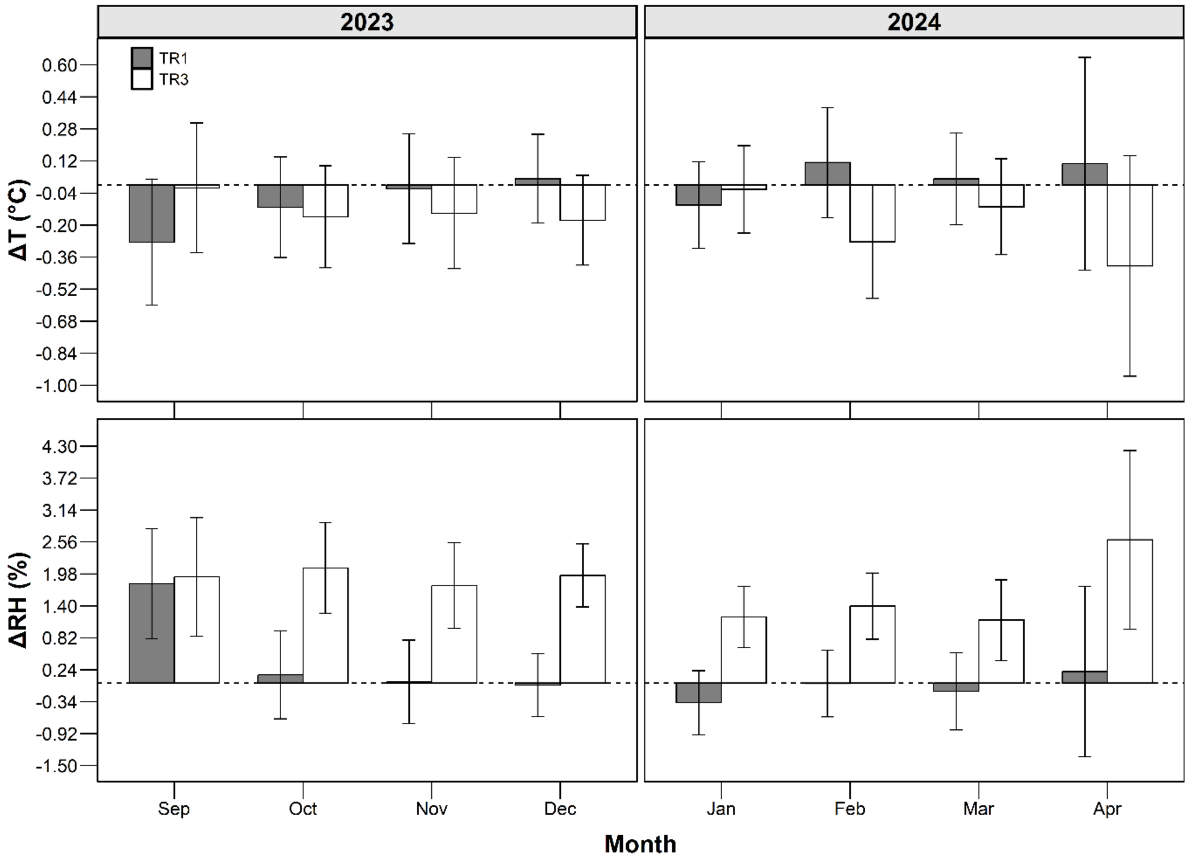

Figure S3. Monthly mean differences (± standard error) in air temperature (ΔT, °C) and relative humidity (ΔRH, %) between (TR1) and under the photovoltaic panels (TR3) compared to the reference area (CT1). The dashed line denotes the zero-difference reference (Δ = 0).

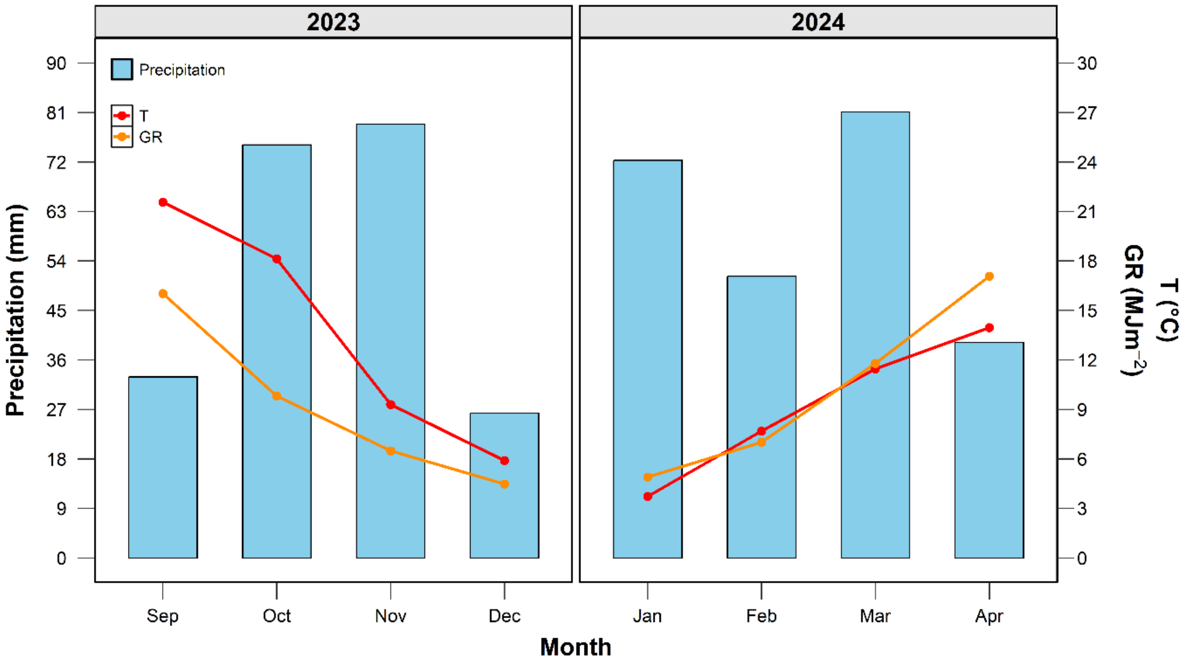

Figure S4. Monthly trends of total precipitation (blue bars), mean air temperature (red line), and mean daily global solar radiation (orange line) recorded at the experimental AVS site.

Table S1. Average (± standard error) of soil temperature (T_{soil}, °C) and volumetric water content (VWC, %) measured during autumn and spring sampling across treatments (CT, TR1-TR4).

Treatment	**T_{soil} (°C)**		**VWC (%)**	
	Autumn	**Spring**	**Autumn**	**Spring**
CT	14.17 ± 0.21	23.00 ± 0.01	38.03 ± 0.35	37.83 ± 5.13
TR1	14.46 ± 0.44	23.66 ± 1.12	43.22 ± 1.72	35.04 ± 2.95
TR2	14.08 ± 0.47	23.73 ± 1.00	44.14 ± 2.65	35.42 ± 2.20
TR3	14.07 ± 0.49	23.48 ± 1.09	20.24 ± 2.22	32.70 ± 1.87
TR4	14.00 ± 0.44	23.00 ± 0.99	42.06 ± 2.69	33.06 ± 2.04

Table S2. Average density (individuals m⁻²) of arthropod taxa, classified by class and order, recorded in autumn and spring across experimental treatments (CT, TR1-TR4).

Class	Order	CT		TR1		TR2		TR3		TR4	
		Autumn	Spring	Autumn	Spring	Autumn	Spring	Autumn	Spring	Autumn	Spring
Chelicerata	Acarina	112.56	212.49	284.03	493.19	180.73	295.77	309.24	129.44	380.12	559.72
	Araneae	-	-	2.31	2.20	1.56	-	2.50	-	3.96	7.69
	Opiliones	-	-	-	-	0.59	-	-	-	-	-
	Pseudoscorpiones	-	-	0.32	-	-	-	-	-	7.14	-
Crustacea	Isopoda	5.19	4.10	22.09	34.83	13.89	0.26	111.27	-	44.48	12.24
Myriapoda	Chilopoda	-	0.53	2.05	11.39	0.29	-	-	-	1.15	14.29
	Diplopoda	-	-	0.61	0.53	8.28	-	-	2.78	7.30	8.33
	Pauropoda	-	-	-	-	3.41	-	-	-	-	-
	Symphyla	-	-	0.43	-	-	-	-	-	1.12	-
Hexapoda Entognatha	Collembola	247.51	117	407.05	195.44	461.76	245.46	198.34	42.78	331.52	122.53
	Diplura	0.17	0.63	-	4.26	-	0.09	3.60	-	-	13.64
	Protura	-	-	0.43	-	1.01	-	-	-	4.55	-
Hexapoda Insecta	Hemiptera	-	-	-	1.38	3.02	6.06	32.06	73.68	14.80	-
	Hymenoptera	19.13	63.55	59.41	139.22	188.16	347.58	87.08	304.68	49.34	109.40

	Psocoptera	-	-	-	-	0.43	-	-	-	-	-
	Thysanoptera	-	-	-	5.72	0.53	-	-	102.78	-	-
Larvae	Coleoptera	12.67	1.16	11.72	11.12	33.77	1.69	31.13	110.53	43.53	31.03
	Dermaptera	-	-	-	-	-	-	-	-	-	-
	Diptera	1.39	0.53	9.57	0.72	2.55	3.09	8.04	133.33	10.99	21.14
	Embioptera	-	-	-	-	-	-	-	-	-	-

Table S3. Fifteen-day mean (± standard error) Fraction of Transpirable Soil Water (FTSW) and Intercepted Soil Radiation (ISR; MJ m^{-2} day^{-1}) from day of the year (DOY) 85 to 100 under shading treatments (TR1–TR4).

Treatment	**FTSW**	**ISR**
TR1	0.76 ±0.03	13.45 ±1.20
TR2	0.96 ±0.05	16.34 ±1.45
TR3	0.76 ±0.01	3.35 ±0.60
TR4	0.95 ±0.01	4.47 ±0.75

Table S4. Pearson's correlation coefficients (r) among Pasture Value (PV), Soil Biological Quality–arthropods (QBS-ar), Fraction of Transpirable Soil Water (FTSW, 15-day average), and Intercepted Soil Radiation (ISR, 15-day average) recorded during spring.

Variable 1	***Variable 2***	**r**
PV	*QBS-ar*	0.53
PV	*FTSW*	-0.31
PV	*ISR*	0.85
QBS-ar	*FTSW*	0.12
QBS-ar	*ISR*	0.73
FTSW	*ISR*	0.22

List of Tables and Figures

Tables

Chapter 3

Chapter 6

Figures

Chapter 3

Figure. 3.3. (A) Graphical 3D representation of the Ravenna APV System created in the GroIMP platform, including the alfalfa rows and the sources of direct and diffuse radiation. The sky dome discretization (72 light nodes) used by the 3D illumination model is indicated. (B) Detailed representation of the field layout, including the positions of the camera and the locations of treatments TR1, TR2, TR3 and the external control.

Figure 3.4 (part 1). Limiting to the common treatments (i.e., TR1, TR2, and TR3), comparison of daily alfalfa fAPAR derived from 2D imaging (e.g., ExG-based GPARExG and Blue Ratio, BR) and from 3D imaging (e.g., Green Ratio, GR, plant height, and volume). Model performance and Akaike's Information Criterion (AIC) are reported to compare 2D- vs 3D-based predictors across mowing cycles. The figure highlights the relative contributions of spectral (2D) and structural (3D) information in tracking daily fAPAR and the recovery dynamics after mowing—TR1 generally shows the fastest recovery, reaching pre-mowing fAPAR more rapidly than TR2 and TR3.

Figure 3.4 (part 2). Comparison between observed and simulated alfalfa fraction of absorbed photosynthetically active radiation (fAPAR). Observed values are derived from field hemispherical photographs; simulated values were modeled using the best predictors derived from 2D-imaging (i.e., Green Plant Area Ratio from ExG—GPARExG—and Blue Ratio, BR) and 3D-imaging (i.e., Green Ratio, GR, and height/volume). The black line represents the 1:1 reference line.

Figure 3.5. Application of the predictive allometric equations based on 2D-imaging (GPARExG and BR) to reconstruct the daily fAPAR trend throughout (A) 2023 and (B) 2024. The individual data represent the mean value of the nine replicates and the locally weighted error smooth, while red vertical lines indicate the mowing dates. Error bars and significance levels from the Tukey post-hoc test are reported (*: $p \leq 0.05$; **: $p \leq 0.01$; ***: $p \leq 0.001$).

Figure 3.6. Evolution of Alfalfa Specific Leaf Area across the three ROIs (TR1, TR2, and TR3) and the different days of year (DOY) in 2023. Each point indicates the mean value from the replicates, with error bars indicating the standard error.

Figure 3.7. Daily yield progression of alfalfa throughout (A) 2023 and (B) 2024 as reconstructed from 2D-derived fAPAR (GPARExG and BR). Red vertical lines correspond to the alfalfa mowing dates. Each data point represents the mean yield from three field observations with an error bar (± standard error); significance from the Tukey post-hoc test is reported (*: $p \leq 0.05$; **: $p \leq 0.01$; ***: $p \leq 0.001$).

Figure 3.8. Seasonal trends of the Fraction of Transpirable Soil Water (FTSW) across the three treatments (TR1, TR2, TR3) and precipitation (mm) during the years 2023 and 2024.

Chapter 4

Chapter 6

Collection of a standardized soil cube (10 × 10 × 10 cm) using a steel corer. (C) Example of an extracted soil sample prior to laboratory processing. (D) Berlese-Tullgren funnels used for microarthropod extraction, with soil samples placed under a light–heat gradient to induce organism migration into the collecting vials.

Figure 3. Average (± standard error) relative cover (%) of plant functional groups (G, L, O) across treatments (CT, TR1–TR4) and seasons (autumn and spring). Different letters above bars indicate significant differences among treatments within the same functional group and season according to Tukey's HSD test ($p < 0.05$).

Figure 4. Average (± standard error) relative abundance (%) of soil microarthropod functional groups (Epiedaphic, Hemiedaphic, Euedaphic) across treatments (CT, TR1–TR4) and seasons (autumn and spring). Different letters above bars indicate significant differences among treatments within the same microarthropod functional group and season according to Tukey's HSD test ($p < 0.05$).

Figure 5. Average (± standard error) PV and QBS index across treatments (CT, TR1–TR4) and seasons (autumn and spring). Different letters above bars indicate significant differences among treatments within the same season according to Tukey's HSD test ($p < 0.05$), while asterisks denote significant differences between seasons for the same treatment ($p < 0.05$).

Figure 6. Principal Component Analysis (PCA) biplot showing the distribution of observations by treatment (TR1–TR4) during spring (DOY 100). Individual points represent replicates, while larger points indicate group centroids. Ellipses depict 95% confidence intervals for each treatment. Variable vectors (arrows) illustrate the contribution and direction of each measured variable to the first two principal components (PC1 and PC2), with the percentage of variance explained indicated on the axes. Variables included are Plant Vegetation index (PV), Soil Biological Quality index (QBS-ar), Fraction of Total Soil Water (FTSW), and Intercepted Soil Radiation (ISR).

Figure 7. Heatmap showing Pearson's correlation coefficients (r) between relative abundance (%) and relative cover (%) of plant (G, L, O) and soil microarthropod (Euedaphic, Hemiedaphic, Epiedaphic) functional groups, respectively, during spring (DOY 100).

List of Scientific Contributions

Publications in indexed journals

Moretta, M., Moriondo, M., Leolini, L., Padovan, G., Staglianó, N., Palchetti, E., Lanini, G. M., Bindi, M., & Rossi, R. (2025). Towards crop monitoring in agro-photovoltaic systems: An image-driven modeling approach for fAPAR-derived biomass estimation. *European Journal of Agronomy*, 170, 127748. https://doi.org/10.1016/j.eja.2025.127748

Moretta, M., Rossi, R., Padovan, G., Staglianò, N., Palchetti, E., Bindi, M., … Moriondo, M. (2025). The Impact of Photovoltaic on Permanent Grassland Composition and Productivity in Central Italy. *AgriVoltaics Conference Proceedings*, *3*. https://doi.org/10.52825/agripv.v3i.1372

Moretta, M., Moriondo, M., Rossi, R., Carvalho, G. M. de C. P., Padovan, G., Dal Prà, A., Palchetti, E., Argenti, G., Staglianò, N., Balingit, A. R., & Leolini, L. (2025). Integrated modelling of shading effects on alfalfa growth across different agrivoltaic systems. *Frontiers in Agronomy,* 7,1699126. https://doi.org/10.3389/fagro.2025.1699126

Conference

Moretta, M., Moriondo, M., Bindi, M., Padovan, G., Staglianó, N. & Rossi, R. (2023). Stima della radiazione intercettata (fPAR) da colture orticole in sistemi AgriVoltaici tramite l'utilizzo di dispositivi LiDAR portatili. Sensoristica digitale e agromotica in ortoflorofrutticoltura - Giornate Tecniche SOI, 45 Ottobre, Pontecagnano (Italia). *Modalità presentazione: Orale*

Moretta, M., Rossi, R., Moriondo, M., Padovan, G., Palchetti, E. & Marco, B. (2023). Monitoring the development of meadow grassland in Agrivoltaic system through LiDAR technology. Atti del LII convegno nazionale della Società Italiana di Agronomia (SIA), 25-27 Settembre, Portici (Italia). *Modalità presentazione: Poster*

Moretta M., Bindi M., Argenti G.,Staglianò N.,Padovan G.,Palchetti E.,Rossi R., Moriondo M. Analyzing the Influence of Shading on Alfalfa Phenotypic Traits in Agrivoltaic Systems: A GroIMP Modeling Approach. In: 5th AISSA Under40 Conference, Agricultural Sciences in the Anthropocene: from productivity to the protection of material and cultural heritage. Florence 26-27 June 2024. *Modalità presentazione: Orale*

Moretta M., Padovan G.,Palchetti E.,Rossi R., Moriondo M., Bindi M.,Time-lapse Image-Based Monitoring of Pasture Growth in Agrivoltaic Environment Using Green Indices Extraction: A Proximal Sensing Approach In:Book of abstract of the 52 annual Annual Meeting of the Italian Society of Agronomy.Matera, 10-13 September 2024. *Modalità presentazione: Orale*

<u>Moretta M.,</u> Bindi M., Padovan G.,Palchetti E.,Rossi R.,Campana P.E., Moriondo M. The Impact of Photovoltaic on Permanent Grassland Composition and Productivity in Central Italy.In: The AgriVoltaics World Conference, Denver, CO, USA, June 11-13, 2024. *Modalità presentazione: Poster*

Other scientific Agrivoltaic activities

Project Author and Winner – PHENO-SHADE (PHEN-ITALY 2024)
Title: Assessing the adaptation of horticultural plant species to shading in agrivoltaic systems through image-based phenotyping

<u>Funding programme:</u> PHEN-ITALY 2024, National Research Infrastructure for Plant Phenotyping

<u>Institutions involved:</u> CNR-IBE (Institute of BioEconomy), ALSIA PhenoLab (Metaponto), and University of Florence (DAGRI).

<u>Description</u>*:* The project investigates the adaptive responses of leafy horticultural crops to heterogeneous shading in agrivoltaic systems using image-based phenotyping. Results aim to identify crop species best suited for cultivation under photovoltaic arrays and to optimize agrivoltaic system design for improved synergy between agricultural yield and energy production.

Project collaborator – SUNBIOSE

<u>Institutions involved:</u> Wageningen Research (Netherlands)

<u>Role:</u> Research collaborator during the PhD period abroad at Wageningen University & Research (The Netherlands), within the modelling and experimental work packages on combining agriculture and photovoltaics.

<u>Description:</u> The project develops and tests agrivoltaic (Agri-PV) systems to understand how agriculture (e.g., strawberries, raspberries, pears, cherries, grass/clover) can be integrated with solar power generation on the same plot. It examines the effect of solar canopies on crop growth, financial viability for the farmer, and regulatory/business-case conditions for large-scale rollout.

Thesis Supervision

Thesis co-supervisor – B.Sc. in Agricultural Sciences, University of Florence *"Agrovoltaico: considerazioni generali e produttività delle colture erbacee nell'ambito dei sistemi a duplice utilizzo di suolo"* (Candidate: **Tommaso Cellai**, University of Florence, 2023).

Thesis co-supervisor – B.Sc. in Agricultural Sciences, University of Florence *"Sistemi agrivoltaici avanzati: quadro normativo, monitoraggio e prospettive di ricerca future"* (Candidate: **Samuel Centrini**, University of Florence, 2025).